

T 36818

*(Handwritten circle with a diagonal line)*

*(Handwritten initials)*

487625

# SACRAMENTO PLANT

GEMINI STABILITY IMPROVEMENT PROGRAM  
(GEMSIP)

Contract AF 04(695)-517

Final Report Volume 5--Development Tools

Report GEMSIP FR-1

31 August 1965

FILE COPY

SSD-TR-66-2

626 765

DDC  
AUG 25 1966



AEROJET-GENERAL CORPORATION  
SACRAMENTO, CALIFORNIA

14  
Report GEMSIP-FR-1-Vol-5

6 GEMINI STABILITY IMPROVEMENT PROGRAM

(GEMSIP),

15  
~~Contract~~ AF/04(695)-517

~~Final Report~~  
Volume 5, Development Tools,

9 final rept.,

11 31 Aug 65

12 241 p.

Sacramento Plant  
Aerojet-General Corporation  
Sacramento, California 007 200

10 W. J. Nerd

18 SSD

19 TR-66-2-Vol-5

*isid*

*and*

ACKNOWLEDGEMENTS

This program was conducted under the auspices of the United States Air Force, Space Systems Division, as a part of the Gemini engine development program. Although the ultimate intent of GEMSIP was to provide a useable injector design for Gemini, the immediate aim of the development effort was to resolve the Stage II stability problem. The nature of this problem required considerably more research, analysis, and other highly technical work to reach a solution than is usually found in development programs. Special credit is due here to the many people in the Air Force, Aerospace Corporation, Universities, and Aerojet-General Corporation who contributed in these areas.

The program was directed by Dr. D. E. Robison, Program Manager, who initiated the program, and jointly with Lt. Col. J. R. Brill, Gemini Engineering Manager, Space Systems Division, and V. H. Monteil, Aerospace Gemini project, established the scope and technical content of the program, with the guidance of Mr. A. L. Feldman, Assistant Manager, Liquid Rocket Operations and Mr. L. D. Wilson, Manager, Gemini Program. The success of this program is in large measure due to their extensive experience in the Titan programs and direct assistance in making Aerojet personnel, equipment, and facilities available at critical times in the program.

Later revisions in the program were made under the direction of Major F. E. Thompson and Capt. R. E. Haydon. The latter continued as GEMSIP project director for Space Systems Division through completion of the program. Major Thompson assisted in early phases of the program and extended his services as its scope increased. Capt. Haydon was in almost daily contact with the program in its later phases, particularly during the cooled baffle development and engine demonstration.

Mr. Monteil was the technical direction representative from Aerospace Corporation. Besides assisting in the planning of both original and the expanded GEMSIP program, he took an active interest in all the analytical and development areas. He and Mr. M. Sliwinski assisted greatly in the design of the cooled baffle.

ACKNOWLEDGEMENTS (cont.)

Mr. G. J. Motsko also is due much credit for the capable and diligent assistance he lent to the program. Mr. O. W. Dykema furnished suggestions in the theoretical investigation of stability and interpretation of test results. Mr. K. D. Shogren and Mr. J. E. Ancell furnished much to the design and use of the instrumentation. Dr. S. Rubin aided in the analysis of feed system effects and supplied a Fourier analysis of one of the engine pulse tests. Other contributing personnel from Aerospace include Messrs. L. R. Sitney and E. C. Hart

The F-1 Ad Hoc Combustion Stability Committee helped jointly and through its several members--Dr. R. J. Priem and Mr. E. W. Conrad of NASA Lewis Laboratories, Mr. R. R. Weiss of the Rocket Propulsion Laboratories, EAFB, Mr. D. T. Harrje of Princeton University and Mr. R. L. Richmond of Marshall Space Flight Center--contributed from their research and experience. Dr. Priem, Mr. Weiss, and Mr. Harrje lent their time and made valuable suggestions relating to combustion stability and other technical aspects of the program.

The LRO Combustion Stability Committee provided expert scrutiny of the technical phases of the program and were very helpful in clarifying problems. Those participating were Dr. C. C. Ross and Dr. P. A. Longwell of Aerojet, Dr. R. H. Sabersky and Dr. B. H. Sage of California Institute of Technology, Prof. H. C. Hottel of the Massachusetts Institute of Technology, Dr. I. Dyer of the firm of Bolt, Beranek and Newman, Dr. A. K. Oppenheim of the University of California, and Prof. N. W. Ryan of the University of Utah.

Special appreciation is extended to Dr. J. R. Osborn, Purdue University, who was a consultant on the program.

Valuable assistance was provided by Mr. F. C. Thompson, Manager, Thrust Chamber Design and Development Department. Mr. J. E. Stammer was Project Engineer and his energy and diligence were important to the program's success. Dr. R. J. Hefner, Manager, Combustion Dynamics Department together with Dr. F. H. Reardon were

GEMSIP FR-1, Volume 5

ACKNOWLEDGEMENTS (cont.)

instrumental in planning the experiments, and with Dr. J. M. Bonnell were the principals in guiding the theoretical phases of the program. They were ably assisted by Messrs. D. A. Fairchild, A. J. Smith, J. M. McBride, and R. C. Waugh. Members of the Gemini Project engineering staff--K. F. Royer, V. D. Brinkman, W. W. Coon, and E. R. White--were very helpful in coordinating AEIP engine tests.

The credit for the many achievements in testing and instrumentation technology is due in large measure to the technical competence and able leadership of Messrs. R. McCabe, D. C. Young, and R. D. Wesley.

The assistance of Mr. W. D. Muir and Mr. T. S. Roche of Aerojet, who with Mr. W. B. Fried of Space Systems Division worked out the fiscal and contractual details of the program, is gratefully recognized.

This report was assembled and edited, and to a great extent organized, by Mr. W. J. Nord of the GEMSIP program office with deeply appreciated help from Messrs. D. G. Bryan, E. Q. Redmond, and S. A. Foster.



D. E. Robison, Manager  
Gemini Stability Improvement Program  
Liquid Rocket Operations

FOREWORD

is reported

This is Volume 5 of the GEMSIP Final Report. It is devoted to the development of special tools and techniques for pulsing the combustion and hydraulic systems. Although this work was carried out merely in support of the primary program, it represented a substantial effort in the program and deserves full documentation. These efforts have added to the understanding of combustion stability beside aiding in the development of a stable injector for GEMINI. Moreover, these tools are now available for other development and production programs as well as for future applied research, which alone represents a worthwhile contribution.

Three significant developments pertain to the devices for perturbing the thrust chamber, or engine system, to determine its level of stability. One of these is the nondirected pulse charge which is mounted in the combustor and reacts directly on the combustion process. The other two are the single and multiple pulse generators that produce acoustic shocks in the propellant feed system. Their use permits the observation of the possible interaction of feed system disturbances with the combustion in the chamber.

The 2-dimensional chamber, discussed in Section IV, is another of the devices for observing combustion photographically, both to derive a feeling for the manner in which the reaction occurs and to correlate visual data with the output of pressure transducers. The technique has been widely applied to subscale work; its present significance is that this is the first occasion where the full scale Titan II profile was represented.

is described

Section V is of special interest to combustion theory. It describes the application of classical laboratory methods to obtain the natural acoustic resonances of the chamber in several configurations, which were then correlated with the resonances observed with these configurations when firing. Noteworthy is the work with the half-scale wooden model, which is a step toward understanding the effects of scaling on combustion.

to page vi

FOREWORD (cont.)

*from page V*

The servo control system, ~~discussed in Section VI~~, is a means to reproduce engine transients, insofar as they are reflected in the thrust chamber, with a simple, low cost, pneumatically pressurized system. Extreme conditions or those of rare occurrence, which cannot be readily produced during engine firing, can be simulated realistically. In addition, multiple data points may be obtained from a single firing, thereby reducing test costs by an order of magnitude.

Space in this volume permits treating only the new tools developed for studying instabilities. For this reason the heat transfer baffle experiment is covered in Volume 4 in connection with the heat transfer analyses and the generation of cooled baffle design data.

The application of new techniques to data gathering is treated in Volume 6, Instrumentation. The extension of already developed techniques, such as the measurement of injector flow distribution are discussed in context in Volume 2 in the test program.

Special appreciation is accorded Dr. S. Rubin of Aerospace, who prepared a Fourier Analysis of an engine pulse test where the single pulse generator was employed, besides lending his assistance in many other ways.

Acknowledgement is due to Dr. R. J. Hefner, Manager, Combustion Dynamics Department, who contributed many original ideas to theoretical development work on these devices. Mr. D. A. Fairchild of the Combustion Dynamics Department guided the development of the pulsing devices and the 2-dimensional motor during the course of which he contributed valuable suggestions. He was assisted in the design by Mr. W. C. Cain and Mr. T. J. Koprowski. Mr. S. E. Veglia followed the actual development of the pulsing devices and wrote the reports on which the text is based. Mr. E. W. Higgins supplied the design section and Mr. J. Robertson the section on photography for the 2-dimensional motor. The section on acoustics was prepared by Mr. J. M. McBride in conjunction with Mr. E. E. Johnson

GEMSIP FR-1, Volume 5

FOREWORD (cont.)

and Mr. R. A. Hewitt, all of the Combustion Dynamics Department. The servo control system was developed by Test Division personnel under the guidance of Mr. R. D. Wesley and Mr. D. C. Young.

GEMSIP FR-1, Volume 5

TABLE OF CONTENTS

<u>Section</u>		<u>Page</u>
I	Nondirected Pulse Change	1
II	Single Pulse Generator	69
III	Continuous Pulse Generator	113
IV	Two-Dimensional Motor	153
V	Acoustic Testing	201
VI	Flow Control Servo System	227

GEMSIP FR-1, Volume 5

LIST OF TABLES

<u>Table No.</u>	<u>Title</u>	<u>Page No.</u>
1	Injector Evaluation Instrumentation	26, 27
2	Comparative Test Values of Selected Explosives	62
3	Calibration Test Data for Fuel Pulse Generator	91
4	Calibration Test Data for Oxidizer Pulse Generator	98
5	Engine Component Performance Data for Various Amounts of Propellant	128
6	Continuous Pulse Generator Test Data	142
7	Continuous Pulse Generator Test Data	143
8	Operating Parameters, Two-Dimensional Thrust Chamber	181
9	Alternative Materials for Viewing Window	182
10	Resonant Frequency and Decay Rate Comparison for Half-Scale Chamber	212
11	List of Symbols	226

GEMSIP FR-1, Volume 5

LIST OF FIGURES

<u>Figure No.</u>	<u>Title</u>	<u>Page No.</u>
1	Aerojet Tangential Pulse Generator	2
2	Installation of Apollo Nondirected Pulse Charge	4
3	Initial GEMSIP Nondirected Pulse Charge	6
4	Shock Wave Produced by GEMSIP Nondirected Pulse Charge	8
5	Erosion of Nondirected Pulse Charge Support Arm	10
6	Uncooled Combustion Chamber after Test No. 1.1-01-TLJ-003	12
7	Injector S/N 1377 after Test No. 1.1-01-TLJ-003	13
8	Nondirected Pulse Charge Locations	14
9	Modified Nondirected Pulse Charge	16
10	Nondirected Pulse Charge Chamber Boss	18
11	GEMSIP Nondirected Pulse Charge Spacer	19
12	Possible Locations of Nondirected Pulse Charge in "Iron Horse" Chamber	20
13	Teflon Casing for GEMSIP Nondirected Pulse Charge	21
14	Uncooled Chamber Instrumentation	22
15	GEMSIP Uncooled Combustion Chamber with Observation Windows	23
16	Injector S/N 269 with Bomb Installed	24
17	Injector S/N 0035 after Test No. 1.1-02-TLJ-002	28
18	Injector S/N 1085 after Test No. 1.1-02-TLJ-006	30
19	Final Design of GEMSIP NDPC Used for Uncooled Combustion Chambers	32
20	Bending of Baffles Caused by 220-Grain Nondirected Pulse Charge	34
21	Tube Dents Caused by 40-Grain Pulse Charge--Destructive Tests	36
22	DuPont E-83 E.B. Cap	38
23	Hardware after Test No. 1.2-04-TLJ-140	40
24	Installation of Nondirected Pulse Charge in Tabular Chamber Cavity	41
25	Chamber Dents Caused by 40-Grain Nondirected Pulse Charge	42
26	Chamber Damage Caused by Detonation of Unprotected Squib	44
27	"Shaping" of the GEMSIP Nondirected Pulse Charge	45
28	Damage Caused by Unshaped Charge	46

GEMSIP FR-1, Volume 5

LIST OF FIGURES (cont.)

<u>Figure No.</u>	<u>Title</u>	<u>Page No.</u>
29	Reduction of Damage Resulting from Shaping of the Charge	47
30	Installation of Nondirected Pulse Charge for GRI-91 Test Series	48
31	Modification of Teflon Casing	50
32	Summary of Delay Squib Firing Time	51
33	GEMSIP Pulse Initiator Circuitry	64
34	Installation of Fuel Single Pulse Generator on 91-5 Engine	68
35	Cross-Section of GEMSIP Single Pulse Generator	70
36	Exploded Assembly of Single Pulse Generator	72
37	Anvil and Hammer Piston	73
38	Belleville Washers	74
39	Belleville Washer Adapter	76
40	Mounting of Single Pulse Generator Microswitch	78
41	Propagation of Impact Wave	80
42	GEMSIP Calibrated Line	82
43	Setup for Pulse Generator Functional Tests	85
44	Trigger Piston Failure	86
45	Cracked Belleville Washer	88
46	Setup for Calibration Tests with Fuel Unit	90
47	Fuel Unit Pulse Amplitude vs "Dome" Pressure	92
48	Modified 91-5 Dome	93
49	Oxidizer Pulse Amplitude vs "Dome" Pressure	94
50	SPG Mounted on Chamber	96
51	View of P <sub>fj</sub> -3A Tap Connection	97
52	GEMSIP Injector	100
53	Helium Bleed Combustion Chamber	101
54	Modified Fuel Discharge Line	102
55	Modified Oxidizer Discharge Line	103
56	Modified Oxidizer Suction Spool	104
57	Modified Fuel Suction Spool	104
58	High Frequency Playback for Test No. 1.2-01-TLA-006	106

LIST OF FIGURES (cont.)

<u>Figure No.</u>	<u>Title</u>	<u>Page No.</u>
59	Installation of Oxidizer Single Pulse Generator on 91-5 Engine	108
60	Installation of Teflon Burst Diaphragm	109
61	High Frequency Playback for Test No. 1.2-01-TLA-007	110
62	Area Change of Propellant Line	114
63	Piston Displacement of Fluid	116
64	Line for Constant Cross-Sectional Area	118
65	Orifice Size and Spacing	119
66	Waveshape for One Cycle	122
67	Waveshape for More Than One Cycle	124
68	Cross-Section of Continuous Pulse Generator	126
69	Shaft-Rotor Center of Gravity and Radius of Gyration Location	132
70	Motor Speed Rise Rate	134
71	Major Components of Continuous Pulse Generator	136
72	Test Setup at Continuous Pulse Generator	138
73	GEMSIP "Calibrated Line"	139
74	Continuous Pulse Generator Oscillograph Trace	140
75	Unmodified Continuous Pulse Generator Configuration	144
76	Modified Continuous Pulse Generator Configuration	144
77	Two-Dimensional Motor	152
78	Simulator, Injector Chamber	156
79	Injector Fuel Manifold	160
80	Injector Oxidizer Manifold	161
81	Injector Assembly, Combustion Chamber	162
82	Simulator Subassembly, Combustion Chamber	169
83	Clamp Assembly, Bridge	170
84	Window, Observation	171
85	Cover Plate, Combustion Chamber	172
86	Bolt, Machine - Double Hexagon Head	173
87	Spacer, Bolt	174
88	Mount Assembly, Injector	175

GEMSIP FR-1, Volume 5

LIST OF FIGURES (cont.)

<u>Figure No.</u>	<u>Title</u>	<u>Page No.</u>
89	Support, Window	176
90	Spacer, Bridge Clamp	177
91	Window, Observation	178
92	Cross-Section of Assembled Motor	180
93	Injector Configurations - Two-Dimensional Chamber	186
94	Photographic Installation--2-D Chamber	192
95	Acoustic Test Setup	200
96	Schematic of Acoustic Test Setup	202
97	Traversing Fixture	204
98	Experimental Results for Transverse Modes	205
99	"Banana" Baffle	207
100	Effect of Baffles on First Tangential Frequency	206
101	Effects of Baffle Length of L-Modes--Acoustic Tests	210
102	Effects of Baffle Length on L-Modes--Calculated	211
103	Effect of Baffles on First Tangential Mode	216
104	Curvilinear Coordinate System	218
105	Generalized C-1 Configuration Philosophy	228
106	TCA Transient with Position Feedback Control	231
107,	C-1 Transient Test Data--Pressure and Flows vs Time	234
108	System for Simultaneous Control of TCA Parameters	236
109	C-1 Closed-Loop Control System Response Data - Open-Loop to Closed-Loop Control	238
110	C-1 Closed-Loop Control System Response Data	239
111	C-1 Closed-Loop Control System Response Data	240

I. NONDIRECTED PULSE CHARGE DEVELOPMENT

For many years the understanding of combustion stability was restricted by the random incidence of instabilities which occurred unexpectedly without allowing preparation for gathering the necessary data. It was observed, however, that nearly all instabilities were preceded by a disturbance of the combustion. This led to the idea of a device to produce such a disturbance on signal during tests specifically arranged to evaluate instability. The sensitivity of the system could be rated by the energy required to render it unstable, the test conditions could be controlled, and for the limited number of tests required, it would be economically feasible to provide extensive instrumentation.

The first such device used to any extent was the tangential pulse gun developed at Aerojet-General in 1958. Some question of this technique was raised, however, that it might preferentially excite only certain modes of instability. Theoretically, the naturally occurring disturbances were nondirectionally oriented and therefore the induced pulse should be also. This was reflected in Paragraph B.5 Exhibit "A," Statement of Work for the GEMSIP contract states:

"Pulsing tests of the YLR 91-AJ-7 combustion chamber with a nondirected high explosive pulse during both component and engine testing shall be conducted to demonstrate achieved improvements in stability. Based on a consideration of comparable rocket engine pulsing, the charge size is specified as 220 grains for the uncooled (boiler plate) testing. For tubular chamber testing, a mutually acceptable charge which will be below the threshold of tubular chamber damage shall be used to verify dynamic stability. These charges are to be located approximately one inch downstream of the baffle tips and midway between the axis of the chamber and the inner wall of the chamber. It is intended that the charge sizes specified herein be smaller than those which would cause chamber damage, and that the size will be verified experimentally."

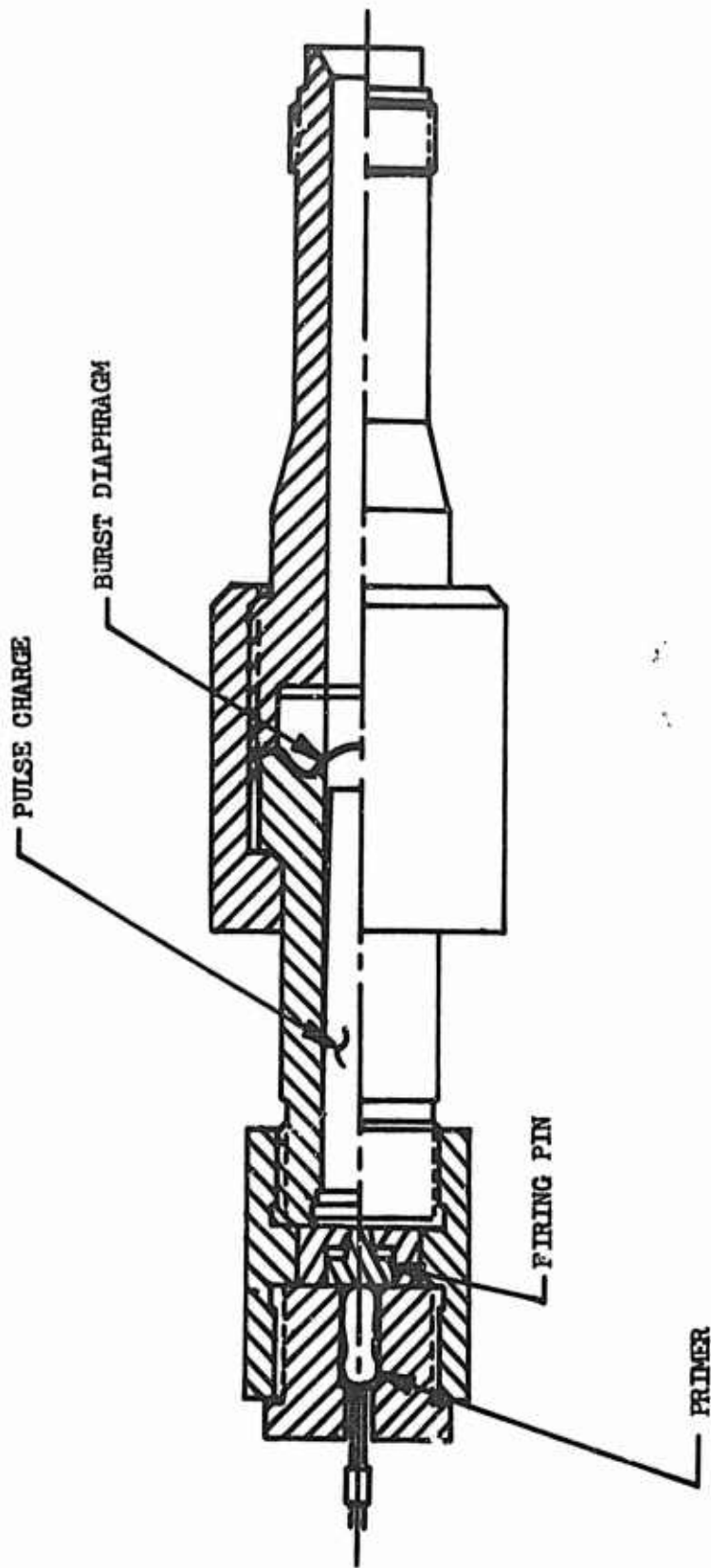


Figure 1 -- Aerojet Tangential Pulse Generator

I, Nondirected Pulse Charge Development (cont.)

Paragraph 6 states:

"Conduct a program of pulse charge technique development to include installation and charge location verification, installation and checkout of the test equipment, and instrumentation system validation."

To fulfill these contractual requirements, the GEMSIP nondirected pulse charge was developed and verification tests were conducted with cooled and uncooled hardware.

A. BACKGROUND

Prior to the inception of the GEMINI Stability Improvement Program, the most common stability rating tool employed was the tangential pulse generator, which has been used extensively at Aerojet-General in research and development programs. The generator consists of a powder charge behind a precision burst diaphragm at the end of a short barrel, as shown in Figure 1. Following ignition of the powder charge, pressure builds up rapidly behind the diaphragm causing it to burst, sending a shock wave down the barrel, and introducing a tangentially directed pulse into the combustion chamber.

A rating, termed the "stability index," is awarded based on the chamber pressure and the maximum magnitude pressure perturbation that the system can withstand before combustion becomes unstable. (Larger stability indices indicate systems which were more stable.) The tangential pulse generator has the inherent disadvantage of producing a wave pattern which simulates that of a spinning tangential mode, and, hence, has a higher probability of triggering transverse modes in the combustor.

The basis for the nondirected bomb is the simulation of naturally occurring perturbations, which may be caused, for example, by delayed combustion of pockets of mixed propellants. In practice, the bomb consists of a charge of

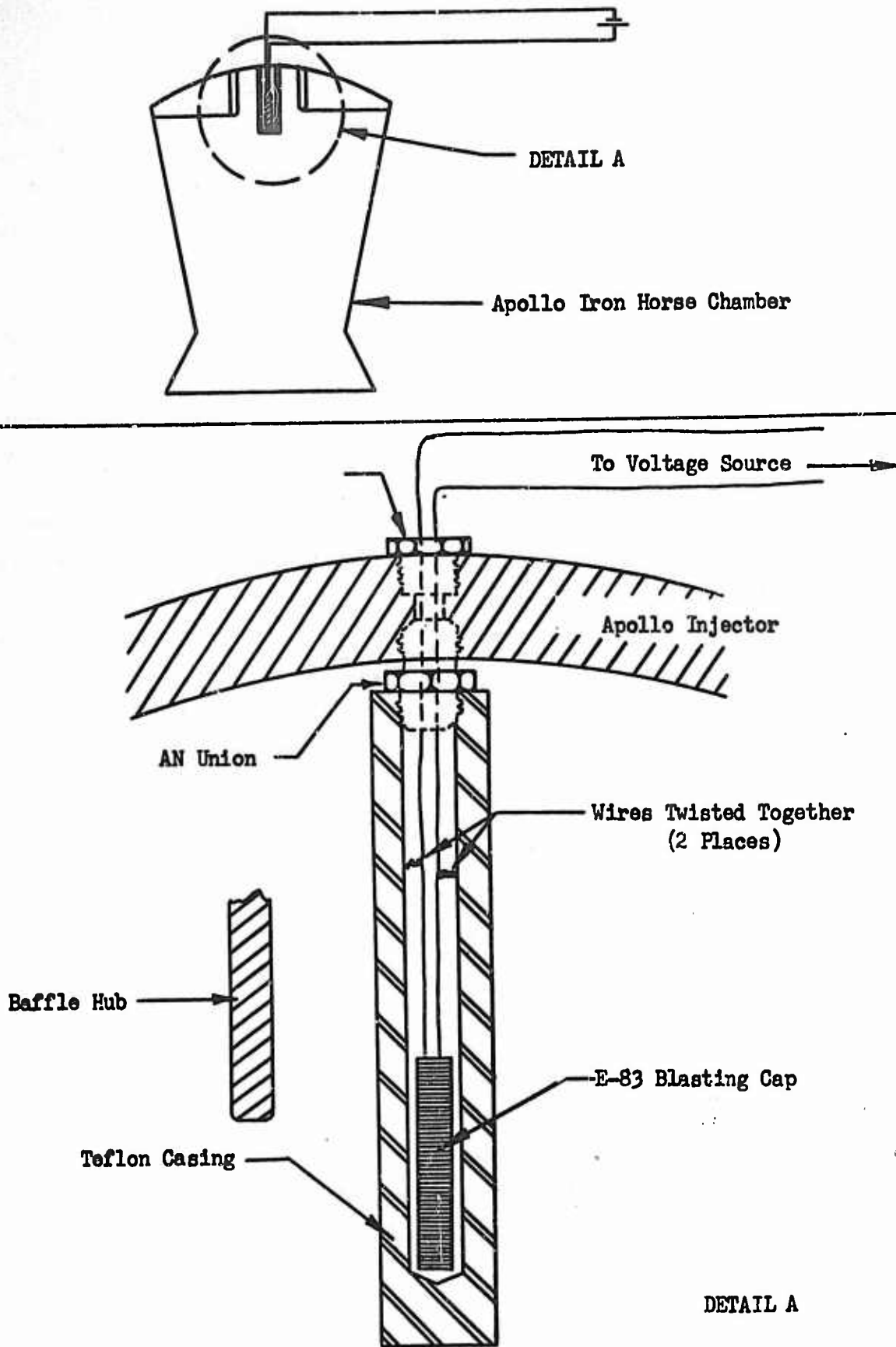


Figure 2 -- Installation of Apollo Nondirected Pulse Charge

I, A, Background (cont.)

high explosive surrounded by a thermal shield and mounted within the combustion chamber cavity. The main charge is detonated by a squib which is initiated either electrically or thermally. The initial shock wave propagating from the bomb is spherical; the nature of the perturbation finally produced depends upon the location of the pulse charge as well as on the combustion chamber geometry. In general, a bomb placed near the axis of the chamber will produce a radial mode; whereas, one located near the wall will tend to favor the tangential modes.

A literature search showed that Rocketdyne had had experience with nondirected pulse charges during the development phases of the Atlas, H-1 and F-1 programs. Their nondirected pulse charge was a high explosive (Composition C-3) contained in a Teflon casing and supported in the combustion chamber with a copper holding fixture. The lead wires from the initiator (or squib) are brought out through the combustion chamber wall for the charges used on "iron horse" hardware and through the injector face for the tubular chamber version. Three different case materials were tested--Teflon, Nylon, and micarta. Teflon proved to be the most satisfactory.

Prior to the GEMINI Stability Improvement Program, some experience with nondirected pulse charges had been gained from the Apollo Program. The Apollo bomb (throughout this report the terms "bomb" and "nondirected pulse charge" will be used interchangeably) consisted of a Teflon outer casing which contained a high explosive (Composition C-4) and an electrically initiated squib. The pulse charge was hung from the injector face as shown in Figure 2.

Two types of nondirected pulse charges were developed for the Gemini Stability Improvement Program: one charge for use in "iron horse" combustion chambers, and another for tubular chamber testing. The development of these two types of pulse charges will be discussed separately.

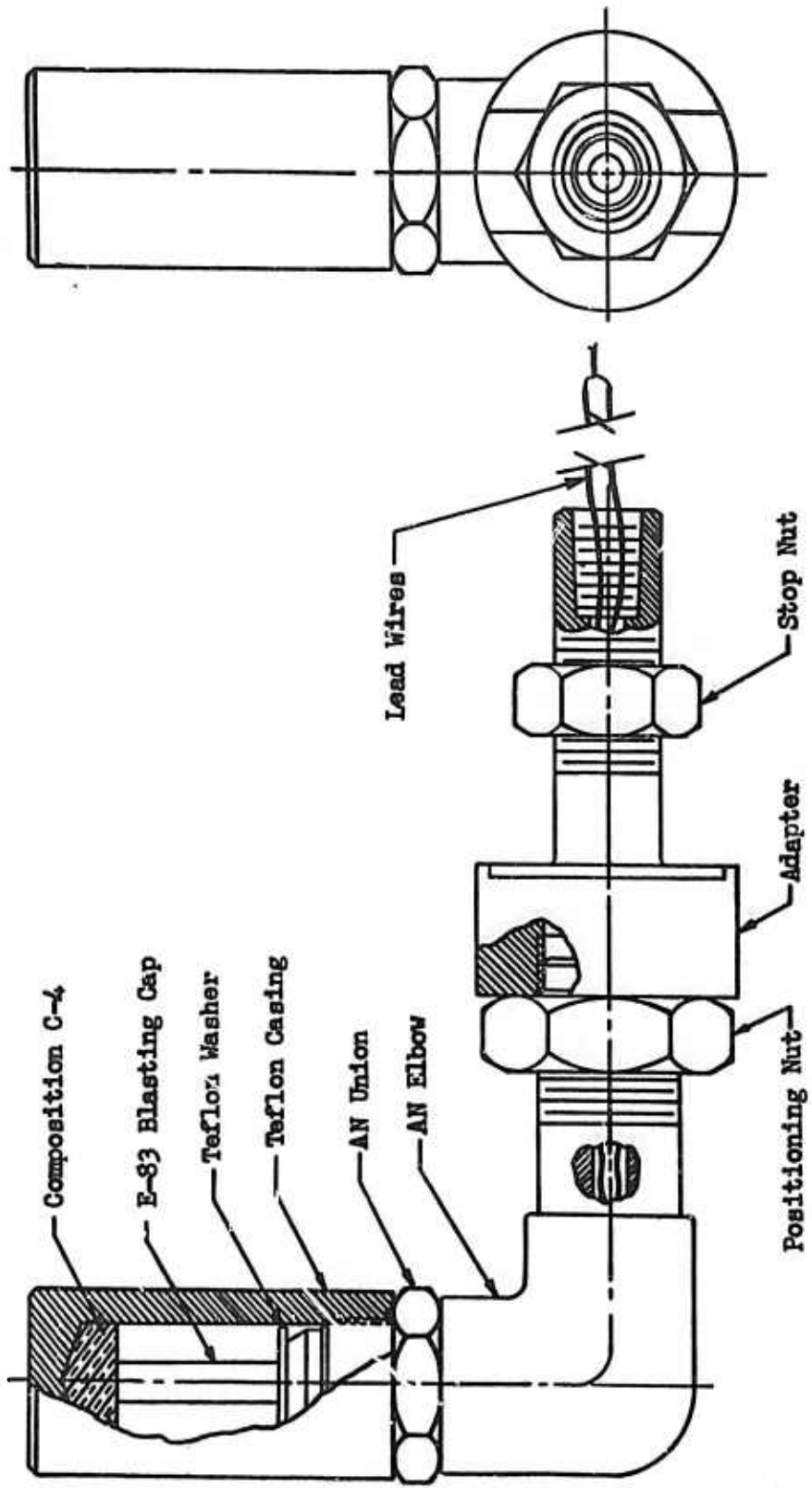


Figure 3 -- Initial GEMSIP Nondirected Pulse Charge

I, Nondirected Pulse Charge Development (cont.)

B. UNCOOLED COMBUSTION CHAMBER PULSE CHARGE

1. Design

The design of the GEMSIP pulse charge was a modification of the Rocketdyne bomb. The charge itself remained basically the same (a Teflon case containing high explosive and an initiating squib), but the support arm was redesigned to simplify sealing problems.

Figure 3 shows the GEMSIP nondirected pulse charge assembly with a 220-grain Teflon casing installed. The E-83 blasting cap is imbedded 0.050 in. to 0.100 in. into the Composition C-4, which ensures detonation of the maximum amount of the main charge. Composition C-4 was used because of its ready availability at Aerojet-General. Appendix A lists the specifications of Compositions C-3 and C-4.

The charge holder (Figure 3) is composed of an AN union, an AN elbow, tubing, a positioning nut, an adapter and a holding nut. A butyl rubber O-ring is used as a hot gas seal between the charge and the holding fixture, while a commercial Conax MH-4-4-2 seal is used to seal the squib lead wires as they pass through the combustion chamber wall. The squib is sequenced to detonate when the TCA has achieved 90% of steady state chamber (approximately 1.6 sec after FS-1).

2. Chino Hills Tests

A series of tests was conducted at the Aerojet-General Chino Hills facilities to determine whether the shock wave generated by the GEMSIP bomb is truly spherical. The pulse charge was secured in a 5-gallon fish tank and enough water was added to cover the charge adequately. The fish tank was placed against and in front of a Fresnel lens with a 19-in. focal length. Optical alignment of the lens and the camera optics was accomplished by moving a simulated point light source about a point at the focal length of the Fresnel lens until the collimated

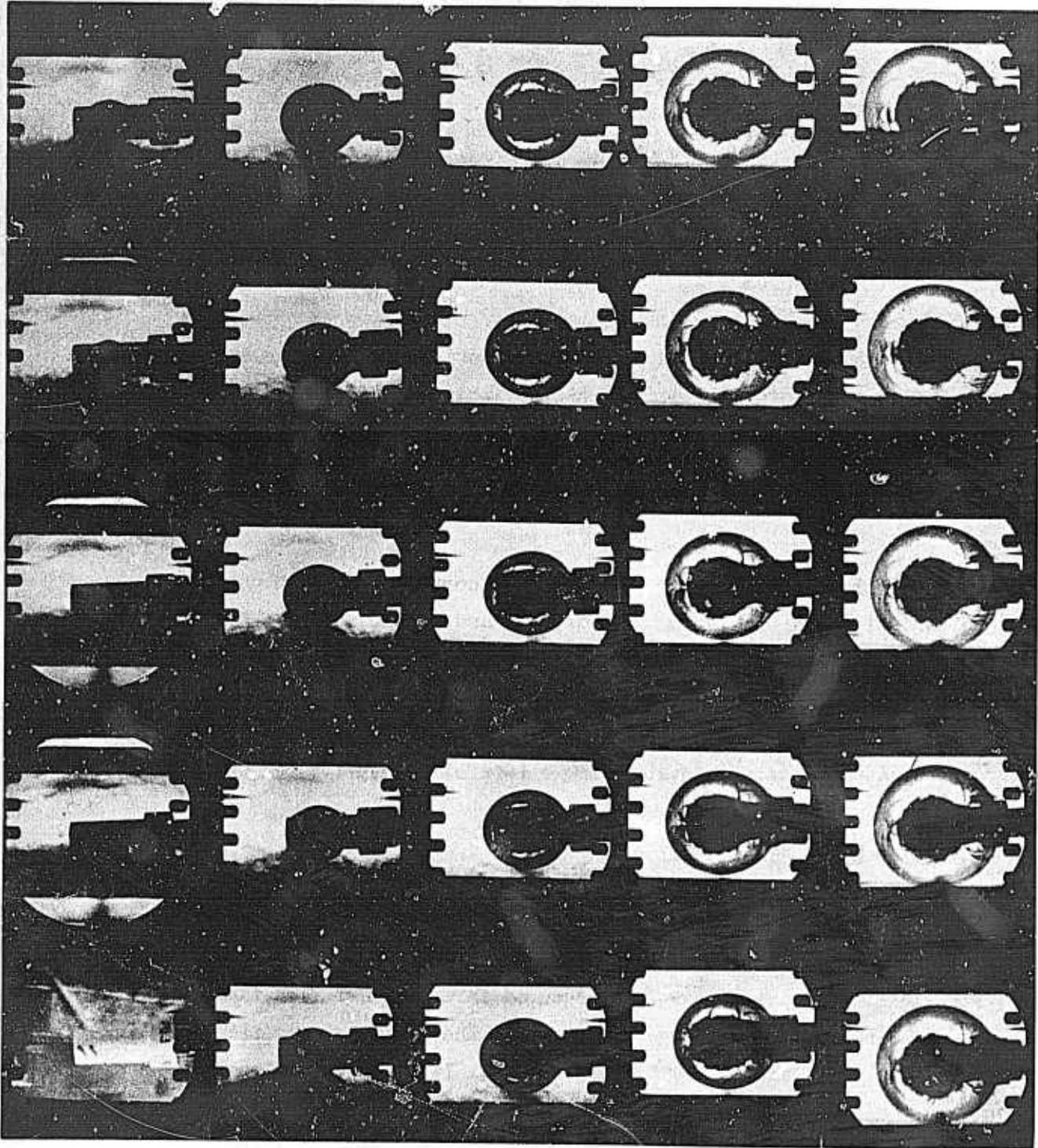


Figure 4 -- Shock Wave Produced by GEMSIP Nondirected Pulse Charge

I, B, Uncooled Combustion Chamber Pulse Charge (cont.)

light appeared through the optical center of the camera lens system. When this alignment was reached, an exploding bridge wire, which is an effective point light source, was secured to the holders at this position and the explosive device was primed.

Figure 4 shows the results of one of these tests. The framing rate was 980,000 frames/sec. It is apparent that the shock wave produced by the nondirected pulse charge is indeed spherical.

3. Demonstration Pulse Tests

a. 2SIN-22 Test Series

Beginning in December 1963, a series of three tests (1.1-01-TLJ-001, -002, and -003) was conducted on Test Stand C-1 to evaluate the GEMSIP nondirected pulse charge in hot firing conditions. Injector S/N 1377, which has a 2SIN-22 pattern and eight radial baffles with a hub, was used for this test series because, although it had a history of 30% instabilities in what is thought to be the first longitudinal mode, pulsing with tangential pulse guns had failed to excite this mode. Therefore, if the GEMSIP nondirected pulse charge proved capable of exciting an instability with an injector using the 2SIN-22 pattern, it would increase confidence that pulse testing with this device could locate incipient instabilities.

The first test was not a pulse test; its purpose was to balance the propellant injection pressures and to test the durability of the bomb support arm. In an attempt to determine the ablation rate of the Teflon bomb casing, a special charge was installed in the chamber without the squib or the C-4 explosive. Two chromel-alumel thermocouples were attached to the inside of a Teflon casing with a 1/4-in. wall.

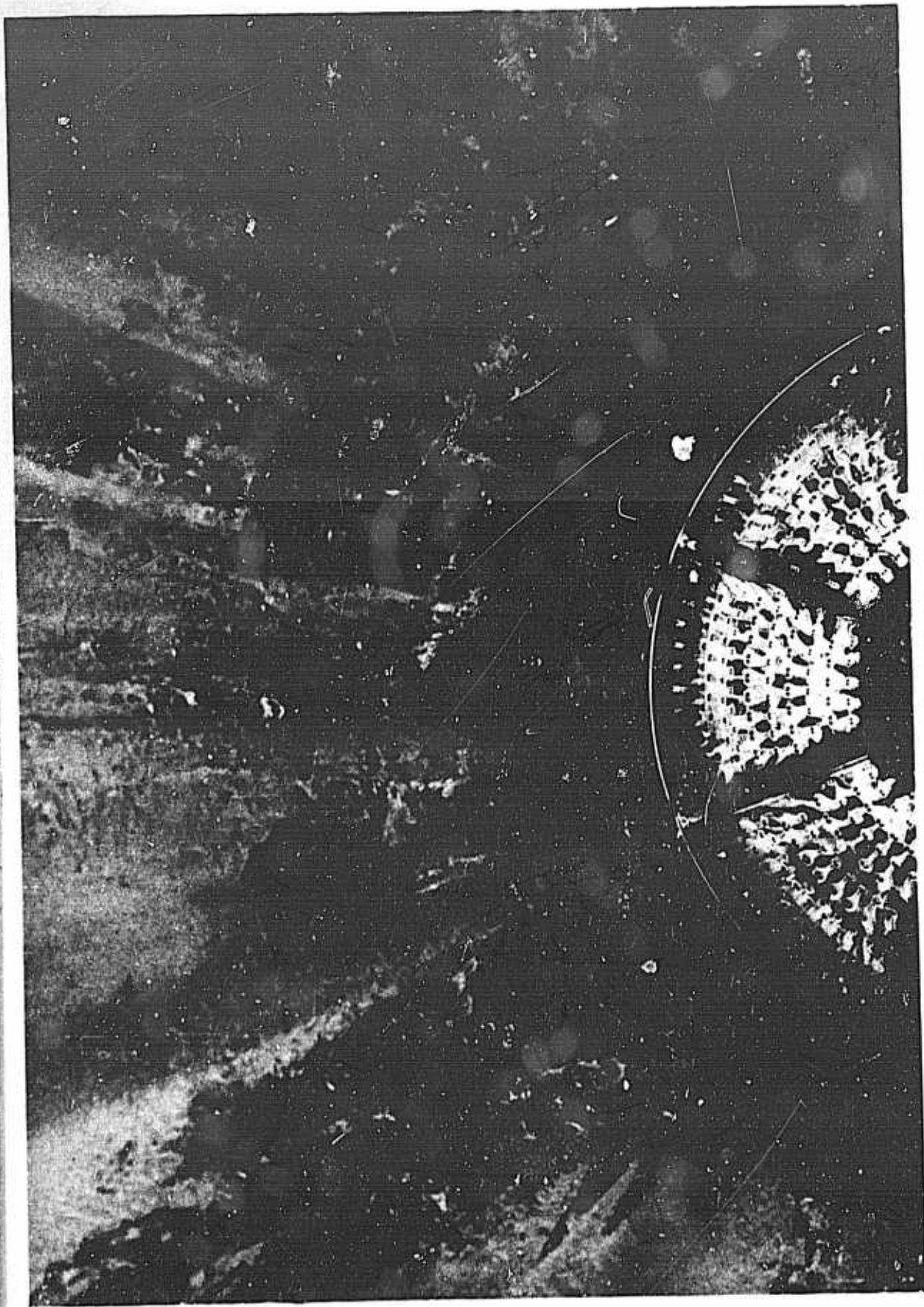


Figure 5 -- Erosion of Nondirected Pulse Charge Support Arm

I, B, Uncooled Combustion Chamber Pulse Charge (cont.)

During the test, both thermocouples failed at FS-1 + 1.46 sec, recording a temperature of approximately 700°F at the time of failure. Figure 5 shows what remained of the pulse charge assembly after a 3.1-sec test. Note the erosion of the chamber wall downstream of the pulse charge holder--the result of an interruption of the fuel film cooling and an increase in turbulence downstream of the support arm.

Because the thermocouples burned out at FS-1 + 1.46 sec, the wall thickness of the Teflon casing was increased to 1/2 in. for Test No. -002 and the squib was sequenced to fire at FS-1 + 1.3 sec. A 220-grain charge was mounted midway between the combustion chamber axis and the wall, and one in. below the baffle tips. The pulse charge support was coated with NRL 1795, an ablative material, to increase the "life" of the arm in the highly erosive atmosphere of the combustion chamber.

The test was satisfactory: a pulse of 250 psi was recorded by all high frequency transducers and damped in 15 msec. The test duration was 3.1 sec and was classified as stable. Five Dynisco high frequency chamber pressure transducers were damaged by Teflon shrapnel from the exploding bomb.

For the third test, the pulse charge mounting was turned 180 deg. This positioned the 220-grain charge in the convergent section of the throat which is a pressure antinode for the longitudinal acoustic modes and, therefore, a location sensitive to perturbations. The bomb detonated at FS-1 + 1.825 sec, triggering a 4300-cps oscillation on all chamber parameters. This 4300-cps oscillation was quite complex and could not be positively identified by phase and amplitude.

Severe erosion occurred again below the pulse charge mounting boss, as shown in Figure 6. The injector suffered damage to the baffle tip strips, cracking those on the radial baffles, completely removing the hub tip strip, and eroding the injector face plate inside the hub, as shown in Figure 7.



Figure 6 -- Uncooled Combustion Chamber after

Test No. 1.1-01-TLJ-003

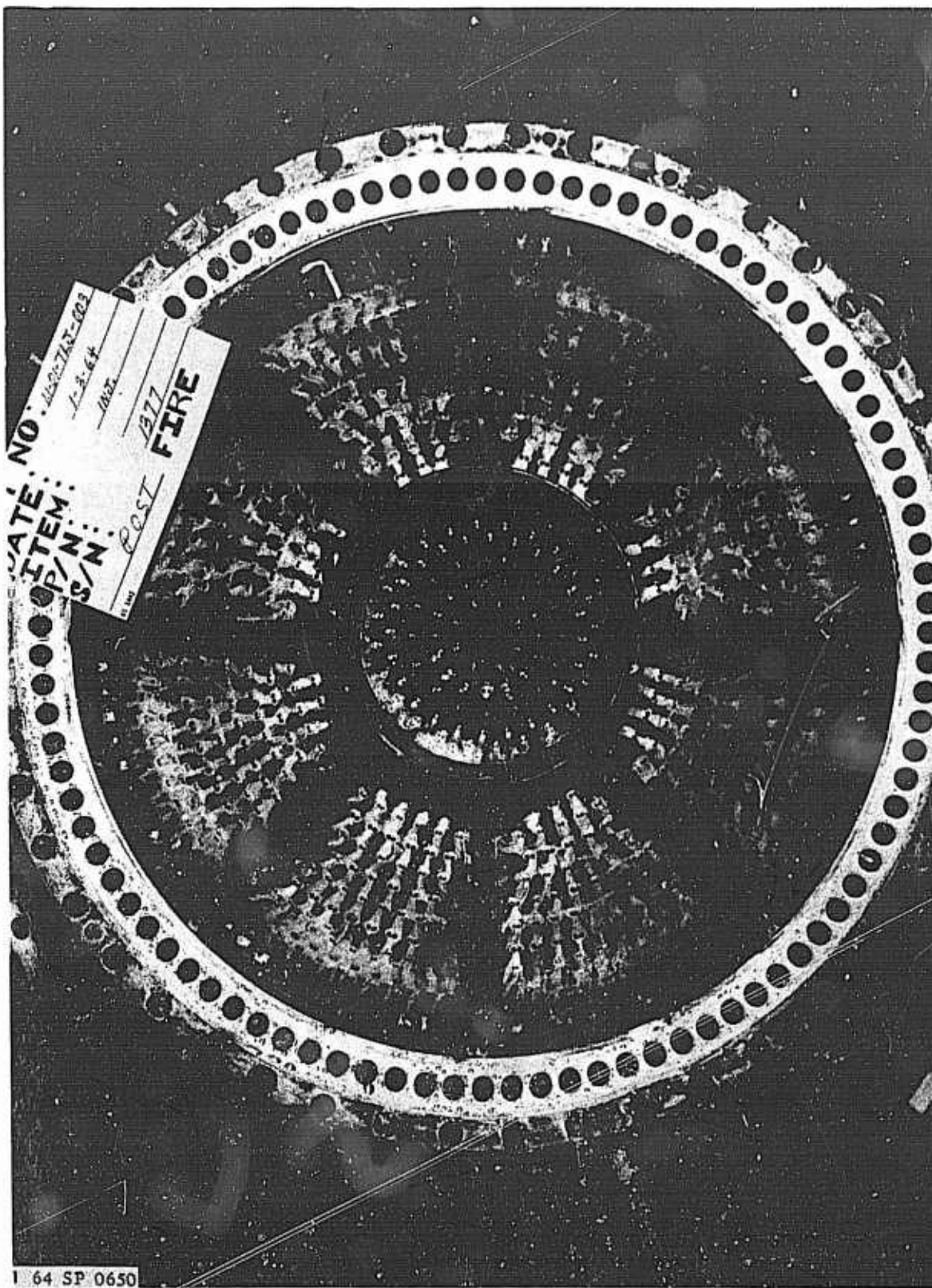


Figure 7 -- Injector S/N 1377 after Test No. 1.1-01-TLJ-003

- GRAIN SIZES
1. 13.5GR
  2. 20 GR
  3. 40 GR
  4. 80 GR
  5. 100 GR
  6. 220 GR

TEST SEQUENCE

<u>TEST NO.</u>	<u>POSITION</u>	<u>CHARGE</u>
1, 2, ..., N	B	1, 2, ..., N
N + 1	D	N - 1
N + 2	D	N
N + 3	D	N + 1
N + 4	I	220

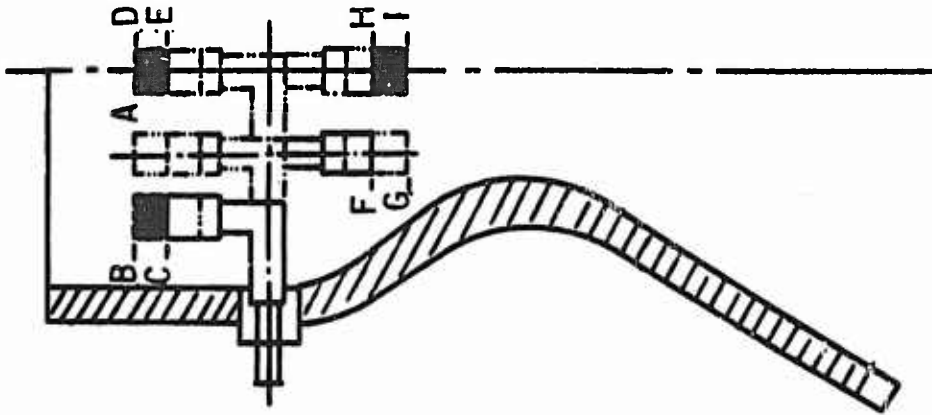


Figure 8 -- Nondirected Pulse Charge Locations

GEMSIP FR-1, Volume 5

I, B, Uncooled Combustion Chamber Pulse Charge (cont.)

Although these tests were unsuccessful in demonstrating the ability of the bomb to produce the predicted mode of instability, they did show that the bomb could excite instability with a marginally stable injector. Moreover, they showed the need to test in various locations to obtain a true measure of total stability.

b. Sensitive Location Test Series--2SXVIIM-2A Injector

The purpose of this test series was (1) to determine the position in the combustor most sensitive to a perturbation, and (2) to establish the threshold pulse charge size for the 2SXVIIM-2A injector. The most sensitive location was necessary for future GEMSIP pulse tests to make meaningful comparison between injector configurations. The establishment of a threshold pulse charge size for the 2SXVIIM-2A injector was used as a base point to demonstrate the degree of improvement of the GEMSIP candidate injector.

Discussions with Rocketdyne personnel indicated, in their experience, that a position close to the chamber wall, near the injector face was the most sensitive to perturbation. Accordingly, the plan for the initial test was to fire 10, 20, 40, 80, 100, and 220-grain charges in ascending order at Position "B" (1 in. from the wall and 1 in. below the baffle tip, Figure 8) until an instability was induced.

For the next test a charge one level less than that which produced the instability would then be fired at Position "D." If no instability was encountered, the charge would be raised one level. If still no instability occurred, it would be assumed that the system was more sensitive to being perturbed from Position "B" in the chamber than from Position "D." If an instability were encountered, further exploration would be conducted. Finally, a 220-grain charge was to be fired at Position "I" in the convergent section of the throat to check the sensitivity of the system to perturbations from this location.

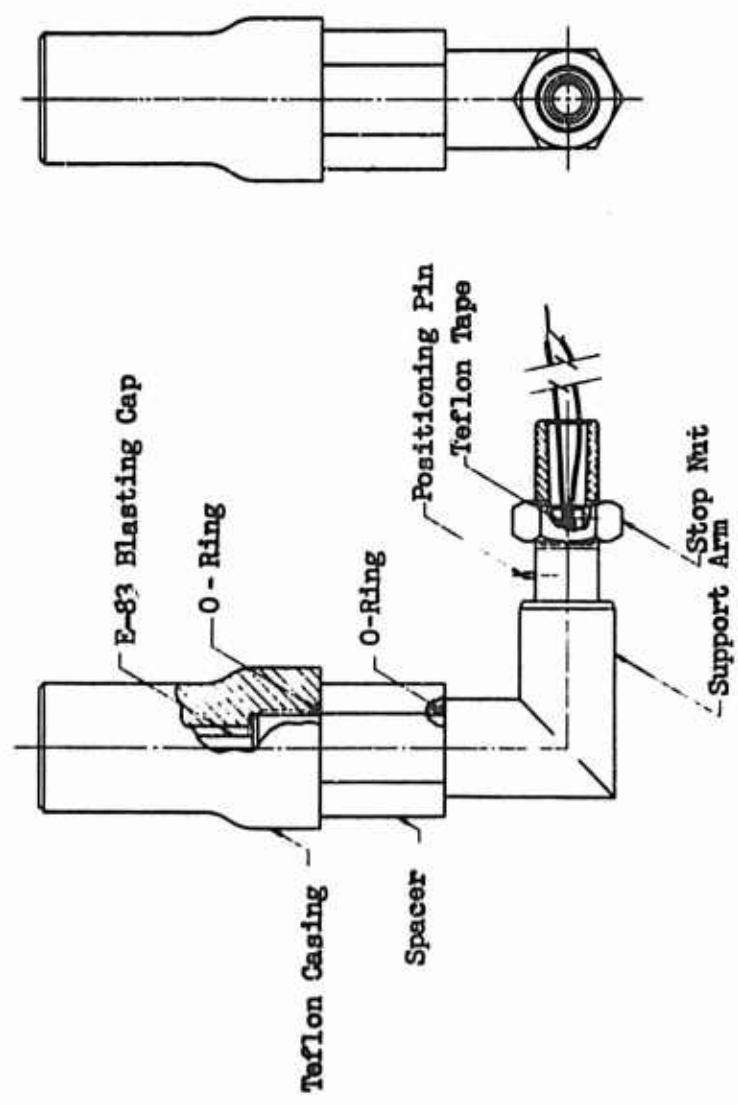


Figure 9 -- Modified Nondirected Pulse Charge

I, B, Uncooled Combustion Chamber Pulse Charge (cont.)

The design of the nondirected pulse charge was modified, as shown in Figure 9, to facilitate easier fabrication, assembly, and installation. The support elbow was fabricated from two pieces of 1-1/8-in. tubing with 3/8-in. wall, cut at 45-degree angles and welded together. Three lengths were designed so that the charge could be positioned (1) at the chamber centerline, (2) midway between the chamber center line and wall, and (3) at the chamber wall. A positioning pin provided the capability of rotating the support arm 360 deg in 45-deg increments. The combustion chamber bomb boss is shown in Figure 10. The spacers, shown in Figures 9 and 11, were fabricated in varying lengths, permitting further positioning capabilities. Figures 12a and 12b show all the possible mounting positions in an iron horse combustion chamber. A Teflon casing modification was necessary (see Figure 13) to contain explosive in 10-grain increments up to 100 grains; a different case was used for 200 grains. As before, the case thickness was maintained at 0.500 in.

A Titan II second-stage "iron horse" chamber was reworked to include provision for extensive high frequency instrumentation. Bosses for six Photocon transducers, one Kistler transducer, one Electro Optical Systems (EOS) water dump transducer, and one Phototransducer were welded on the combustion chamber at the locations shown in Figures 14a and 14b. An EOS transducer and a Microsystems high frequency transducer were inserted through the flange to monitor chamber pressure and the pressure of the fuel in Channel 17 of the injector, respectively. Numerous other close-coupled and flush-mounted high frequency transducers were installed at the locations shown in Figures 14a and 14b.

This GEMSIP uncooled chamber also contained horizontal and vertical strip film windows as well as a general observation window located near the throat (Figure 15). Fastex streak film cameras were used at the horizontal and vertical windows and a 1000-frame/sec Fastex camera was used at the observation window.

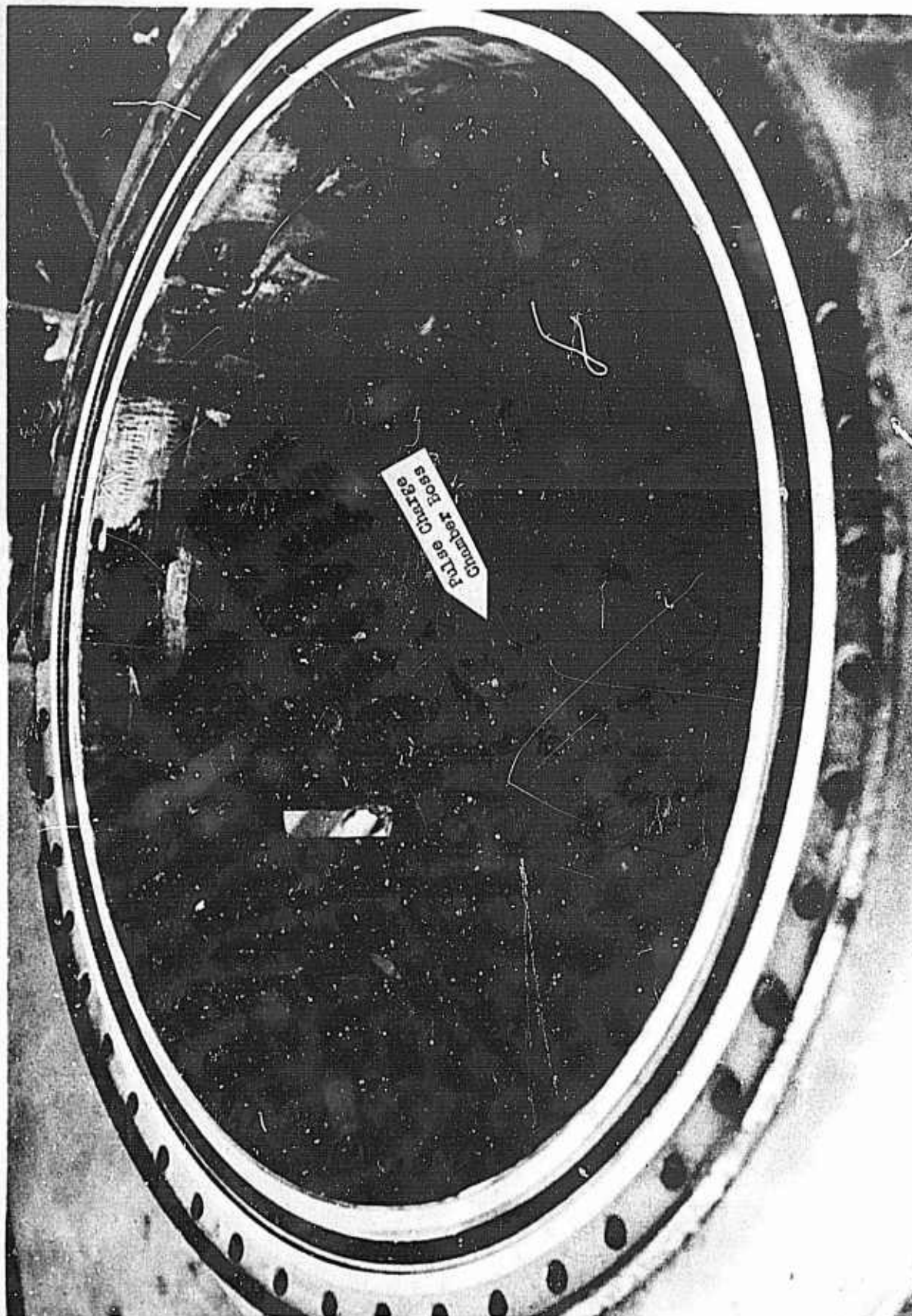


Figure 10 -- Nondirected Pulse Charge Chamber Boss

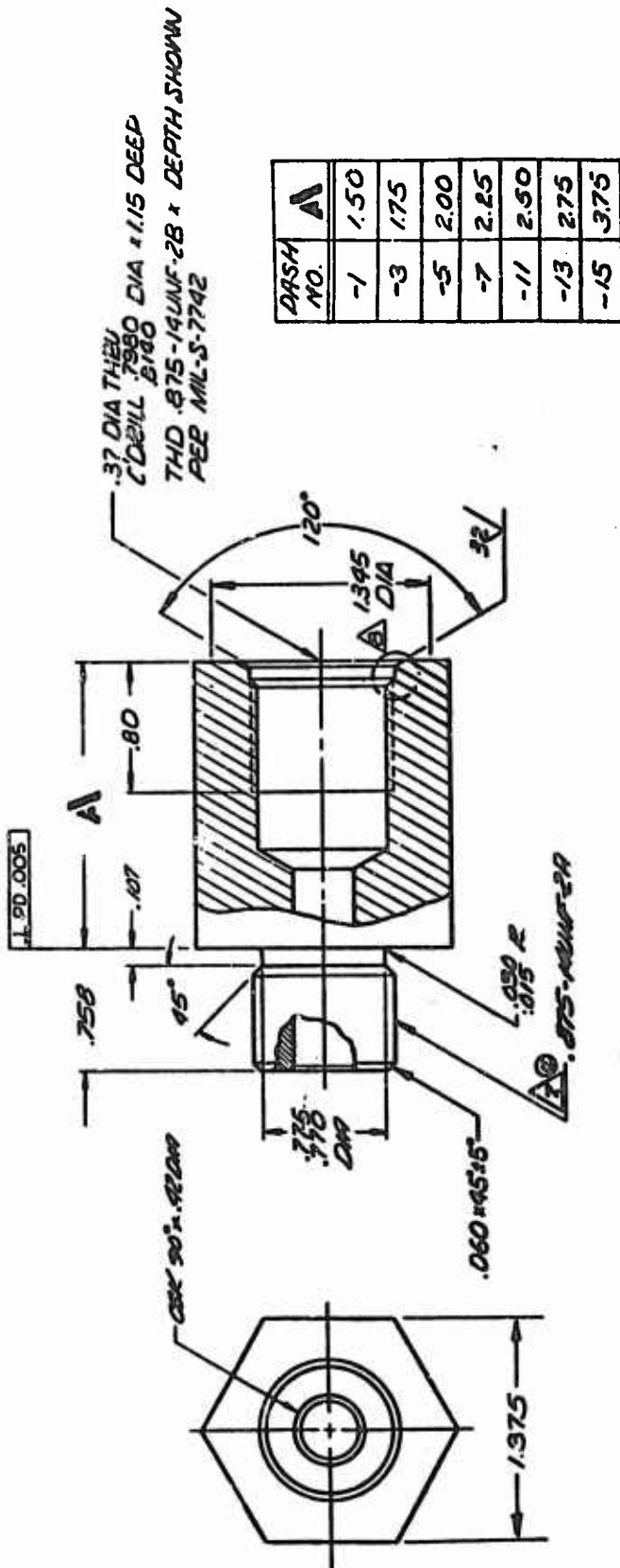
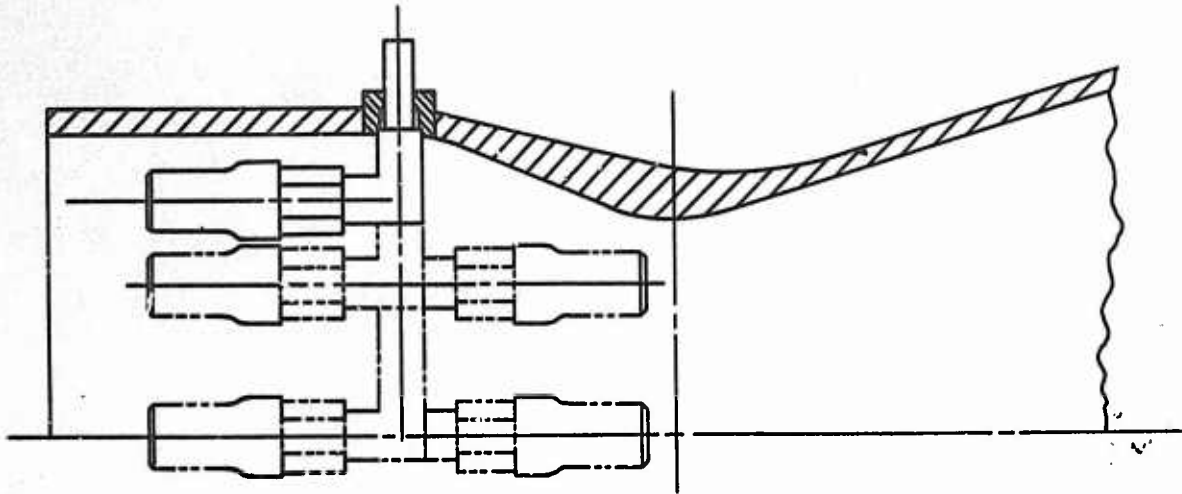


Figure 11 --- GEMSIP Nondirected Pulse Charge Spacer



A.

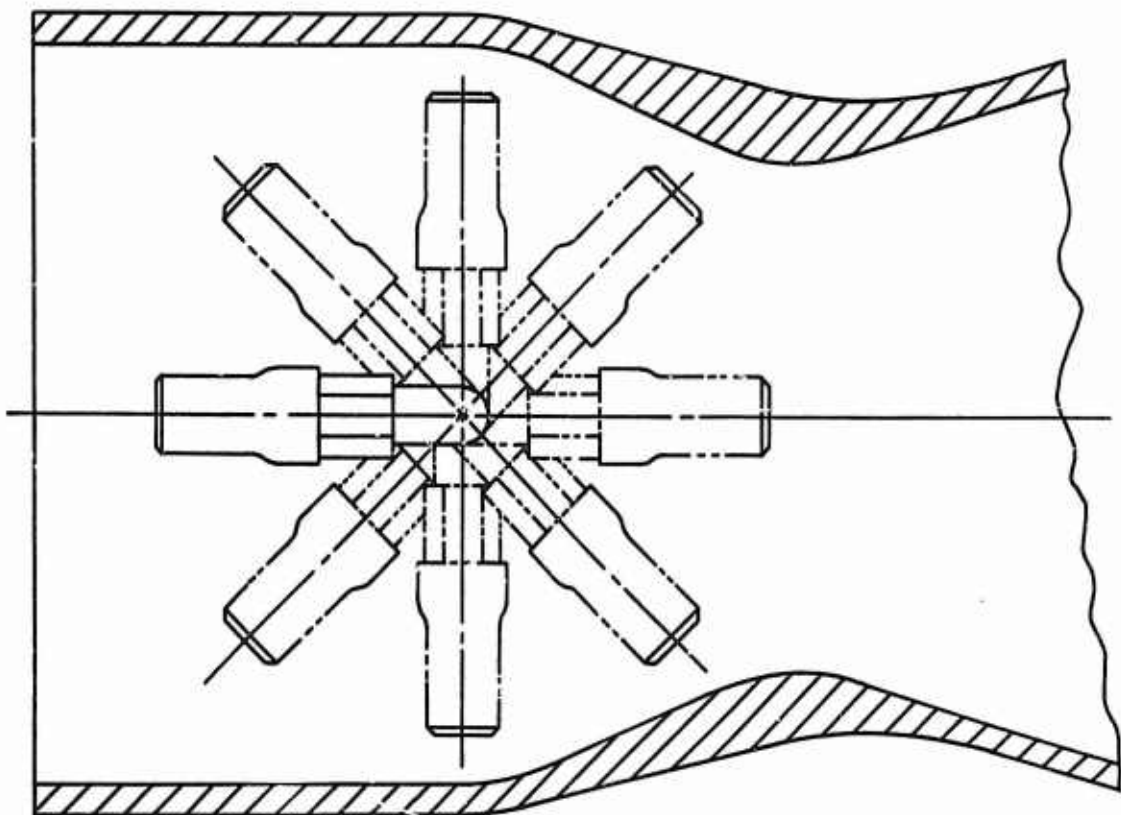


Figure 12 -- Possible Locations of Nondirected Pulse Charge  
in "Iron Horse" Chamber

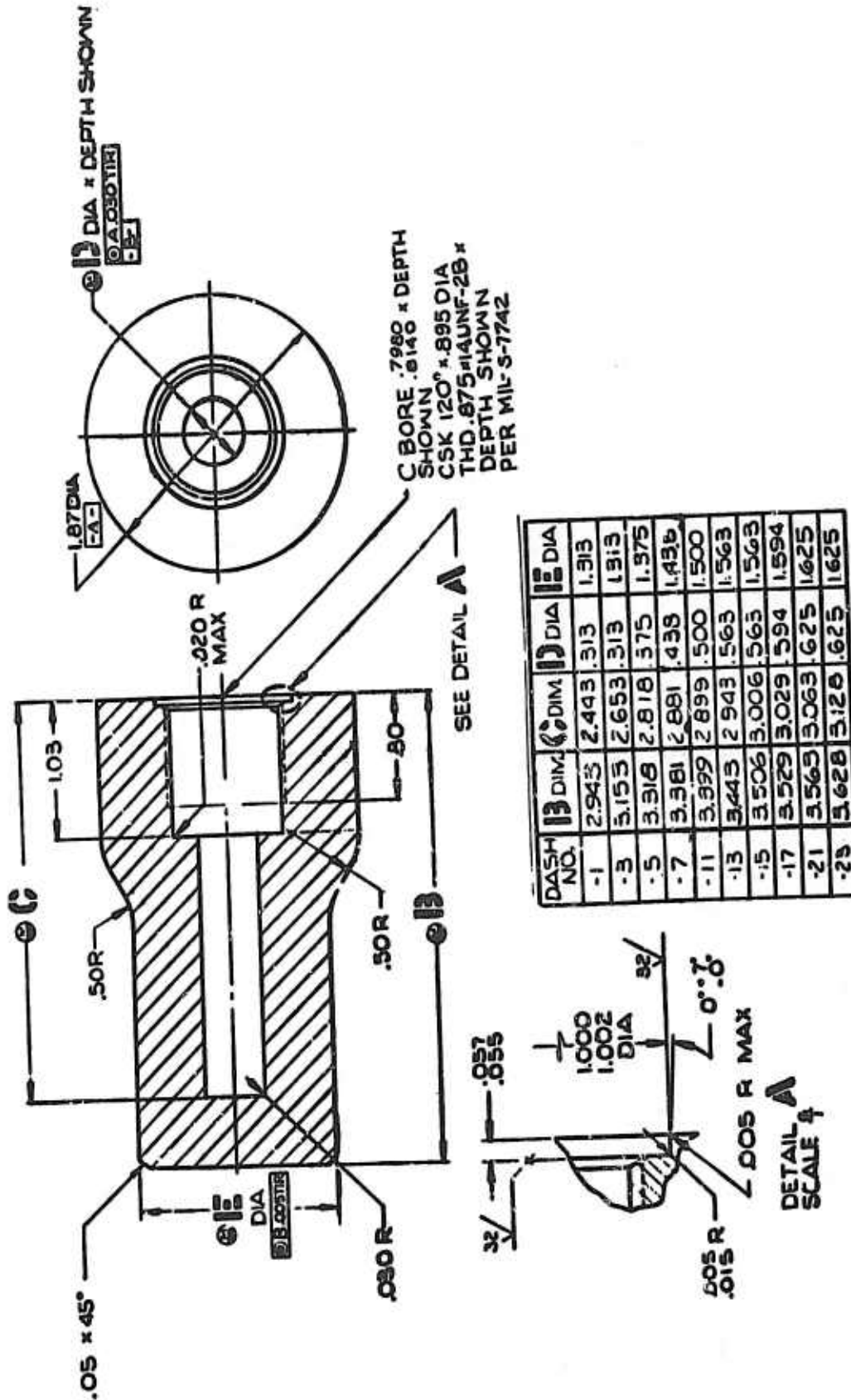
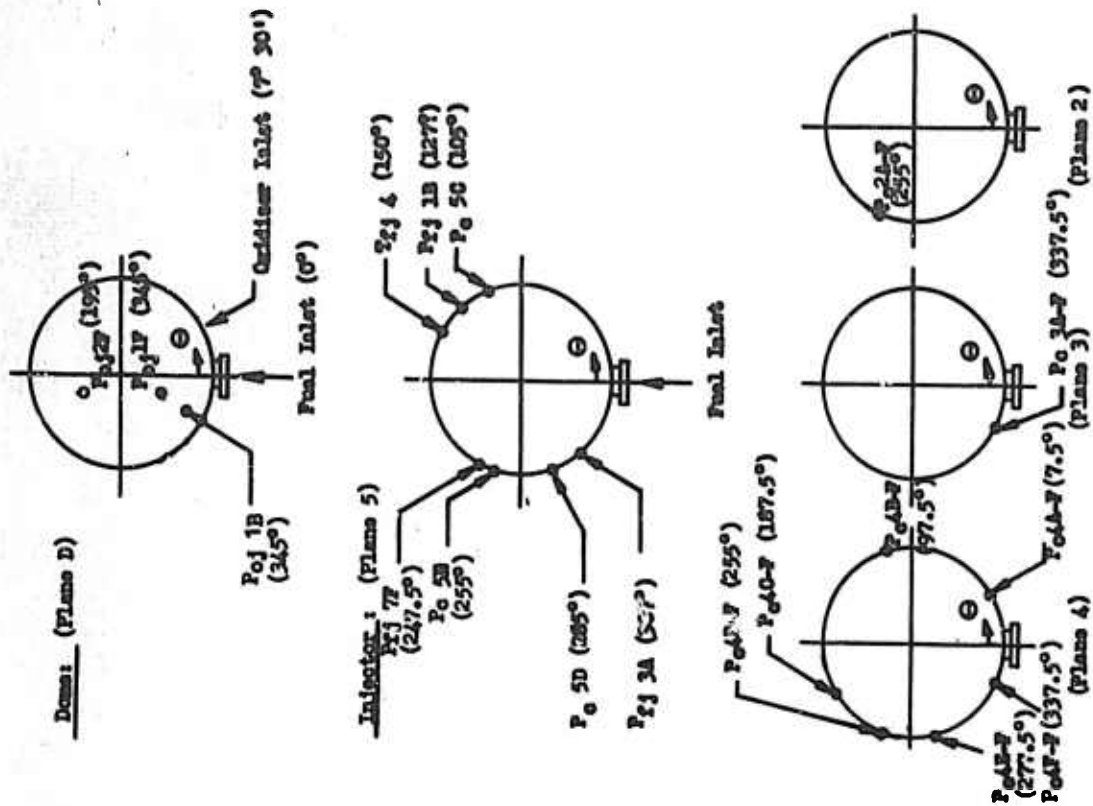
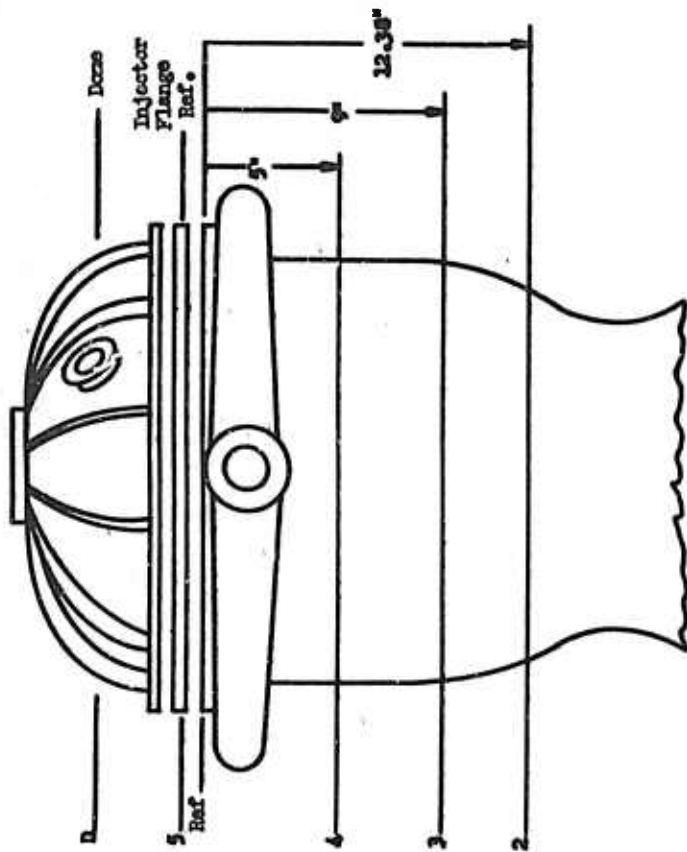


Figure 13 --- Teflon Casing for GEMSIP Nondirected Pulse Charge



B.



Test Applicability

Task I:

- a. N-D Bomb Evaluation
- b. Quadet Threshold and Location Sensitivity
- c. Baffle Configuration Evaluation
- d. Injector Flow Distribution Evaluation

Figure 14 -- Uncooled Chamber Instrumentation

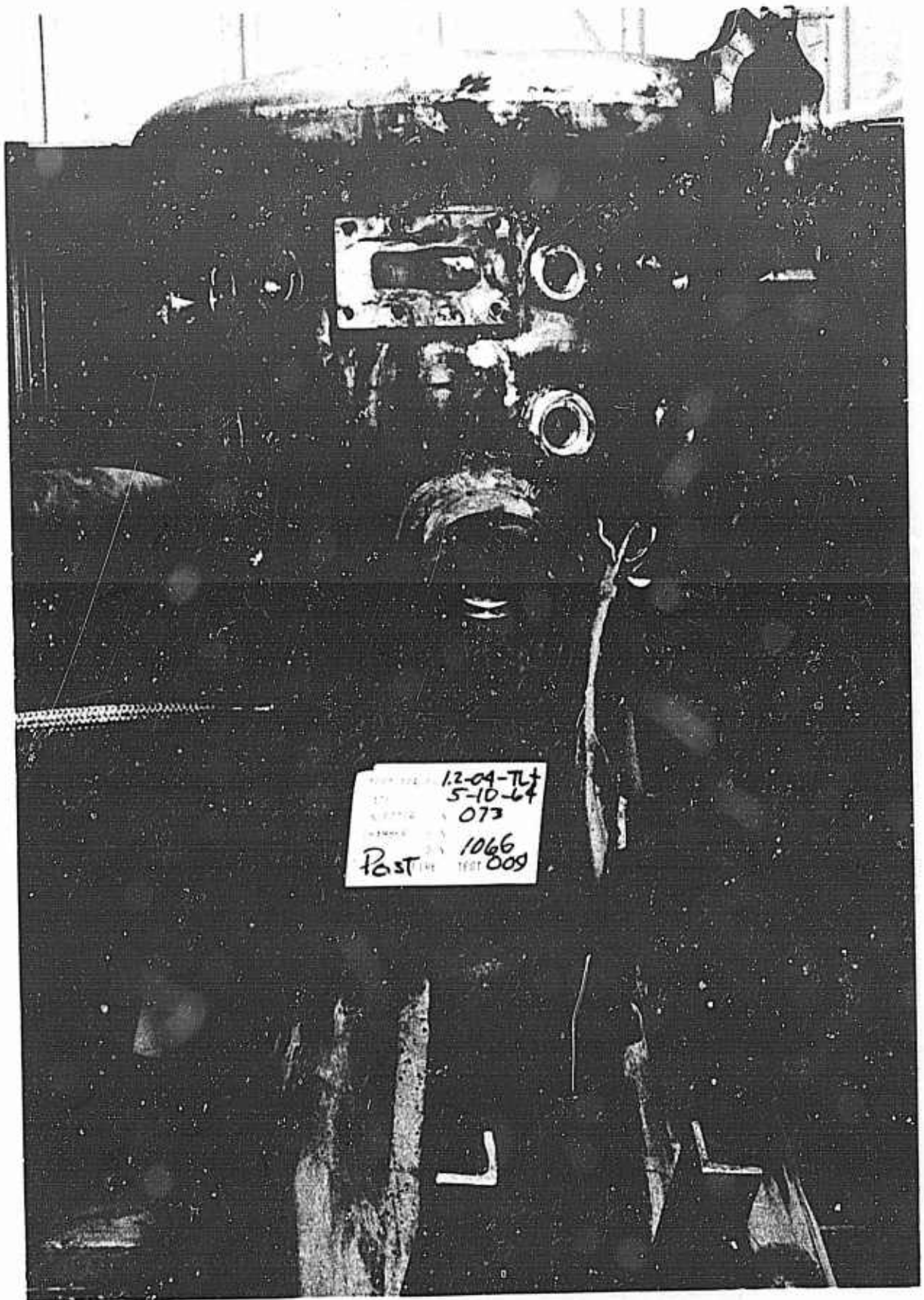


Figure 15 -- GEMSIP Uncooled Combustion Chamber with  
Observation Windows

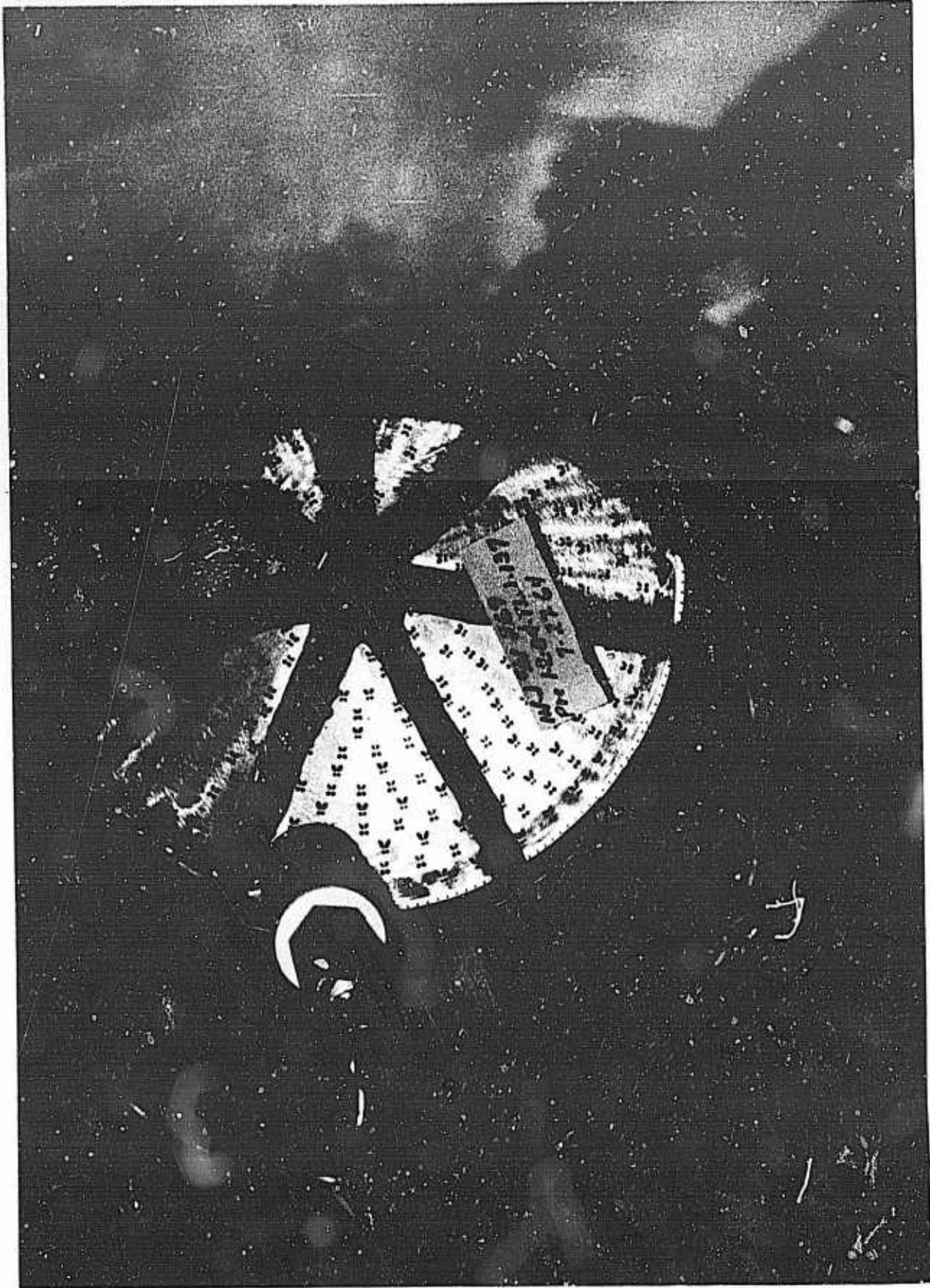


Figure 16 -- Injector S/N 269 with Bomb Installed

GEMSIP FR-1, Volume 5

I, B, Uncooled Combustion Chamber Pulse Charge (cont.)

As a result of a meeting with the customer, the test objectives and number of tests to be conducted during this series were changed. It was decided that, when the threshold pulse charge size was determined at Position "B," a change, one size less than the "threshold bomb," would be fired at Positions "D" and "I." If no instability resulted, then it could be concluded that these positions were not grossly more sensitive than Position "B" at least within the gradations of bomb size. From the standpoint of economy as well as because the intended goal was a marked improvement over Titan, extensive mapping of the threshold sensitivity seemed unwarranted.

A standard 2SXVIIM-2A quadlet Gemini prototype injector (S/N 035) was used in conjunction with GEMSIP uncooled combustion chamber S/N 1065 in Test No. 1.1-02-TLJ-001. The total instrumentation is listed in Table 1. The combustion stability monitor (CSM) monitored Pcj-1B, a close-coupled Microsystems high frequency transducer, and was set to trip at a frequency equal or greater than 1000 cps with a minimum amplitude of 100 psi peak-to-peak for a duration of 30 msec. An unloaded bomb case, shown in Figure 13, was installed 1.0 in. below the baffle tip and 1.0 in. from the chamber wall. The test objectives were to balance the system to check the procedures and instrumentation, and to observe the rate of ablation of the bomb case. Figure 16 shows the bomb installed in the chamber.

The test was shut down after 0.8 sec by the CSM. Postfire examination of the high frequency records showed that the CSM shutdown was invalid and was caused by a high amplitude oscillation of Pcj-1B only. During the test, the pulse charge positioning pin had sheared and the bomb arm rotated. The thermocouple located in the Teflon case recorded a maximum temperature of 1200°F.

Test No. 1.1-02-TLJ-002 was conducted to attain the objectives that were missed by the previous test using the same hardware and test setup. The instrumentation was the same except for the addition of a helium-cooled Kistler transducer at Pc4E. Because a Microsystems transducer had caused an invalid shutdown during the previous test, a Taber transducer was used for the combustion stability monitor for Test No. -002.

TABLE 1

## INJECTOR EVALUATION INSTRUMENTATION

<u>Function</u>	<u>Range</u>	<u>R-1</u>	<u>R-2</u>	<u>Brown</u>	<u>Milli</u>	<u>Ampex</u>	<u>On Line Miller</u>	
FS	Switch Trace	X				X	X	
P <sub>WP</sub>	0-500 Taber		X	X	X			
PgOPR	0-1500 Taber		X	X	X			
PgFPR	0-1500 Taber		X	X	X			
Pc4A-F(P)	0-1500 Photocon.					X		
Pc4B-F(P)	0-1500 Photocon					X		
Pc4C-F(P)	0-1500 Photocon					X		
Pc4D-F(P)	0-1500 Photocon.				RS	X	X	
Pc4E-F(K)	Kistler 500 pk to pk					X		
Pc4F-F(P)	0-1500 Photocon	X			RS	X	X	
Pc3A-F(P)	0-1500 Photocon				RS	X	X	
Pc2A-F(M)	0-1500 P(EOS)					X		
Pc4G-F	Fiber Optics	Per Special Instructions						
Pc5E(M)	0-1500 (EOS)					X	X	
Pc5D	0-1500 Taber			X	RS			
Pc5C <sup>1</sup> -M(M)	0-1500 Micro					X		
P <sub>FJ</sub> 3A	0-1500 Taber		X	X	X			
P <sub>FJ</sub> 7F-F(M)	0-1500 Micro				RS	X	X	
T <sub>FJ</sub> <sup>4</sup>					X			
P <sub>FJ</sub> 1B-M(M)	0-1500 Micro					X		
P <sub>OJ</sub> 3F-F(M)	0-1500 Micro					X		
T <sub>OJ</sub>					X			

TABLE 1 (cont.)

<u>Function</u>	<u>Range</u>	<u>R-1</u>	<u>R-2</u>	<u>Brown</u>	<u>Milli</u>	<u>Ampex</u>	<u>On Line Miller</u>
P <sub>OJ</sub> <sup>2</sup> -F(M)	0-1500 Micro				RS	X	
P <sub>OJ</sub> <sup>1</sup> -F(M)	0-1500 Micro					X	
P <sub>OJ</sub> <sup>1</sup> B	0-1500 Taber		X	X	X		
P <sub>OT</sub>	0-1500 Taber		X	X	X		
P <sub>fT</sub>	0-1500 Taber		X	X	X		
PoTCV	0-1500 Taber	X					
PcTCV	0-1500 Taber	X					
Pci	0-1500 Taber	X					
L <sub>TCFV</sub>	Potentiometer	X	X				
L <sub>TCOV</sub>	Potentiometer	X	X				
FM <sub>o</sub>	0-300 lbs/sec	X	X	X	RS		
FM <sub>f</sub>	0-175 lbs/sec	X	X	X	RS		
CSM <sup>(1)</sup>	Switch Trace	X	X			X	X
1 KC Time	Trace	X	X			X	X
Squibs	Switch Traces	X				X	X

Special Note - The following functions should have a common coded, 1 KC time correlation signal:

Strip film cameras  
 Fastax camera for combustion photographs  
 Miller  
 Ampex  
 R-1

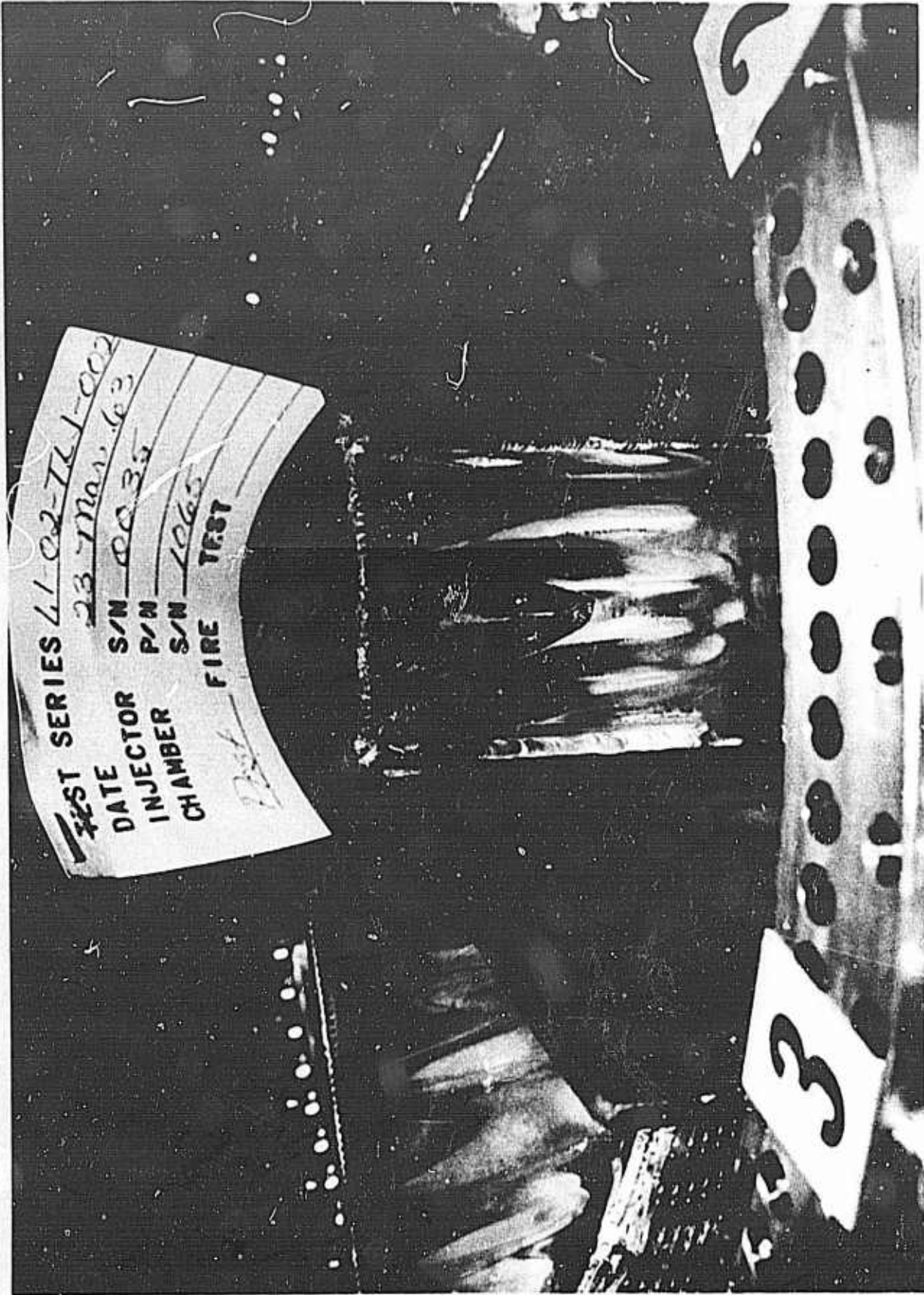


Figure 17 -- Injector S/N 0035 after Test No. 1.1-02-TLJ-002

I, B, Uncooled Combustion Chamber Pulse Charge (cont.)

The thrust chamber assembly operated 4.189 sec at nominal chamber pressure and mixture ratio. Postfire examination of the hardware revealed that the injector sustained severe, unexplainable erosion on the hub as shown in Figure 17. Again, the thermocouple located in the dummy Teflon case recorded a maximum temperature of 1200°F. The hydraulic balance was obtained for the system and the instrumentation verified.

Test No. 1.1-02-TLJ-003 was the first test scheduled for threshold sensitivity rating. Because of the severe baffle damage incurred on the previous test, injector S/N 1085 (another 2SXVIIM-2A) was used for Test No. -003. A 13.5-grain (blasting cap only) pulse charge was installed in the chamber at Position "B." For this test, the CSM unit was monitored from Poj-1F(M) using a flush-mounted Microsystems transducer. It was thought that Poj would be less likely to cause shutdown from a spurious signal than Pfj.

The combustion stability monitor terminated the test after 0.919 sec because the transducer at Poj-1F was defective and produced a noisy high amplitude signal which triggered the CSM unit. No hardware damage occurred during this test.

Because the previous test terminated before detonation of pulse charge, the next tests had the same objectives as Test No. -003. On Test No. -004, a 13.5-grain charge was located in Position "B" and sequenced to fire at FS-1 + 1.300 sec. The test was satisfactory: a 252-psi peak-to-peak pulse was recorded at a Pc4 plane transducer which damped in 12 msec. The test was classified as stable and there was no hardware damage.

For Test No. 1.1-02-TLJ-005, the pulse charge was still located at Position "B" but was increased to 20 grains. The test had a duration of 3.476 sec. A 268-psi peak-to-peak pulse occurred at FS-1 + 1.312 sec, damping in 10 msec. The test was therefore stable and the hardware remained undamaged.

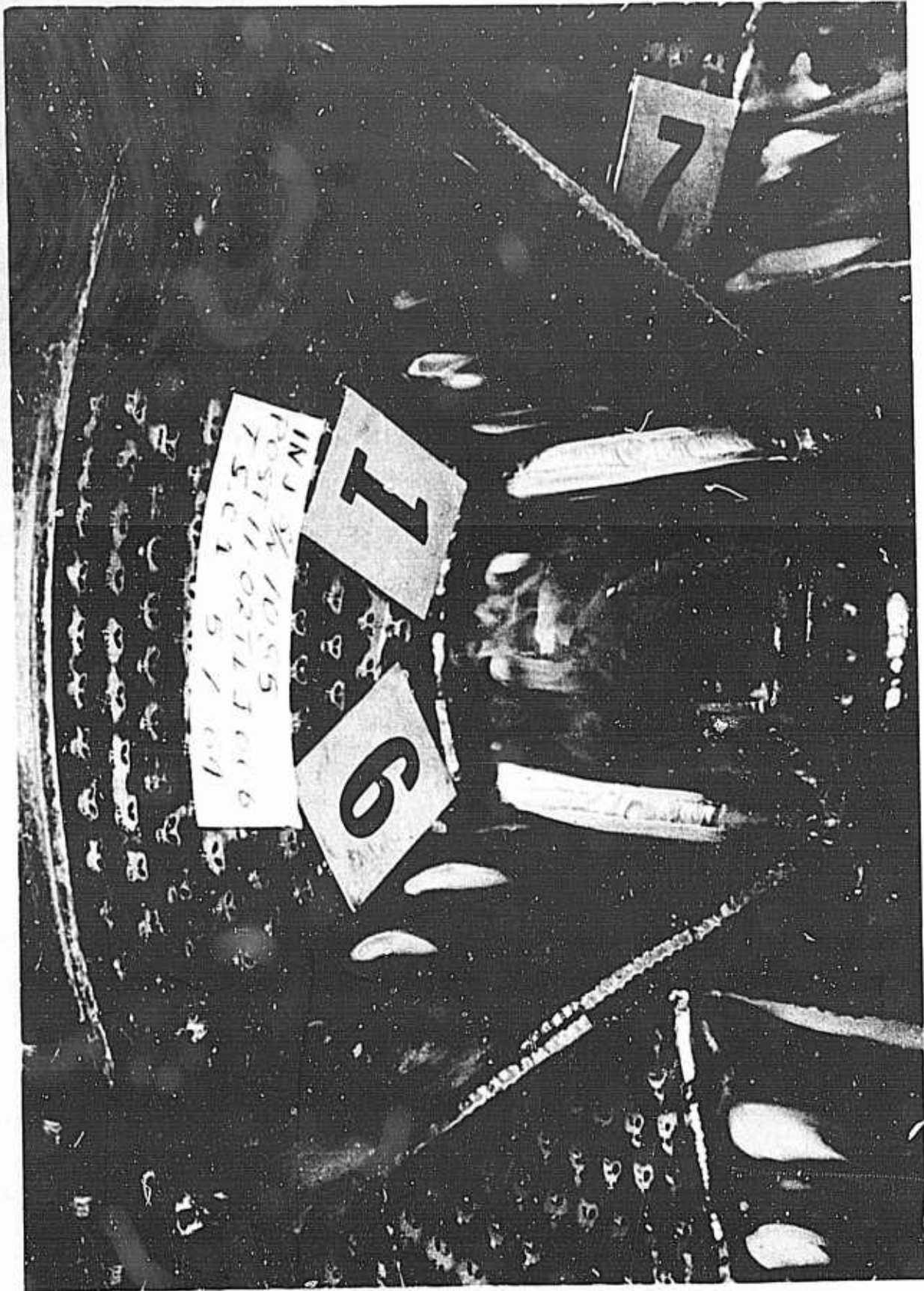


Figure 18 -- Injector S/N 1085 after Test No. 1.1-02-TIJ-006

GEMSIP FR-1, Volume 5

I, B, Uncooled Combustion Chamber Pulse Charge (cont.)

A 40-grain nondirected pulse charge was located in Position "B" for Test No. 1.1-02-TLJ-006. For this test, a dual CSM unit was utilized to provide against premature shutdown from a single invalid signal. The dual CSM requires that two transducers concurrently monitor oscillations, which meet the CSM "trip" criteria, for a duration of 30 msec.

The test was conducted on 7 May 1964 and was terminated at FS-1 + 1.354 sec by the combustion stability monitor. Figure 18 shows the damage to injector S/N 0035. An analysis of the high frequency playback led to the conclusion that the instability was initially a standing fourth tangential mode (5400 cps) which later shifted to a standing third tangential mode (4200 cps). This fixed the threshold at Position "B" between 20 grains and 40 grains for the Titan/Gemini injector.

On Test No. 1.1-02-TLJ-007, the nondirected pulse charge was moved to Position "D" (Figure 8) and the size was decreased to 20 grains. Injector S/N 0035, which had been damaged on Test No. -002 and was subsequently weld repaired, was installed on the thrust chamber assembly for Test No. -007. The test was conducted for a total duration of 2.420 sec with the pulse charge exploding at FS-1 + 1.307 sec. A 156-psi pulse resulted and was damped in 4 msec. The test was classified as stable and no hardware was damaged. It was concluded that Position "D" was not more sensitive than Position "B."

On Test No. 1.1-02-TLJ-008, a 20-grain bomb was located at Position "I," near the throat on the chamber centerline. The test duration was 2.209 sec and the charge detonated at FS-1 + 1.307 sec.

The amplitude of the pulse was 136-psi peak-to-peak and damped in 4 msec, marking a stable test. No hardware damage resulted.

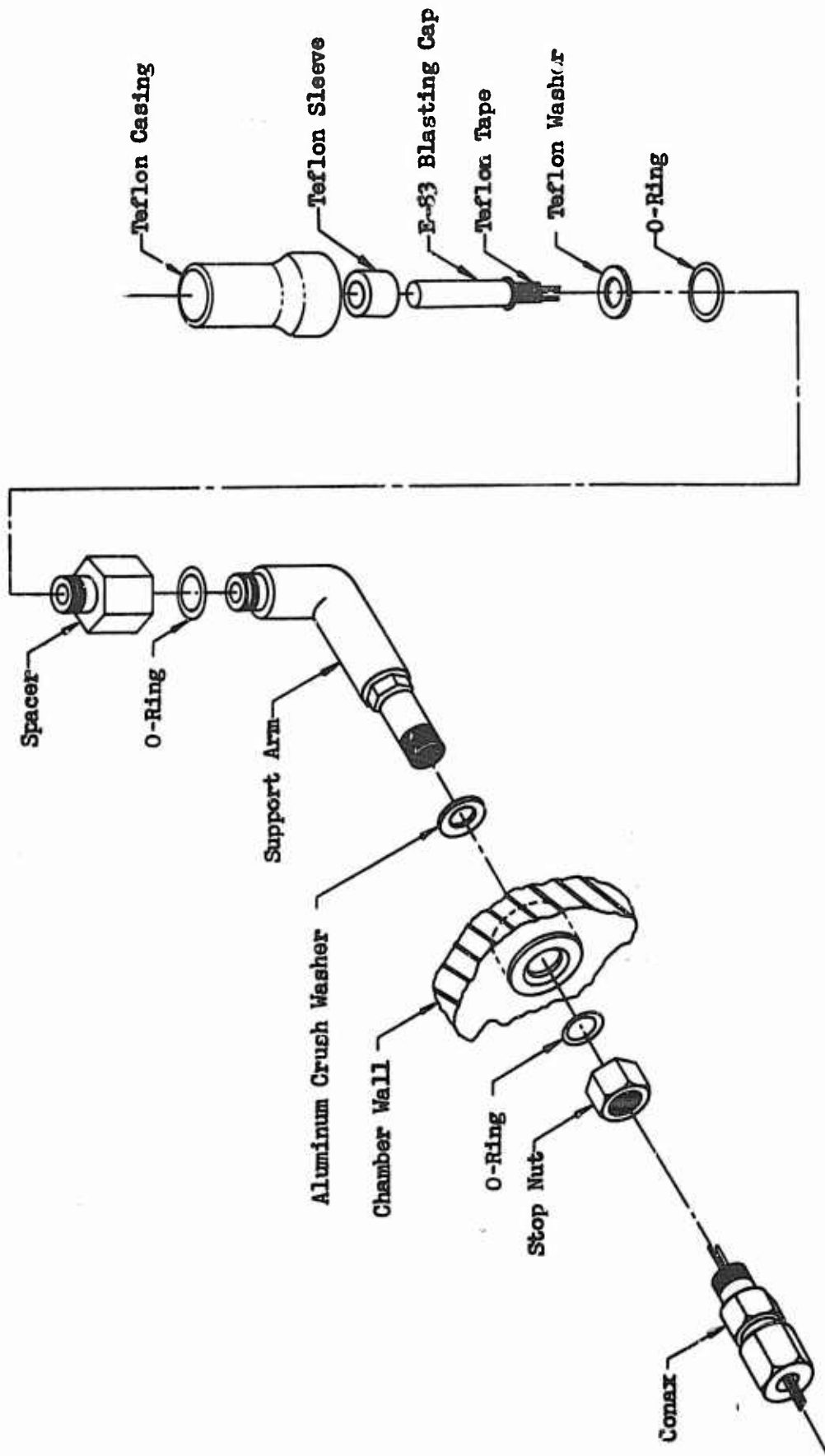


Figure 19 -- Final Design of GEMSIP NDFC Used for Uncooled Combustion Chambers

GEMSIP FR-1, Volume 5

I, B, Uncooled Combustion Chamber Pulse Charge (cont.)

Test No. 1.1-02-TLJ-008 concluded this series; it had been demonstrated that none of the other positions were grossly more sensitive to pulsing than Position "B."

Because the pulse charge positioning pin sheared during two of the tests, the design of the support arm was modified to incorporate a hexagonal shank as shown in Figure 19. The assembly procedure was changed also to include the placement of a Teflon spacer around the blasting cap to ensure axial alignment of the squib in the Teflon case. Experience indicated that the nonreproducibility of the magnitude of the perturbation may have been caused by a misalignment of the squib, which resulted in a primary detonation of only a portion of the main charge of C-4 explosive.

With these final modifications, the GEMSIP nondirected pulse charge was considered to be fully operable. During the baffle and injector pattern evaluation phases of the Gemini Stability Improvement Program, approximately sixty 100-grain and 220-grain nondirected pulse charges were used successfully. Figure 16 shows a 220-grain bomb installed in an uncooled chamber. It was noted that when 220-grain charges were used with the candidate injector with seven regeneratively cooled baffles, the detonation shock wave caused bending of the baffle nearest the charge. Figure 20 shows the postfire condition of such an injector. For this reason, only 100-grain charges were subsequently used to demonstrate the dynamic stability of the candidate injector.

C. TUBULAR COMBUSTION CHAMBER PULSE CHARGE

1. Design

The design of the nondirected pulse charge to be used for the tubular chamber tests differed from the uncooled version only in the method of mounting. Because there is no way to attach the pulse mounting assembly to the

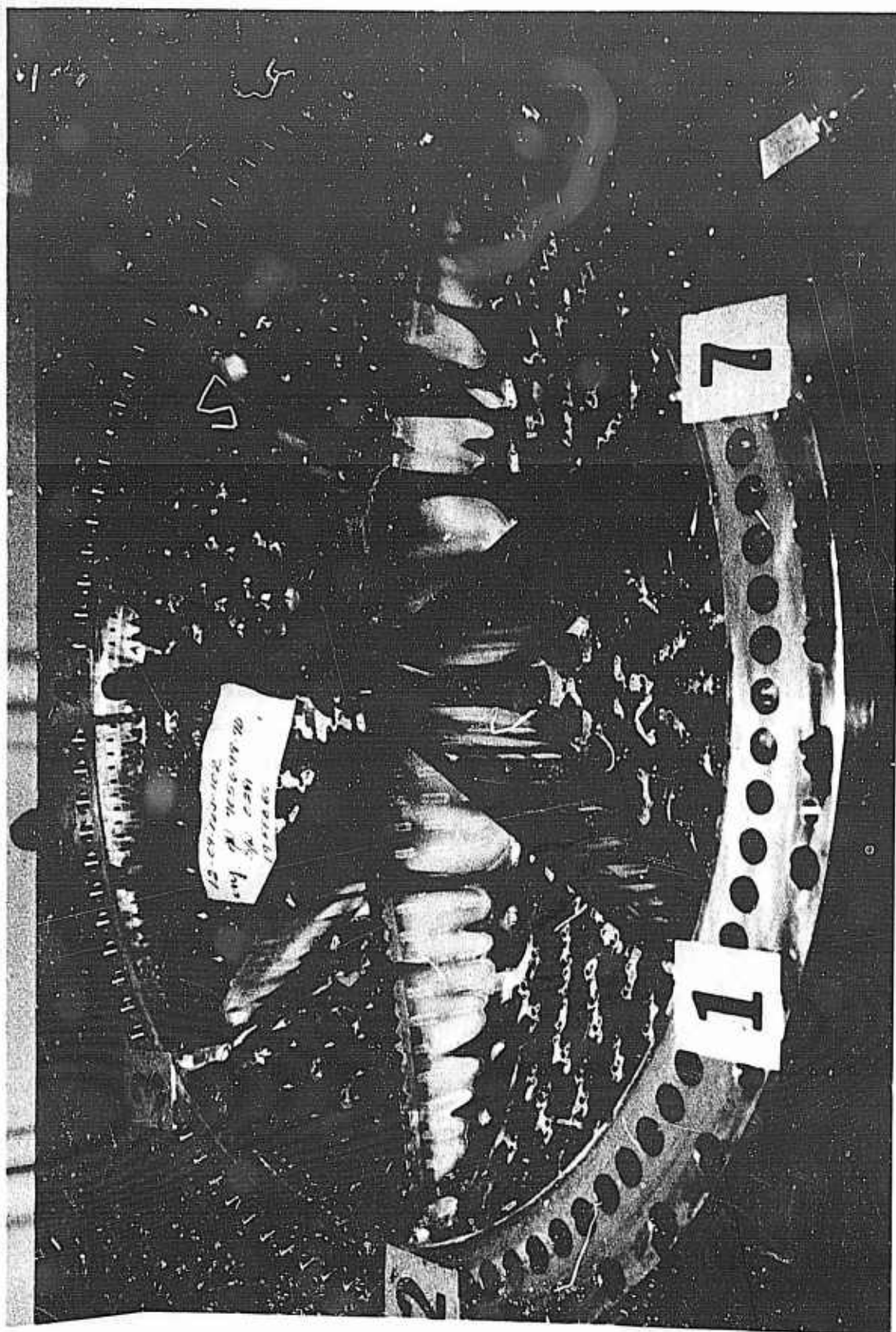


Figure 20 -- Bending of Baffles Caused by 220-Grain  
Nondirected Pulse Charge

I, C, Tubular Combustion Chamber Pulse Charge (cont.)

chamber wall, three alternative methods of mounting the charge were considered: (1) use of a long wand, inserted through the throat to position the pulse charge; (2) attachment of the pulse charge holder to a baffle; and (3) suspension of the charge holder from the injector face.

Method (1) was not feasible because a long unsupported wand would vibrate severely, causing possible tube denting in the chamber throat. Also, the wand might fail before the charge was fired and certainly would require replacement after each test. Methods (2) and (3) had approximately the same advantages and disadvantages, except that Method (2) required the welding of a new holding fixture to the baffle each time the configuration was changed. Therefore, suspension from the injector face was chosen as the best method for supporting the nondirected pulse charge in a tubular chamber.

2. Damage Threshold Testing

Before hot firings in tubular chambers, a series of pulse tests at ambient nonfiring conditions was conducted to determine the pulse charge size that would be just below the threshold of tubular chamber damage. These tests were conducted using combustion chamber SN 1491 (which was no longer suitable for hot firing) and injector SN 1377. For all these tests, the Teflon case thickness was reduced to 1/4 in. to allow for the ablation of the Teflon prior to detonation of the charge in the combustor.

For the first test (1.1-01 TLC-001) a 13.5-grain bomb (actually only the blasting cap detonator) was mounted on the chamber centerline immediately downstream of the tip of the hub. The charge fragmented into rather large pieces and the fragmentation seemed to be distributed equally around the chamber. The dents were small and were limited to a 2 in. circumferential band.

For Test No. -002, a 20-grain charge was positioned as in the previous test and the damage was similar, but the dents were smaller and more numerous. This indicated that the larger grain size caused more extensive fragmentation of the case and that the smaller pieces had less momentum.



Figure 21 -- Tube Dents Caused by 40-Grain Pulse Charge--

Destructive Tests

I, C, Tubular Combustion Chamber Pulse Charge (cont.)

For Test No. -003, a 40-grain charge was located as in the previous tests and the damage was again limited to a 2-in. band. On this test, it was noted that Teflon fragments striking between two tubes caused deeper dents than a fragment hitting directly in the center of a tube, as shown in Figure 21. No tube fractures were observed after this test.

For the next test (1.1-01-TLC-004) and 80-grain charge was located approximately 5 in. closer to the throat than in the previous tests so that the Teflon fragments would strike "virgin territory" and the tube dents would be identified separately from those previously incurred. Postfire examination showed the field of damage to be limited to a heavily dented 1-in. band of 360 degrees. Again, no tube ruptures were observed.

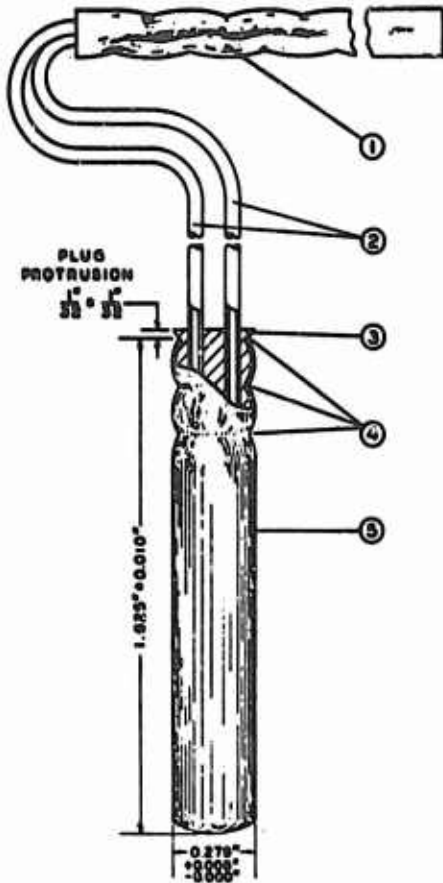
The bomb size was reduced to 40-grains for Test No. -005 and was located near the baffle tip midway between the chamber centerline and wall. The damage was similar to that encountered in Test No. -003, but was localized to an 80-degree arc immediately adjacent to the charge. No tube ruptures were detected.

The last test of the series (-006) utilized a 220-grain bomb located at the geometric center of the plenum and the extent of damage was not measurable. Numerous tubes were split wide open and Teflon fragments of all sizes and description were found imbedded in the wall of the combustion chamber.

Based on the results of these tests, it was concluded that an 80-grain nondirected pulse charge is the largest that can be exploded in a YLR91-AJ-5 tubular chamber without probability of tube fractures. Although an 80-grain charge caused heavy denting during these cold tests, it was thought that a hot firing would produce less tube damage because the tubes would be pressurized with propellant and the Teflon fragments would be subjected to ablation while directed at an angle to this wall by the momentum of the chamber gases.

To confirm this reasoning, a thrust chamber assembly pulse test was conducted during August 1964, with an 80-grain nondirected pulse charge in a

# DUPONT E-83 E. B. CAP



- (1) SHUNT - CELLOPHANE-LINED ALUMINUM FOIL APPROXIMATELY 2-1/2 IN. LONG ROLLED AROUND BARED ENDS OF LEG WIRES.
- (2) LEG WIRES - PLASTIC INSULATED TINED COPPER, BOTH YELLOW, 22 GAGE IS STANDARD FOR LENGTHS LESS THAN 30 FT., 20 GAGE IS STANDARD FOR 30 FT. OR LONGER. UPON SPECIAL REQUEST THE VARIOUS GAGES AND LENGTHS MAY BE INTERCHANGED. CONDUCTIVE ENDS BARED FOR A DISTANCE OF 1-7/8 TO 2-1/4 IN.
- (3) RUBBER PLUG - MOLDED TO LEG WIRES AND HAVING BRIDGE WIRE ATTACHED TO BRIDGE POSTS.
- (4) CRUOPS - COMPLETELY AROUND SHELL.
- (5) SHELL - ALUMINUM ALLOY SHELL.

RESISTANCE OF COMPLETE ASSEMBLY - RESISTANCE OF THIS CAP IS  $1.16 \pm 0.25 \text{ OHMS} + 0.0332 \text{ OHM}$  FOR EACH DOUBLE FOOT OF 22 GAGE TINED COPPER WIRE OR  $0.0702 \text{ OHM}$  FOR EACH DOUBLE FOOT OF 20 GAGE TINED COPPER WIRE.

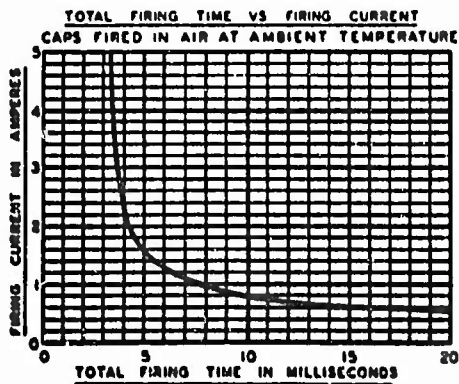
### PERFORMANCE CHARACTERISTICS

THE PROPERTIES GIVEN BELOW ARE BASED ON BACKGROUND INFORMATION OR WERE DETERMINED IN THE LABORATORY ON INITIAL LOTS OF THE CAP. THE DATA MAY VARY WITH MORE EXHAUSTIVE TESTS AND ARE, THEREFORE, SUBJECT TO CHANGE.

- GENERAL - THIS CAP IS AN ALUMINUM SHELL VERSION OF THE E-78 CAP AND WAS FIRST MANUFACTURED FOR PICATINNY ARSENAL IN 1955.
- FIRING TIME - TIME FROM APPLICATION OF CURRENT UNTIL FLASH FROM CAP ACTIVATED A PHOTOCELL STOP CIRCUIT IS SHOWN IN THE GRAPH AT LEFT.
- MINIMUM FIRING CURRENT - APPROXIMATELY 0.38 AMP.
- STATIC SENSITIVITY - MAXIMUM ENERGY BY CONDENSER DISCHARGE FOR IGNITION PROBABILITY OF ZERO - 0.117 JOULE.
- STORAGE PROPERTIES

TEMPERATURE	SATISFACTORY AFTER THE FOLLOWING TIME
225°F.	24 HRS.
160°F.	3 YRS.
-180°C. (LIQ. O <sub>2</sub> )	30 HRS.

THE MAXIMUM STORAGE LIFE UNDER ALL OF THE ABOVE CONDITIONS IS UNKNOWN.
- WATER RESISTANCE - FUNCTIONED SATISFACTORY AFTER 4 HRS. AT 400 LB./SQ. IN. AND 2 WEEKS AT 250 LB./SQ. IN.



THIS DRAWING HAS BEEN FURNISHED BY E.I. DUPONT DE NEMOURS & CO. INC. THE INFORMATION AND DATA THEREON MAY BE REPRODUCED WITHOUT THE WRITTEN PERMISSION OF DUPONT. INQUIRIES CONCERNING THIS PRODUCT SHOULD SHOW PRODUCT DESIGNATION, PAGE DATE, AND BE ADDRESSED TO:

SALES DIVISION  
EXPLOSIVES DEPARTMENT  
E.I. DUPONT DE NEMOURS & CO. INC.  
WILMINGTON DE, DEL.

DATE 1-9-61



PAGE B-12

Figure 22 -- DuPont E-83 E. B. Cap

I, C, Tubular Combustion Chamber Pulse Charge (cont.)

tubular chamber. The pulse mount was welded to the baffle, halfway between the chamber centerline and wall. A time delay blasting cap (Figure 22), actuated at FS-1, with a 1.600-sec delay was used to detonate the main charge of C-4. (Appendix B describes the circuitry used to initiate the squib.) The insulated detonator lead wires were brought out through the throat and burned off at thrust chamber ignition.

The damage caused by this 80-grain charge, shown in Figure 23, was heavier than anticipated, possibly because the strength of the stainless steel coolant tubes was decreased at the high combustion temperature and, therefore, the tubes were more susceptible to damage. Based on these test results, 40 grains was established as the maximum pulse to be detonated in a tubular chamber.

3. Early Engine Test Series

During the months of August through November 1964, a series of 91-5 engine pulse tests was conducted in conjunction with the Feed System Improvement Phase of the GEMSIP. One of the purposes of these tests was to further develop techniques of mounting nondirected pulse charges in tubular combustion chambers for later application during engine demonstration. One balance test and six pulse tests were conducted during this test series. These tests are described in detail in Volume 2, Section III,A.

For the first pulse test, the nondirected charge support arm was attached to the injector face as shown in Figure 24. The support arm is coated with NRL 1795, an ablative material, to shield the steel support from the severe thermal environment. A time delay blasting cap with a 1.600-sec delay time was used to detonate the charge.

Post fire examination after Test No. 1.1-01-TLA-002 revealed a heavy concentration of dents opposite the end of the bomb (Figure 25). The same

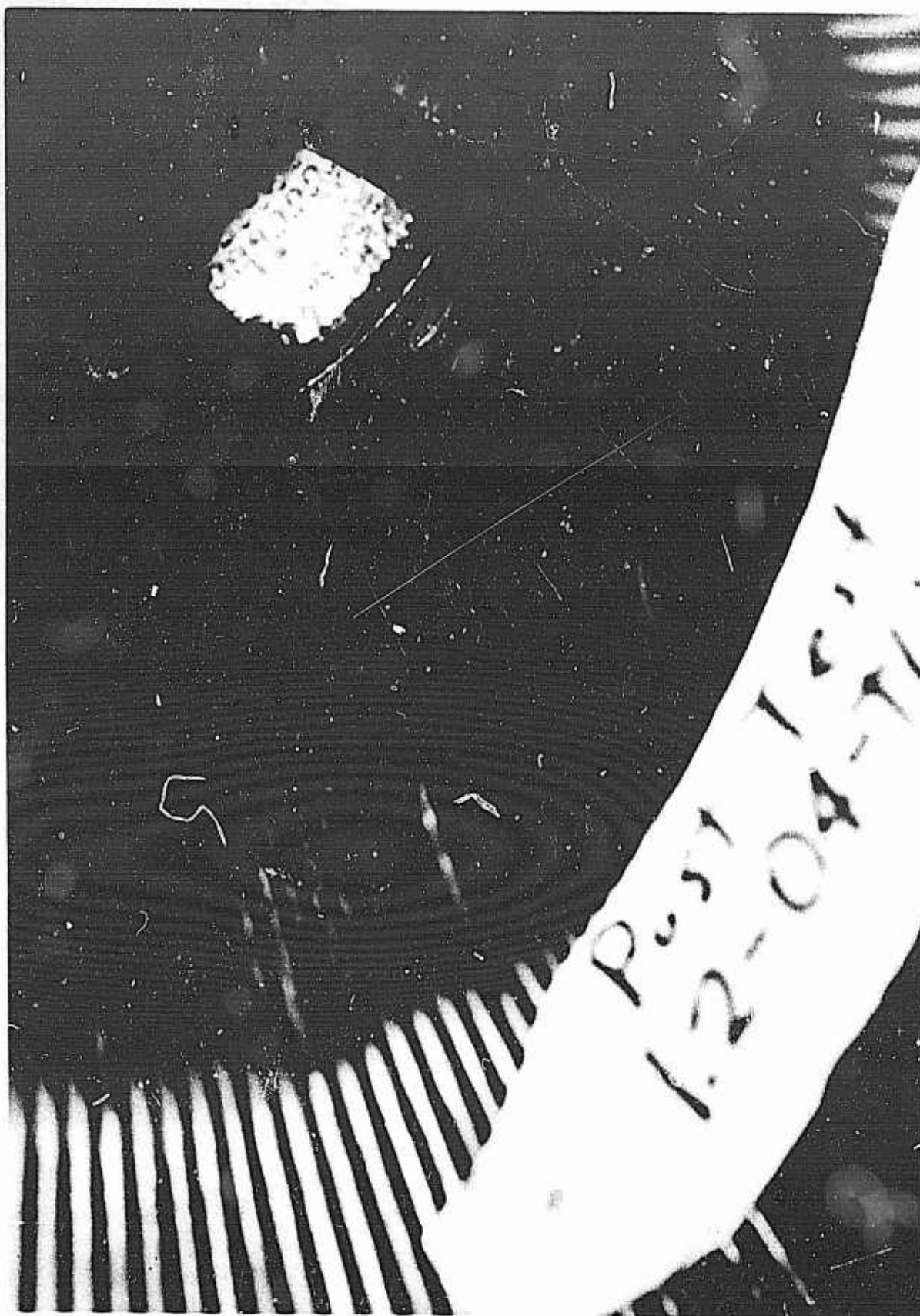


Figure 23 -- Hardware after Test No. 1.2-04-TLJ-140

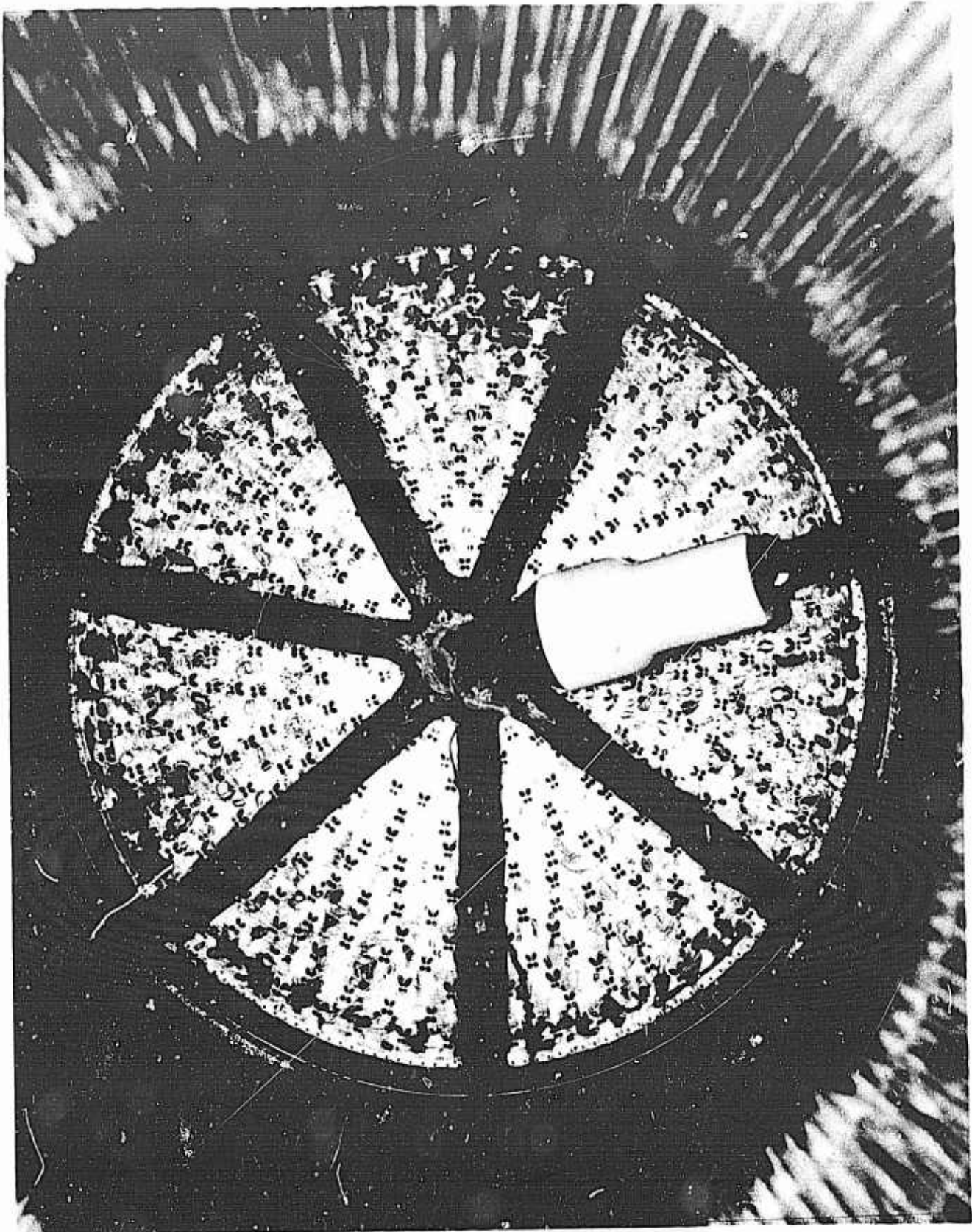


Figure 24 -- Installation of Nondirected Pulse Charge  
in Tabular Chamber Cavity

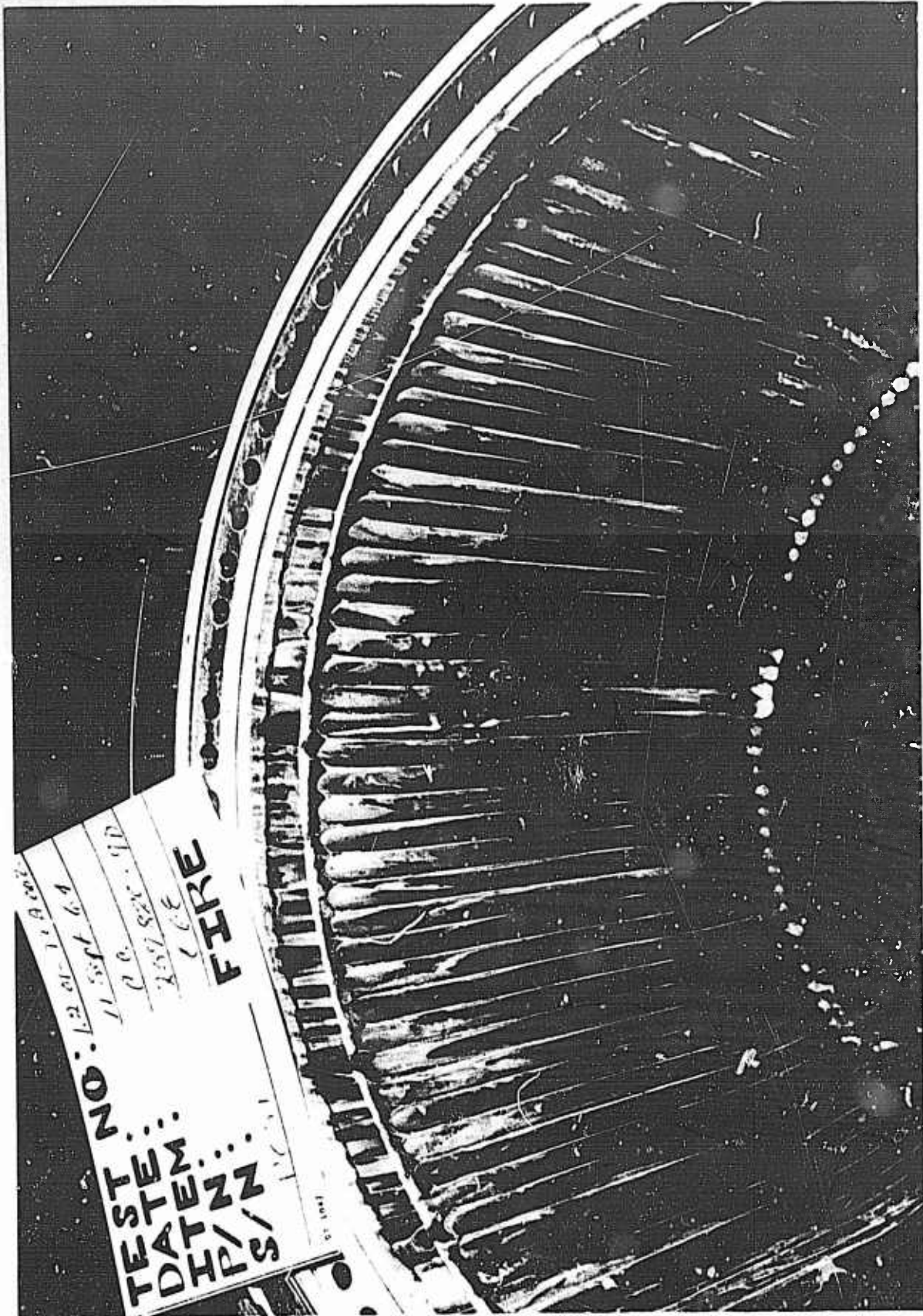


Figure 25 -- Chamber Dents Caused by 40-grain Nondirected

Pulse Charge

I, C, Tubular Combustion Chamber Pulse Charge (cont.)

damage occurred during Test No. -003. For the remaining four tests, therefore, the charge was positioned on the chamber centerline, pointed straight down toward the throat. Tests No. -004 and -005 were satisfactory bomb tests; but during Tests No. -006 and -007, the Teflon containing the main charge of C-4 ejected from the chamber prior to detonation of the squib. When the unprotected brass squib detonated, the chamber tubes were punctured as shown in Figure 26.

Because of the heavy concentration of dents opposite the end of the bomb observed on Tests No. -002 and -003, an attempt was made to minimize the momentum of the fragments traveling toward the wall. This could be done by decreasing the size of the fragments or their velocity. Decreasing the size was chosen because it could be done easily by shaping the C-4 explosive slightly at the end (Figure 27) to cause greater fragmentation of the end of the Teflon case, and hence, less damage to the chamber coolant tubes.

A series of tests conducted in the Solid Rocket Operations high explosives test area verified the advantages of this proposed modification. Figure 28 shows the damage done by an unshaped charge, and Figure 29 illustrates the lesser destruction resulting from the shaped charge.

Shaping of the end of the charge causes a slight distortion of the spherical shock wave, which somewhat alters the "nondirectional" effect of the bomb, but this distortion was not considered to be critical because the dynamic stability of the GEMSIP candidate injector had previously been demonstrated with an uncooled thrust chamber assembly using a truly nondirectional bomb.

4. Engine Demonstration Pulse Tests

The Engine Demonstration Phase of the Gemini Stability Improvement Program was conducted during the months of March, April, and May 1965. A part of this phase of the program was a series of pulse tests conducted on Engines GR1-91 and GR3-91.

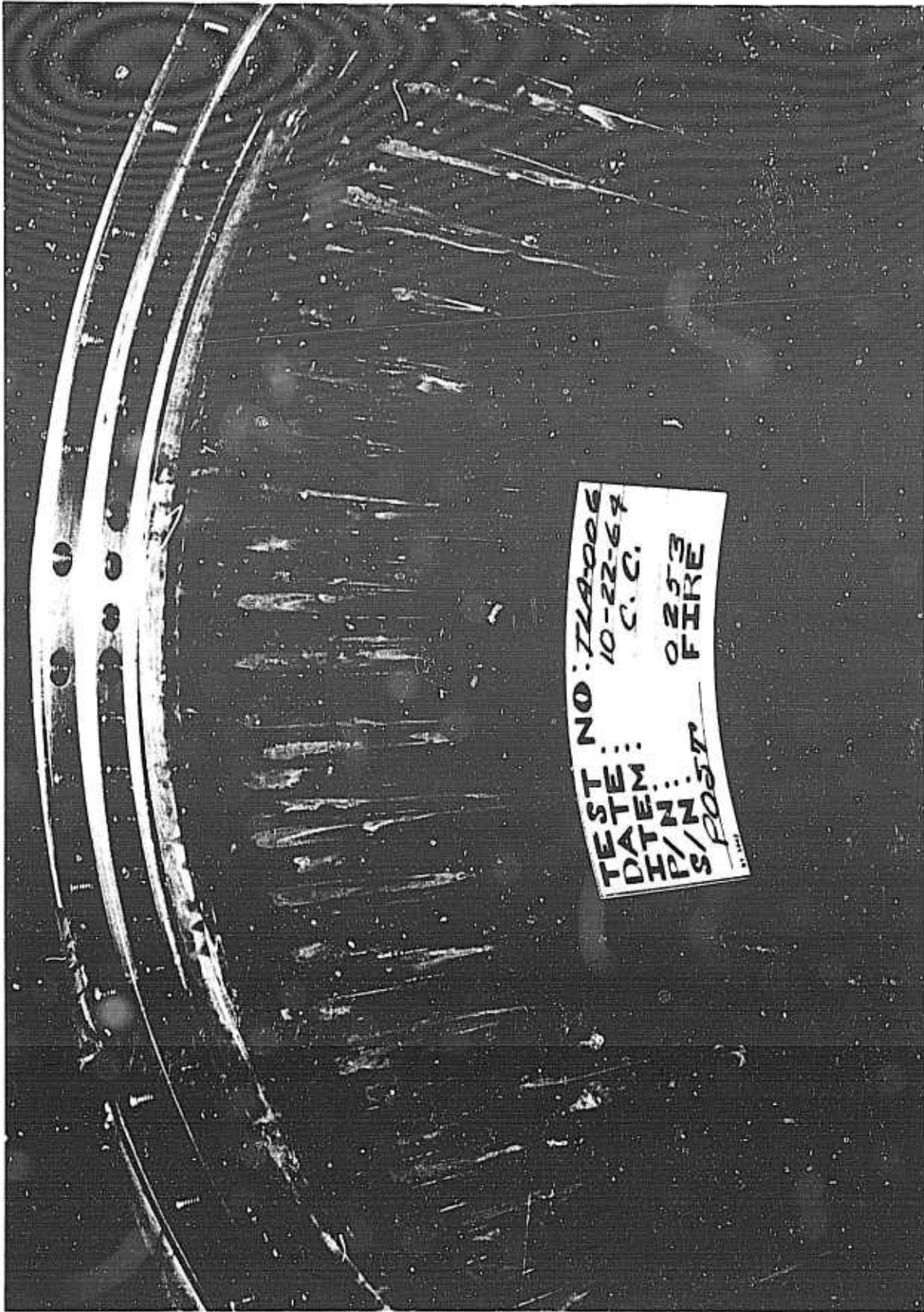


Figure 26 -- Chamber Damage Caused by Detonation of Unprotected

Squib

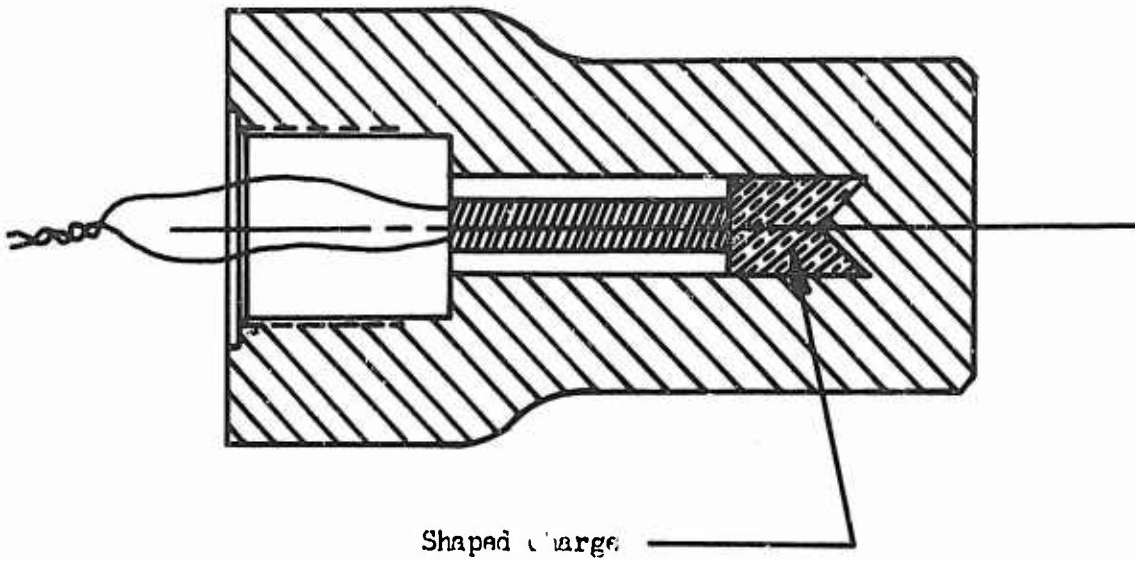
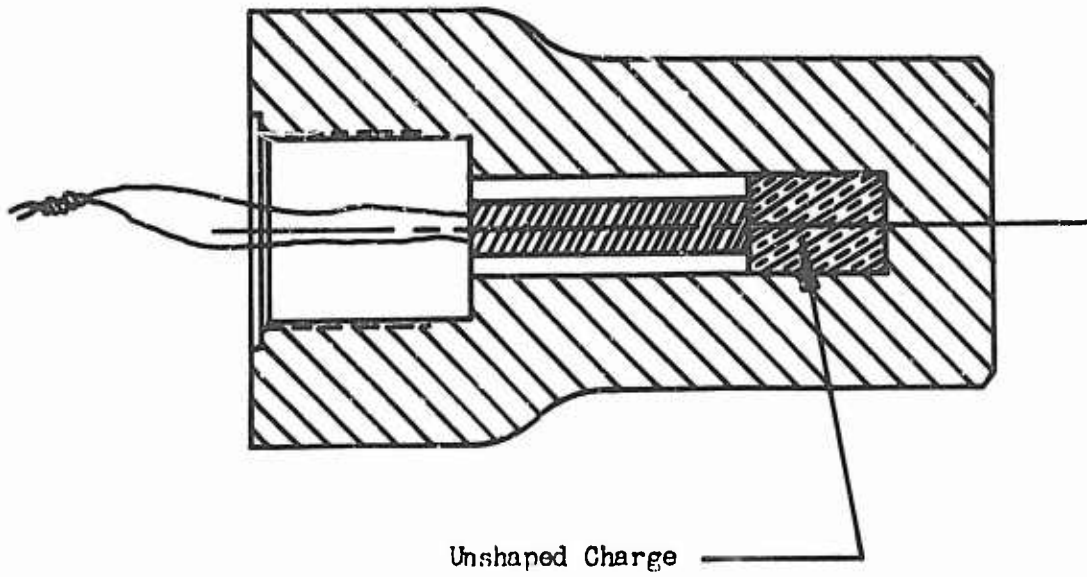


Figure 27 -- "Shaping" of the GEMSIP Nondirected Pulse Charge

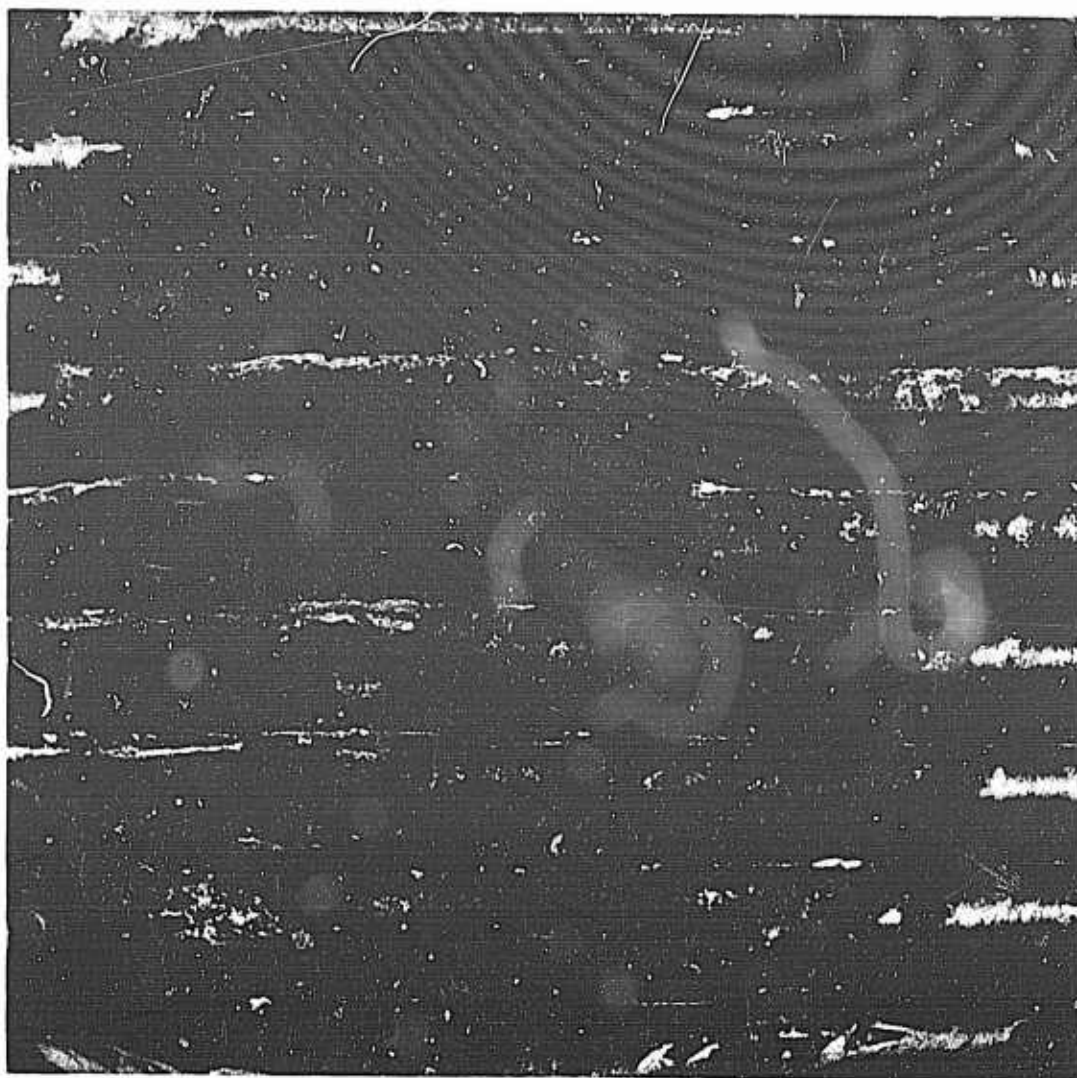


Figure 28 --- Damage Caused by Unshaped Charge



Figure 29 -- Reduction of Damage Resulting from Shaping of the Charge

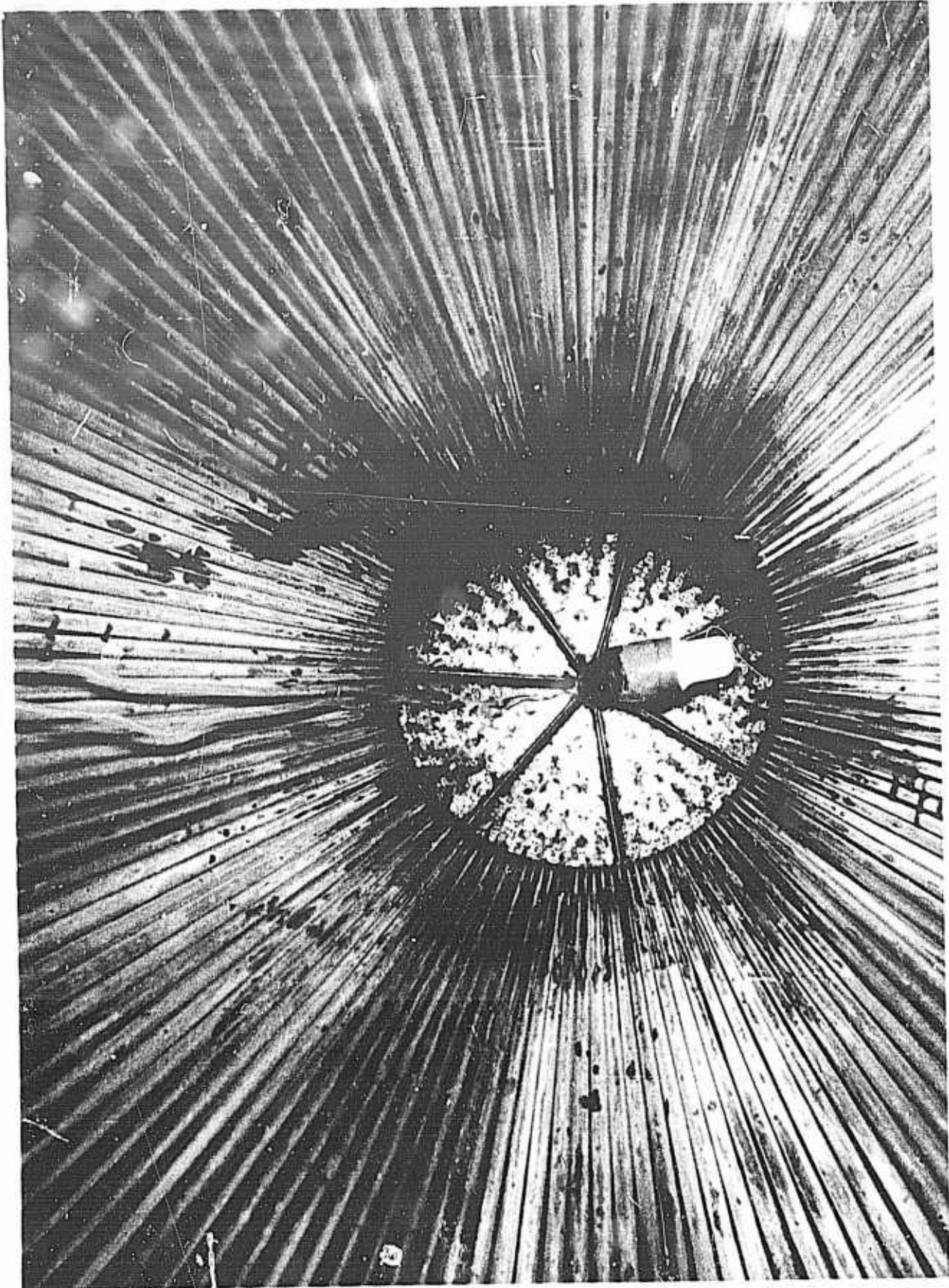


Figure 30 -- Installation of Nondirected Pulse Charge for GRI-91  
Test Series

I, C, Tubular Combustion Chamber Pulse Charge (cont.)

The GR1-91 tests used nondirected pulse charges, which were mounted as shown in Figure 30. Five tests were conducted, three successfully. During Tests No. -002 and -004, the Teflon case of the bomb broke loose from the charge holder and ejected from the chamber prior to detonation of the squib. As happened during the Early Engine Test Series, the chamber tubes were punctured at numerous locations when the unshielded squib detonated.

To reduce the possibility of further failures of this type, the design of the Teflon case was modified slightly to incorporate a larger radius on an internal corner (shown in Figure 31), thereby reducing a high local stress concentration factor. Also, the test procedure was changed so that the time delay squib would be initiated 0.250 sec prior to FS-1 (instead of at FS-1) and detonate at FS-1 + 1.35 sec. This was done because experience had shown that the reliability of the nondirected pulse charge is marginal after 0.80 sec of exposure to combustion in the chamber, which begins at approximately FS-1 + 0.55 sec.

During the Engine GR3-91 test series, five successful pulse tests were conducted. There was a sixth test in which the Teflon case failed in the manner described previously, but this test took place prior to this latest charge.

Based on the experience of all the GEMSIP testing, the tubular chamber nondirected pulse charge was considered a useful and reliable stability rating tool. The only problem area remaining is the tolerance of the time delay blasting cap. Figure 32 presents a summary of the firing times of all the delay caps used during the Gemini Stability Improvement Program. Although the caps were manufactured by Hercules Powder Company with a 1.600-sec  $\pm$  10% delay, the firing times ranged from 1.35 to 2.00 sec. This variance may be attributed to a distortion of the initial fabrication tolerances caused by the elevated temperatures in the combustion chamber.

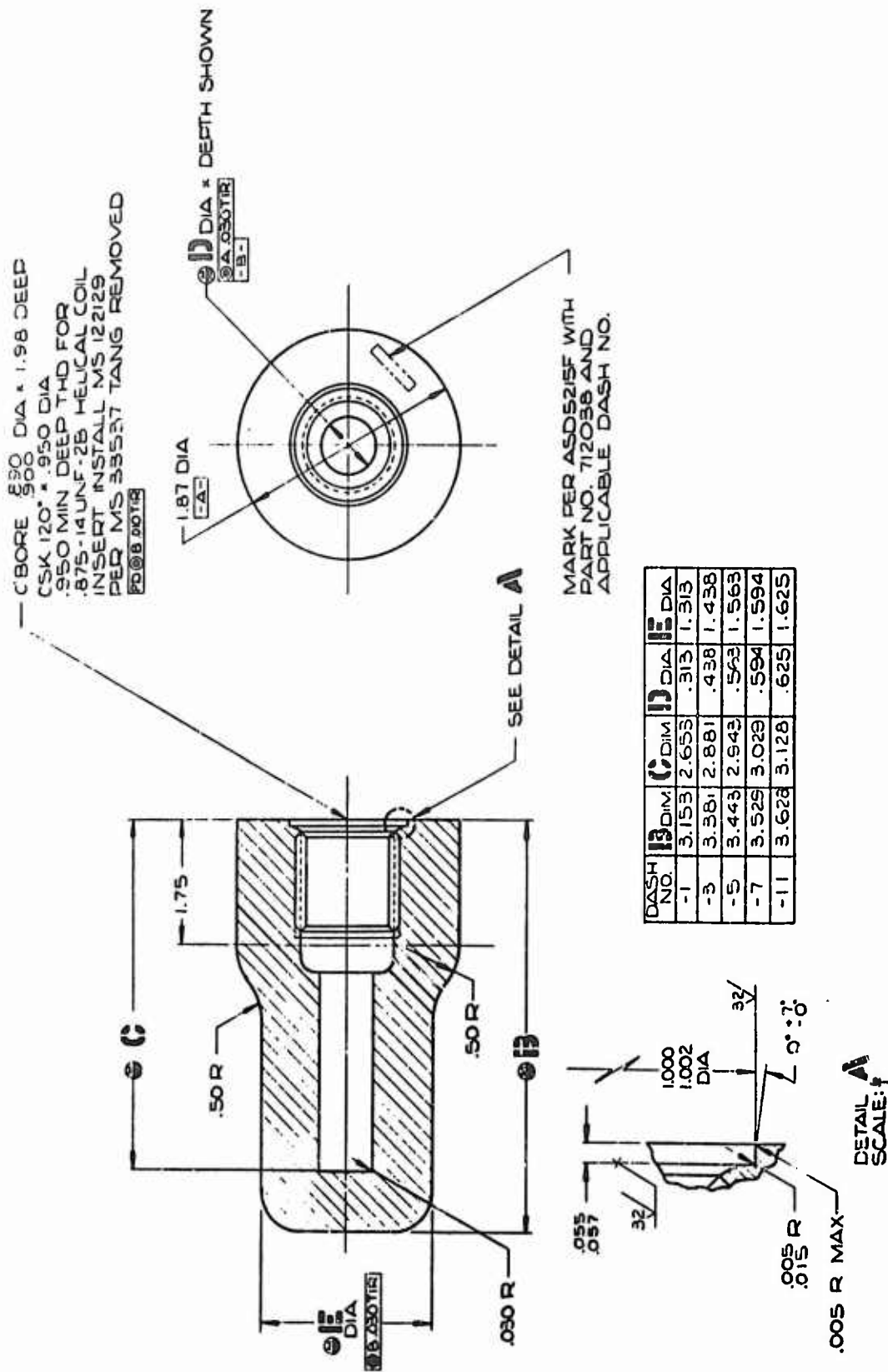


Figure 31 -- Modification of Teflon Casing

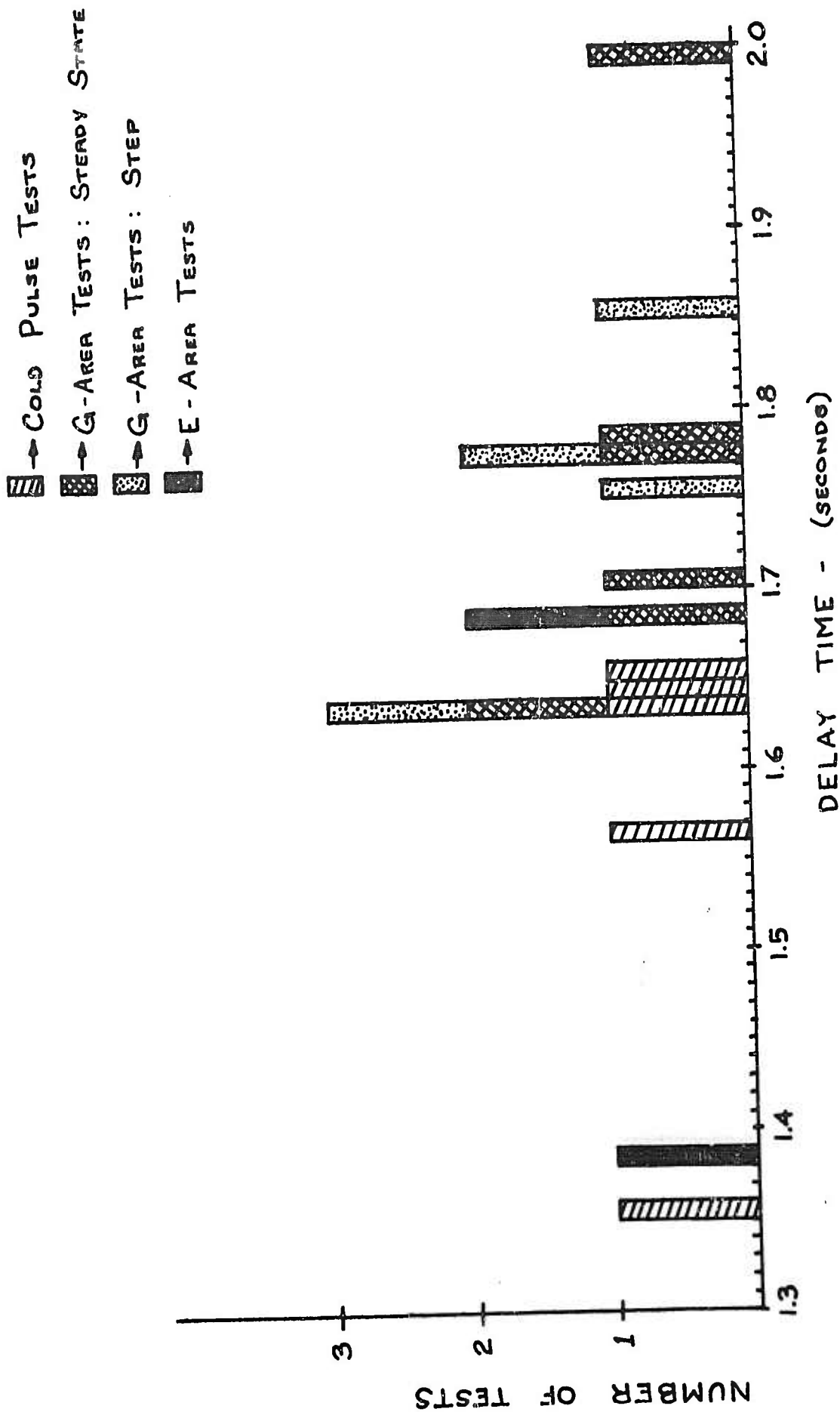


Figure 32 -- Summary of Delay Squib Firing Times

I, Nondirected Pulse Charge Development (cont.)

D. CONCLUSIONS AND RECOMMENDATIONS

Based on the experience from the development testing of the nondirected pulse charge, the following conclusions were drawn:

1. The GEMSIP nondirected pulse charge generates a truly spherical shock wave.
2. A 40-grain nondirected pulse charge will drive the 2SXVIIM-2A injector unstable.
3. A position close to the chamber wall and near the injector face is satisfactory for preliminary pulse test evaluation. Other locations should be probed, however, before final conclusions are drawn respecting the total stability of a particular injector.
4. The nondirected pulse charge can be successfully initiated in tubular combustion chambers using a time delay squib.
5. A 40-grain GEMSIP bomb is the largest charge which can be detonated in regeneratively cooled combustion chambers without causing significant damage.

It is recommended that:

1. Extreme care should be used in assembling the nondirected pulse charge to ensure high reliability. Experience has shown that slight deviations from the established procedure can cause the bomb to malfunction.

I, D, Conclusions and Recommendations (cont.)

2. Further tests should be conducted to determine the ablation and deformation rate of the Teflon bomb casing. Optimization of the wall thickness of this casing would minimize chamber and transducer damage.

3. The tolerance of the timing fuse in the Hercules time delay blasting cap should be decreased from  $\pm 10\%$  to  $\pm 5\%$  and made less sensitive to thermal stress if at all possible.

GEMSIP FR-1, Volume 5

APPENDIX A, SECTION I

EXPLOSIVES USED FOR NONDIRECTED PULSE CHARGES

I. COMPOSITION C-4

A. ALTERNATE NOMENCLATURE

Harrisite  
Plastic Explosive (along with other Composition C-series explosives)

B. COMPOSITION

Cyclonite -----	91.0%
Polyisobutylene -----	2.1%
Motor Oil -----	1.6%
Di-(2-ethylhexyl) sebacate --	5.3%

C. CHARACTERISTICS

Composition C-4 is a dirty white to light brown, puttylike, hand-tamped explosive. It will explode when subjected to a temperature of 290°C for five sec. Composition C-4 has a higher stability than Composition C-3. It is essentially nonhygroscopic. It will not harden at -57°C and will not undergo exudation at 77°C. Composition C-4 is less sensitive to impact and slightly more brisant than Composition C-3. The two compositions are about equal in sensitivity to initiation.

D. MANUFACTURE

The isobutylene plasticizer, previously made up in ether, is mixed with cyclonite (crystals of 44 microns or less) either by machine or by hand-kneading and rolling (machine-mixing uses a Schrader Bowl mixer). The mixture is then dried at 60°C.

E. USES

Composition C-4 is used primarily for demolition blocks. It is well suited for underwater demolition if properly packaged. It is ideally suited for cutting through steel because of its plasticity and its high velocity of detonation.

I, Composition C-4 (cont.)

F. COMMENTS

Composition C-4 has been developed to improve the instability and hygroscopicity of Composition C-3 (see entry). It has not, however, entirely replaced Composition C-3.

II. COMPOSITION C-3

A. ALTERNATE NOMENCLATURE

Plastic Explosive (along with other Composition C-series explosives)

B. COMPOSITION

Cyclonite -----	77.1%
Tetryl -----	3.0%
Mononitrotoluene ----	5.0%
Dinitrotoluene -----	10.0%
TNT -----	4.0%
Wet Nitrocellulose --	0.9%

C. CHARACTERISTICS

Composition C-3 is a yellowish, puttylike, hand-tamped explosive. It will detonate when subjected to a temperature of 280°C for five sec. Two classes of Composition C-3 (Class A and Class B) are manufactured, in accordance with military specifications. The two classes differ only with respect to acidity (see Uses below). Composition C-3 is pliable at normal temperatures and can be easily molded to suit requirements. It is hygroscopic, but its brisance is unchanged after total immersion in water. It is more brisant than TNT, but less brisant than tetryl. Its sensitivity to impact is similar to that of TNT, but

II, C, Characteristics (cont.)

much less than that of cyclonite. Composition C-3 is somewhat unstable. When exposed to air at 25°C for five days, it loses 1.2% of its weight because of its volatility. Moreover, it becomes hard and brittle at -29°C and undergoes considerable exudation at 77°C.

D. MANUFACTURE

Tetryl, nitrocellulose, and the nitrotoluenes are mixed together to form the plasticizing agent. This plasticizer is then heated to 100°C and wet cyclonite is added. The mixture is stirred and heated until the composition is uniform and all the water has been driven off.

E. USES

Class A Composition C-3 is used for the manufacture of demolition blocks. Class B Composition C-3 is used both for the manufacture of demolition blocks and the loading of ammunition where a lower acidity is desired.

F. COMMENTS

Composition C-3 was developed to improve the instability of Composition C-2. It has not been completely satisfactory in this respect, and is being replaced by Composition C-4.

III. CYCLONITE

A. ALTERNATE NOMENCLATURE

Cyclotrimethylene-trinitramine

Trimethylenetrinitramine

NOTE: The term "RDX," although British in origin, is often used interchangeably with "cyclonite" in the U.S.

III, Cyclonite (cont.)

B. COMPOSITION

$(\text{CH}_2)_3\text{N}_3(\text{NO}_2)_3$  or  $\text{C}_3\text{H}_6\text{N}_6\text{O}_6$ --chemical compound containing the following percentages by weight of the elements:

Carbon -----	16.22%
Hydrogen -----	2.72%
Nitrogen -----	37.84%
Oxygen -----	43.22%

C. CHARACTERISTICS

Cyclonite is a colorless or white press-loaded high explosive melting at 204°C. It will detonate when subjected to a temperature of 260°C for five sec. Cyclonite is classified into two types, in accordance with military specifications. Type A must have a minimum melting point of 200°C (the melting point given above is for pure cyclonite) and a maximum acidity of 0.05% (as nitric acid). Type B must have a minimum melting point of 190°C and a maximum acidity of 0.02% (as acetic acid). There is also a slight difference in granulation between the two grades. Type B is the less pure of the two types, the impurity consisting mainly of HMX. Cyclonite has no reaction with aluminum or stainless steel. It reacts slightly with copper, brass, mild steel, and cadmium, and when damp it also reacts slightly with nickel and zinc. Cyclonite is nonhygroscopic at 30°C and 90% relative humidity. It is as stable as TNT at temperatures under 100° to 150°C. It has been stored for ten months at 85°C without any change in stability. Cyclonite has the same sensitivity to impact as tetryl, but is more sensitive to friction than tetryl. Both types of cyclonite are equally sensitive to impact, friction, heat, and initiation. Cyclonite is more powerful than tetryl and is considered the second most powerful standard military explosive (nitroglycerin being the first).

III, Cyclonite (cont.)

D. MANUFACTURE

Formaldehyde is reacted with ammonia to yield hexamethylene-tetramine, which in turn is nitrated to yield crude cyclonite. The cyclonite is collected by filtration and is washed and ground.

E. USES

Cyclonite is used mainly in mixtures (Composition A, Compositions B and B-2, Compositions C, C-2, C-3, and C-4, Torpax, PTX-1, and PTX-2), but can be used alone as a subbooster, booster, and bursting charge.

F. COMMENTS

The chief impurity occurring in the manufacture of cyclonite is HMX. Its presence in cyclonite is not considered harmful.

Comparative test values of these explosives are shown in Table 2.

Reference for all explosive specifications: Encyclopedia of Explosives, Ordnance Technical Intelligence Agency, Durham, North Carolina.

TABLE 2

COMPARATIVE TEST VALUES OF SELECTED EXPLOSIVES

<u>Explosive</u>	<u>Impact Sensitivity</u> 2- kg wgt. hgt. in cm.	<u>Brisance</u> sand test 200 gm. Bomb gms of sand	<u>Power</u> Ballistic Mortar % TNT	<u>Detonation Rate</u> meters/sec. at density (gm/cc)
Composition C-3	100 +	53.1	126	7625 @ 1.60
Composition C-4	100 +	55.7	130	3040 @ 1.59
Cyclonite	32	60.2	150	8180 @ 1.65

GEMSIP FR-1, Volume 5

APPENDIX B, SECTION I

GEMSIP PULSE CHARGE INITIATOR FIRE CHECK SYSTEM

GEMSIP FR-1, Volume 5  
Appendix B, Section I

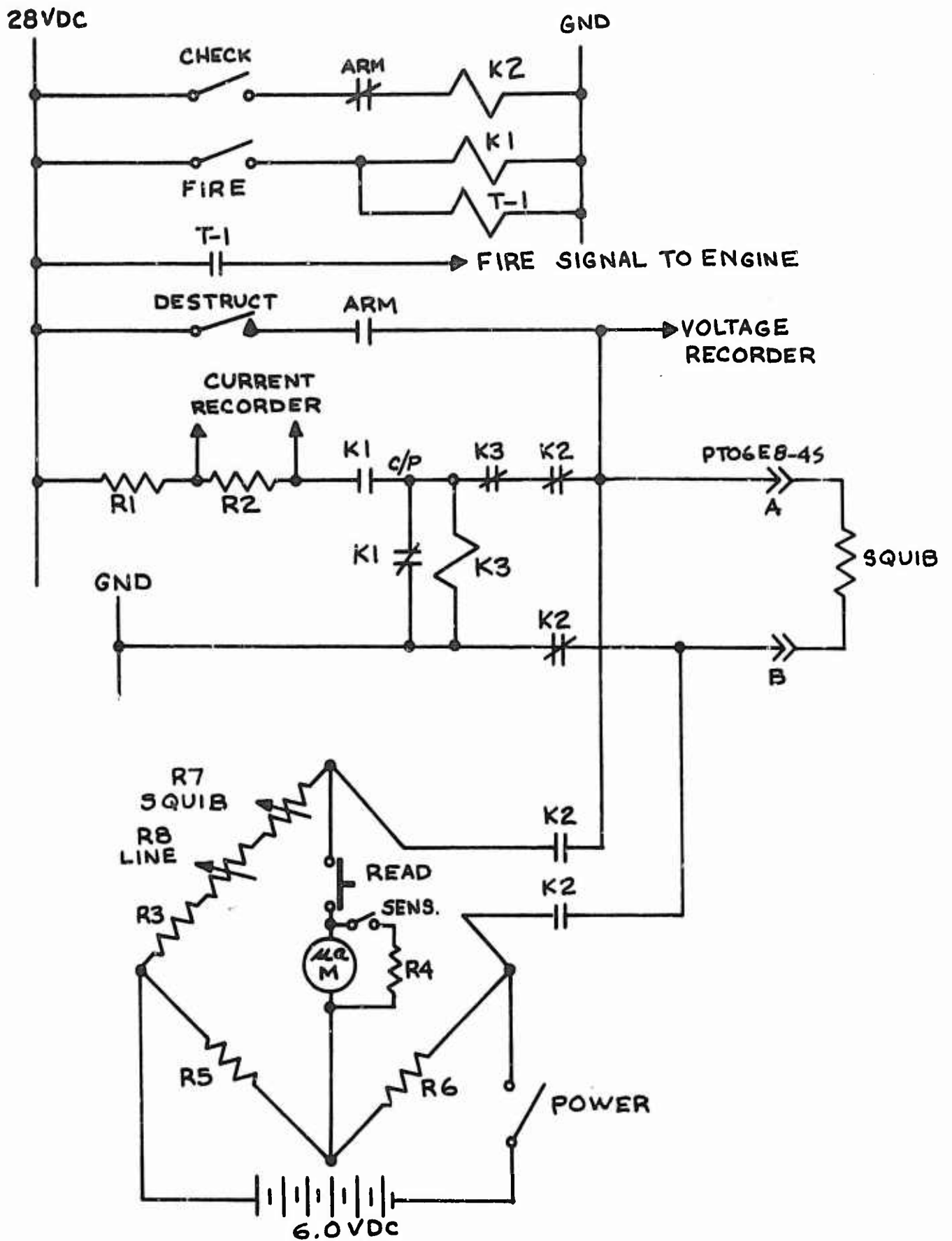


Figure 33 -- GEMSIP Pulse Initiator Circuitry

I. DESIGN REQUIREMENTS

- A. Provide 28 vdc firing circuit limited to 2 amps max.
- B. Provide independent 28 vdc destruct circuit without current limitation.
- C. Provide remote squib resistance check circuit current limited to 10 ma max. with a measuring range of 0 to 10 ohms and sensitivity of 0.050 ohms.

II. CIRCUIT DESCRIPTION (See Figure 33)

A. CHECK CIRCUIT

The check circuit is comprised of a Wheatstone-type resistance bridge utilizing 0.01% tolerance resistors. The bridge ratio is established at 100:1 by the fixed ratio of R5 to R6. Values of line and squib are measured directly by use of 10-turn precision potentiometers R7 and R8 equipped with direct reading dials. R3 provides current limitation at 10 ma max. The null indicator is 50-0-50 micrometer protected by sensitivity resistor R4. The check power source is a 6.0 vdc mercury cell battery.

B. FIRING CIRCUIT

The firing circuit is a 28 vdc system current limited by resistor R1 to 2 amps max. Firing relay K1 is wired to apply a direct short to the squib until energized by manual fire switch. At fire switch, K1 shuttles to remove short and apply power in a break-before-make operation to prevent inadvertent grounding of the power source at initiation. Timer T1 provides a delayed sequence to engine ignition, allowing pre-ignition of the pulse squib. T1 is a variable R-C timer repeatable to set within 0.005 sec. Squib firing current is measured and recorded by a current sensing galvanometer whose voltage source is the voltage drop across resistor R2.

II, B, Firing Circuit (cont.)

Initiation time is measured and recorded by use of a voltage switch trace. The firing circuit is protected from short circuiting by relay K3, which receives fire signal simultaneous with squib and disconnects power source within 7-msec relay pick-up time.

III. THEORY OF OPERATION

A. The check circuit is energized by the control room switch energizing relay K2, which cuts off the firing circuit and connects the resistance bridge.

B. A direct short circuit is applied in place of the squib at the test stand. The squib dial is set to zero and the line dial is rotated to provide a meter null. The line dial is locked in this position. Line resistance is now irrelevant to the measuring circuit.

C. The short circuit is now removed and the squib is installed. Step B, above, is repeated using the squib dial to obtain squib resistance.

D. The check switch is cut off automatically at the engine sequence arm to prevent accidental firing into the measuring bridge instead of the squib which would cause a system and test malfunction.

E. Firing is automatically initiated by engine command fire switch and a manual destruct capability is provided after engine sequence arm switch to override firing circuit in case of a malfunction.

IV. VARIATIONS AVAILABLE

A. K1 may be wired to receive initiation from a pressure sensitive switch (TCDS) for applications of pulsing system at some fired Pc level.

B. Additional pulse circuits may be gauged and timer sequenced to ignite in a series arrangement at either some preset time or some predetermined Pc levels.



Figure 34 -- Installation of Fuel Single Pulse Generator on 91-5

Engine

II. SINGLE PULSE GENERATOR

Unstable combustion has often been attributed to disturbances in the propellant feed system. The early work of Summerfield explored in this direction, and from these studies he developed a model for unstable combustion induced by feed system perturbations. It is now known that this is only one of the ways by which unstable combustion may be excited and that it is associated with the lower frequency chamber oscillations usually referred to as "chugging."

No standard of amplitude, rise rate, or duration has yet been generally accepted for classifying the tolerance of rocket engines for feed system pulsing. For the GEMSIP Program, the requirement as set forth in Exhibit A, Paragraph B.3, states:

"Pulsing tests of the engine feed system in both the fuel and oxidizer lines shall be conducted to evaluate the response and coupling characteristics of the feed, injection and combustion systems and to determine the effect on injector stability. This pulse shall be 20% greater than the working pressure of the system at the point injected or the limiting pressure, whichever is less. The pressure rise rate shall be equal to or greater than 350,000 psi per second."

Several techniques have been used for producing feed system perturbations, but no one has been recognized as best for all occasions. For GEMSIP, two devices were developed -- the continuous pulse generator, discussed in Section III of this volume, and the single pulse generator which follows here (Figure 34).

A search of the literature revealed that the Rocketdyne Division of North American Aviation had developed a single pulse generator that had been used for both the H-1 and F-1 programs. The Rocketdyne reports state that the pulse generator operated in the following manner: a smokeless powder charge, contained within a cavity behind a "hammer," was ignited electrically. When the burning

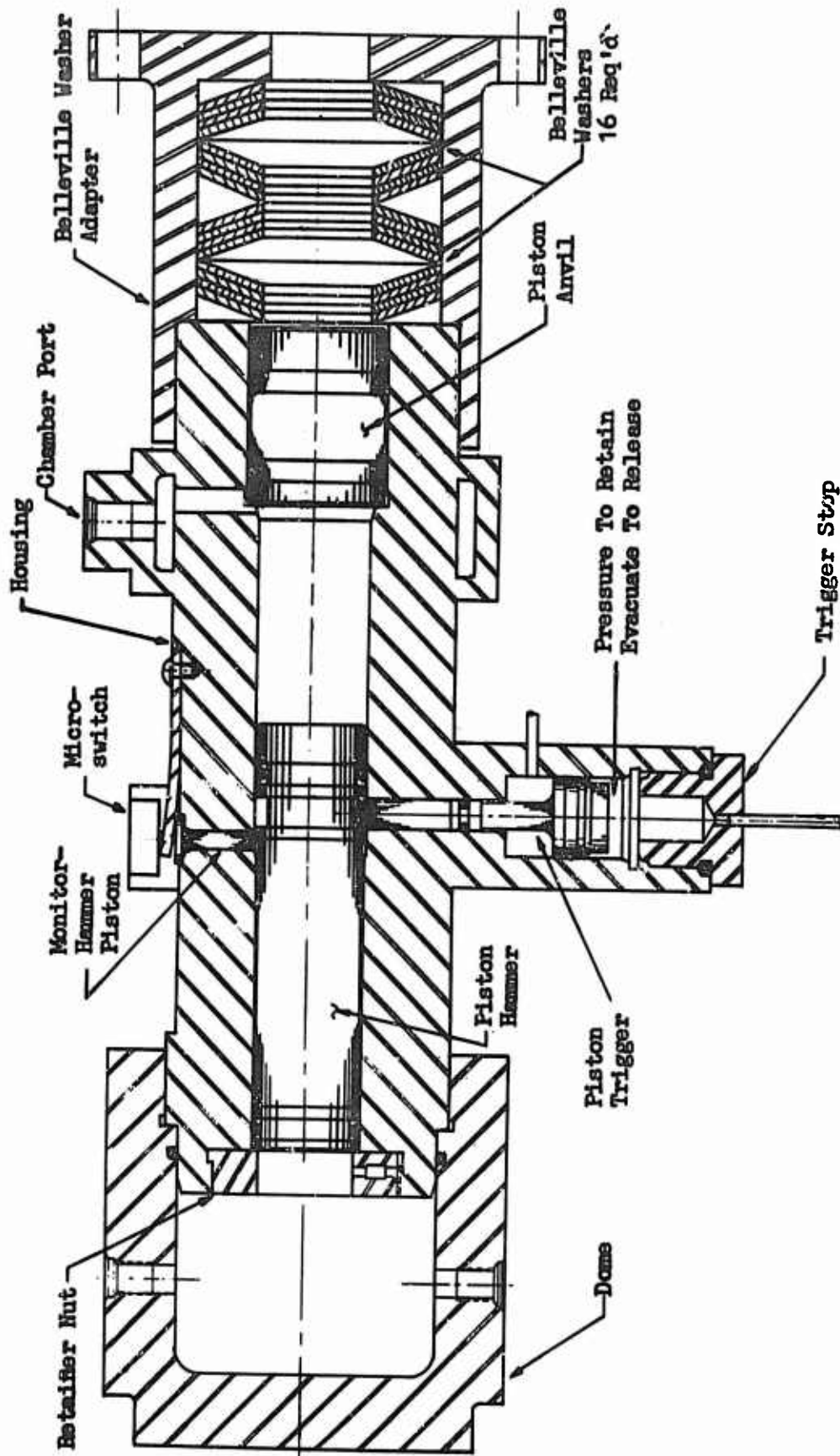


Figure 35 -- Cross-Section of GEMSIP Single Pulse Generator

II, Single Pulse Generator (cont.)

charge had generated sufficient pressure, two hammer-holding pins sheared, permitting the hammer to impact upon the backside of a piston, the frontside of which was in intimate contact with the working fluid. The resulting compression of the liquid generates a high-energy short-duration pressure pulse.

A. DESIGN

The single pulse generator (P/N 704716) designed for use on the GEMSIP is similar to the Rocketdyne pulser in that it utilizes the mechanism of one piston striking another to produce a steep-fronted high-energy wave. However, high pressure nitrogen gas instead of a powder charge produces the driving force for the hammer. Figure 35 shows a cross-section of the GEMSIP single pulse generator.

The single pulse generator consists of the following seven major components: anvil piston, hammer piston, trigger piston, housing, Belleville washers, Belleville washer adapters, and "dome." Figure 36 shows an exploded assembly of these components.

The anvil piston (Figure 37) is machined from 431 stainless steel, which is heat-treated to a hardness of Rockwell C 38-43. It is 1.362 in. in diameter and 1.850 in. long. Two grooves are machined in the anvil piston to accept butyl rubber O-rings and Teflon back-up rings.

The hammer piston (Figure 37) is also machined from 431 stainless steel with a hardness of Rockwell C 38-43. It is 1.183 in. in diameter and 4.421 in. long. Heat-treated AISI 431 stainless steel was chosen to prevent mushrooming at the impact end of the piston.

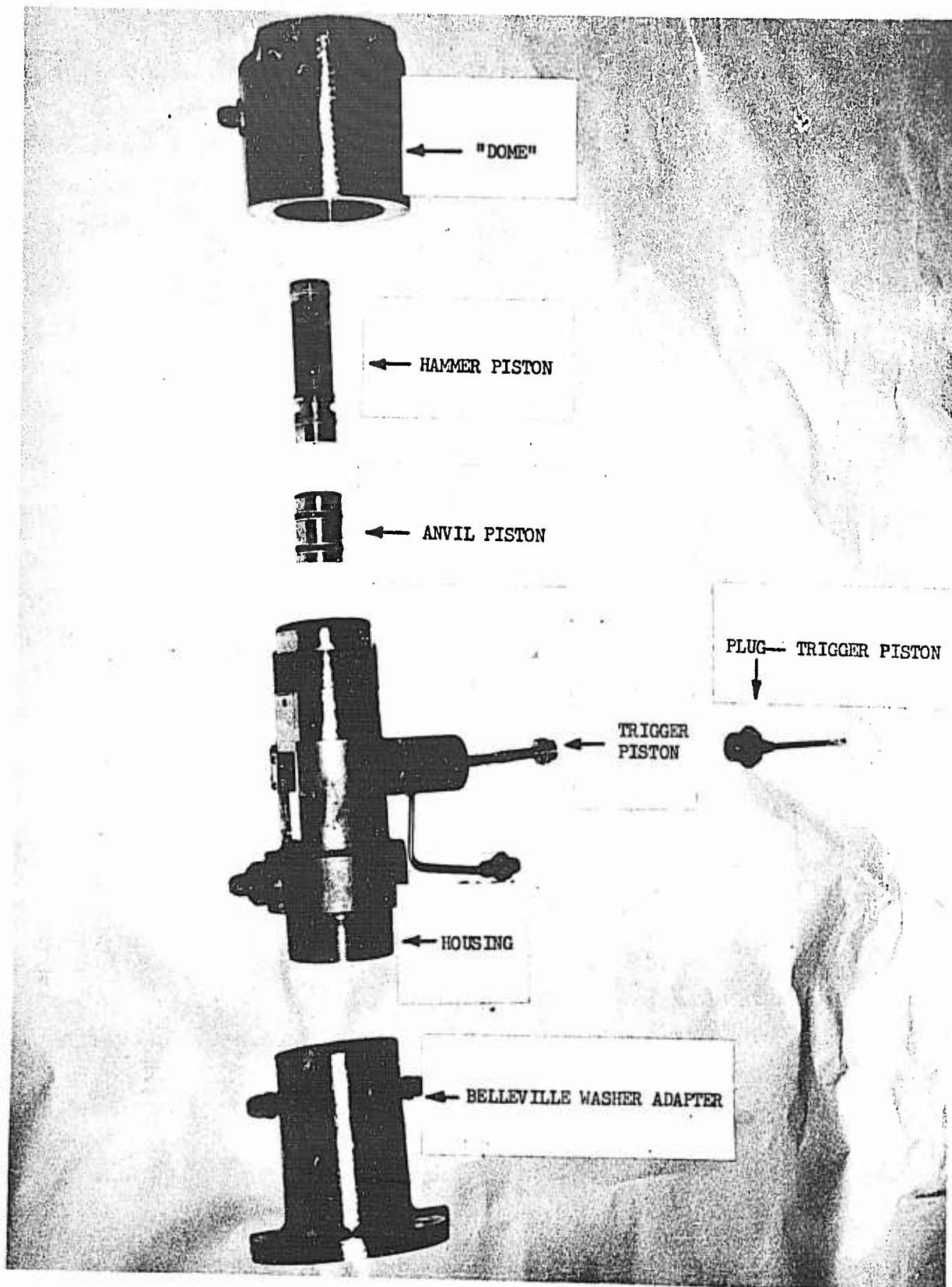


Figure 36 -- Exploded Assembly of Single Pulse Generator

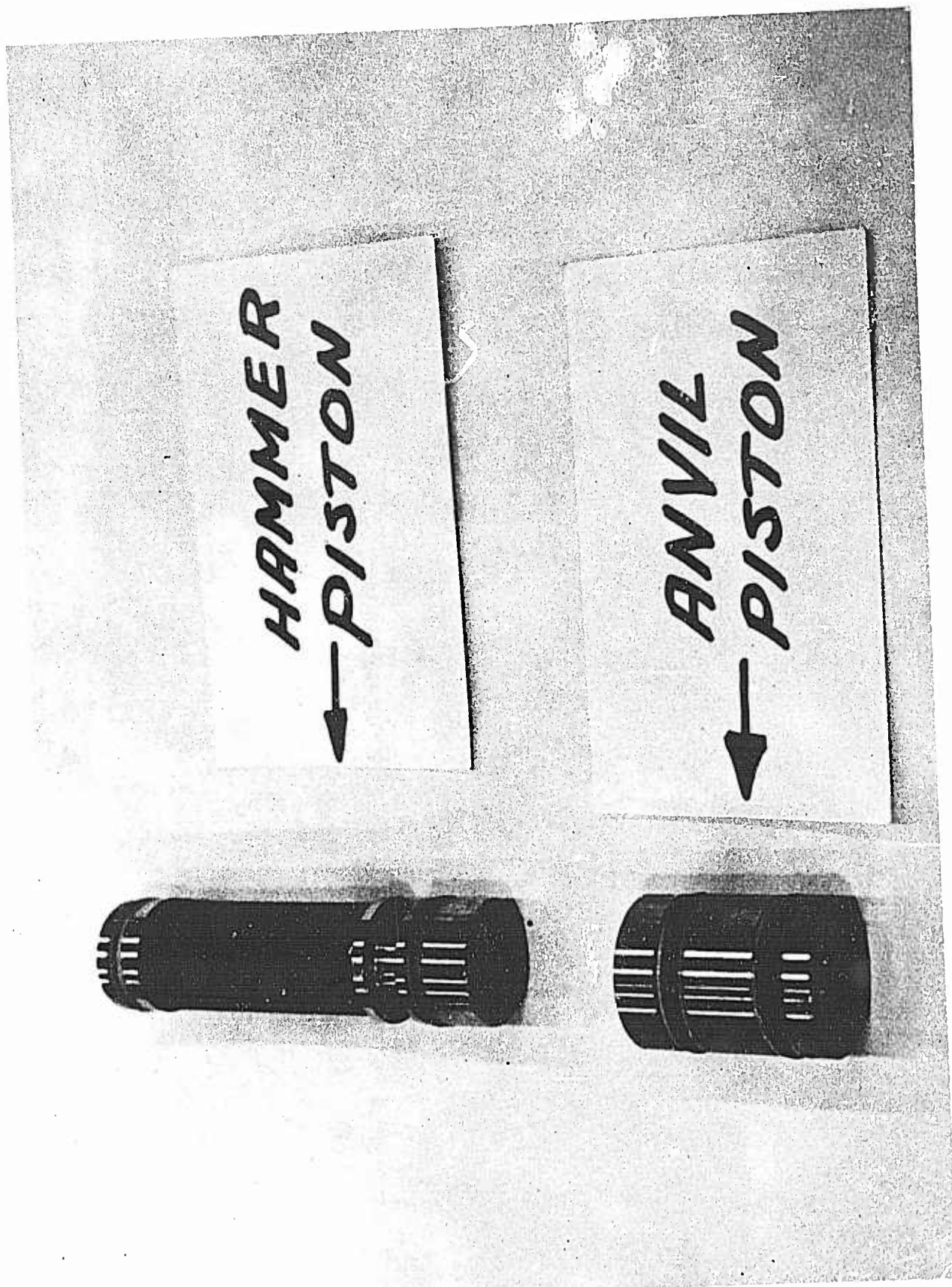


Figure 37 -- Anvil and Hammer Piston

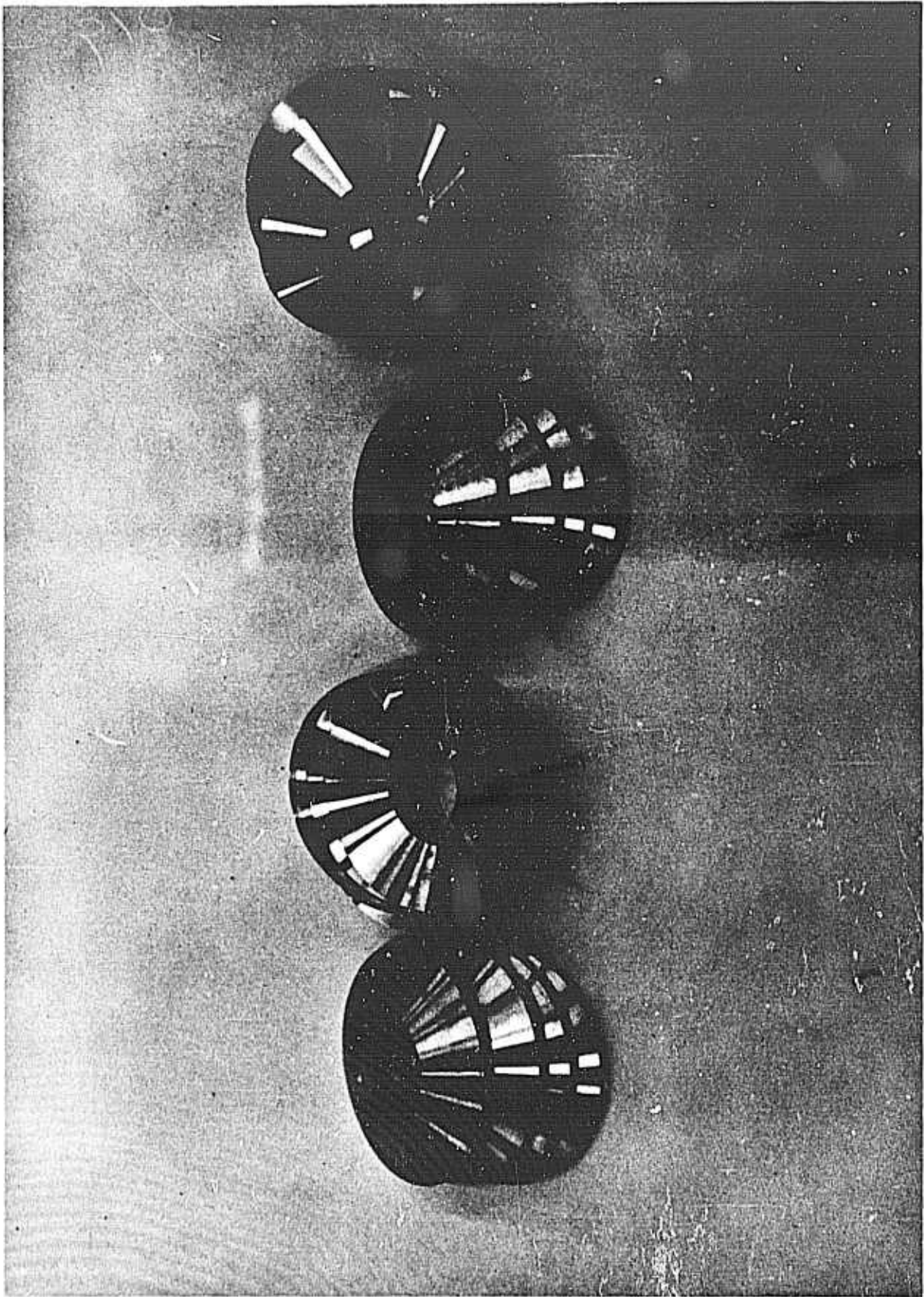


Figure 38 -- Belleville Washers

II, A, Design (cont.)

Two O-ring grooves are machined, one at each end of the hammer piston, and another deeper groove is machined for insertion of the trigger piston (see Figure 35). Butyl rubber O-rings with Teflon slipper seals are used for dynamic sealing in order to decrease the coefficient of dynamic friction.

The trigger piston (see Figures 35 and 36) is machined from AISI 440C stainless steel which has been heat-treated in the following manner:

- (a) Two hours at 1850° to 1900°F; quenched in oil at 150 to 200°F.
- (b) Double stress-relieved at 350°F for 15 minutes; quenched with water.
- (c) Tempered at 1100 to 1150°F for two hours to a hardness of Rockwell C 35-45. The hardness of Rockwell C 35-45 is required so that wear on the tip of the trigger piston will be minimized. The 1100 to 1150°F tempering temperature avoids the brittle zone (750 to 1050°F), so that the trigger piston will be relatively ductile. The AISI 440C stainless steel was chosen because of its high strength which is required because the trigger piston is subjected to a high bending - tension load.

The housing is machined from AISI 431 stainless steel, which has been heat-treated to a hardness of Rockwell C 38-43 (see Figures 35 and 36). The hammer and anvil piston bores are ground to an 8-microin. finish; the trigger piston bore has a 16-microin. finish. This high surface finish is required to minimize sliding friction and wear of the dynamic seals.

The Belleville washers absorb the momentum of the anvil piston after the pulse has been transmitted to the fluid. These washers are machined from PH 15-7 Mo stainless steel, chosen because of its high modulus of elasticity, high tensile strength, and high fatigue strength. They are heat-treated to a hardness of Rockwell C 42-47. Figure 38 shows sixteen Belleville washers.

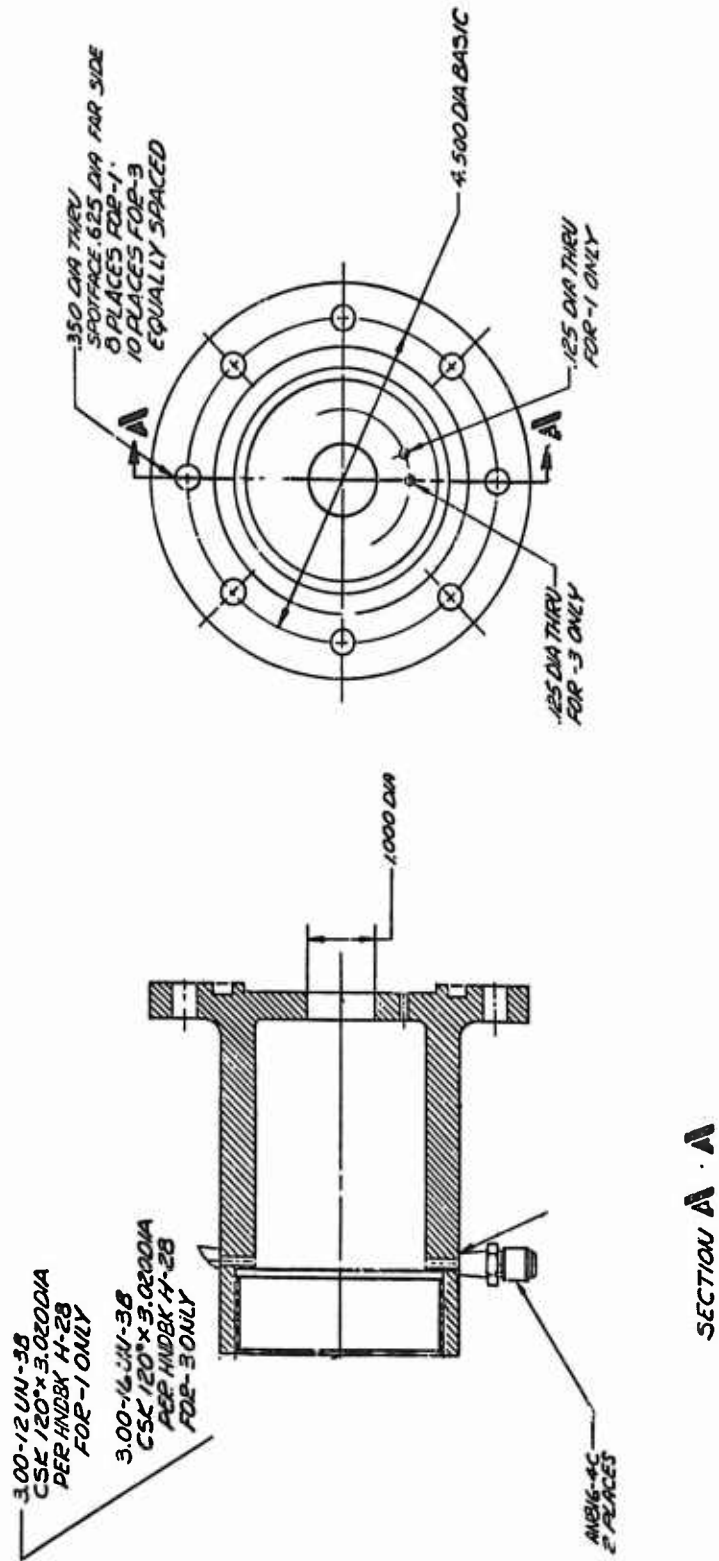


Figure 39 -- Belleville Washer Adapter

II, A, Design (cont.)

The belleville washer adapter contains the belleville washers and provides a means of bolting the generator assembly to the attachment point on the feed system. (See Figure 39). To prevent the possibility of mounting a fuel system pulse generator on the oxidizer circuit, or vice-versa, the belleville washer adapters for the two system units were fabricated with different bolt hole patterns. The adapter for the oxidizer unit has ten bolt holes and 3.00-16UN-3B threads, while the fuel unit has eight bolt holes and 3.00-12UN-3B threads. Welded to the adapter are two AN816 unions, through which air can be bled from the belleville washer cavity after the unit has been attached to a feed system. The hole through the belleville washer adapter is 1.000 in. in diameter.

The dome of the single pulse generator (see Figures 35 and 36) is machined from 347 stainless steel designed for working pressures up to 1500 psi.

B. FUNCTIONING OF THE SINGLE PULSE GENERATOR

The GEMSIP single pulse generator operates in the following manner:

1. The dome and back side of the trigger piston are vented.
2. The chamber portion between the hammer and anvil pistons and the front side of the trigger piston are pressurized. This causes the trigger piston to retract and the hammer piston to be forced up against the retainer nut. When the hammer piston is in the full-up piston, a microswitch is actuated (Figure 40), which verifies the position of the hammer by lighting a light on the control panel.
3. With the front side of the trigger piston pressurized, the back side is then pressurized to drive the trigger piston forward to engage the hammer piston groove. (The trigger piston moves forward when equal pressure is applied to the front and back because of the differential area).

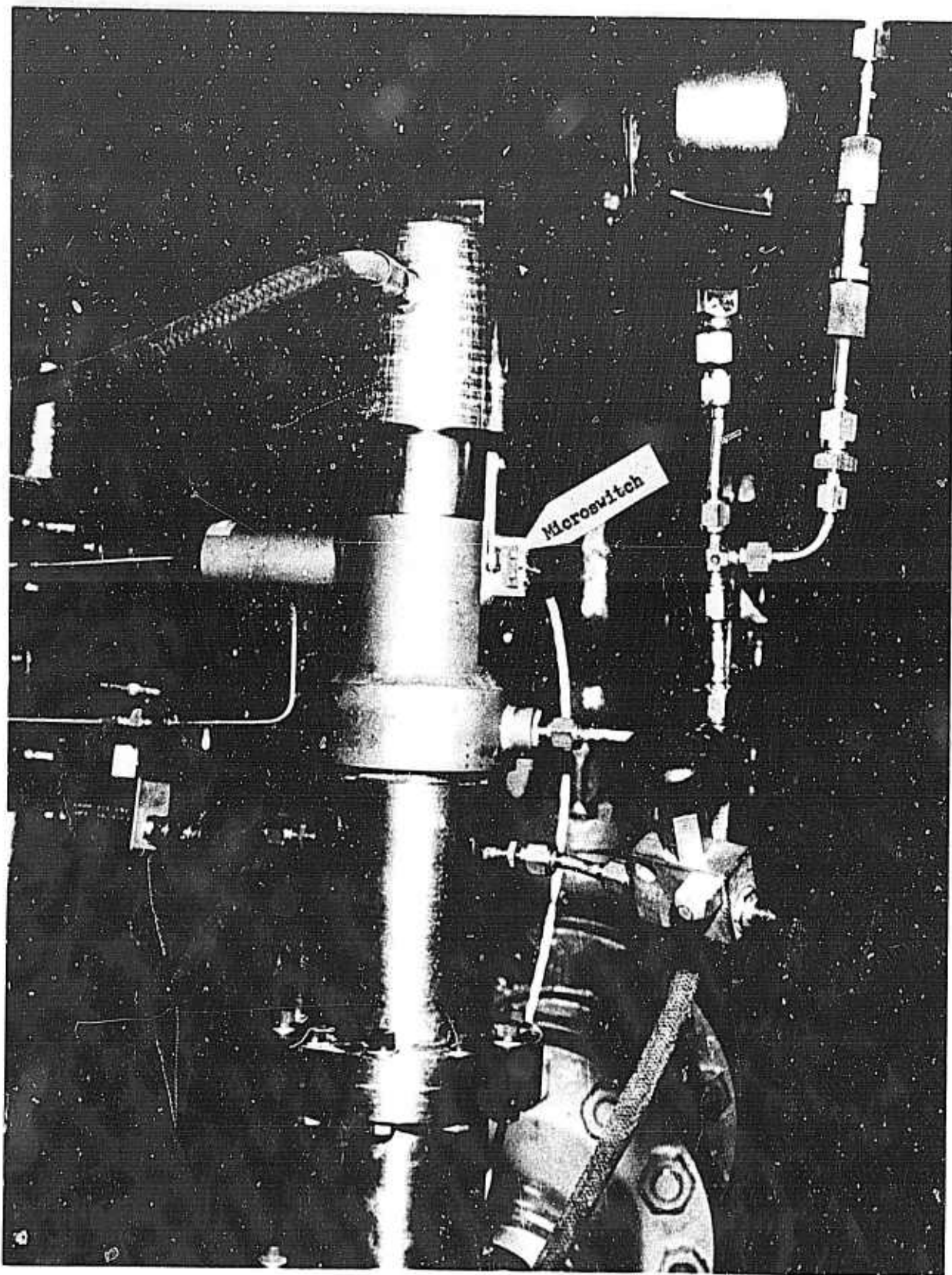


Figure 40 -- Mounting of Single Pulse Generator Microswitch

II, B, Functioning of the Single Pulse Generator (cont.)

4. The dome is pressurized, and the chamber is evacuated. The single pulse generator is now ready to fire.

5. The back side of the trigger piston is vented, which retracts the trigger. This allows the hammer piston to travel down the bore at high velocity and strike the anvil piston, thus transferring energy to the anvil piston through impact. The anvil piston, in turn, transfers the impact energy to the fluid, producing a pulse in the feed system.

C. TRANSFER OF ENERGY THROUGH IMPACT

Figure 41 depicts the propagation of the impact wave through the hammer and anvil pistons. The velocity of an impact wave is dependent upon the velocity of sound in the material in which it travels. Since both pistons are made of the same material, the impact wave travels at the same velocity in both.

In Figure 41, (1) is the hammer piston and (2) is the anvil piston. Figure 41b shows the impact waves traveling opposite directions, with each wave containing some finite energy,  $\bar{A}$ . At the same time shown in Figure 41d, the wave in (2) reaches the end of the piston exposed to the fluid and part of the wave is transmitted to the fluid, while the remainder is reflected back into piston (2).

Let  $K\bar{A}$  equal the part transmitted to the fluid and  $(1-K)\bar{A}$  be the reflected portion of the wave. The  $(1-K)\bar{A}$  wave continues to travel through the anvil piston (2), passes into the hammer piston (1) and through the  $\bar{A}$  wave. At the time shown in Figure 41i, the  $\bar{A}$  wave reaches the contact end of the hammer (1) piston. At this time, the anvil piston (2) moves away from the hammer piston (1).

Wave  $(1-K)\bar{A}$  remains echoing in piston (1), losing some energy every time it is reflected from an end face, until it decays.

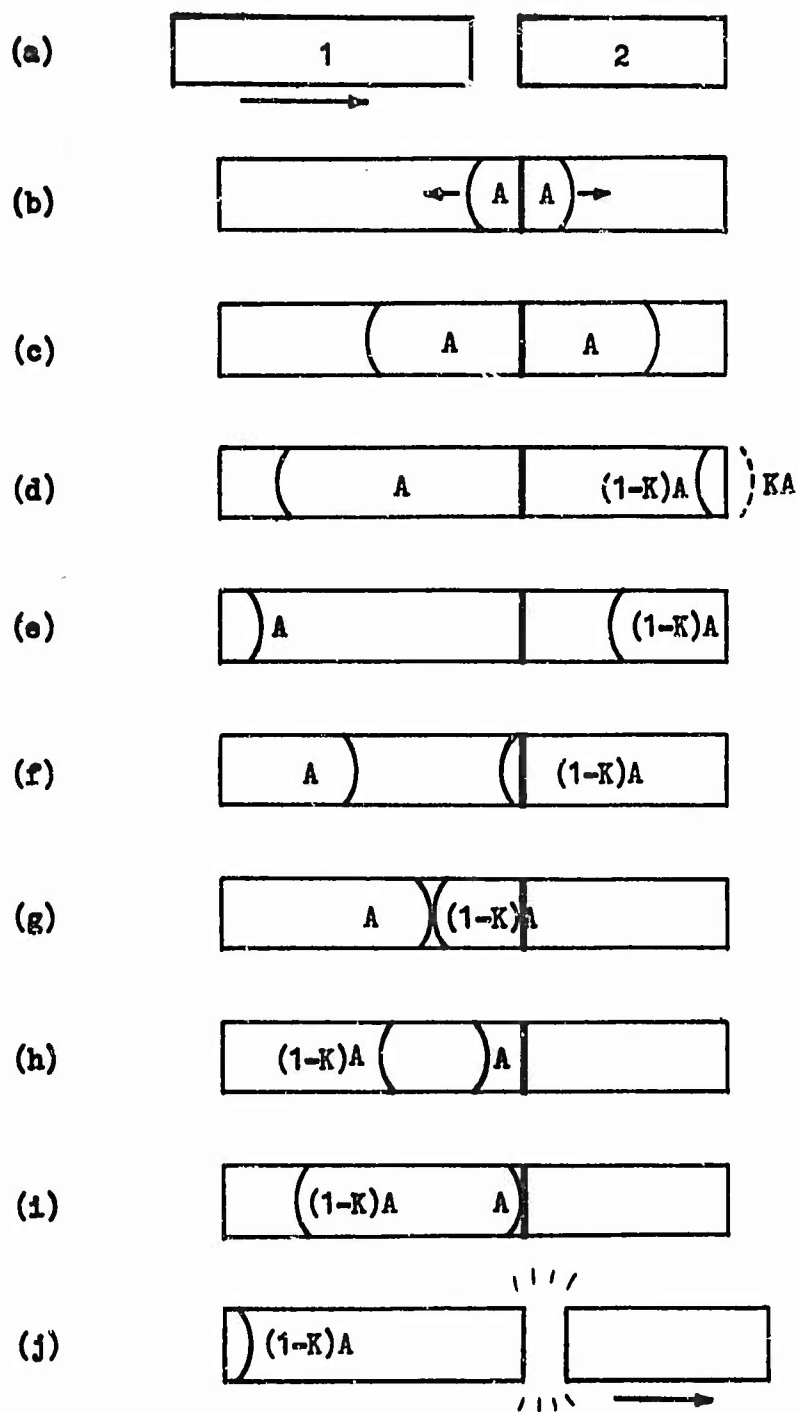


Figure 41 -- Propagation of Impact Wave

II, C, Transfer of Energy Through Impact (cont.)

It is possible to calculate the magnitude of the wave transmitted to the fluid using the method described by Goldsmith\*.

Step 1. Calculation of the velocity of the hammer piston at impact:

$$F = M a = P A_1 \text{ or} \quad (1)$$

$$A = \frac{P A_1}{M_1} \quad (3)$$

Where:

a = Piston acceleration

F = Force on back side of hammer piston

$M_1$  = Mass of piston (1) =  $0.03 \frac{\text{lb} \cdot \text{sec}^2}{\text{ft}}$

P = dome pressure =  $1000 \text{ lb/in.}^2$

$A_1$  = Area of piston (1) =  $0.95 \text{ in.}^2$

For the conditions above, and the following assumptions:

- a. Constant pressure during stroke
- b. No losses due to friction
- c. No back pressure buildup (i.e. evacuated "chamber")

$$s = 1/2 at^2 \text{ or } t = \frac{\sqrt{2s}}{a} \text{ where} \quad (4) \text{ and } (5)$$

$$a = 31,600 \text{ ft/sec}^2 \text{ and}$$

$$s = \text{stroke length} = 0.187 \text{ ft.}$$

then

$$t = 0.00344 \text{ sec} - \text{hammer piston traveltime}$$

$$V = at = \text{velocity of hammer piston at impact}$$

$$V = 94.8 \text{ ft/sec}$$

\*W. Goldsmith, Impact (Edward Arnold Publishers: 1960) pp. 267-276.

II, C, Transfer of Energy Through Impact (cont.)

Step 2. Calculation of Stress at Piston Impact

$$\text{Stress} = \rho V_0 C = 83,700 \text{ lb/in.}^2$$

Where

$$\rho = \text{density of piston material} = 15.3 \frac{\text{lb/sec}^2}{\text{ft}^4}$$

$$C = \text{acoustic velocity in material} = 5,400 \frac{\text{ft}}{\text{sec}}$$

$$V = \text{average velocity of two pistons at impact} = \frac{(94.8 + 0)}{2} \text{ ft/sec}$$

Assuming elastic impact.

Step 3: Calculation of the stress transmittal ratio (amount of shock energy transferred to the fluid)

$$\text{Stress transmittal ratio} = \frac{2A_p \rho_p C_p}{A_p \rho_p C_p + A_f \rho_f C_f}$$

where the subscripts p and f denote piston and fluid acoustic properties respectively.

$$\text{Stress transmittal ratio} = 6.75\%$$

Step 4: Calculation of the magnitude of the stress wave transmitted into the fluid caused by the initial impact of the pistons.

$$\begin{aligned} \text{Transmittal Wave} &= (\text{stress transmittal ratio}) \times (\text{Impact Stress}) \\ &= 5,650 \text{ psi} \end{aligned}$$

II, C, Transfer of Energy Through Impact (cont.)

It is apparent that this predicted 5650-psi wave (pulse) would adequately fulfill the contractual requirement of a 20% overpressure at the point of applications because the nominal line pressures for the 91-5 feed system are approximately 1000 psi.

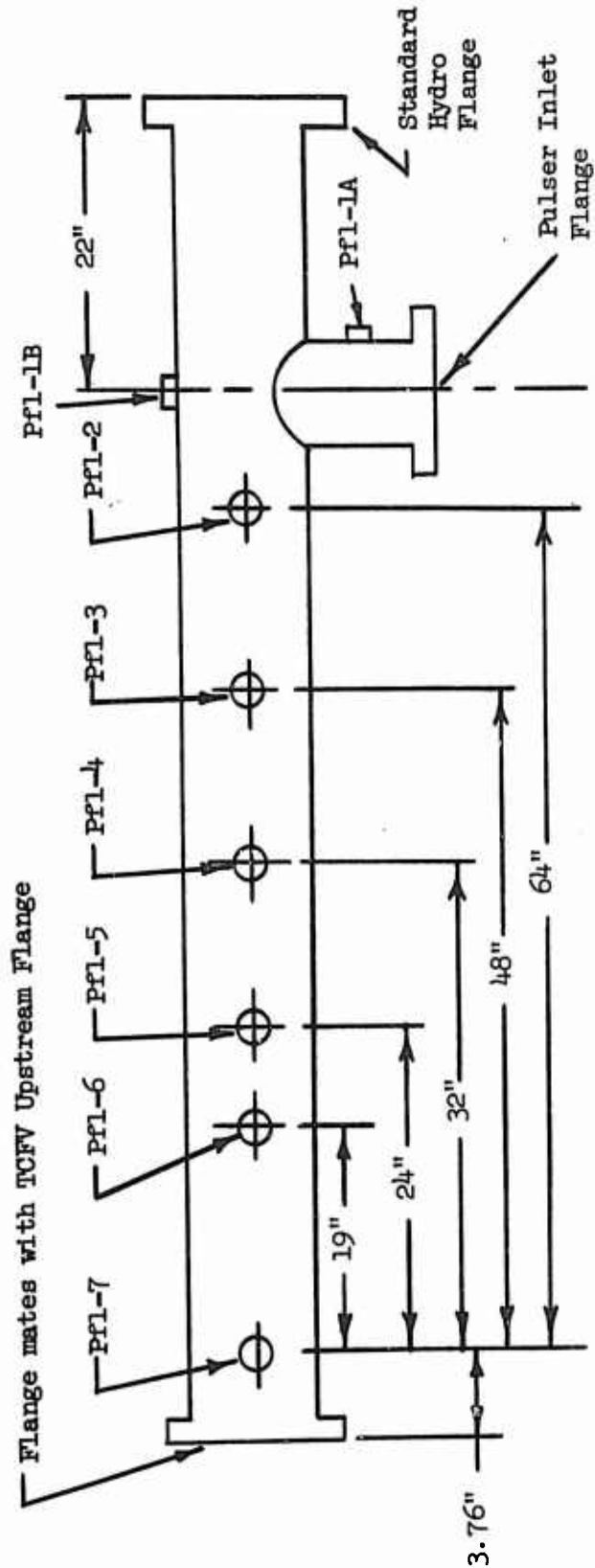
D. DEVELOPMENT TESTING

The development testing of the GEMSIP single pulse generators involved three phases: (1) the functional testing of the pulsers on a calibrated line; (2) the calibration testing of the pulse generators on a 91-5 thrust chamber assembly consisting of a dome, injector, combustion chamber, and inlet elbows; and (3) an evaluation and demonstration series on a hot firing second stage Titan engine system.

1. Functional Testing

The functional testing phase involved the pulsing of a calibrated line (T605011) in the Research and Development Shops Hydraulics Laboratory (Figure 42). The line was flowed with water at nominal engine flowrates corrected to water flow with a back pressure of 1000 psi. The calibrated line is a straight section of pipe with approximately the same inside diameter as the engine propellant line. Welded to the calibrated line is a flange for attaching the single pulse generator. Figure 43 depicts the test set up. This calibrated line provided the capability for mounting six Microsystems PT3F-C2 high frequency pressure transducers at various locations down the line, and one Kistler 701 transducer directly opposite the pulser inlet.

Initially, multirecording capability was not available in the hydro-lab; only one function at a time could be monitored on an oscilloscope with a Polaroid picture recording the trace. This method proved to be both inadequate and time-consuming. Therefore, a portable Ampex tape recorder was obtained and all



- Notes:
- 1) Line is made of 3-in. nominal x 0.337 wall--CRES 304 Pipe
  - 2) Inside Diameter is 2.76-in.
  - 3) Pfl-2 through Pfl-7 Accept Microsystems PF3FC2 Flush Mounted High Frequency Transducers
  - 4) Pfl-1A and Pfl-1B Accept Kistler 701 Flush-Mounted High Frequency Transducers

Figure 42 -- GEMSIP Calibrated Line

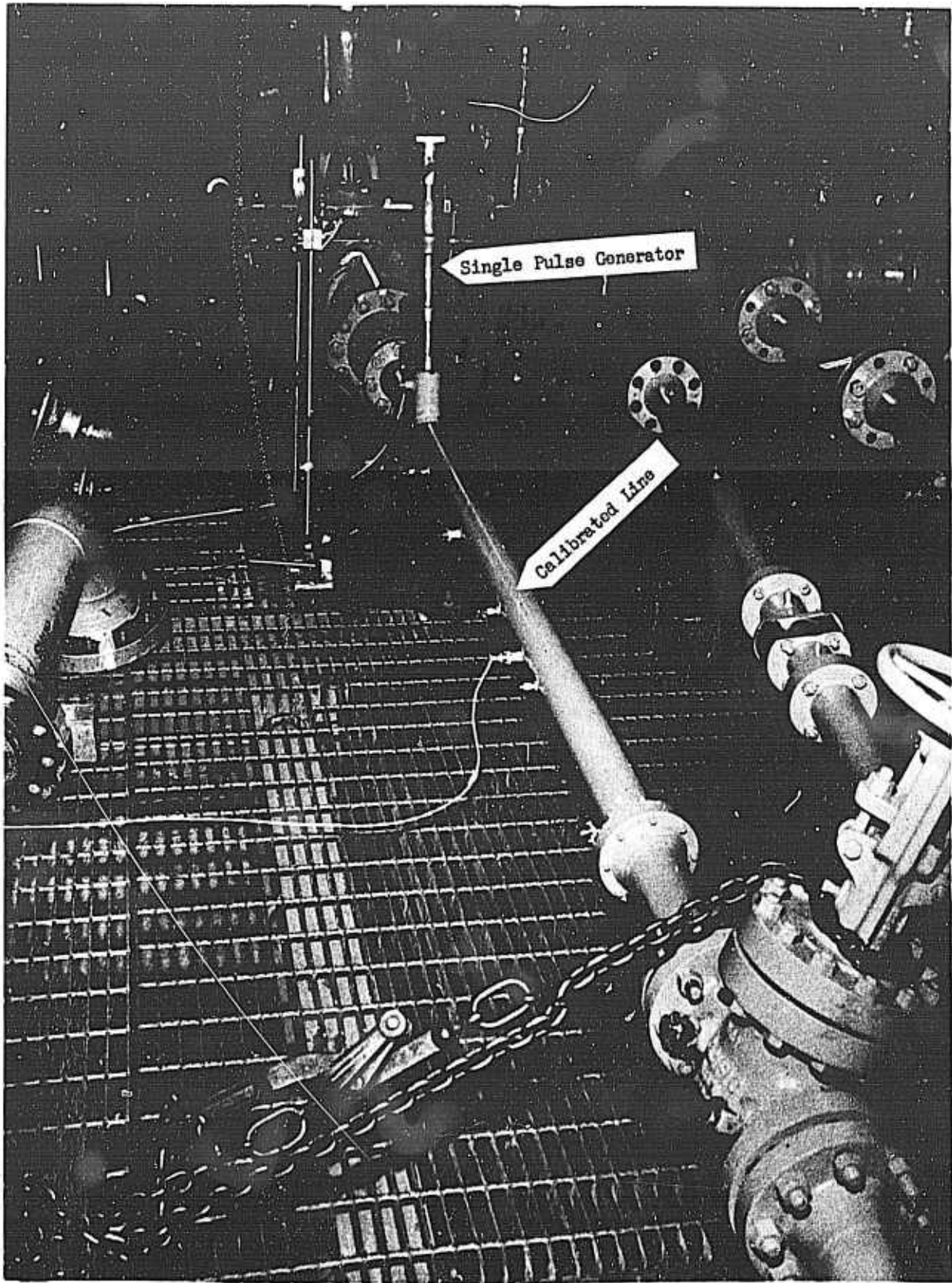


Figure 43 -- Setup for Pulse Generator Functional Tests

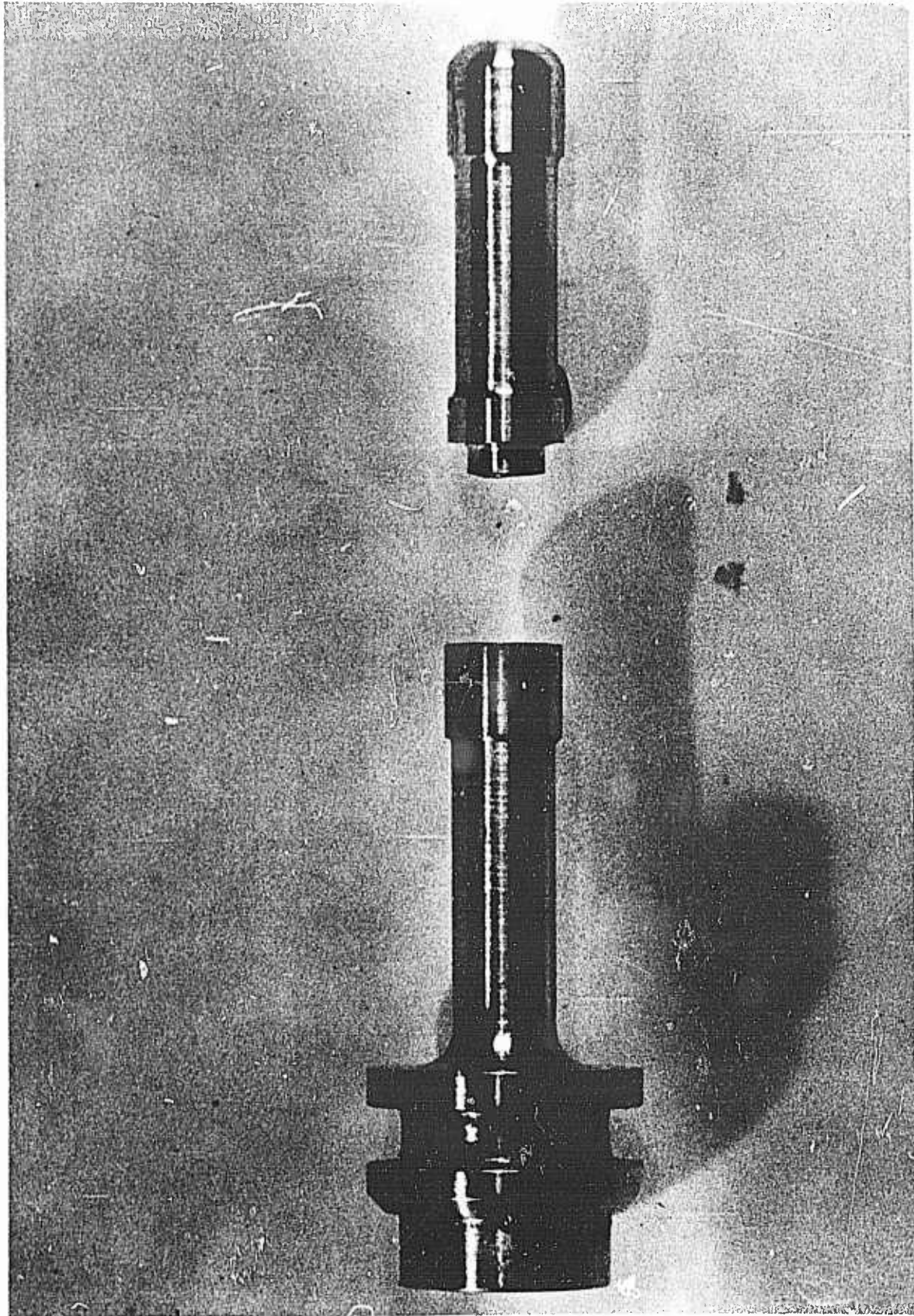


Figure 44 -- Trigger Piston Failure

II, D, Development Testing (cont.)

transducers were monitored simultaneously on tape. The tape was played back at a reduced speed and the output was recorded by a standard oscillograph. This technique had advantages of high readout speed, good resolution of pressure spikes, and the capability for producing filtered playbacks if necessary.

During the functional tests with the fuel single pulse generator, the trigger piston failed as shown in Figure 44. An analysis indicated that there was a crystalline or fatigue-type failure which was the result of a combination of two causes: (1) an improper heat treatment resulted in a hardness of Rockwell C 28 instead of the required C 35-45; and (2) during the first series of tests, the hammer piston was inadvertently pushed to the upper position while the trigger piston protruded through the wall (again refer to Figure 35). This put a severe bending load on the trigger piston and accelerated a fatigue-type failure.

To prevent repetition of the error, the control system was modified so that it now is impossible to move the hammer piston while the trigger piston is protruding into the chamber cavity. Subsequent firings of the single pulse generator have not produced another damaged trigger piston.

Approximately 250 functional tests were conducted with the two pulse generators. During these tests, three belleville washers failed in the manner shown in Figure 45. This failure rate is unimportant since there is a total of 16 of these washers in each unit, and they can be checked and replaced very easily.

During the functional testing of the pulse generators, it was necessary to disassemble and reassemble the units several times. The assembly of the pulse generator can be accomplished by one man in about two hours. The major assembly problem is the installation of the trigger and hammer pistons with the Teflon slipper-seals in place. Teflon is a light material and tears very easily. Installation of these slipper-seals is facilitated by applying a generous coat of Dow Corning Lubricant (DC-11) and working the seals lightly with the fingers.

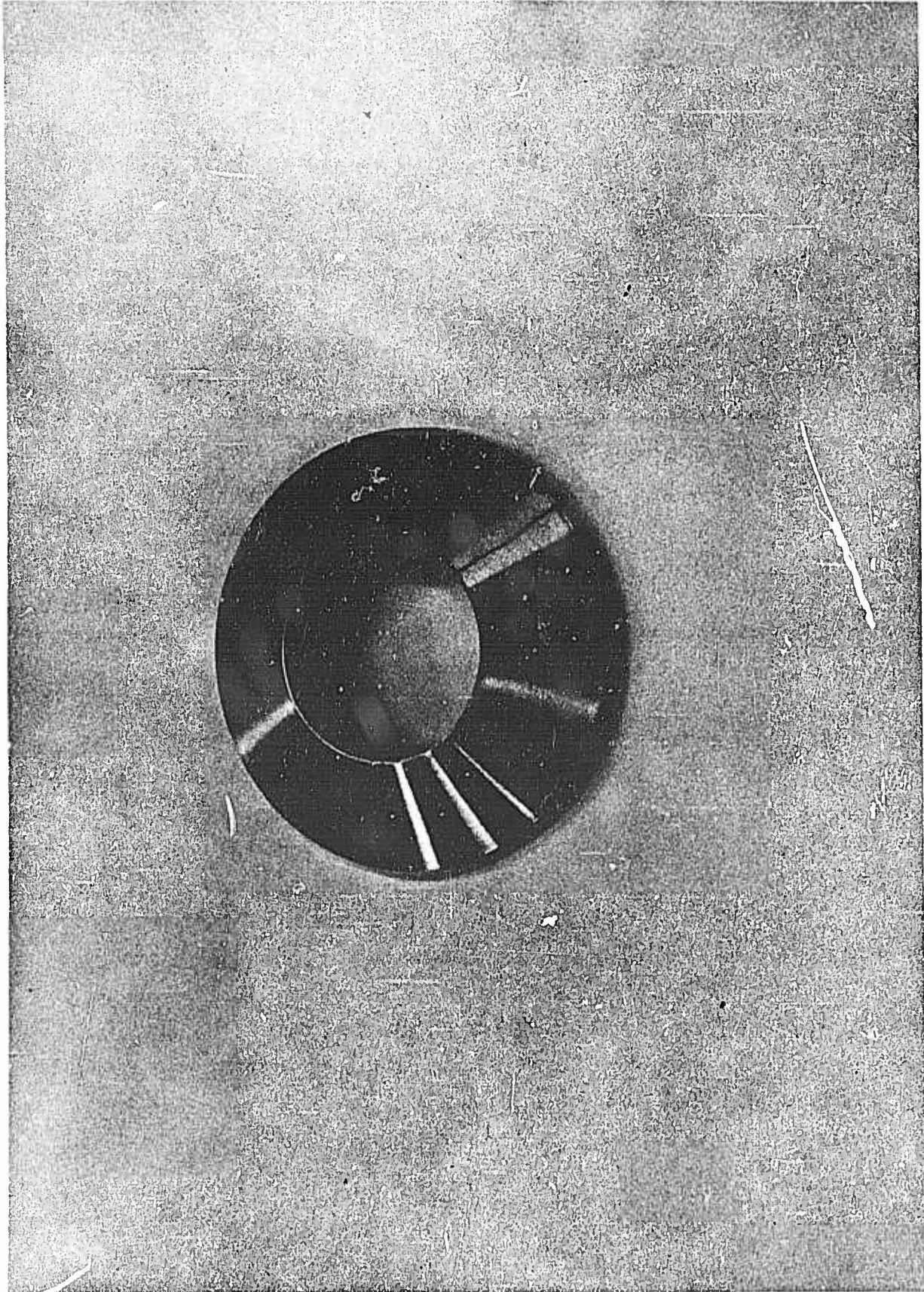


Figure 45 -- Cracked Belleville Washer

II, D, Development Testing (cont.)

A little pressure must be applied to seat the pistons into place. All the pistons should be completely packed with DC-11 and all seals coated liberally with the exception of the durabula gasket used between the housing and the belleville washer adapter.

2. Calibration Testing

A 91-5 thrust chamber assembly was set up in the hydraulics laboratory for the calibration testing of the single pulse generators. The purpose of these calibration tests was to determine the amplitude and transmission characteristics of the pulse as a function of the pulse generator dome pressure.

For the series of tests with the fuel pulse generators, the calibrated line was attached to the fuel inlet elbow, simulating the fuel discharge line to which the single pulse generator was to be attached during engine testing. Figure 46 shows the test setup. The system was flowed with water at 114 lb/sec which allowed to discharge to ambient pressure in the combustion chamber. Static pressure of 350 psi in the calibrated line was maintained by flow control valves.

Data were recorded for pulser dome pressure varying from 100 psi to 900 psi in 100 psi increments. The results of this test series are tabulated in Table 3 and represented graphically in Figure 47. It is evident that a pulser dome pressure of 400 psi will produce the required pulse of 20% overpressure.

For the oxidizer system tests, a 91-5 oxidizer dome was modified to accept the single pulse generator and Microsystem high frequency transducers as shown in Figure 48. The system was flowed at 169 lb/sec of water, which produced a pressure of 300 psi in the dome.

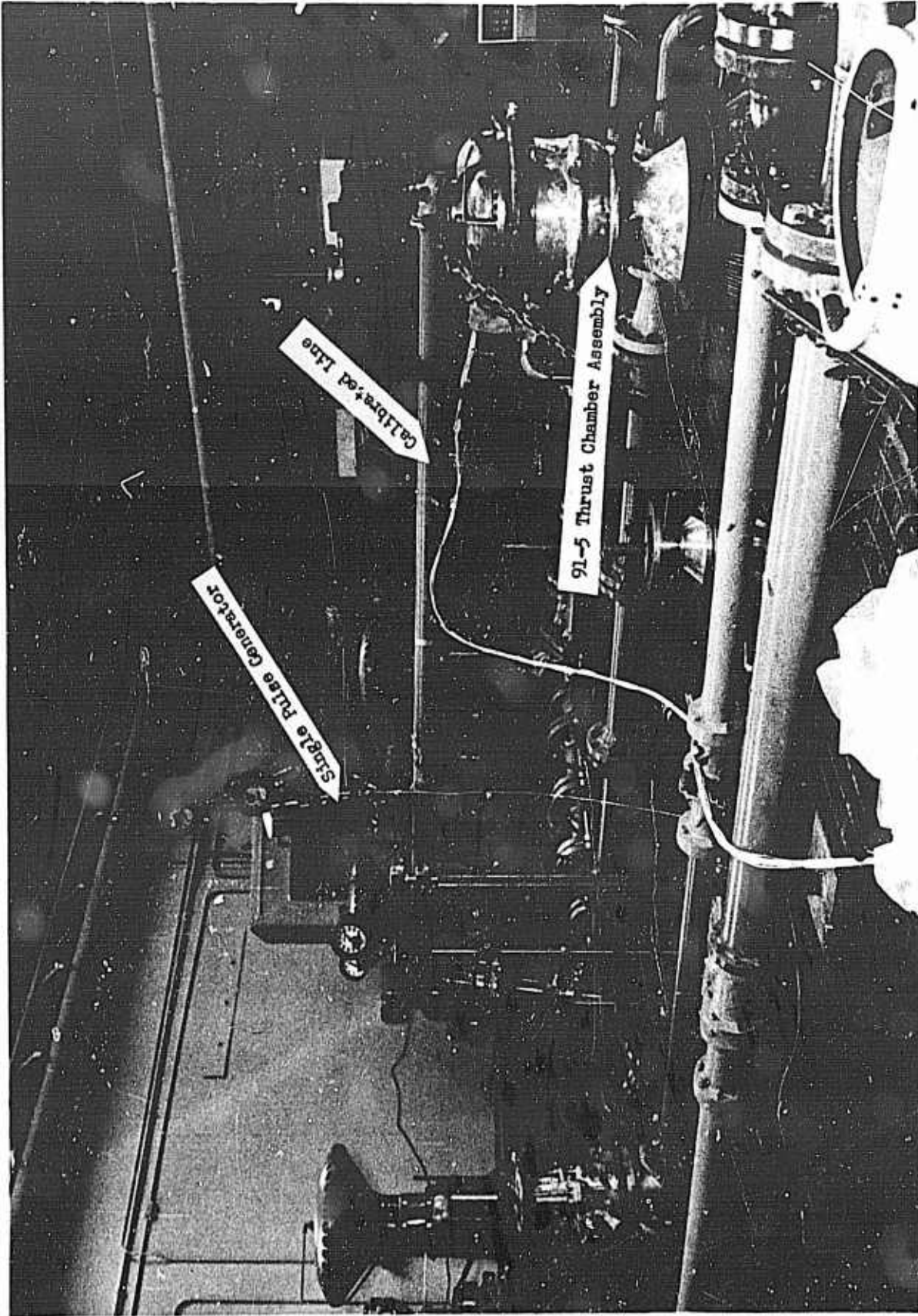


Figure 46 -- Setup for Calibration Tests with Fuel Unit

GEMSIP FR-1, Volume 5

Table 3 -- Calibration Test Data For Fuel Pulse Generator

Test No	SPG Dome Pres.	Pci-2C		Pci-2D		PfJ-1B		PfJ-7F		PfJ-3A		Remarks
		Spike Ampl.	Press Rise Rate									
		psi	psi/sec x 10 <sup>6</sup>									
-050	100	206	4.16	106	2.68	42.8	0.86	22.2	0.89	--	---	PfJ-3A is questionable
-051	200	229	3.85	159	5.34	57.1	1.92	32.2	1.08	--	---	
-052	300	238	4.80	219	7.35	73.5	1.85	45.1	1.81	35.2	1.42	
-053	500	203	11.3	217	10.9	114	3.28	64.4	2.60	47	1.89	
-054	700	182	6.16	212	11.7	143	4.12	83.8	3.38	53.0	2.14	
-055	900	208	5.24	205	114	183	4.62	100	338	76.5	1.93	

Test No	Dome Pres.	Pci-2B		Pci-2A		PfJ-1B		PfJ-2A		PfJ-3A		Remarks
		Spike Ampl.	Press Rise Rate									
		psi	psi/sec x 10 <sup>6</sup>									
-040	300	200	14.3	-	-	109	2.76	66	2.21	38	1.09	Pci-2A lost because of system shcrt
-041	500	205	20.7	-	-	150	4.32	69	2.31	55	1.58	
-042	700	210	21.2	-	-	180	6.07	88	3.54	82	2.07	
-043	900	191	19.3	-	-	188	6.32	105	4.23	62	2.08	

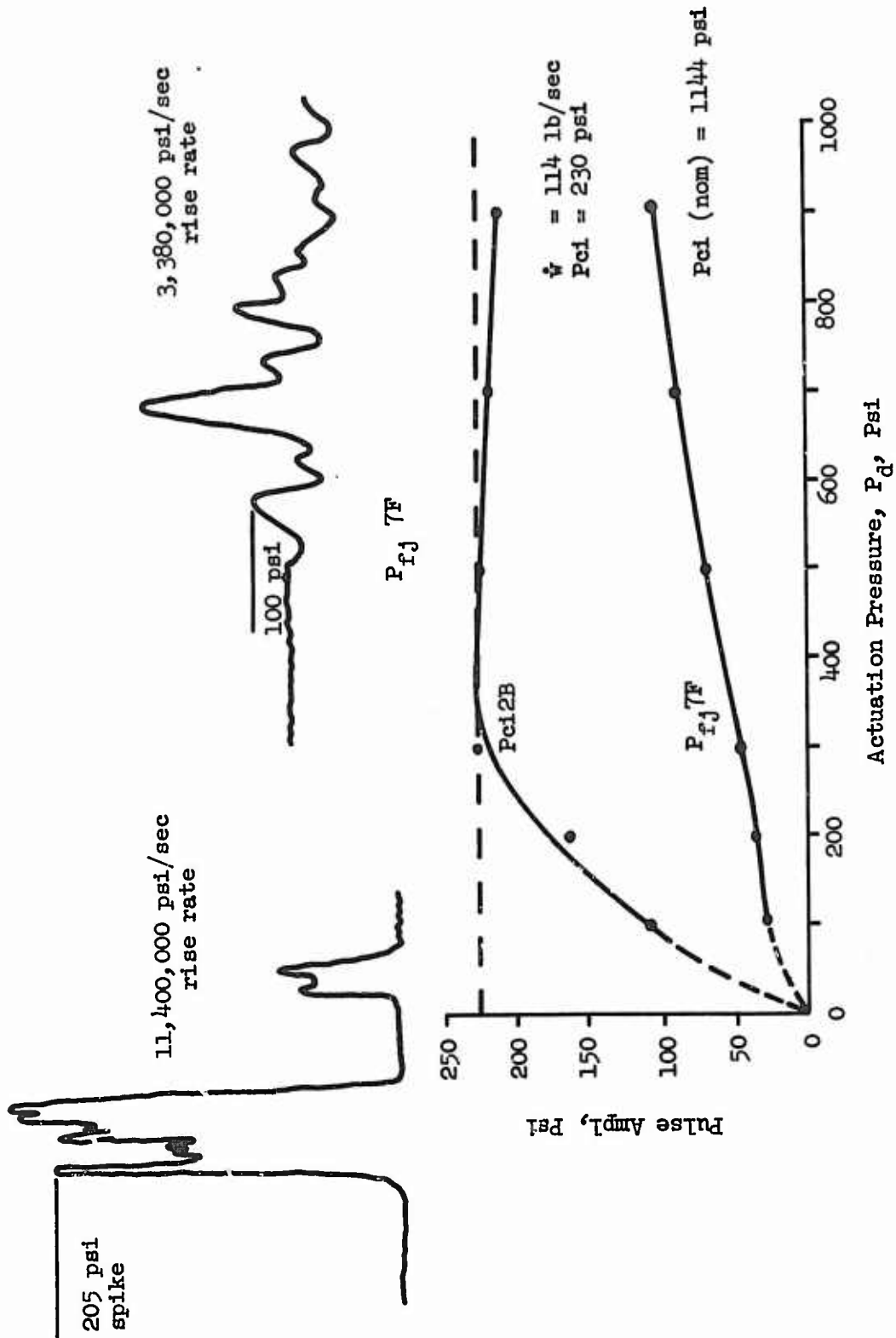


Figure 47 -- Fuel Unit Pulse Amplitude vs "Dome" Pressure

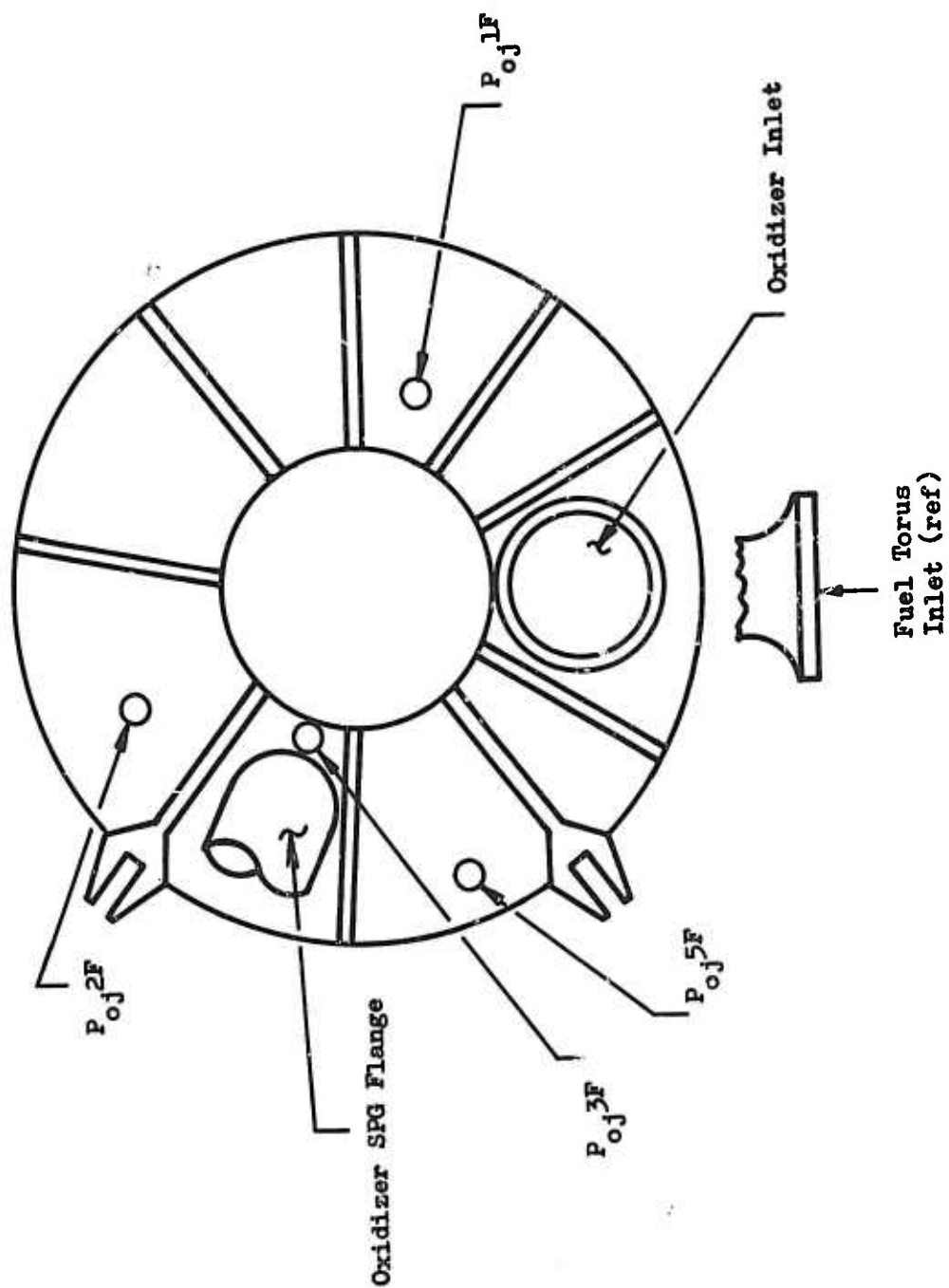


Figure 48 -- Modified 91-5 Dome

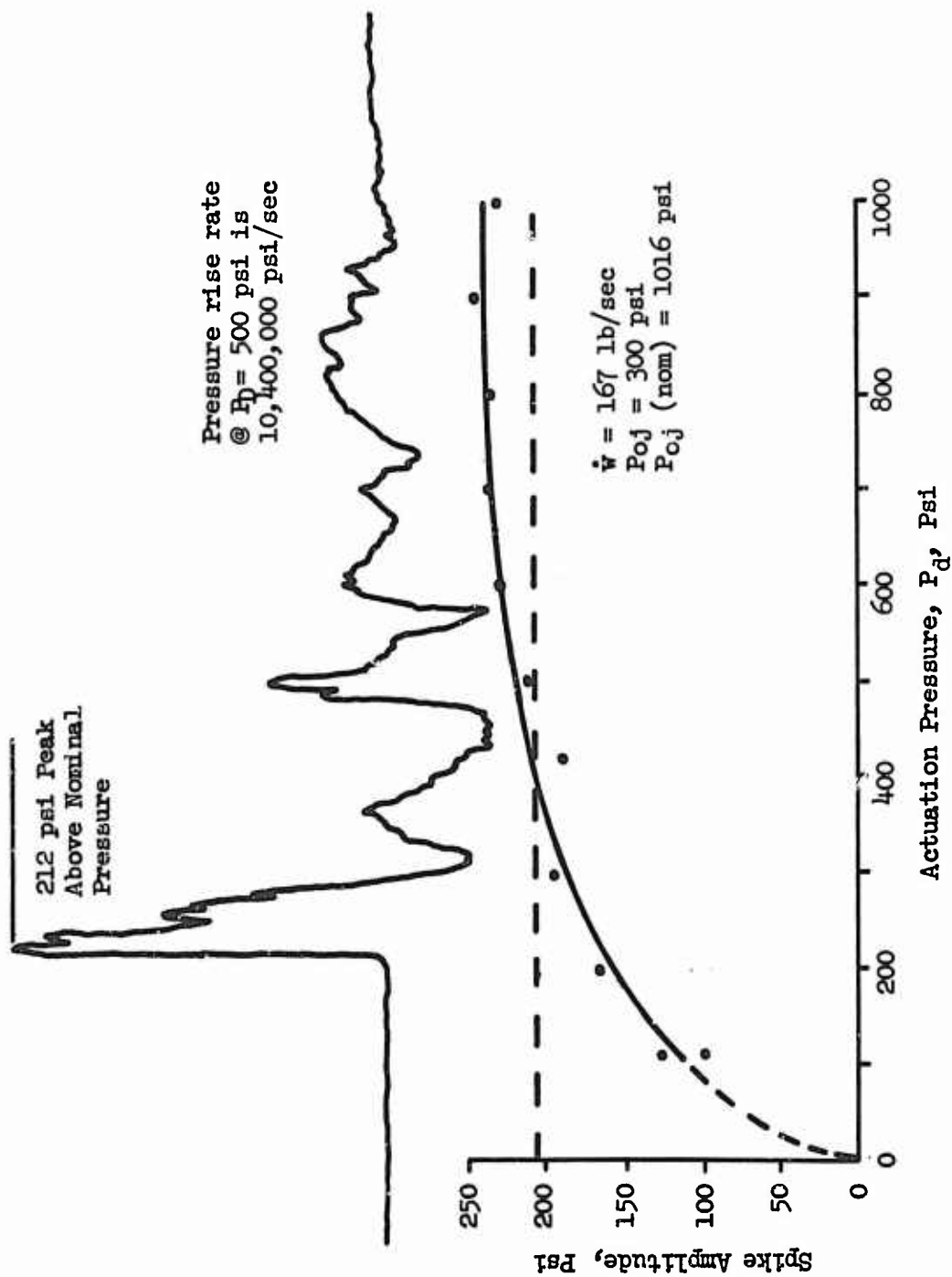


Figure 49 -- Oxidizer Pulse Amplitude vs "Dome" Pressure

II, D, Development Testing (cont.)

Again, the pulse generator dome pressure was varied from 100 psi to 900 psi in 100-psi increments. The results are tabulated in Table 4 and represented graphically in Figure 49 where it is apparent that a pulser dome pressure of 500 psi will produce a contractually acceptable pulse.

After the calibration test series on both the fuel and the oxidizer systems, an attempt was made to pulse the fuel system through the  $P_{fj}$ -3A boss. ( $P_{fj}$ -3A measures the pressure of the fuel in Channel 17 of the injector). An adapter was fabricated to reduce the area of the hole through the belleville adapter from 1.00-in. diameter to 0.007-in. diameter. The test setup is shown in Figures 50 and 51.

This test series showed that the transmission losses through the 0.125 in. tubing attenuated the pulse so much that even at pulser dome pressures of 900 psi,  $P_{fj}$ -7F, located 9 in. from  $P_{fj}$ -3A, showed only a 10 psi increase in noise level.

3. Engine Tests

The single pulse generator was used in conjunction with the GEMSIP early engine test series for two purposes:

(1) To demonstrate the ability of an engine to absorb a perturbation in the feed system without going unstable, when using a candidate injector with a tip-injecting baffle configuration.

(2) To demonstrate the capability of the single pulse generator to produce the required perturbation in the engine feed system.

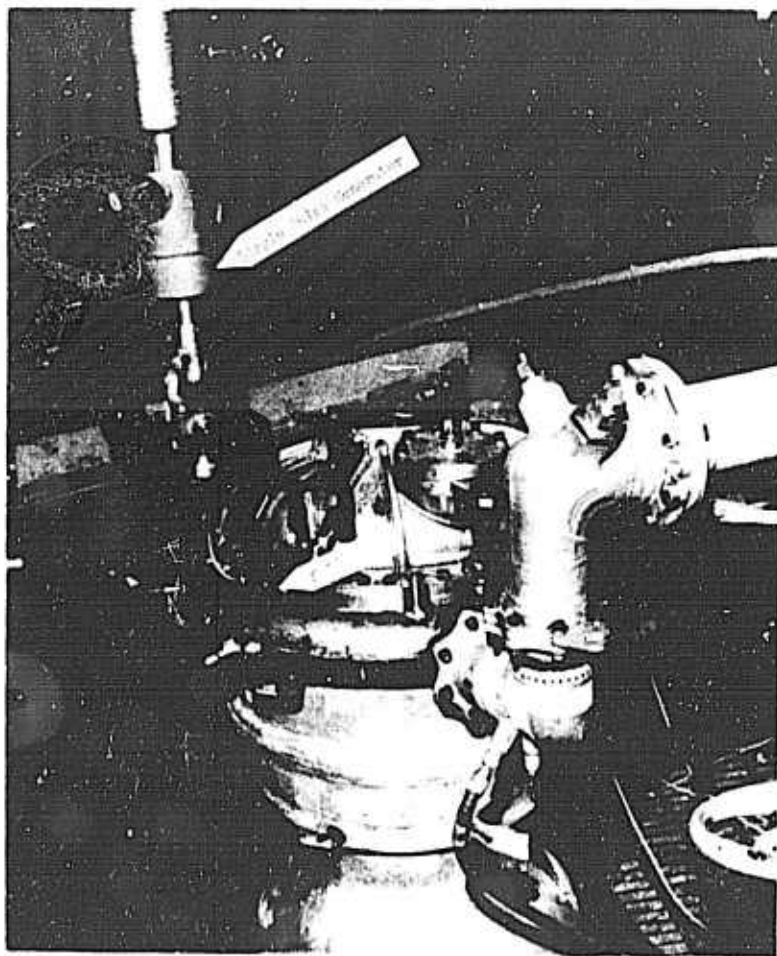


Figure 50 -- SPG Mounted on Chamber

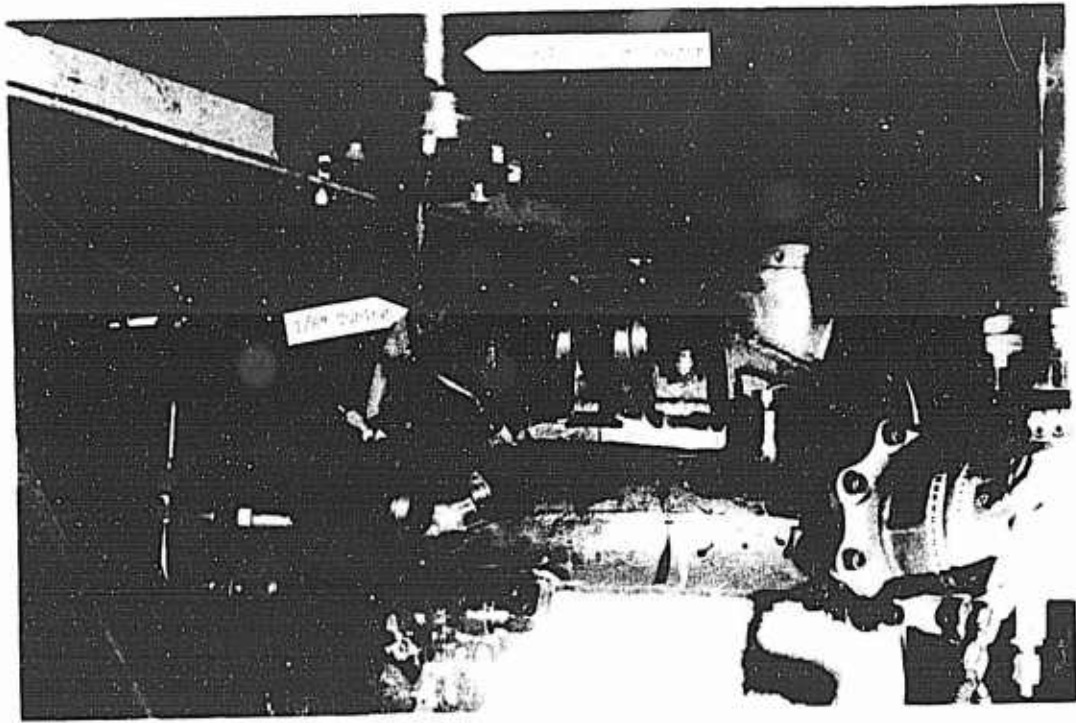


Figure 51 -- View of P<sub>fj</sub>-3A Tap Connection

GEMSIP FR-1, Volume 5

Table 4 -- Calibration Test Data for Oxidizer Pulse Generator

Test No.	Dome Press.	PoJ-3		PoJ-2		PoJ-1		Remarks
		Spike Ampl.	Press. Rise Rate	Spike Ampl.	Press. Rise Rate	Spike Ampl.	Press. Rise Rate	
	psig	psi	psi/ sec x 10 <sup>6</sup>	psi	psi/ sec x 10 <sup>6</sup>	psi	psi/ sec x 10 <sup>6</sup>	Dome - S/N 1020 Injector - S/N 246 Comb. Chb. S/N 1495
-038	100	111	3.93	78.3	2.25	80	2.23	
-040	100	127.7	8.49	83.5	2.62	99.7	3.14	
-041	200	167.7	11.08	116.8	3.31	120	2.41	
-042	300	194.5	12.9	139	4.61	134.3	3.34	
-043	400	191	10.9	158.5	5.27	105.6	2.21	
-044	500	212	10.4	180.5	5.13	171.3	3.57	
-045	500	229	11.8	183	5.21	162.6	3.24	
-046	700	236	12.6	191	6.34	168.5	3.53	
-047	800	232	15.2	228	6.69	188.4	4.69	
-048	900	244	12.0	244	6.94	194	4.29	
-049	1000	229	12.9	223	7.33	197	4.36	

II, D, Development Testing (cont.)

For this test series, a second stage Titan engine was assembled with a special dome, combustion chamber, discharge lines, and suction lines which provided the capability for extensive high frequency instrumentation (see Figures 51 through 56).

For Test No. 1.2-01-TLA-004, the fuel unit was attached to the fuel discharge line as shown in Figure 57. Prior to the test, fuel was bled down to the thrust chamber valves by opening the oxidizer and fuel high point bleed valves. The belleville washer adapter bleed on the pulser was also opened during this time to eliminate air from the cavity immediately adjacent to the anvil piston. The single pulse generator dome pressure was set at 500 psi and the trigger piston actuation pressure was set at 900 psi.

An electrical timer was used to signal the triggering mechanism at FS-1 + 2.2 sec. However, a shutdown caused by the combustion stability monitor (CSM) occurred at FS-1 + 0.943 sec, which was prior to the actuation of the single pulse generator. An examination of the records showed the CSM shutdown to be caused by oscillating amplifiers and therefore invalid.

For Test No. 1.2-01-TLA-005, the fuel unit was mounted on the fuel discharge line with the trigger actuation pressures set at 900 psi. The pulse generator was cycled three times with 500-psi pulser dome pressure prior to the test. Because the generator was actuated in a "dry" system (no propellant in the cavity of the belleville washer adapter), several belleville washers were cracked during these functional tests and had to be replaced.

As in the first test, the pulser was sequenced to operate at FS-1 + 2.2 sec. However, though the control unit for the trigger piston functioned properly, the trigger piston did not retract and, consequently, the pulser did not operate.

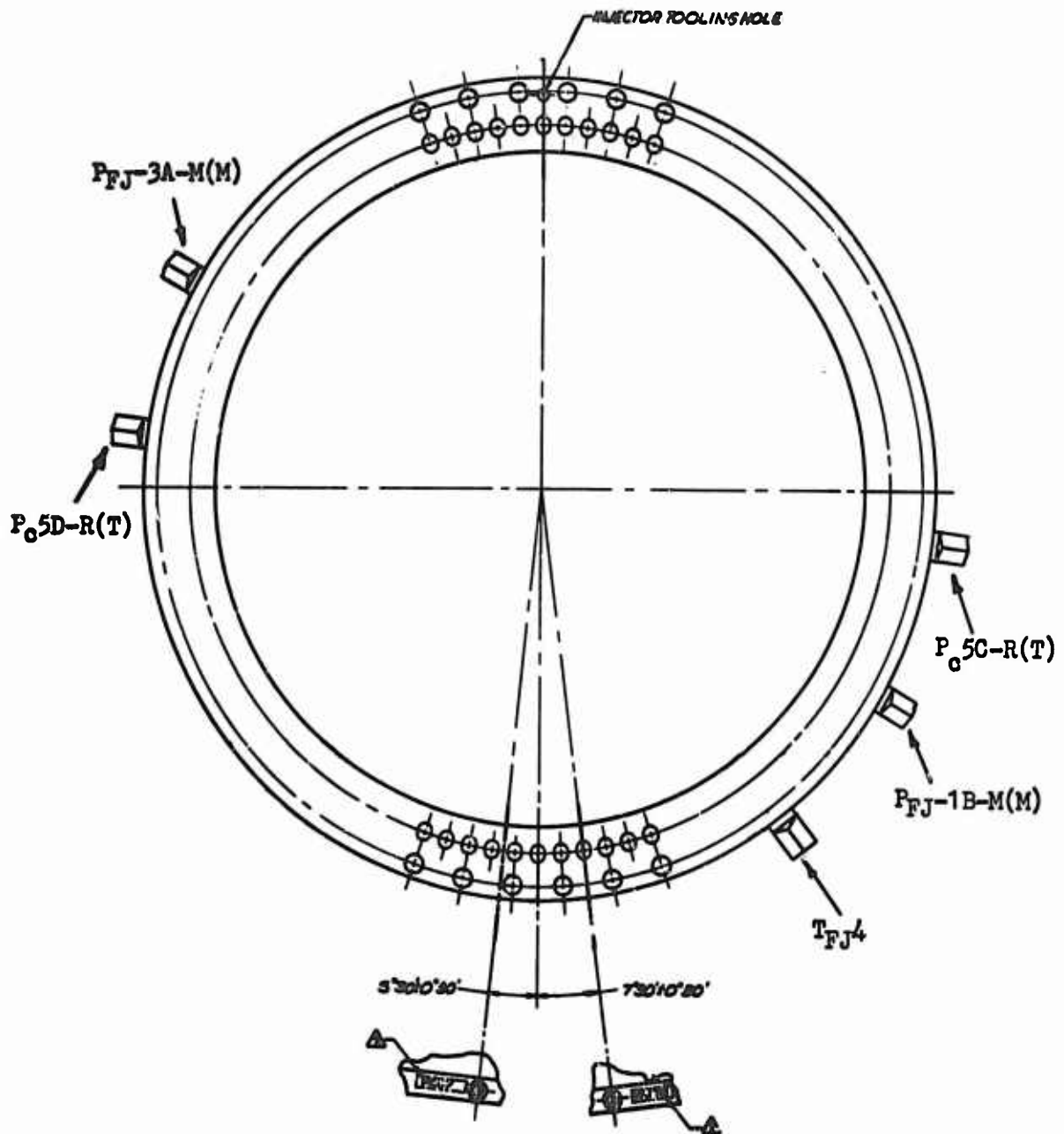


Figure 52 -- GEMSIP Injector



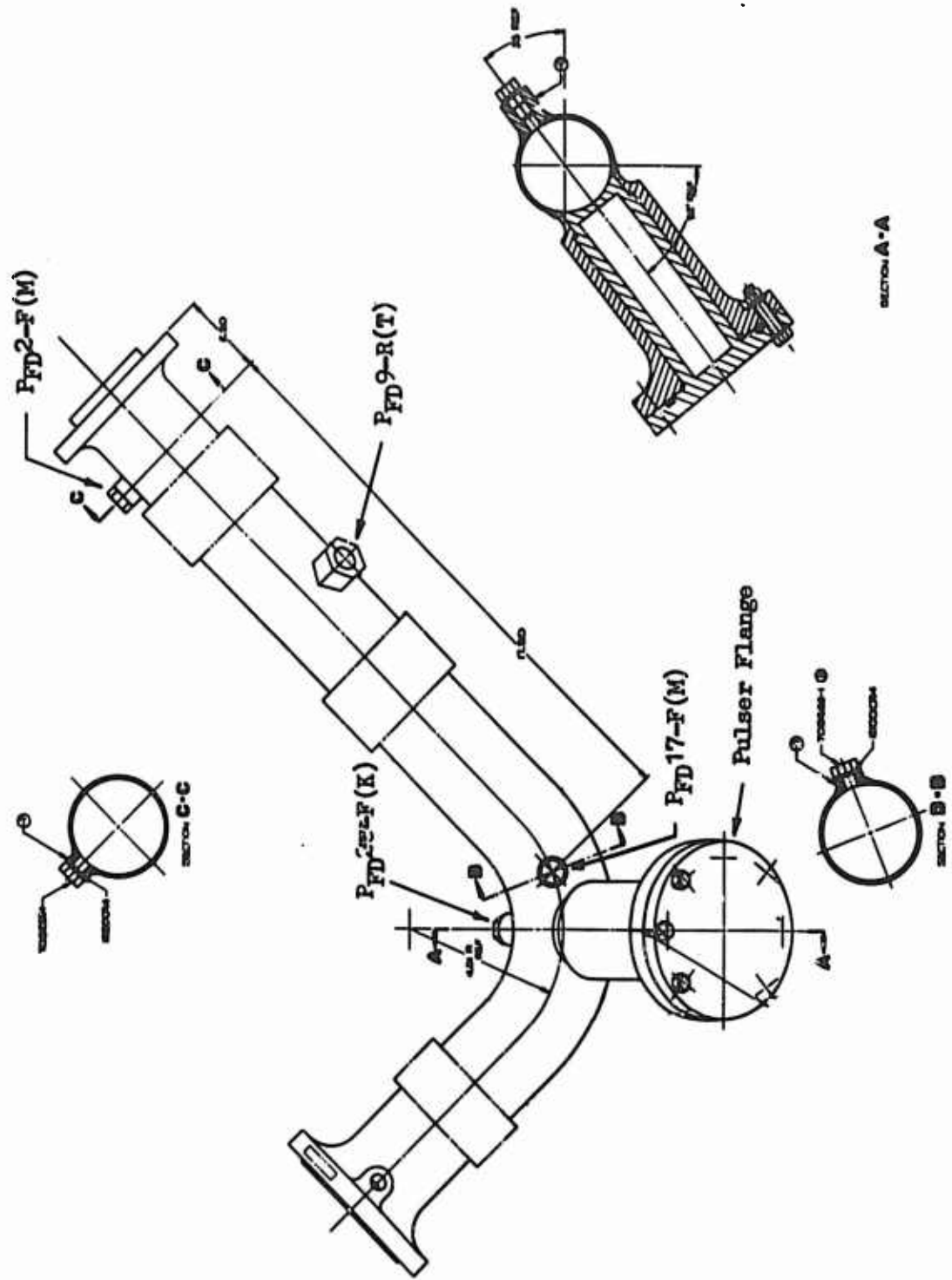


Figure 54 -- Modified Fuel Discharge Line



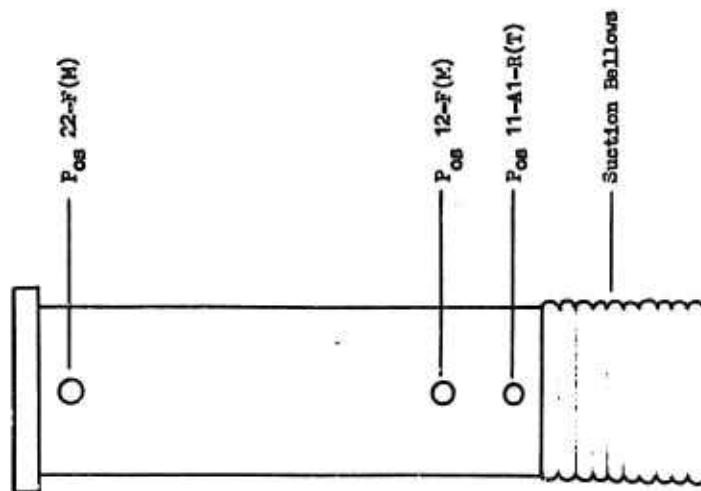
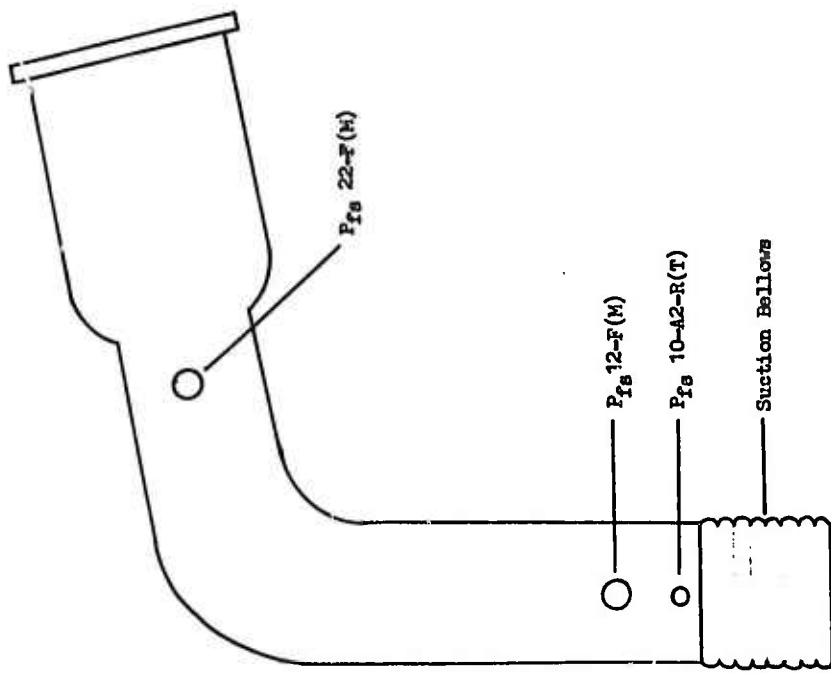


Figure 57 -- Modified Fuel Suction Spool

II, D, Development Testing (cont.)

A visual inspection of the pulse generator revealed some scoring marks on the trigger piston bore, which were thought to have been caused by a sharp edge on the "neck" of the trigger piston. The sharp edges on the trigger piston were removed, and 0.0005 in. of material was honed from the walls of the damaged bore to remove the scoring.

The fuel pulse generator was attached to the fuel discharge line for Test No. 1.2-01-TLA-006. The trigger piston actuation pressures were set at 1000 psi, and the dome pressure was set at 400 psi. A Teflon block was substituted for the belleville washers to prevent further breakage of the washers, and the pulser was cycled successfully 15 times with no propellant in the lines.

During one of these functional tests, all the high frequency transducers on the engine system were monitored on Ampex tape to determine if the transducers would be sensitive to the mechanical vibrations transmitted through the structure. The data showed that none of the transducers was sensing structural vibrations.

The Teflon block was removed, and the belleville washers were replaced. The trigger piston was actuated at FS-1 + 2.2 sec, and the pulse generator fired at FS-1 + 2.45 sec. The 0.25-sec delay can be attributed to the vent time of the trigger cavity, the time required for the trigger and hammer pistons to overcome inertial forces, and the travel time of the hammer piston prior to striking the anvil piston.

The pulse generator produced a 326-psi pulse at  $P_{ci} - 20$  with an 820,000-psi/sec rise rate as shown in Figure 58. None of the chamber pressure transducers showed the pulse.

GEMSIP FR-1, Volume 5

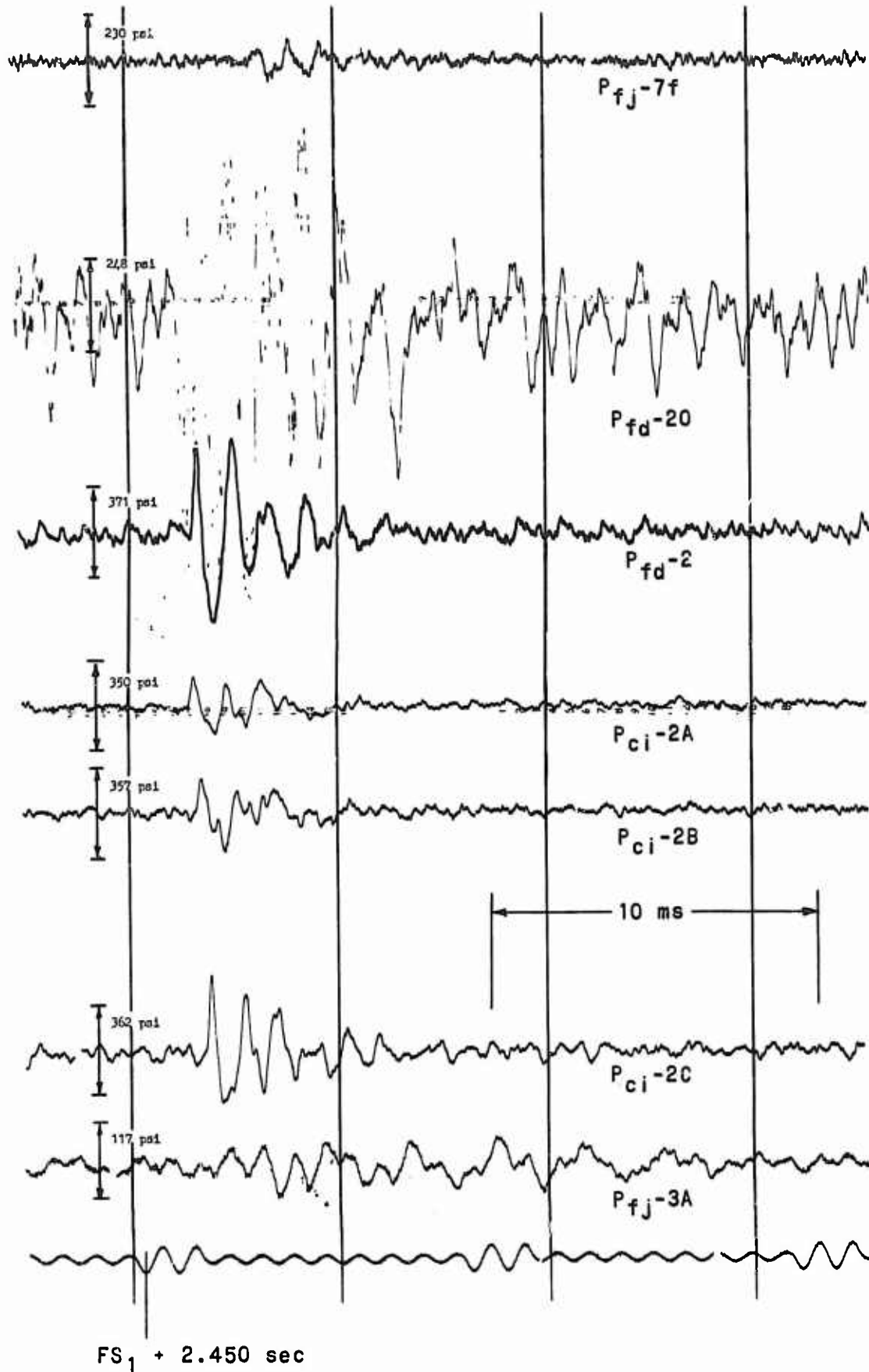


Figure 58 -- High Frequency Playback for Test No. 1.2-01-TLA-006

II, D, Development Testing (cont.)

For Test No. 1.2-01-TLA-007, the oxidizer single pulse generator was mounted on the second stage Titan dome as shown in Figure 59. Because it was thought that the volume of the mounting flange might have an adverse effect on the 91-5 engine start transient, a method was devised to offset this volume during start. A Teflon "orange-peel" burst diaphragm was designed to fit on a serrated seat, located flush with the interior of the oxidizer dome contour (Figure 60). Prior to the test, the cavity between the diaphragm and the pulse generator was filled with nitrogen tetroxide at 40-psi pressure. During the test, as the oxidizer dome pressure increased to 1000 psi, the diaphragm did not rupture because of the liquid prefill on the back side. However, at FS-1 +1.8 sec, this cavity was vented through the belleville adapter bleed port, and the diaphragm ruptured because of the differential pressure. At FS-1 + 2.0 sec, the bleed port was closed.

The pulse generator was actuated with 1000-psi pressure on the trigger piston and 500-psi dome pressure at FS-1 + 2.2 sec, and the pulse generator fired at FS-1 + 2.434 sec. Figure 61 shows the playback of the high frequency records. As can be seen, PoJ-3F shows a 360-psi overpressure with a 3,500,000-psi/sec rise rate. Pc5E (a water dump Electro Optical Systems transducer) showed a slight increase in the combustion noise level.

These test results show that the single pulse generators designed and developed for use in conjunction with the Gemini Stability Improvement Program are capable of producing significant (20% or greater) pressure perturbations, with high rise rates, in the 91-5 feed system.

E. CONCLUSIONS

As a result of the development testing of the GEMSIP single pulse generators, the following conclusions have been made: (1) the GEMSIP single pulse generators are capable of producing significant (20% or greater) pressure perturbations, with high rise rates, in the 91-5 feed system; (2) a pulser "dome"

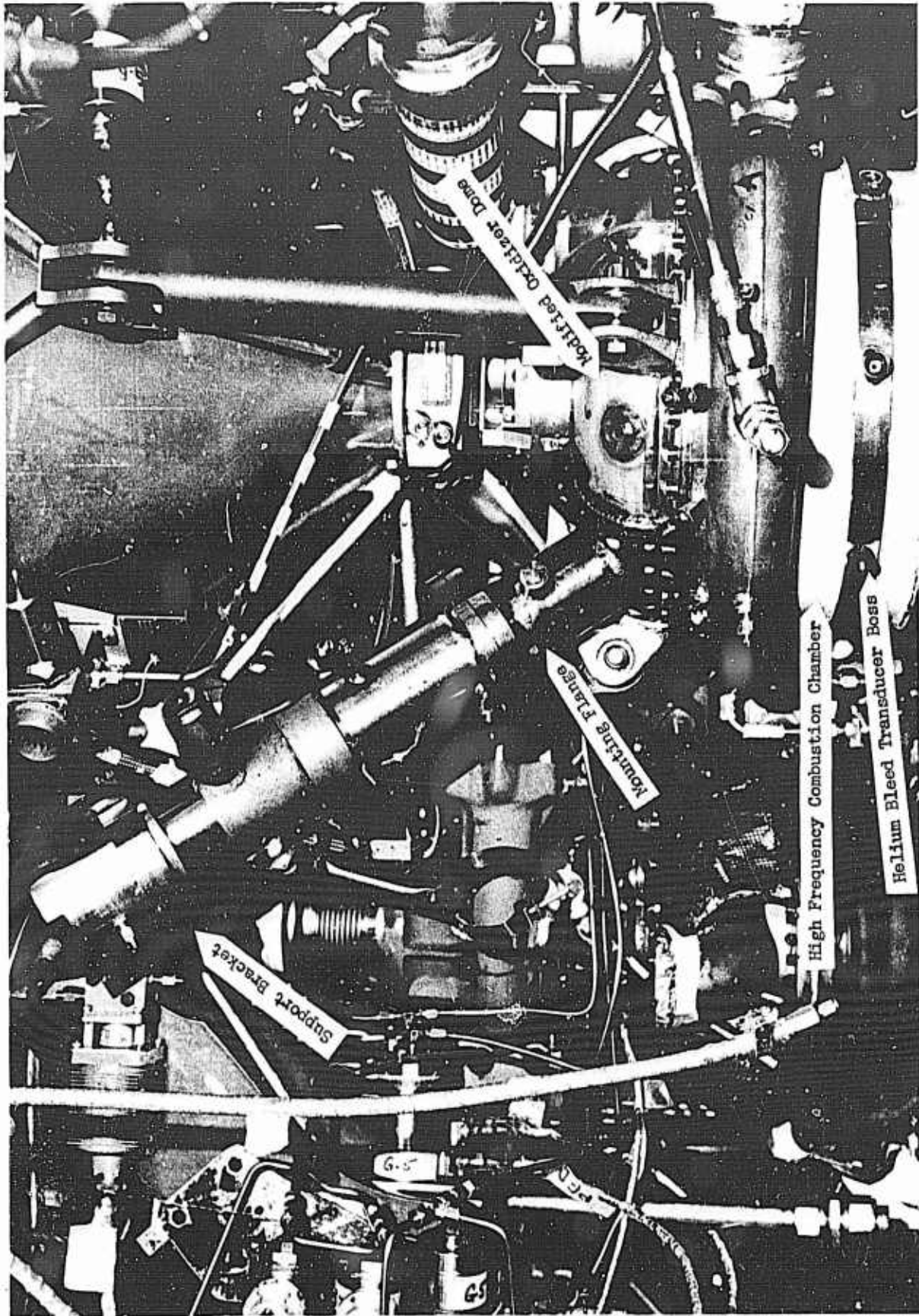


Figure 59 -- Installation of Oxidizer Single Pulse Generator on  
91-5 Engine

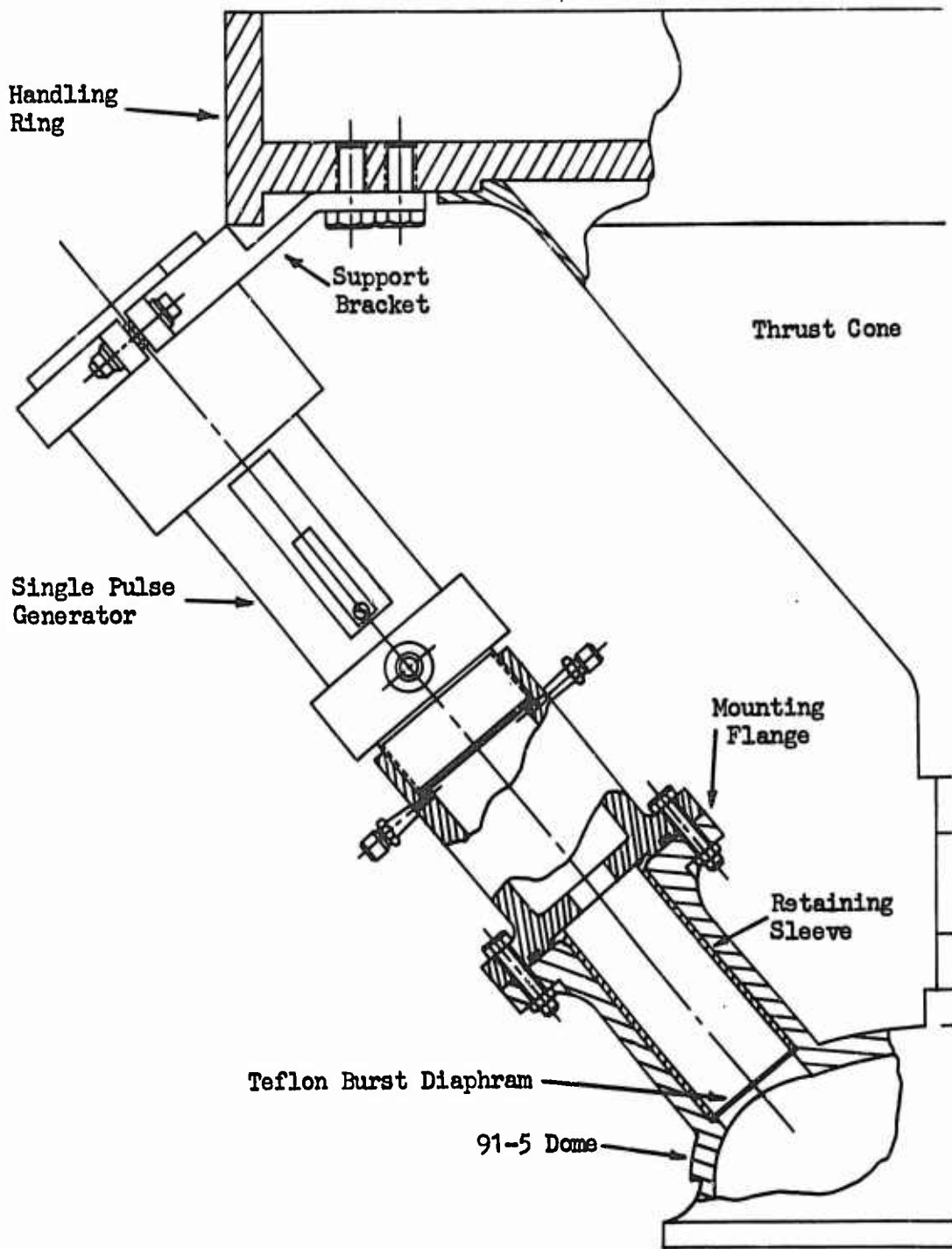


Figure 60 -- Installation of Teflon Burst Diaphragm

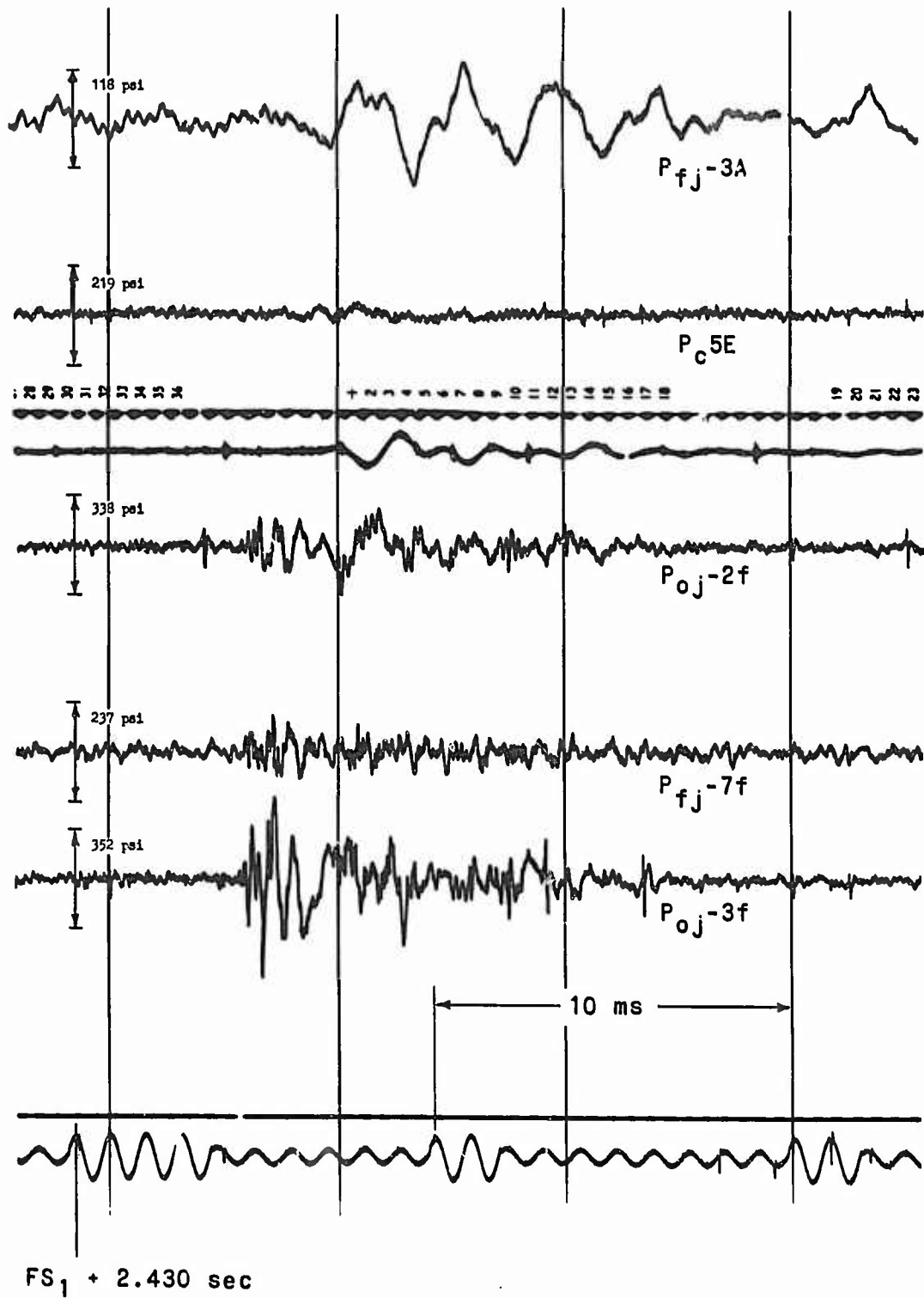


Figure 61 -- High Frequency Playback for Test No. 1.2-01-TLA-007

II, E, Conclusions (cont.)

pressure of 400 to 500 psi is sufficient to produce a significant perturbation; (3) a trigger actuation pressure of 1000 psi insures high reliability of pulser operation; (4) extreme care should be taken in the installation of the Teflon slipper seals on the hammer and trigger pistons -- because of close tolerances, any scoring or tearing may cause the seals to bind or fail; and (5) the belleville washers may crack when subjected to heavy loading or an extreme number of cycles, but this failure is of no consequence because the bellevilles are easily replaced.

III. CONTINUOUS PULSE GENERATOR (FLOW MODULATOR)

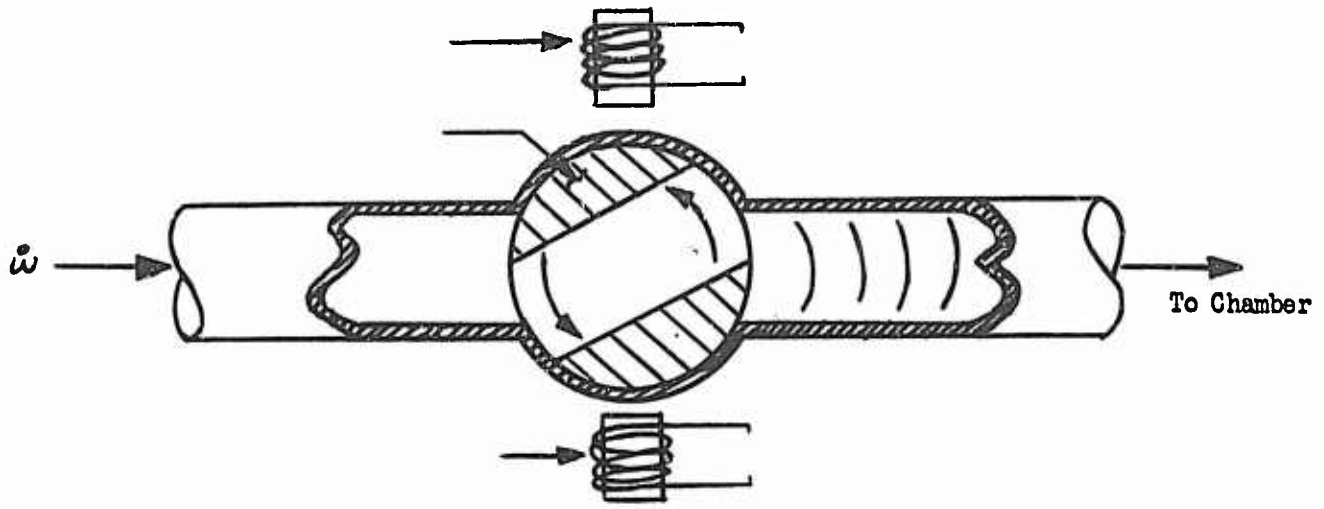
Some 91-5 engine test firings exhibited what appeared to be a correlation between low frequency (400 to 500 cps) oscillations and subsequent damaging instabilities. To assist in establishing the exact role of the oscillations in instabilities, a device to introduce controlled perturbations was designed and fabricated so that the stability sensitivity of the combustion process to oscillations and the dynamic response characteristics of the feed system could be determined.

A. DESIGN REQUIREMENTS--CONTINUOUS PULSE GENERATOR

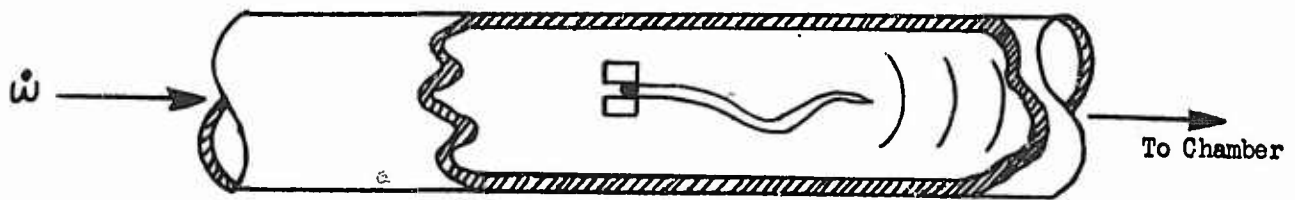
A literature search revealed that both Bell Aircraft Company and Rocketdyne had fabricated pulse generators for use on rocket engine feed systems. The work done by Bell Aircraft was for small-scale engines with flowrates less than 1 lb/sec. Their pulse generator was a simple "ball valve" mechanism producing frequencies up to 500 cycles per second.

The Rocketdyne pulser was mentioned briefly in a final report for the Atlas Program giving few details. Arrangements, therefore, were made for two members of the Combustion Dynamics Department to meet in Canoga Park with Rocketdyne personnel and discuss the design and development of their continuous pulse generator. It was learned that the Rocketdyne pulser produced measurable oscillations only at discrete frequencies and the maximum amplitude was 50 psi peak-to-peak with an operating propellant line pressure of 600 to 700 psi.

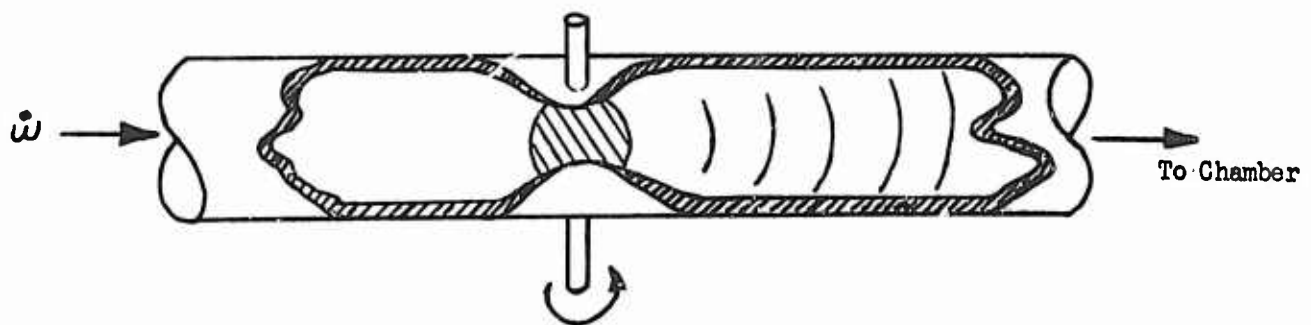
The primary objective was to design a device that would introduce a sinusoidal pressure oscillation into either the fuel or oxidizer circuit at frequencies ranging from 100 to 1000 cps, the amplitude of the perturbation to be sufficient to be discernible above normal combustion and "flow noise."



A. Electrically Driven



B. Vibrating Reed



C. Mechanically Driven

Figure 62 -- Area Change of Propellant Line

III, A, Design Requirements--Continuous Pulse Generator (cont.)

To fulfill the requirements, four concepts were considered:

1. Intermittent variation of the internal flow area of the propellant feed line.
2. Intermittent increase of the propellant pressure.
3. Intermittent injection of propellant into the lines.
4. Intermittent release of propellant overboard.

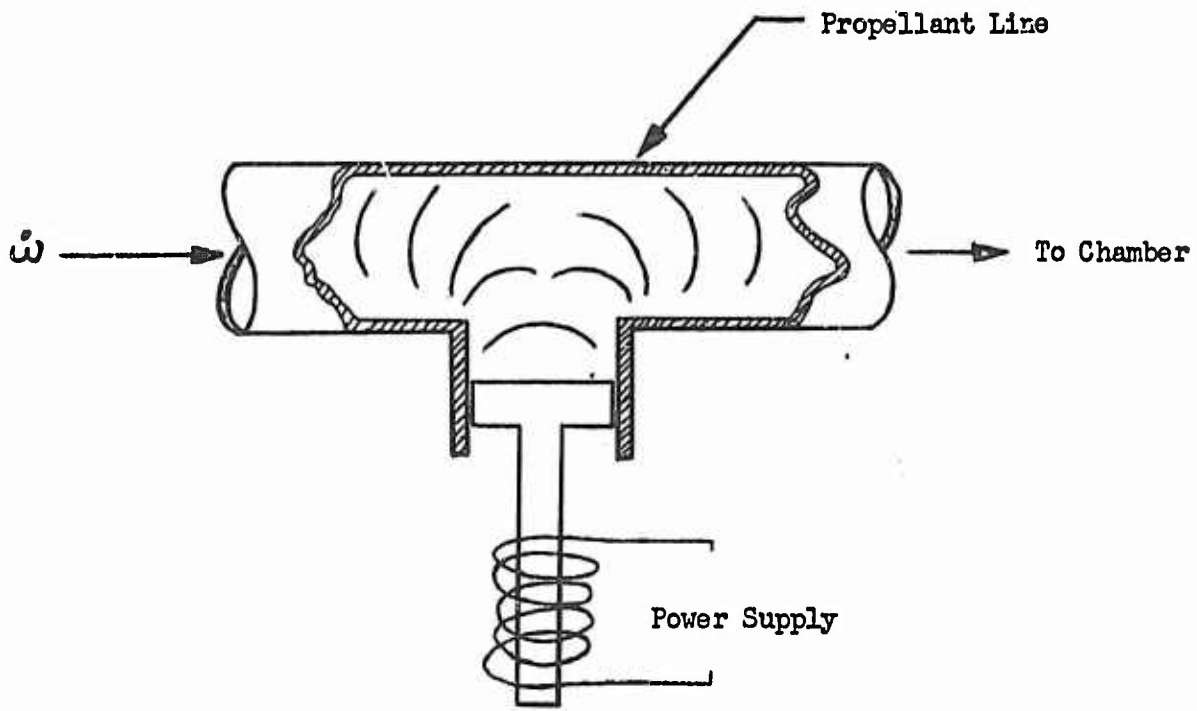
Of the four concepts considered, No. 1 had the most advantages in that line geometry changes would be minimum and closer correlation to actual engine conditions would be realized. It did, however, present power media and sealing difficulties. The various concepts and the results of the analysis are listed:

1. Internal Flow Area Change

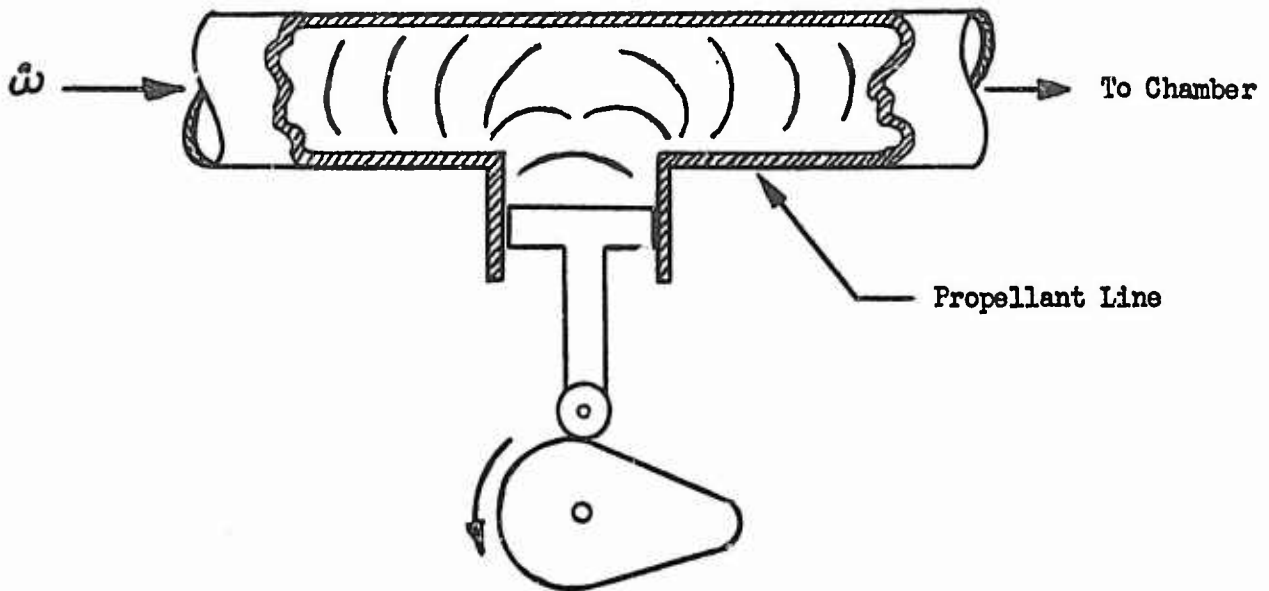
Rotating Butterfly (Figure 62a) studies conducted indicate that the amplitude of the pressure oscillation would meet requirements only if two lobes were used. This would necessitate 30,000 rpm and result in cavitation.

2. Vibrating Reed

This concept (Figure 62b) showed considerable promise; however, preliminary studies indicated that the amplitude of the pressure oscillation was a function of the transverse motion of the reed, which in turn was a function of the length of the reed. If the reed was driven by the energy of the stream, its vibrating (natural) frequency was also a function of its length. It thus became evident that it was necessary to drive the reed by some other means to control both its transverse motion and its length. Laboratory models demonstrated the concept's feasibility, but considerable development work was necessary.



A. Electrically Driven



B. Mechanically Driven

Figure 63 -- Piston Displacement of Fluid

III, A, Design Requirements--Continuous Pulse Generator (cont.)

3. Magnetically Driven Rotor

Preliminary studies were conducted to determine the feasibility of using an orificing rotor inside the feed line (Figure 62c). The rotor would turn when driven by fields located outside the periphery of the propellant line. The rotor would be hexagonal in cross-section and would be matched by an insert of the same shape in the feed line. Then, as the rotor turned one revolution, six pulses would be produced. To control the speed of the rotor, the frequency of the supplied current would be varied. In a laboratory model, an ac variable speed motor with a commutator mounted on its output shaft provided a means of alternating dc current at a variable frequency. Using a bank of fixed capacitors, the concept proved feasible. Varying the capacitance with the frequency proved to be impractical with available equipment. Because of development time necessary, the concept was discarded for use in the GEMSIP program.

4. Intermittent Pressure Increase

An analysis was conducted to determine whether varying the propellant pressure was feasible in this application (Figure 63a). It showed that the power requirements would be excessive.

5. Intermittent Increase in Propellant Flow Rate

This concept proved to be practical with low power requirements (Figure 63b). It did, however, require an additional propellant source which made it undesirable.

6. Overboard Release System

Of all the concepts considered, the overboard release system appeared to be the most practical. It consisted of a tee in the propellant line through which intermittently a metered amount of propellant would be released

III, A, Design Requirements--Continuous Pulse Generator (cont.)

producing local pressure perturbations. Parametric studies showed that release of up to 50 lb/sec of the propellants was possible. Design effort was concentrated on this device using the experience derived from the work of others in the industry that had tried the overboard bleed.

B. DESIGN PARAMETRIC STUDY

In a chemical rocket engine, the feed system configuration determines the injection rate response to pressure changes in the chamber shown by the transfer function,  $G = \frac{\dot{W}}{p}$ . G is determined by the feed system configuration. To determine G at the injector, it is necessary to know the value of G at some point in the system and how it can be extended through the system to the injector.

The transfer function G can be extended through a duct using one dimension wave theory.\* It is possible to start at the propellant tankage, where G is known, and extend G to the injector face, except that little is known about the effect of the pump on G. It is, therefore, necessary to measure G somewhere downstream of the pump. This can be accomplished by using the continuous pulse generator to force a weight flow oscillation in the system.

Since there are no readily available methods of measuring weight flow oscillations directly, pressure measurements can be used to obtain the transfer function, G, utilizing the relationship shown in Figure 64 for a constant cross-sectional area line:

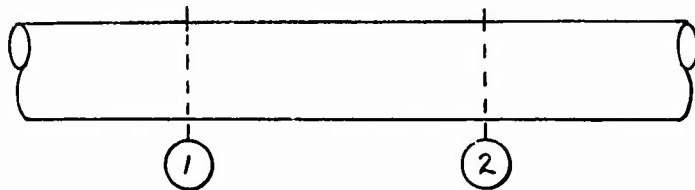


Figure 64 -- Line for Constant Cross-Sectional Area.

\*Discussion contained in ETDR 9645-010, "Low Frequency Stability Analysis," by R. C. Waugh.

## III, B, Design Parametric Study (cont.)

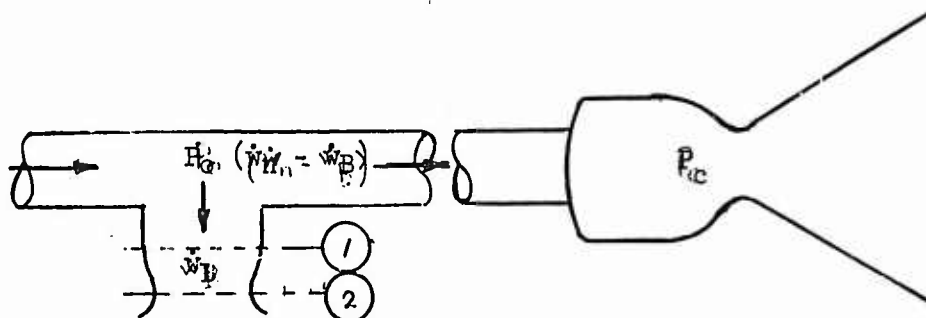
$$G = \frac{\frac{P_2}{P_1} - \cosh Tw}{\frac{C i}{Ag} \sinh Tw} \quad (1)$$

where:  $P_1$  = Pressure at 1  
 $P_2$  = Pressure at 2  
 $L$  = Distance from 1 to 2  
 $A$  = Area of line  
 $c$  = Speed of sound in fluid  
 $g$  = Acceleration due to gravity  
 $T$  =  $L/c$  = Period of oscillation  
 $f$  = Frequency of oscillation  
 $\omega$  =  $2 \pi f$

It is, therefore, necessary to measure two pressures in a constant area line to determine the transfer function at some point in the feed system. For this reason, a set of 91-5 pump discharge lines instrumented with high frequency Microsystems pressure transducers was fabricated.

The orifice size and spacing were determined using the method shown in Figure 65 for quasi-steady state conditions.

Figure 65 -- Orifice Size and Spacing



## III, B, Design Parametric Study (cont.)

where the parameters are defined as:

- $\dot{w}_n$  = nominal flowrate
- $\dot{w}_B$  = bleed flowrate
- $P_c$  = chamber pressure
- $P_o$  = pressure in propellant line
- $A_T$  = total area of the bleed line
- $A_P$  = area of partially opened orifice
- $P_1$  = pressure at 1
- $P_2$  = pressure at 2
- $U_1$  = velocity at 1
- $U_2$  = velocity at 2
- $C_D$  = discharge coefficient
- $K$  = effective adiabatic bulk modulus
- $\rho$  = density of propellant
- $\phi$  = effective area ratio

$$P_o - P_c = K \omega (\dot{w}_n - \dot{w}_B)^2 \quad (1)$$

$$\dot{w} = \rho U_2 A_P \quad (2)$$

$$\frac{P_o - P_1}{K} = \frac{U_1 - U_o}{C} \quad (3)$$

$$\frac{P_1 - P_2}{K} = 1/2 \left( \frac{U_1}{c} \right)^2 \left[ \frac{1}{\phi^2} - 1 \right] \quad (4)*$$

$$\phi = \left( \frac{A_P}{A_T} \right) C_D \quad (5)*$$

$$U_1 = U_2 \phi \quad (6)$$

\*From W. A. Woods; "Method of Calculating Liquid Flow Fluctuations in Rocket Motor Supply Pipes," ARS Journal, November 1961, pp 1560-1567.

## III, B, Design Parametric Study (cont.)

When:

$$K_{\omega} = \frac{P_o - P_c}{(\dot{w}_n)^2} \quad (7)$$

Examining (4) and solving for  $U_1^2$ 

$$U_1^2 = 2c^2 \left( \frac{P_1 - P_2}{K} \right) \left( \frac{\phi^2}{1 - \phi^2} \right) \quad (8)$$

Since  $U_o = 0$  (3) may be rewritten

$$\frac{P_o - P_1}{K} = \frac{U_1}{c} \quad (9)$$

Squaring (9) and solving for  $U_1^2$ 

$$U_1^2 = \left( \frac{c}{K} \right)^2 (P_o - P_1)^2 \quad (10)$$

Setting (10) equal to (8) and gathering terms.

$$P_1^2 - P_1 \left[ 2 P_o + \frac{2K \phi^2}{1 - \phi^2} \right] + \left[ P_o + \frac{2K P_2 \phi^2}{1 - \phi^2} \right] = 0 \quad (11)$$

Let

$$B = - \left[ 2 P_o + \frac{2K \phi^2}{1 - \phi^2} \right]$$

$$D = \left[ P_o + \frac{2K P_2 \phi^2}{1 - \phi^2} \right]$$

$$\therefore P_1 = \frac{-B - (B^2 - 4D)^{1/2}}{2} \quad (12)$$

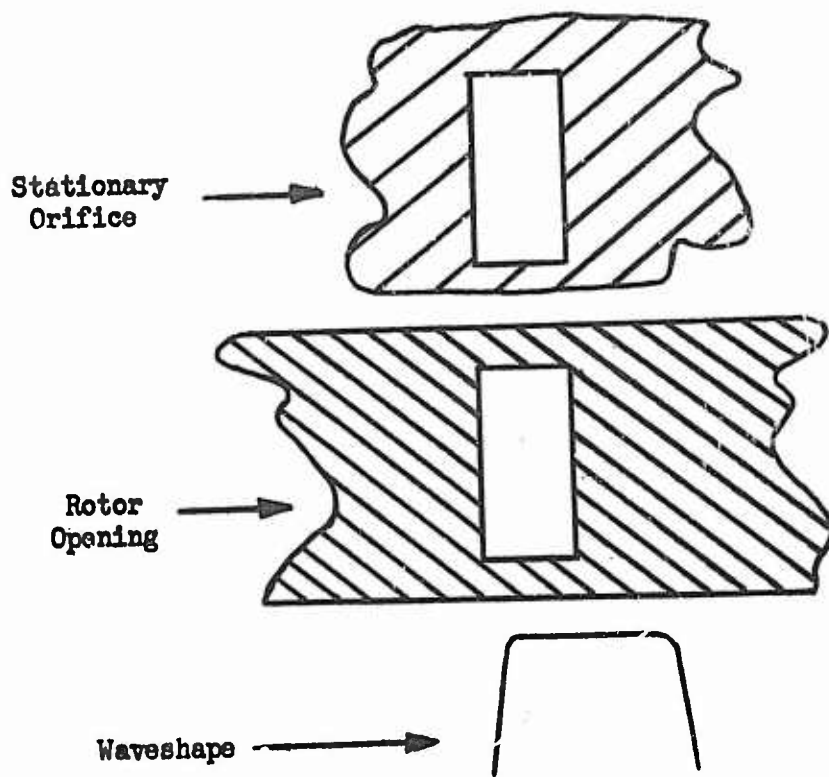


Figure 66 -- Waveshape for One Cycle

## III, B, Design Parametric Study (cont.)

And substituting (6) into (4)

$$U_2 = C \left[ \frac{2(P_1 - P_2)}{K} \frac{1}{(1 - \phi^2)} \right]^{1/2} \quad (13)$$

$$\dot{w}_B = U_2 \rho A_p$$

Knowing these equations it is possible to increment  $A_p$  and calculate a new  $P_0$  each time. Hence, the pressure and flow waveshape for a time varying orifice may be approximated. Using this method, a computer program was written from which it was determined that the rotor openings should be made 0.350 in. wide by 2.220 in. high.

It was also determined from the computer program that, if the rotor opening and the stationary orifice are the same width, the waveshape during the "open path" portion of the cycle would appear as shown in Figure 66. It followed that the openings in the rotor would have to be spaced  $4\omega$  apart in order to approximate a sinusoidal waveshape as shown in Figure 67.

Using the method described below, it was determined that the flow through a time-varying orifice is in phase with the pressure drop and the orifice open area (that is, independent of frequency) for frequencies less than 1200 cps.

Assume that the open area of the orifice,  $A$ , is increased by an amount  $dA$ . The problem is to find out how long it takes the fluid to accelerate through the channel,  $dA$ , to full port velocity,  $A_0$ . The fluid being accelerated has a length approximately equal to the hydraulic diameter of the port. Then

$$\frac{\rho L}{g} \frac{dU}{dt} = \Delta P - \frac{U^2}{2g} \quad (1)$$

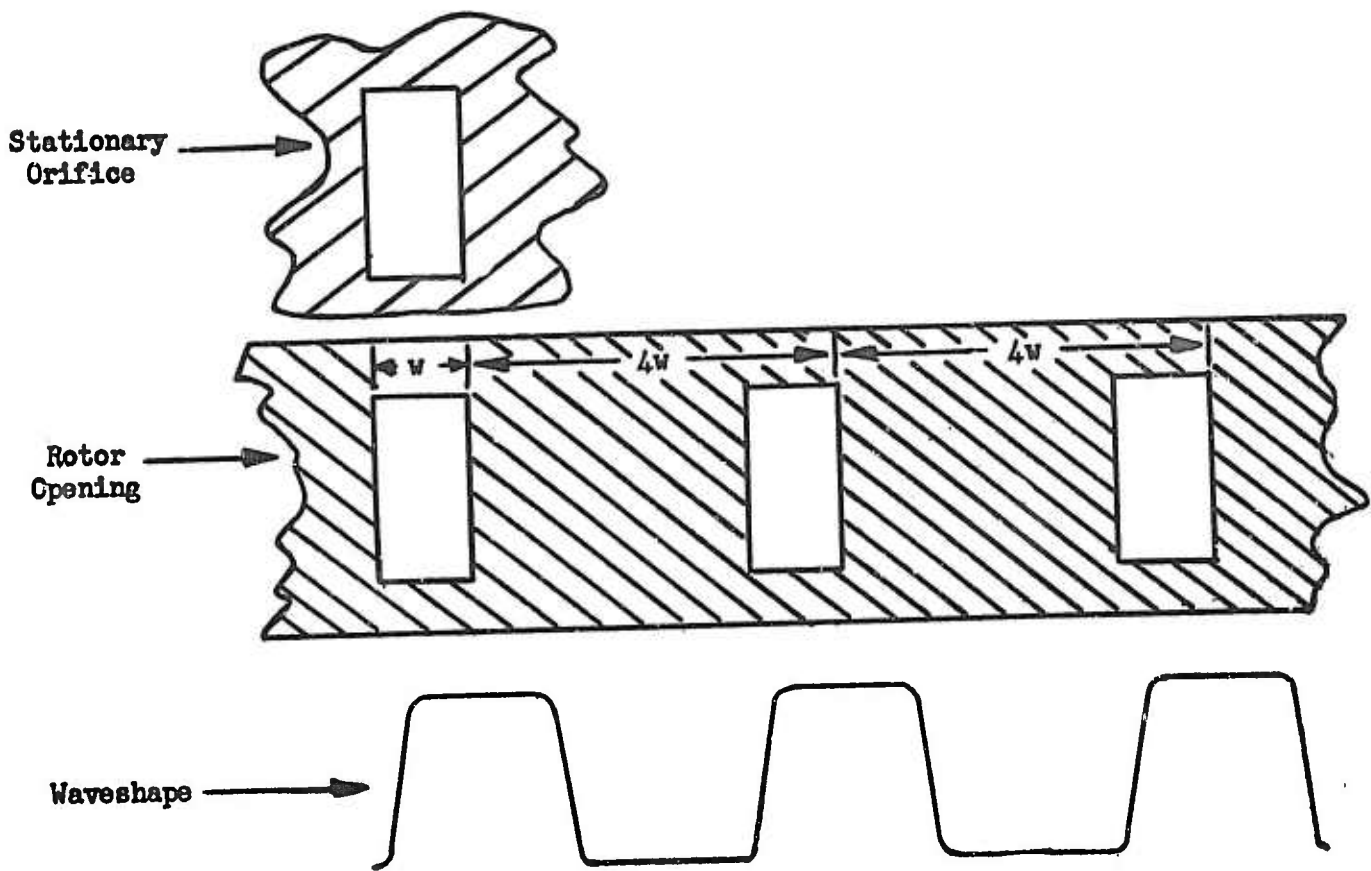


Figure 67 -- Waveshape for More Than One Cycle

## III, B, Design Parametric Study (cont.)

Or

$$\frac{dU}{U_o^2 - U^2} = \frac{dt}{2L} \quad (2)$$

This integrates to

$$\text{tanh}^{-1} \left( \frac{U}{U_o} \right) = \frac{U_o t}{2L} \quad (3)$$

or

$$\frac{U}{U_o} = \tanh \left( \frac{U_o t}{2L} \right) \quad (4)$$

Since these two functions have the same origin and asymptotes, and are equal at  $t/\tau = 1$ , this is the same as:

$$\frac{U}{U_o} = 1 - e^{-t/\tau} \quad (5)$$

Where:

$$\tau = \frac{2L}{1.43 U_o} \quad (6)$$

Now for  $U_o = 1000$  fps,  $L = 0.350$  in.,  $\tau = 4.1 \times 10^{-5}$ , the port area increment will contribute usefully to the flow if  $T$  is on the order of 1/10 the time the increment is open. The average increment may be open about half the cycle. Then an upper frequency limit is on the order of

$$f_u = 1/20 \tau$$

$$f_u = 1200 \text{ cps}$$

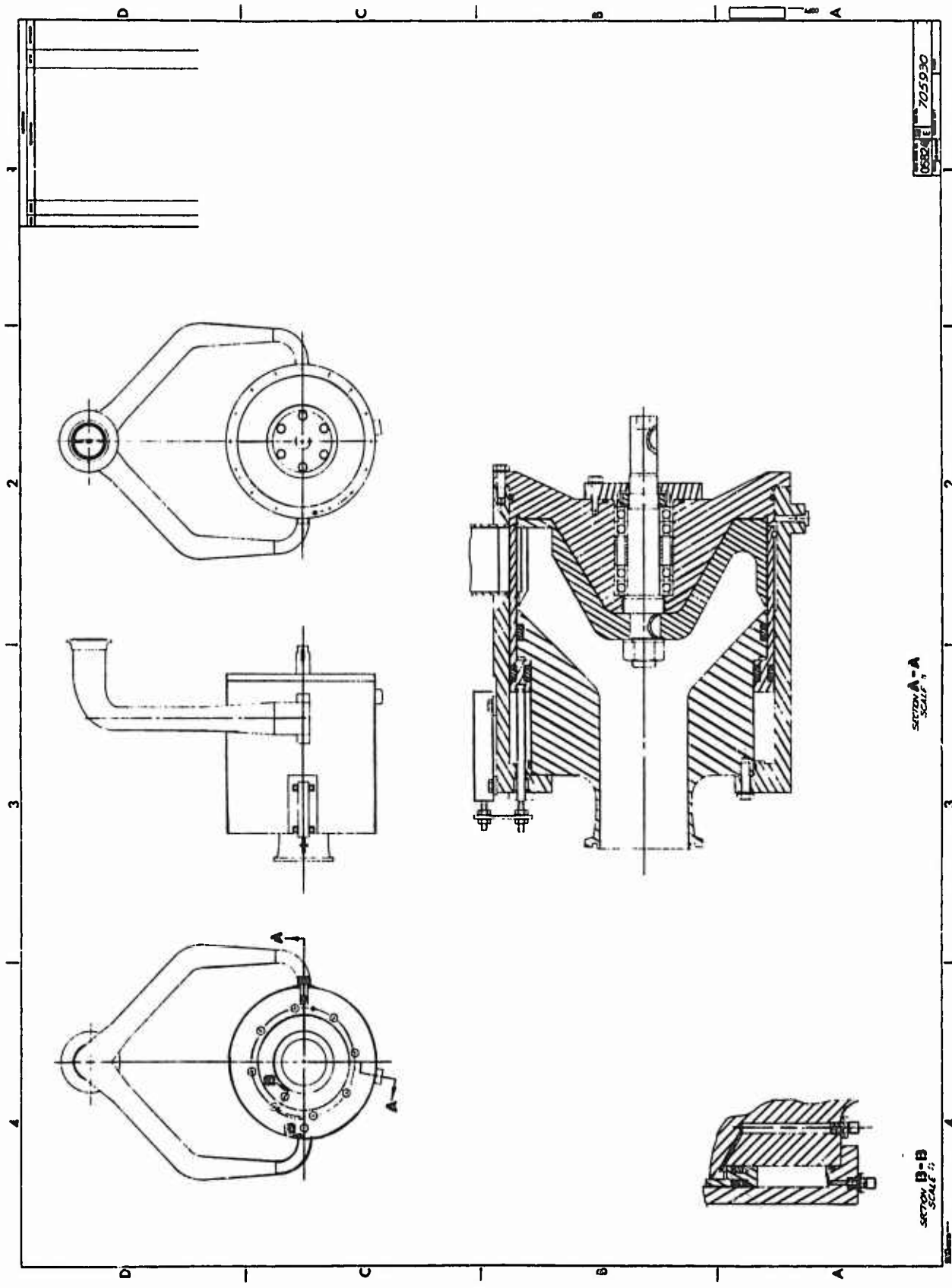


Figure 68 -- Cross-Section of Continuous Pulse Generator

III, B, Design Parametric Study (cont.)

Since engine operating parameters are affected by bleeding off propellant during the run, the Systems and Controls Division was requested to use the YLR91-AJ-5 analytical model to predict engine component performance for the following conditions:

1. Oxidizer bleed at pump discharge
2. Oxidizer bleed at injector dome
3. Fuel bleed at pump discharge
4. Fuel bleed at cooling jacket inlet (torus)

The amount of oxidizer flow rate dumped overboard was varied from 0 to 50 lb/sec and the fuel flow rate from 0 to 25 lb/sec at either tap-off location. Table 5 presents a brief steady state history of engine component performance for various flow rates of propellant discharged overboard. It may be concluded that these amounts of propellant bleed will not drastically affect engine performance.\*

C. DESIGN

The final design of the continuous pulse generator used high pressure propellant piped through a "Y" to diametrically opposed slots on the outside of a housing assembly. A rotor, supported on two sets of matched high angular-contact stainless-steel radial ball bearings, turns inside the housing and is driven by a protruding shaft (Figure 68). Openings in the periphery of the rotor are spaced so that a path for propellant flow is alternately opened and closed as the rotor turns. Side loads on the rotor are opposite and cancelling.

To prevent longitudinal oscillations, the rotor is designed so that the longitudinal center of gravity is located between the support bearings. Also, the pulsed stream of fluid is directed so as to impinge between the support bearings

---

\*From "Continuous Pulse Generator Analysis," Memo from C. K. Leeper to D. E. Robison, dtd 26 December 1963.

TABLE 5  
ENGINE COMPONENT PERFORMANCE DATA FOR VARIOUS  
AMOUNTS OF PROPELLANT BLEED

A. OXIDIZER DUMPED AT PUMP DISCHARGE

Unit	Amount Dumped in lb/sec			
	0	10	20	30
<u>Thrust Chamber</u>				
Thrust Chamber Pressure (P <sub>c5</sub> )	826	808	789	770
Oxidizer Flow	206.9	199.9	192.8	185.7
Fuel Flow	110.3	109.2	108.1	107.0
Mixture Ratio	1.876	1.831	1.784	1.735
<u>Oxidizer Pump</u>				
Oxidizer Density	90.83	90.83	90.83	90.83
Total Suction Pressure	41.0	41.0	41.0	41.0
Total Discharge Pressure	1130	1091	1053	1015
Non-Cavitating Head	1769	1706	1644	1583
Oxidizer Flow	207.3	210.3	213.2	216.1
Suction Specific Speed	14994	14926	14852	14772
Shaft Speed	8431	8333	8235	8136
<u>Fuel Pump</u>				
Fuel Density	56.65	56.65	56.65	56.65
Total Suction Pressure	44.5	44.5	44.5	44.5
Total Discharge Pressure	1212	1186	1160	1133
Non-Cavitating Head	3103	3027	2952	2878
Fuel Flow	122.3	121.1	119.9	118.7
Suction Specific Speed	21998	21631	21268	20908
Shaft Speed	23760	23483	23206	22929
<u>Gas Generator</u>				
Chamber Pressure	438	433	427	422
Oxidizer Flow	0.432	0.425	0.418	0.411
Fuel Flow	4.910	4.856	4.802	4.746
Mixture Ratio	0.0880	0.0876	0.0871	0.0866
<u>Gas Turbine</u>				
Gas Flow	5.018	4.991	4.933	4.874
Total Inlet Pressure	431	426	421	416
Shaft Speed	23760	23483	23206	22929
<u>Tap-Off</u>				
Tap-Off Pressure Total (P <sub>od</sub> )		1082	1043	1004
			966	928

Table 5 -- Engine Component Performance Data for Various Amounts of Propellant

B. OXIDIZER DUMPED AT INJECTOR DOME

	Unit	Amount Dumped in lb/sec			
		0	10	20	30
<u>Thrust Chamber</u>					
Thrust Chamber Pressure ( $P_{c5}$ )	psia	826	807	787	768
Oxidizer Flow	lb/sec	206.9	199.0	191.1	183.2
Fuel Flow	lb/sec	110.3	109.5	108.7	108.0
Mixture Ratio	--	1.876	1.818	1.758	1.697
<u>Oxidizer Pump</u>					
Oxidizer Density	lb/ft <sup>3</sup>	90.83	90.83	90.83	90.83
Total Suction Pressure	psia	41.0	41.0	41.0	41.0
Total Discharge Pressure	psia	1130	1097	1065	1032
Non-Cavitating Head	ft	1769	1716	1663	1610
Oxidizer Flow	lb/sec	207.3	209.5	211.6	213.6
Suction Specific Speed	$\frac{\text{rpm} \sqrt{\text{ft}}}{\text{lb}^{1/2}}$	14994	14917	14836	14748
Shaft Speed	rpm	8431	8345	8258	8170
<u>Fuel Pump</u>					
Fuel Density	lb/ft <sup>3</sup>	56.65	56.65	56.65	56.65
Total Suction Pressure	psia	44.5	44.5	44.5	44.5
Total Discharge Pressure	psia	1212	1188	1163	1138
Non-Cavitating Head	ft	3103	3033	2963	2892
Fuel Flow	lb/sec	122.6	121.4	120.5	119.6
Suction Specific Speed	$\frac{\text{rpm} \sqrt{\text{ft}}}{\text{lb}^{1/2}}$	21998	21691	21386	21081
Shaft Speed	rpm	23760	23517	23272	23024
<u>Gas Generator</u>					
Chamber Pressure	psia	438	433	428	422
Oxidizer Flow	lb/sec	0.432	0.425	0.417	0.410
Fuel Flow	lb/sec	4.910	4.859	4.807	4.754
Mixture Ratio	--	0.088	0.0874	0.0868	0.0862
<u>Gas Turbine</u>					
Gas Flow	lb/sec	5.048	4.993	4.937	4.879
Total Inlet Pressure	psia	431	426	421	416
Shaft Speed	rpm	23760	23517	23272	23024
Tap-Off Pressure Total ( $P_{of}$ )	psia		982	949	916
				888	850

Table 5 -- Engine Component Performance Data for Various Amounts of Propellant

C. FUEL DUMPED AT PUMP DISCHARGE

	Unit	Amount Dumped in lb/sec					
		0	5	10	15	20	25
<u>Thrust Chamber</u>							
Thrust Chamber Pressure ( $P_{c5}$ )	psia	826	813	799	785	771	757
Oxidizer Flow	lb/sec	206.9	206.2	205.6	205.0	204.4	203.9
Fuel Flow	lb/sec	110.3	107.0	103.9	100.7	97.5	94.4
Mixture Ratio	--	1.876	1.927	1.980	2.036	2.097	2.161
<u>Oxidizer Pump</u>							
Oxidizer Density	lb/ft <sup>3</sup>	90.83	90.83	90.83	90.83	90.83	90.83
Total Suction Pressure	psia	41.0	41.0	41.0	41.0	41.0	41.0
Total Discharge Pressure	psia	1130	1115	1100	1084	1068	1052
Non-Cavitating Head	ft	1769	1743	1717	1691	1665	1638
Oxidizer Flow	lb/sec	207.3	206.7	206.0	205.4	204.9	204.3
Suction Specific Speed	$\frac{rpm \text{ ft}^{3/4}}{\text{lb/sec}}$	14994	14873	14753	14632	14511	14388
Shaft Speed	rpm	8431	8376	8321	8265	8208	8150
<u>Fuel Pump</u>							
Fuel Density	lb/ft <sup>3</sup>	56.65	56.65	56.65	56.65	56.65	56.65
Total Suction Pressure	psia	44.5	44.5	44.5	44.5	44.5	44.5
Total Discharge Pressure	psia	1212	1177	1142	1107	1073	1040
Non-Cavitating Head	ft	3103	3013	2924	2837	2750	2665
Fuel Flow	lb/sec	122.6	124.1	125.8	127.6	129.3	131.1
Suction Specific Speed	$\frac{rpm \text{ ft}^{3/4}}{\text{lb/sec}}$	21998	22012	22020	22023	22022	22016
Shaft Speed	rpm	23760	23606	23450	23293	23132	22968
<u>Gas Generator</u>							
Chamber Pressure	psia	438	432	427	421	416	410
Oxidizer Flow	lb/sec	0.432	0.429	0.426	0.423	0.419	0.416
Fuel Flow	lb/sec	4.910	4.481	4.773	4.704	4.634	4.564
Mixture Ratio	--	0.0880	0.0886	0.0892	0.0898	0.0905	0.0910
<u>Gas Turbine</u>							
Gas Flow	lb/sec	5.048	4.980	4.912	4.884	4.775	4.706
Total Inlet Pressure	psia	431	426	420	415	409	404
Shaft Speed	rpm	23760	23606	23450	23293	23132	22968
<u>Tap-Off</u>							
Tap-Off Pressure Total ( $P_{fd}$ )	psia		1160	1124	1089	1055	1021

Table 5 --- Engine Component Performance Data for Various

Amounts of Propellant

D. FUEL DUMPED AT COOLING JACKET INLET

Unit	Amount Dumped in lb/sec				
	0	5	10	15	20
<u>Thrust Chamber</u>					
Thrust Chamber Pressure (P <sub>c5</sub> )	826	809	794	778	762
Oxidizer Flow	206.9	206.1	205.5	204.8	204.2
Fuel Flow	110.3	106.2	102.6	99.1	95.5
Mixture Ratio	1.876	1.941	2.002	2.067	2.138
<u>Oxidizer Pump</u>					
Oxidizer Density	90.83	90.83	90.83	90.83	90.83
Total Suction Pressure	41.0	41.0	41.0	41.0	41.0
Total Discharge Pressure	1130	1111	1094	1077	1059
Non-Cavitating Head	1769	1736	1708	1679	1648
Oxidizer Flow	207.3	205.6	205.9	205.2	204.6
Suction Specific Speed	14994	14847	14714	14579	14442
Shaft Speed	8431	8363	8302	8239	8174
<u>Fuel Pump</u>					
Fuel Density	56.65	56.65	56.65	56.65	56.65
Total Suction Pressure	44.5	44.5	44.5	44.5	44.5
Total Discharge Pressure	1212	1179	1145	1111	1078
Non-Cavitating Head	3103	3016	2929	2842	2754
Fuel Flow	122.6	123.2	124.6	125.9	127.3
Suction Specific Speed	21998	21901	21860	21812	21756
Shaft Speed	23760	23569	23396	23219	23036
<u>Gas Generator</u>					
Chamber Pressure	438	431	425	418	412
Oxidizer Flow	0.432	0.426	0.425	0.421	0.417
Fuel Flow	4.910	4.823	4.747	4.669	4.590
Mixture Ratio	0.0880	0.0888	0.0895	0.0902	0.0909
<u>Gas Turbine</u>					
Gas Flow	5.048	4.962	4.887	4.810	4.732
Total Inlet Pressure	431	424	418	412	406
Shaft Speed	23760	23569	23396	23219	23036
<u>Tap-Off</u>					
Tap-Off Pressure Total (P <sub>c1</sub> )		1105	1070	1036	1001
					967

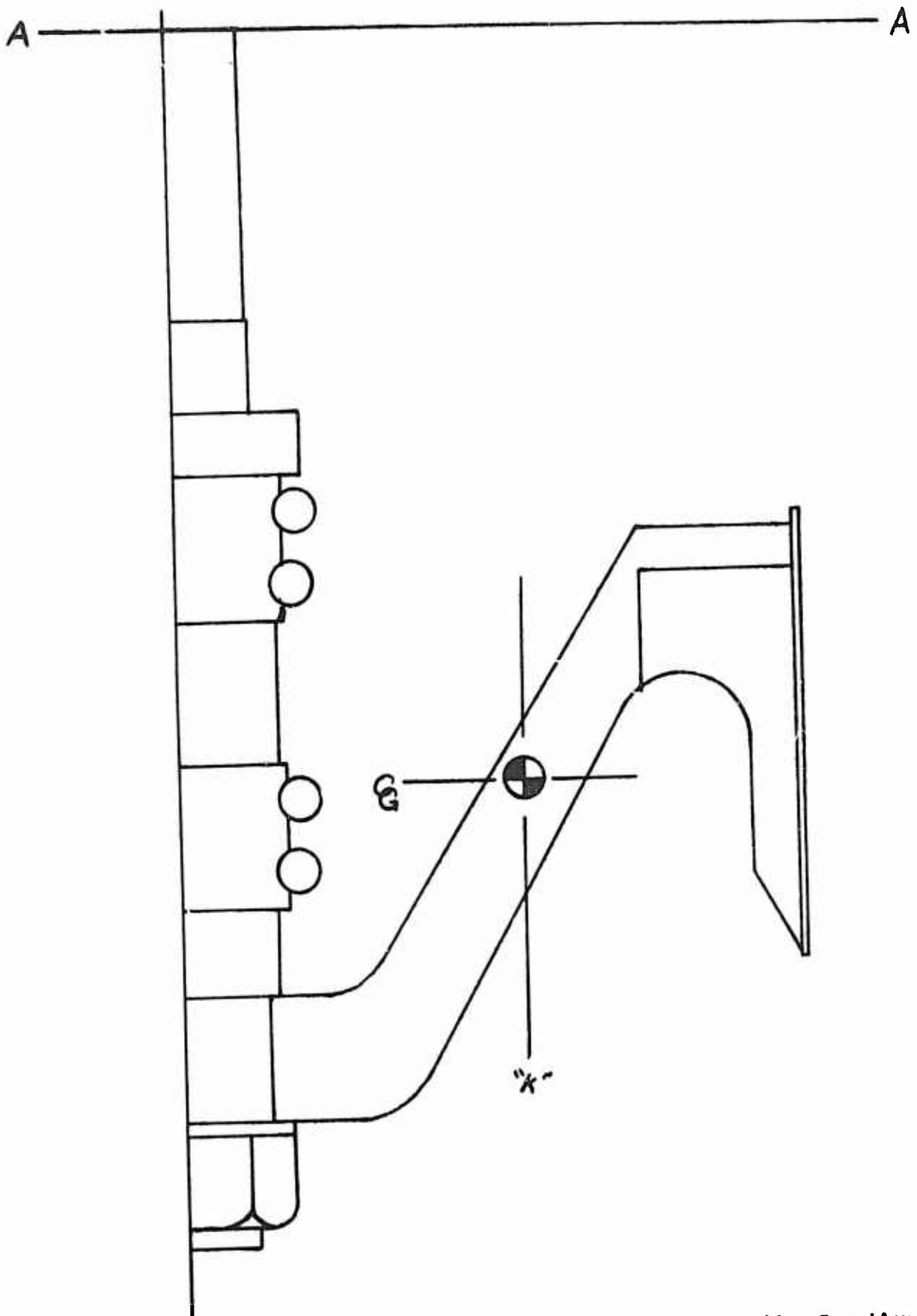


Figure 69 — Shaft-Rotor Center of Gravity and Radius of Gyration Location

III, C, Design (cont.)

on the rotor (Figure 69) and is deflected at right angles by the rotor. The rotor contains 20 slots around the periphery, producing 20 pulses for each revolution. The frequency of the transmitted pulses is controlled by regulating the speed of the slotted rotor. To control the orifice sizes during or between runs, a sliding gate moves to vary the orifice area (Figure 68). The discharged propellant is carried through piping to catch tanks.

The driving system requirements were met by a commercially available 7-1/2-hp explosion-proof variable-speed electrical motor with a vari-drive speed controller capable of accelerating the unit from 352 to 3000 rpm (producing 1000 cps in the pulse generator at full speed) in 2.4 sec (Figure 70). The motor was manufactured by U.S. Motors, Model No. VE-JV-GH, Frame No. 44-254U-41.

Details of the continuous pulse generator design are as follows:

1. Rotor

The rotor is an overhung type with a protruding conical surface. The fluid travelling through the slots strikes the conical surface and deflects downward. The rotor was machined from CRES Type 416 and was heat-treated to a hardness of Rockwell C 39-43 prior to final machining. It weighed 18 lb upon completion.

2. Shaft

The shaft was designed to withstand the torsional loads imposed by the severe acceleration. It was fabricated from CRES Type 416 (heat-treated to a hardness of Rockwell C 39-43).

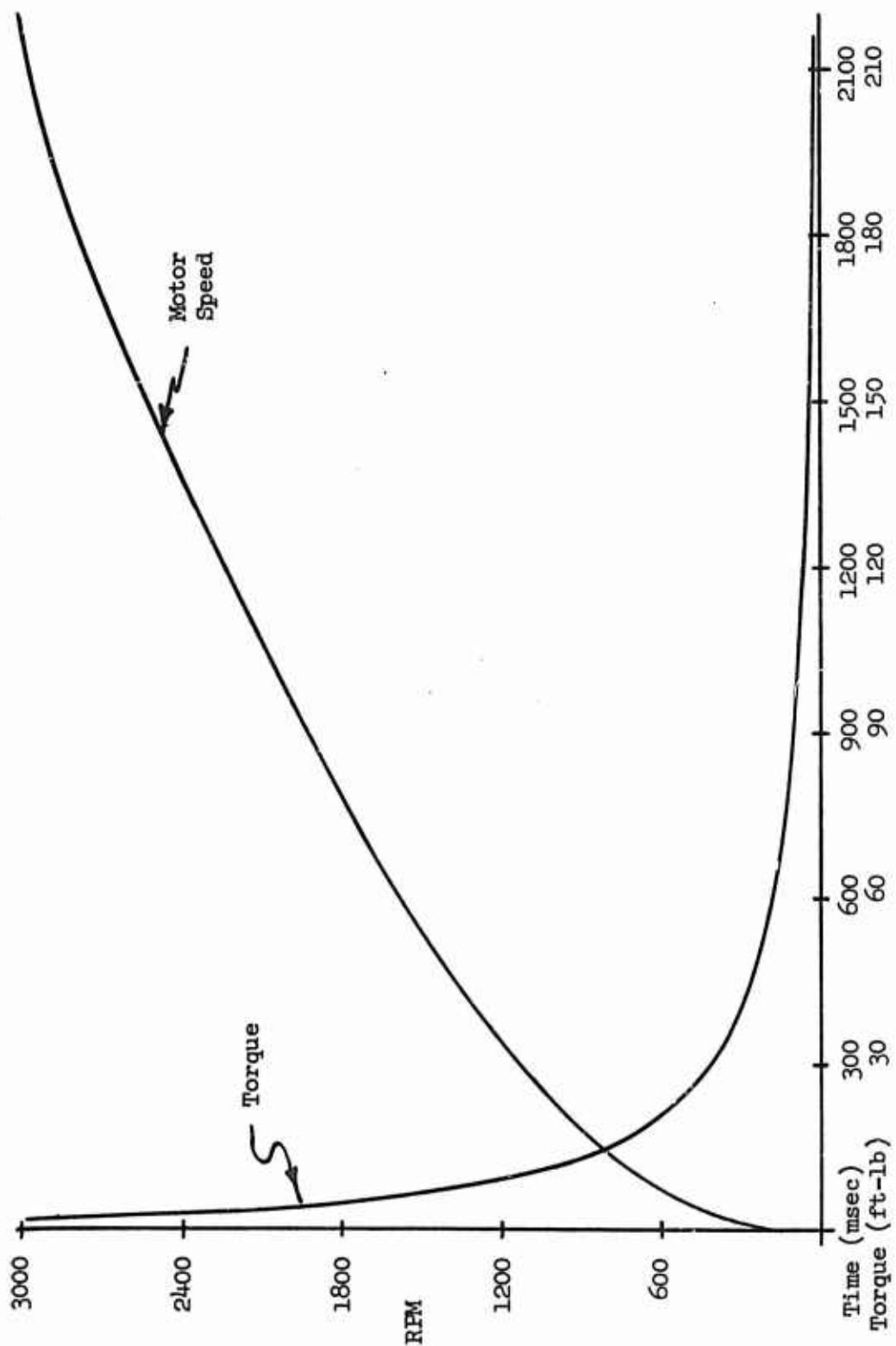


Figure 70 -- Motor Speed Rise Rate

III, C, Design (cont.)

3. Bearings

The bearings were assembled to the shaft in such a manner as to oppose longitudinal oscillations during rotation. Because only three sets of stainless steel Class 7 bearings were available, one pulse generator was assembled using standard weld steel bearings.

4. Seals

To seal against the corrosive attack of the propellants, slotted Teflon O-rings (produced by the Parco Engineering Co.) were utilized. To prevent possible leakage, two O-ring seals were used in parallel. The lips of the seals were mounted with the lip on the liquid side.

5. Gate

The gate was machined from CRES Type 416 and heat-treated to a hardness of Rockwell C 28-32.

6. Bearing Housing

The housing was made from CRES Type 416 heat-treated to a hardness of Rockwell C 28-32. It had a conical surface to match the inside of the rotor. Because the design required two seals in parallel, it became necessary to provide a means adjacent to the bearings for venting between the seals. This would in effect minimize both the possibility of pressure building up between the seals and provide a path for heat to escape from the bearings and lubricant.

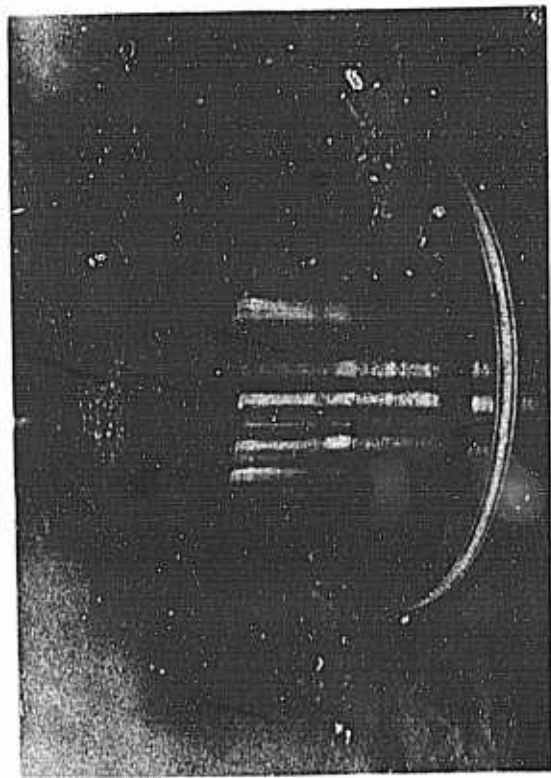
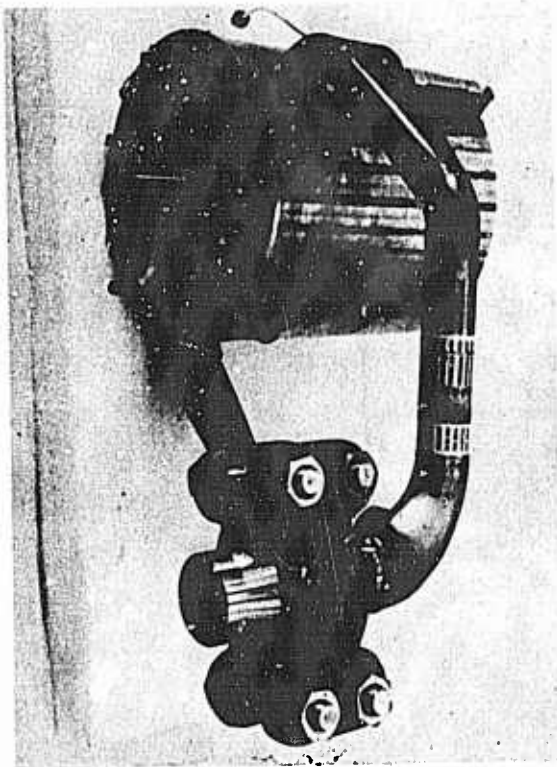
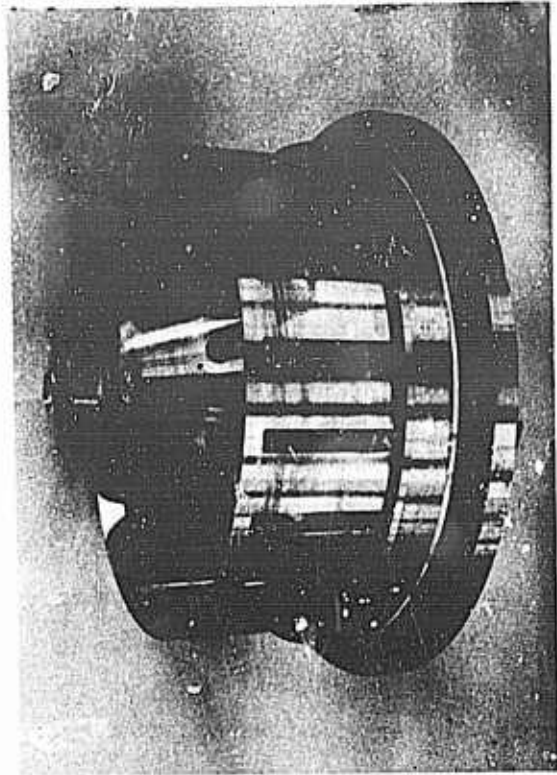
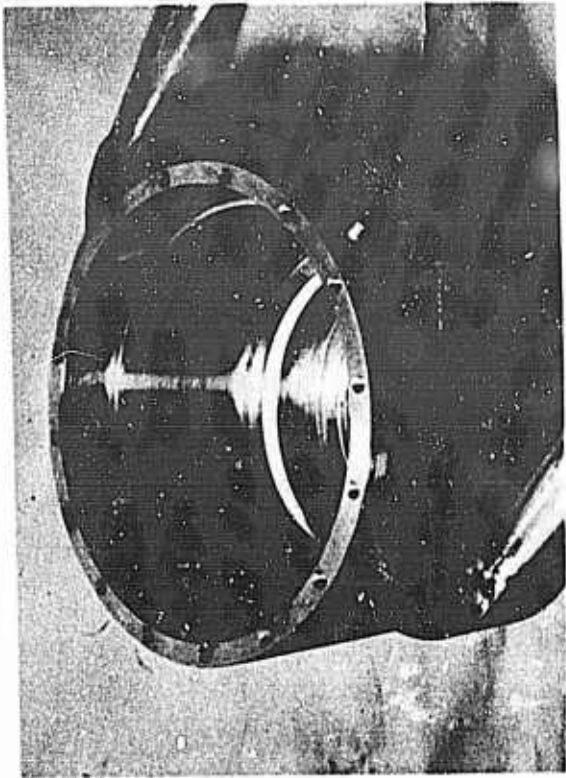


Figure 71 -- Major Components of Continuous Pulse Generator

III, C, Design (cont.)

7. Position Indicator

A linear potentiometer was mounted on the outside of the pulse generator. A shaft which extended into the bearing was connected to the potentiometer by a connecting link. It was thus possible to determine the position of the gate remotely at any time during the run.

D. DEVELOPMENT TESTING

Fabrication of the two pulser units (PN 705930-9 and 705930-19) was completed in the Aerojet-General research and development shop in July 1964. Figure 71 shows pictures of some of the major components. The development testing phase involved the pulsing of a calibrated line (T-605011) in the research and development hydraulics laboratory. The line was flowed with water at the nominal engine flow rate (corrected to water flow) and with a back pressure of 1000 psig. (See Figure 72 for test setup.)

The calibrated line is a section of straight pipe with approximately the same internal diameter as the engine propellant line. Welded to the calibrated line is a flange for attaching the continuous pulse generator connecting lines. This calibrated line provided the capability for mounting six Microsystems PT3F-C2 high frequency pressure transducers at locations calculated to be the quarter wavelength of various discrete frequencies between 200 and 1000 cps (Figure 73).

The oxidizer unit was the first continuous pulse generator to be tested. Early developmental testing of the unit revealed serious flow and actuation problems. The gate that controlled the flow area jammed in the housing and would travel only 25% of its intended distance, that is, the gate traveled only between 75% and full-open. At this gate setting, the flow rate through the pulser varied from 119 to 132 lb/sec of water. A flow rate of this size would mean that, if the pulser were installed on the engine feed lines during a hot firing, the engine performance would

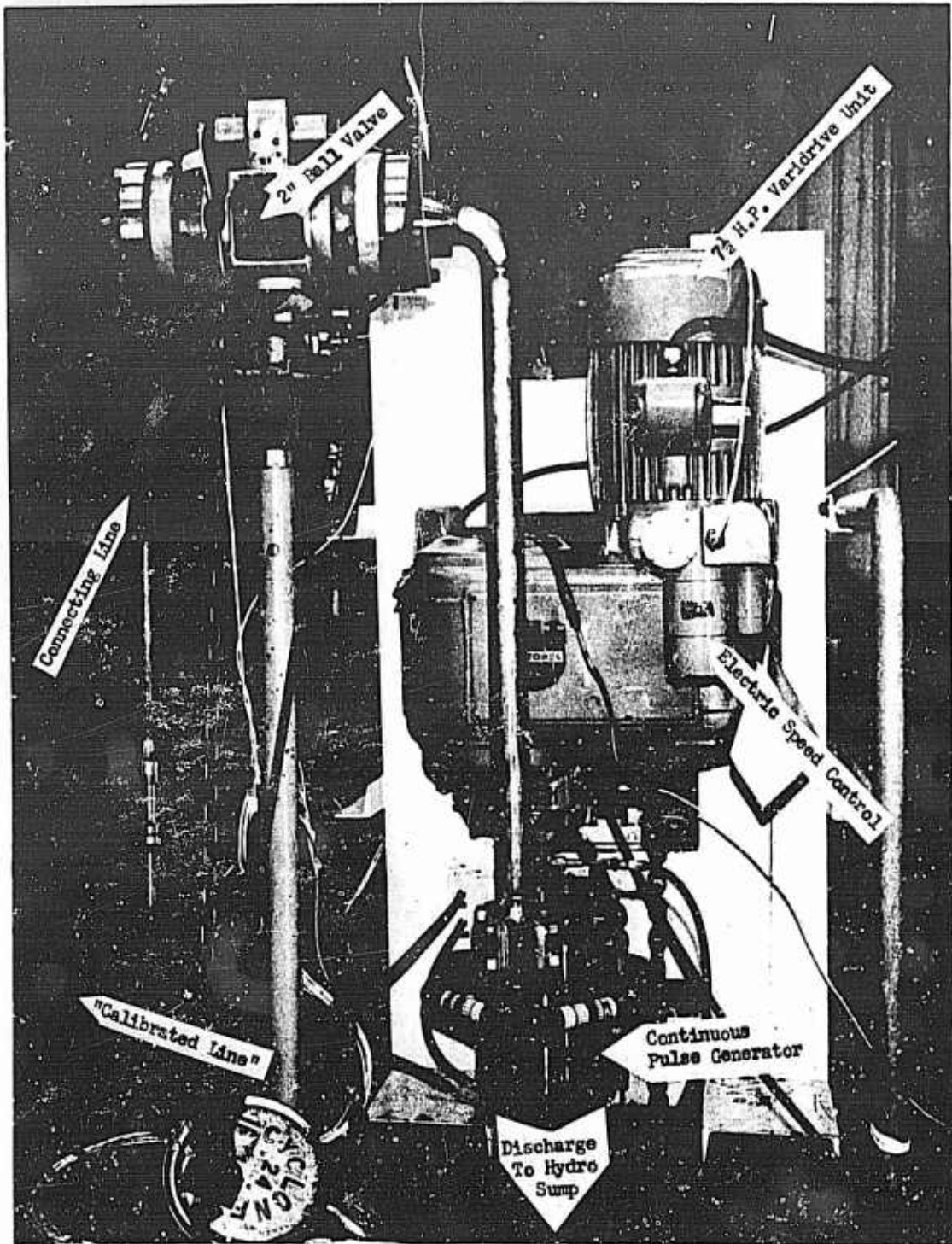
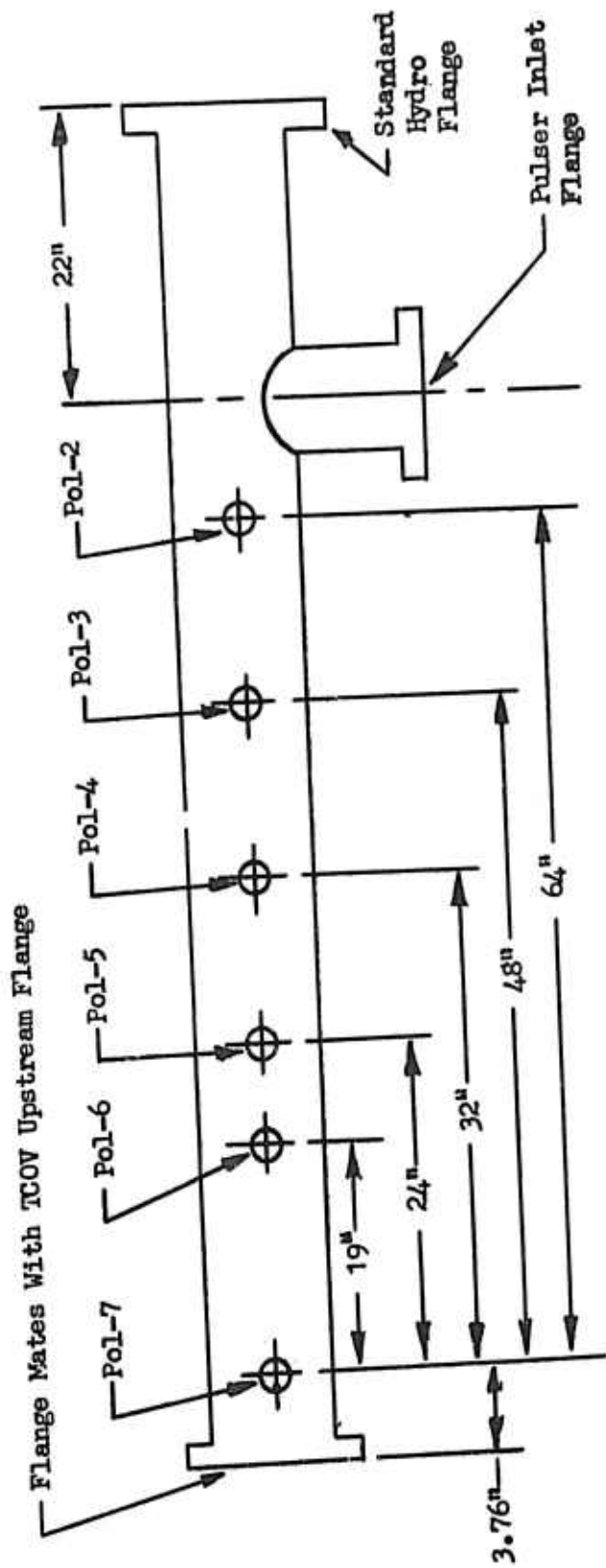


Figure 72 -- Test Set-up of Continuous Pulse Generator



- Notes: 1) Line is made of 4" nominal x .337 wall — CRES 304 Pipe
- 2) Inside Diameter is 3.76"
- 3) Transducer Bosses Accept MICROSYSTEMS PT3F-C2 Flush Mounted High-Frequency Transducers

Figure 73 — GEMSIP "Calibrated Line"

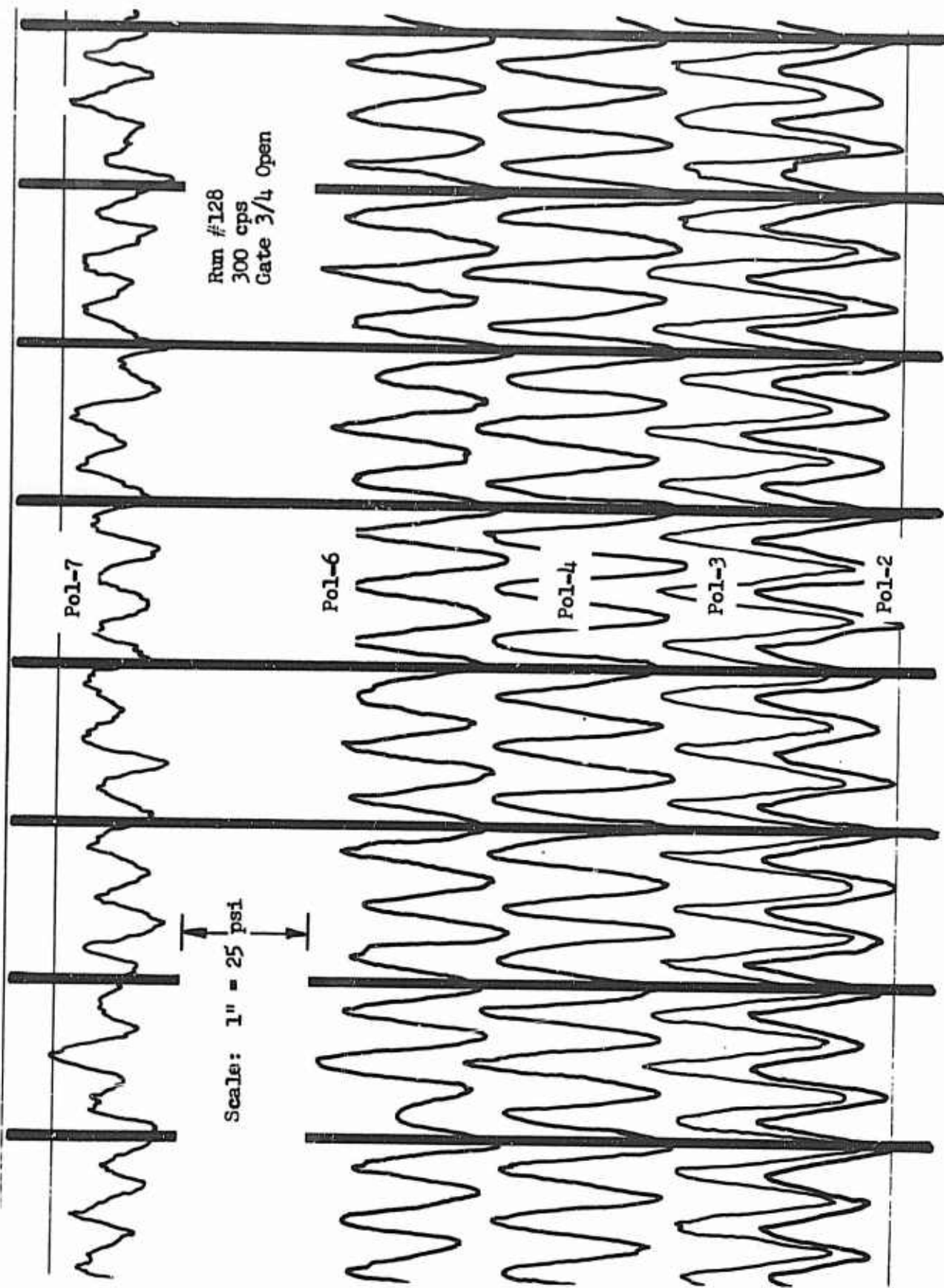


Figure 74 -- Continuous Pulse Generator Oscillograph Trace

III, D, Development Testing (cont.)

be affected drastically, and severe hardware damage would result. However, at these high flow rates, pressure perturbations up to 80 psi and frequencies from 200 to 400 cps were transmitted successfully to the calibrated line. (See Figure 74 for typical oscillograph trace.)

The unit was therefore sent to the assembly shop and disassembled to see why the regulating gate was jamming. It was found that the ball between the gate and the housing (used to prevent the rotation of the gate) had gouged some material from both the gate and the housing because the slot it traveled in was of improper size. At this time it was decided to remove the requirement for the ball from the assembly print and operate the pulsers without the ball. Both units were disassembled and then reassembled without the ball.

The second series of hydraulics laboratory tests began when the fabrication of the fuel circuit pulser was complete. The testing of the fuel unit showed that the operation of the gate was satisfactory without the anti-rotation ball, and that the flow of fluid through the pulser could be controlled to a satisfactory quantity; however, at these low bleed flow rates the magnitude of the pressure perturbations in the calibrated line was not sufficient. The pulses ranged from a low of 9 psi at acceptable flow rates to a high 40 psi at nonacceptable flow rates. Tables 6 and 7 contain the tabulated results of these tests.

This test series also showed that water was leaking into the rotor bearing cavity in both pulsers because the vent plug had inadvertently been left in while the unit was running. This oversight caused both seal and bearing failure in one unit but only seal failure in the other. The bearings in the fuel unit had to be replaced because of corrosion caused by the above mentioned leakage. (These bearings were not made of stainless steel as listed on Drawing 705930 because of the unavailability of the proper stainless steel bearings.)

Table 6 -- Continuous Pulse Generator Test Data

RUN NO.	UNIT	GATE POSITION	CFS	PcPcI (psig)	PULSER Kw	FLOW RATES (lb/sec)		Δ P (PEAK TO PEAK) (psig)							REMARKS		
						IN	OUT	F <sub>1-1</sub>	F <sub>1-2</sub>	F <sub>1-3</sub>	F <sub>1-4</sub>	F <sub>1-5</sub>	F <sub>1-6</sub>	F <sub>1-7</sub>			
CFG-001	Oxidizer	3/4 open	200	-	-	-	-	-	-	-	-	-	-	-	-	-	No Good Data
-002	Oxidizer	3/4 open	200	ND	-	-	-	-	-	-	-	-	-	-	-	-	No Good Data
-003	Oxidizer	3/4 open	200	ND	-	137	119	34.4	33.6	33.6	33.6	33.6	33.6	33.6	33.6	33.6	Nominal Ox. Flow = 169 lb/sec
-004	Oxidizer	3/4 open	300	-	-	136.5	124	47.0	81.7	81.7	81.7	81.7	81.7	81.7	81.7	81.7	
-005	Oxidizer	3/4 open	300	-	-	136.5	124	41.1	54.0	54.0	54.0	54.0	54.0	54.0	54.0	54.0	
-006	Oxidizer	Full open	383	-	-	128.5	132	32.4	21.6	21.6	21.6	21.6	21.6	21.6	21.6	21.6	
-007	Fuel	1/4 open	290	705	2.08	104.5	55.1	17.0	21.4	21.4	21.4	21.4	21.4	21.4	21.4	21.4	Nominal Fuel Flow = 117 lb/sec
-008	Fuel	1/4 open	430	710	2.07	104.5	55.1	15.5	22.4	22.4	22.4	22.4	22.4	22.4	22.4	22.4	
-009	Fuel	1/4 open	570	720	2.04	104.9	54.7	16.6	16.1	16.1	16.1	16.1	16.1	16.1	16.1	16.1	
-010	Fuel	1/4 open	715	725	1.95	105.4	52.4	14.8	-	-	-	-	-	-	-	-	
-011	Fuel	1/4 open	290	870	1.29	104.7	38.1	13.4	14.5	14.5	14.5	14.5	14.5	14.5	14.5	14.5	
-012	Fuel	1/8 open	430	872	1.29	104.7	38.1	12.0	13.5	13.5	13.5	13.5	13.5	13.5	13.5	13.5	
-013	Fuel	1/8 open	570	875	1.28	104.9	37.9	9.0	9.1	9.1	9.1	9.1	9.1	9.1	9.1	9.1	
-014	Fuel	1/8 open	715	880	1.24	105.1	36.8	13.4	10.0	10.0	10.0	10.0	10.0	10.0	10.0	10.0	
-015	Fuel	1/16 open	200	850	1.23	109.4	36.0	13	11	11	11	11	11	11	11	11	
-016	Fuel	1/16 open	300	850	1.23	109.4	36.0	12	14.6	14.6	14.6	14.6	14.6	14.6	14.6	14.6	
-017	Fuel	1/16 open	400	855	1.22	109.7	35.7	16	16.7	16.7	16.7	16.7	16.7	16.7	16.7	16.7	
-018	Fuel	1/16 open	500	855	1.21	109.7	35.5	17	17	17	17	17	17	17	17	17	
-019	Fuel	1/16 open	600	858	1.20	109.7	35.3	13	12.7	12.7	12.7	12.7	12.7	12.7	12.7	12.7	
-020	Fuel	1/16 open	700	862	1.16	109.7	34.1	11	12	12	12	12	12	12	12	12	
-021	Fuel	1/16 open	800	888	1.11	110.1	33.2	10	18	18	18	18	18	18	18	18	
-022	Fuel	1/2 open	200	545	3.73	97.9	87.8	13	15	15	15	15	15	15	15	15	
-023	Fuel	1/2 open	300	550	3.71	98.3	87.1	26	23	23	23	23	23	23	23	23	
-024	Fuel	1/2 open	400	555	3.69	98.5	86.9	23	21	21	21	21	21	21	21	21	
-025	Fuel	1/2 open	500	560	3.64	98.5	86.1	26	16	16	16	16	16	16	16	16	
-026	Fuel	1/2 open	600	572	3.52	99.4	84.3	15	12	12	12	12	12	12	12	12	
-028	Fuel	3/4 open	200	392	5.10	90.3	101.1	12	9	9	9	9	9	9	9	9	
-029	Fuel	3/4 open	300	392	5.09	90.5	100.9	18	16	16	16	16	16	16	16	16	
-030	Fuel	3/4 open	400	397	5.05	90.5	100.1	20	17	17	17	17	17	17	17	17	
-031	Fuel	3/4 open	500	407	4.95	90.6	100.1	20	17	17	17	17	17	17	17	17	
-032	Fuel	3/4 open	600	425	4.74	91.8	97.6	15	13	13	13	13	13	13	13	13	

Table 7 -- Continuous Pulse Generator Test Data

RUN NO.	UNIT	GATE POSITION	CPS	PULSES (PULG)	PULSER IN	FLOMRATES (#/sec)		A.P. (PEAK TO PEAK) (psi)							REMARKS	
						THRU	OUT	F-1	F-2	F-3	F-4	F-5	F-6	F-7		
101	Oxidizer	1/8 open	200	878	1.28	37.8	161.5	199.3	16	17	17	17	-	12	14	
102	Oxidizer	1/8 open	300	876	1.24	36.6	162.7	199.3	13	10	18	14	-	15	10	
103	Oxidizer	1/8 open	400	876	1.22	36.2	162.7	198.9	15	14	14	14	-	12	10	
104	Oxidizer	1/8 open	500	875	1.24	36.6	162.7	199.3	13	15	14	14	-	13	11	
105	Oxidizer	1/8 open	600	880	1.22	36.2	162.7	198.9	12	11	12	12	-	12	9	
106	Oxidizer	1/8 open	700	876	1.24	36.6	162.1	198.7	9	10	9	9	-	11	9	
107	Oxidizer	1/8 open	800	876	1.21	35.8	162.1	197.9	13	13	12	12	-	12	8	
108	Oxidizer	1/16 open	200	928	0.74	22.5	165.2	187.7	9	7	12	12	-	12	13	
109	Oxidizer	1/16 open	300	928	0.74	22.5	165.2	187.7	9	11	13	12	-	12	9	
110	Oxidizer	1/16 open	400	930	0.74	22.5	165.2	187.7	10	11	11	11	-	11	11	
111	Oxidizer	1/16 open	500	930	0.74	22.5	165.2	187.7	10	12	12	13	-	13	12	
112	Oxidizer	1/16 open	600	932	0.72	21.9	165.8	187.7	10	11	9	9	-	10	9	
113	Oxidizer	1/16 open	700	933	0.72	21.9	165.8	187.7	9	13	11	11	-	13	12	
114	Oxidizer	1/16 open	800	933	0.70	21.4	165.8	187.2	12	12	12	14	-	12	12	
115	Oxidizer	1/16 open	900	935	0.70	21.4	165.8	187.2	15	13	14	14	-	15	19	
116	Oxidizer	1/4 open	200	832	1.60	46.2	159.6	205.8	13	13	14	14	-	13	-	
117	Oxidizer	1/4 open	300	832	1.60	46.2	159.6	205.8	14	13	15	15	-	17	10	
118	Oxidizer	1/4 open	400	834	1.57	45.3	159.6	204.9	14	14	14	14	-	18	15	
119	Oxidizer	1/4 open	500	836	1.57	45.3	159.6	204.9	12	14	11	11	-	16	10	
120	Oxidizer	1/4 open	600	837	1.57	45.3	159.6	204.9	10	11	12	12	-	13	15	
121	Oxidizer	1/4 open	700	840	1.56	45.3	159.6	204.9	12	18	12	12	-	14	14	
122	Oxidizer	1/2 open	200	666	4.00	103.2	156.5	259.7	14	14	12	12	-	14	9	
123	Oxidizer	1/2 open	300	670	3.96	102.6	157.1	259.7	34	40	38	38	-	33	18	
124	Oxidizer	1/2 open	400	667	3.95	101.9	157.1	259.0	20	13	18	18	-	27	30	
125	Oxidizer	1/2 open	500	663	3.93	101.2	157.1	258.3	16	22	19	19	-	20	20	
126	Oxidizer	1/2 open	600	672	3.88	100.8	157.1	257.9	7	7	8	8	-	12	9	
127	Oxidizer	3/4 open	200	415	5.90	120.2	139.5	259.7	13	12	10	10	-	9	9	
128	Oxidizer	3/4 open	300	418	5.89	120.2	139.5	259.7	26	35	38	38	-	31	14	
129	Oxidizer	3/4 open	400	427	5.72	118.1	139.5	257.6	16	12	14	14	-	23	27	
130	Oxidizer	3/4 open	500	425	5.69	117.3	139.5	256.8	14	23	27	27	-	18	20	
131	Oxidizer	Full open	200	340	6.97	128.8	135.9	264.7	12	14	13	13	-	12	7	
132	Oxidizer	Full open	300	346	6.93	128.8	135.9	264.7	11	15	13	13	-	11	8	
133	Oxidizer	Full open	400	352	6.93	128.1	135.9	264.0	13	12	14	14	-	15	15	

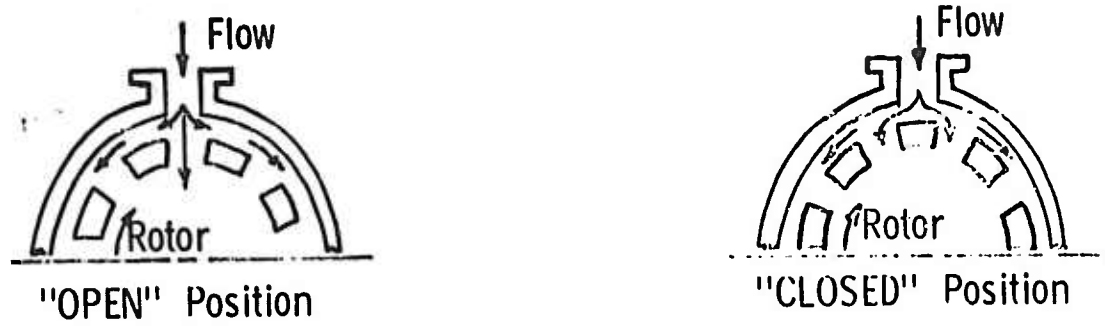


Figure 75 — Unmodified CPG Configuration



Figure 76 — Modified CPG Configuration

III, D, Development Testing (cont.)

Studies were conducted to determine modifications to the pulser that would produce higher pressure perturbations within the limit of acceptable bypass flow rates. These resulted in a design change requiring the welding of restrictor blocks into the pulser housing and the machining of two inlet holes in the gate. (Refer to Figures 75 and 76.) This modification permits a much more restricted path to the fluid flowing through the pulser and eliminates the excessive bleed between the housing and the rotor that occurred with the original design. The full open condition now occurs when the gate is in the upper position rather than in the lower position and prevents the flow of any free fluid between the housing and the rotor.

The fully modified oxidizer continuous pulse generator was returned to the hydraulics laboratory for the third series of checkout and functional tests on 21 September 1964. The setup was complete 23 September 1964. The calibrated line was flowed at 169 lb/sec of water at 1000 psig back pressure. Flow and gage readings were taken for future flow calculations.

The noise level of the pulser with the modification was much higher than it had been before, and the pulses being transmitted to the calibrated line were causing the line and entire system to vibrate severely. The vibrations backed nuts off flanges on the line that were originally tightened to 300 to 500 in.-lb of torque. Before the recording oscillograph could be actuated to record the perturbations in the line, galvanometer adjustments had to be made.

Visual observation of the perturbations being received by the oscillograph showed the range to be over 2 in. of deflection on an adjusted scale of 100 psi/in. of deflection; or a perturbation in excess of 200 psi peak-to-peak. These perturbations were seen with the pulser shaft turning 600 rpm, thus giving an effective pulse frequency of 200 cps. This pulser operation was not permanently recorded because of a structural failure of one of the housing inlet elbows.

III, D, Development Testing (cont.)

The faulty elbow cracked in a longitudinal direction and across the weld between PN's 705975-9 and 706099-1. The crack is approximately 2-in. long with a maximum gap of approximately 1/8-in. at the midpoint. The crack apparently started in the weld joint between the parts listed and propagated into the parent material of the adapter, PN 706099-1, and along the weld joint of the elbow, PN 705975-9. This failure could have been caused by a discrepant weld; however, previous weld penetration inspections and proof tests on the unit before it was assembled tend to discredit this theory.

A more likely explanation of the failure would be that the crack was the result of severe vibrational loading while the pulser was operating, causing fatigue in the weld joints. Before the continuous pulse generators are run again at pressures above 600 psig, a thorough inspection of the welds on the inlet lines should be made to assure the soundness of all welded joints. On September 10, 1964, all development testing of the continuous pulse generator was cancelled because of program redirection.

The last test series on the oxidizer unit (S/N 002) also developed leakage through the shaft seals and into the bearing cavity. This condition has existed on all tests to date. It was noted after the first test series that the Teflon shaft seals had caused a 0.001 to 0.002-in. scoring on the rotor shaft. Because of this scoring, there may have been insufficient compression on the Teflon seals, which resulted in leakage. Before these units are operated again, a detailed inspection should be made of the rotor shaft and the Teflon shaft seals measured accurately.

Test results indicate that the overboard bleed concept is a feasible method for producing oscillations in the 91-5 feed system, but the GEMSIP pulse generators are not ready for use with a fireable engine. The bearing seal and inlet elbow problems must be solved and further development testing in the hydraulics laboratory would be necessary before these units would be completely functional.

GEMSIP FR-1, Volume 5

APPENDIX, SECTION III

FINAL DISPOSITION OF HARDWARE

I. UNITS SENT TO SUBSTORES

A. OXIDIZER UNIT

Oxidizer unit PN 705930 was sent intact to Substore No. 11. It is recommended that this unit be disassembled, cleaned, and reassembled prior to operation again.

B. FUEL UNIT

The following components of the fuel unit were sent to Substore No. 11:

<u>PN</u>	<u>Name</u>
705923-1	Shaft
705924-1	Bearing Housing
705925-1	Rotor
705926-1	Bearing Cover
705927-1	Bearing Spacer
705927-3	Bearing Spacer
705928-1	Gate
705977-9	Body and Flange
705932-1	Nut
705933-1	Positioning Rod
706280-9	Manifold and Housing Assy

The unit requires the following parts to complete assembly.

<u>PN</u>	<u>Name</u>
706276-1	Retainer
706277-1	Plate
706278-1	Retainer Plug
SSQH0LO6DT-S5	Bearing (2 sets required)
52821	Hub
50807	Ring
48502	Clamp

GEMSIP FR-1, Volume 5, Appendix, Section III

II. SPARE PARTS ON ORDER

The following is a list of all spare parts ordered for the assembly of the continuous pulse generators that are presently on hand in Substore No. 11.

<u>PN</u>	<u>Name</u>	<u>Quantity on Hand</u>	<u>Quantity Required for Assembly</u>
FRP2103-445	Teflon Ring	23	2
FRP2103-446	Teflon Ring	22	2
FRP2103-447	Teflon Ring	23	2
FRP2103-010	Teflon Ring	120	2
FRP9020-3	Teflon Ring	79	1
FRP9020-4	Teflon Ring	76	1
FRP9020-5	Teflon Ring	74	1
FRP568-445	O-Ring	9	1
FRP568-446	O-Ring	10	1
FRP568-447	O-Ring	10	1
FRP568-271	O-Ring	12	1
FRP568-266	O-Ring	11	1
FRP568-010	O-Ring	79	1
FRP9020-2	O-Ring	79	1
FRP2120-023	O-Ring	8	1
FRP2120-029	O-Ring	16	2
MS35337-80	Lockwasher	42	6
MS35337-81	Lockwasher	14	2
MS35337-82	Washer	48	6
MS35337-83	Lockwasher	177	24
MS24392-3	Union	10	1
MS24392-4	Union	2 (8 on order)	1
MS24391-2L	Plug	3	1
NAS625-H6	Bolt	84	14
AN44C7A	Bolt	16	2

GEMSIP FR-1, Volume 5, Appendix, Section III

II, Spare Parts on Order (cont.)

<u>PN</u>	<u>Name</u>	<u>Quantity on Hand</u>	<u>Quantity Required for Assembly</u>
AN520C8R5	Screw	124	4
AN507C836R4	Screw	106	2
AN340C8	Nut	20	2
AN315C3R	Nut	20	2
AN5CH10A	Bolt	0 (48 on order)	8
MS172207	Washer	23	1
MS20913-1CR	Plug	19	1
AN581-4-24	Pin	106	1
AN960-C-1416	Washer	12	1
AN315C14R	Nut	12	1
AN4CH7A	Bolt	48	6
AN122719	Dowel Pin	10	2

Both U.S. Motors Varidrive units and frames were sent to D-Area stores (but actually stored at the City Annex).

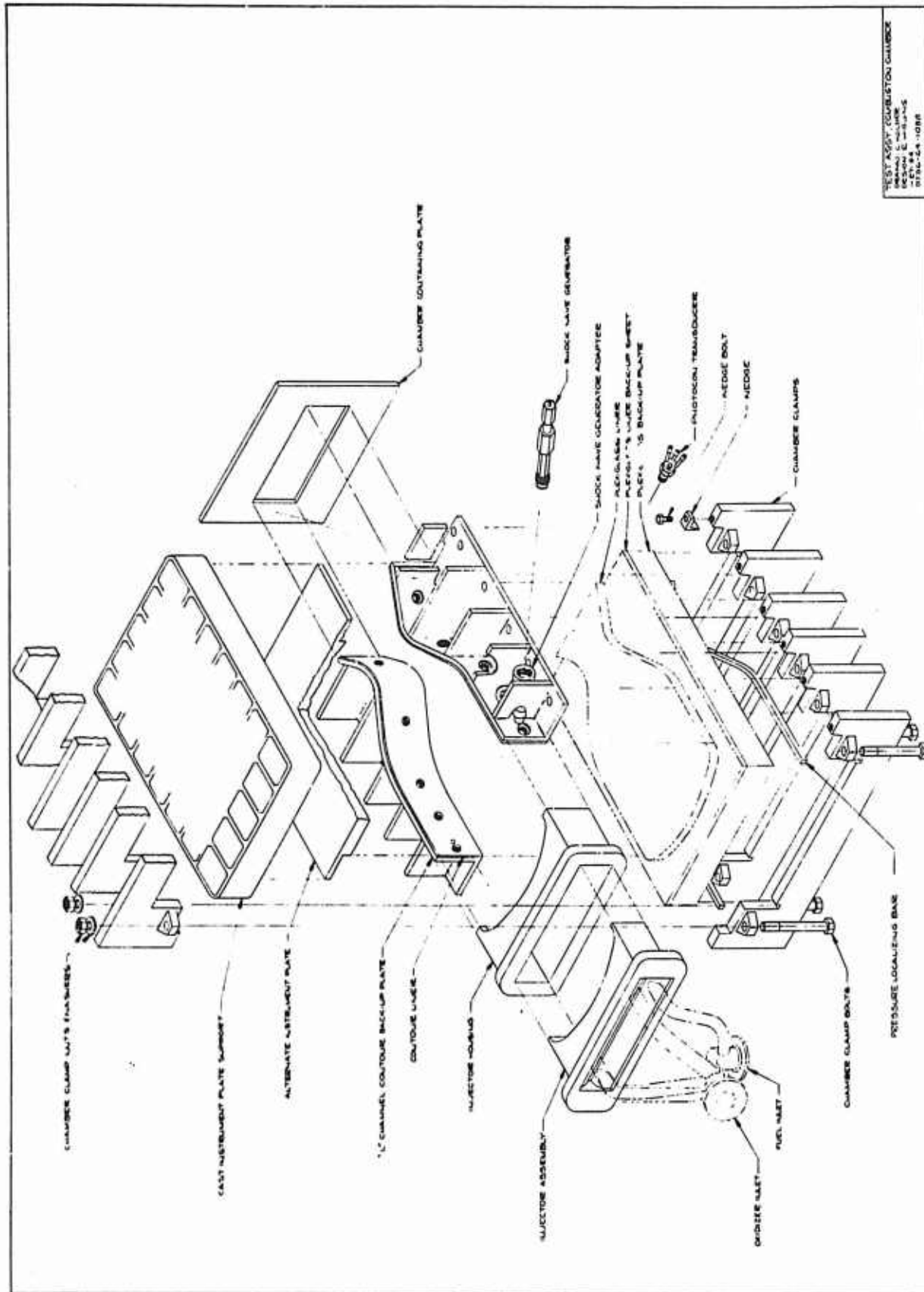


Figure 77 -- Two-Dimensional Motor

IV. TWO-DIMENSIONAL MOTOR

The objective was to design a 2-dimensional motor which could be used to study visually the combustion phenomena and the interaction of induced pressure perturbations on the combustion process. The gross properties of the combustion phenomena were to be made variable by utilizing several different injection concepts and both unbaffled and uncooled baffled injectors. (See Figure 77.)

A. DESIGN APPROACH

The motor was to duplicate or simulate the full-scale TCA as closely as possible in the following respects:

- a) Mass flow rate per unit of cross sectional chamber area.
- b) Chamber pressure.
- c) Valve mixture ratio.
- d) Cross-sectional size and shape.
- e) Injector pattern variation capability.

In addition, the motor design was to encompass the following features:

- a) Interchangeable, replaceable, transparent side walls.
- b) Interchangeable, replaceable, instrumented side walls.
- c) All pressure instrumentation to be of the high frequency response type.
- d) Rugged construction.
- e) Maximum access for instrumentation, perturbation, and viewing.
- f) On-stand replacement of windows
- g) Propellant lines and thrust attachments to mate with LR91-AJ-5 TCA and test stand.

IV, A, Design Approach (cont.)

The basic concept of the motor was an axial cross section of the full-scale combustion zone with a finite depth. The assembly was envisioned as a rugged "boilerplate" design, employing large safety factors, manufactured from commonly available materials. A working pressure of 2000 psia was selected, based on the nominal chamber pressure plus possible pressure overshoot multiplied by a safety factor of two. The most conservative approach to the stress analysis was taken with all components. Mild steel was selected as the material to be used on all components of the motor where its use would not compromise the main objectives of the program. Other materials would be selected as applicable.

It was decided to conduct a material evaluation study to determine the most suitable material for use as the observation windows (See Section II B). The high frequency response pressure transducers selected were the Photocon Model 352A for the hot gas transducers and Microsystems Model PT3JC2 for the propellant circuits. The locations of the transducer bosses was selected for best correlation of pressure data with visual observations and the motor designed around the boss locations. The adapters for the perturbing devices were designed to fit the standard Photocon boss.

The perturbing devices selected were the tangential pulse gun and a nondirected bomb of a new design.

In order to keep the mass flow rate per unit cross-sectional area constant, the throat "diameter" had to be increased. The forward-end contour was kept identical to the full-scale chamber, and the convergence angle increased to allow for the decreased throat "diameter."

IV, Two-Dimensional Motor (cont.)

B. COMPONENT DESCRIPTION

The simulator, or 2D motor, Figure 78, was designed as an assembly of fuel and oxidizer manifolds, Figures 79 and 80; injector, Figure 81; simulator sub-assembly, Figure 82; clamp assemblies, Figure 83; windows and/or cover plates, Figures 84 and 85; bolt assemblies, Figure 86; bolt spacers, Figure 87; thrust mount, Figure 88; window supports, Figure 89; clamp spacers, Figure 90; and window, Figure 91.

The design incorporated all the required design parameters with emphasis placed on simplicity of fabrication and durability of the structure. All components were designed to yield at an internal pressure of 2000 psia.

A thickness of 3.0 in. was selected for the combustion zone; a compromise between (1) the thin width desired for photographing the combustion phenomena, (2) the thick width desired for reducing the boundary layer effect, and (3) the physical size required to accommodate the Photocon pressure transducers and sufficient elements in the injector pattern to produce a gross simulation of the full-scale pattern.

All threaded connectors were through bolts with nuts wherever possible. Internally threaded holes were only used in locations where clearances made the use of through bolts impossible.

The injector simulator subassembly interface was sealed with a standard size butyl O-ring. The simulator subassembly-to-window (or cover plate) interface was sealed with a silicon O-ring extrusion protected by trowelled-in RTV-60 rubber.

The detailed design parameters selected for the motor are shown in Table 8. Figure 92 shows a typical section through the assembled motor.

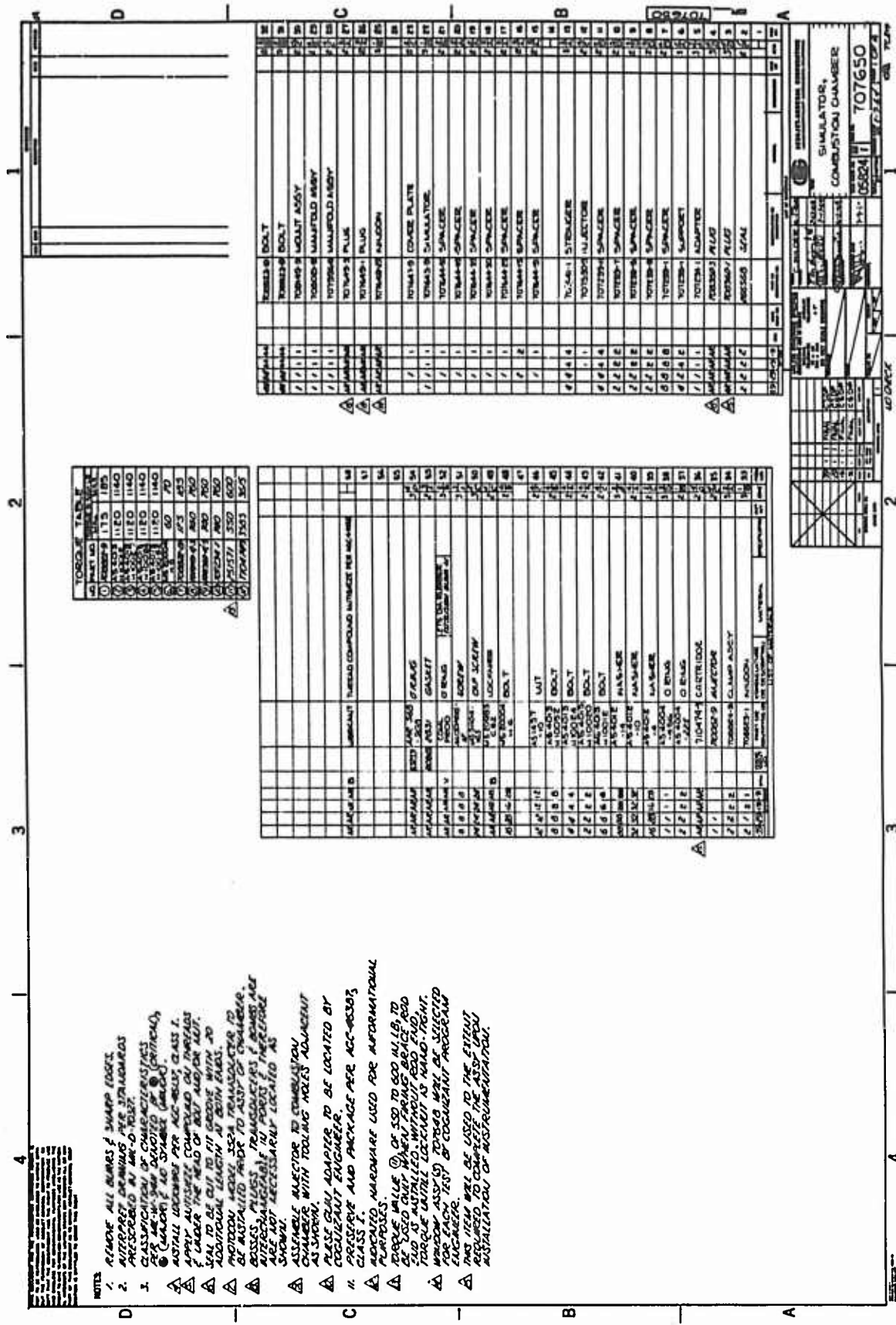


Figure 78a -- Simulator, Injector Chamber

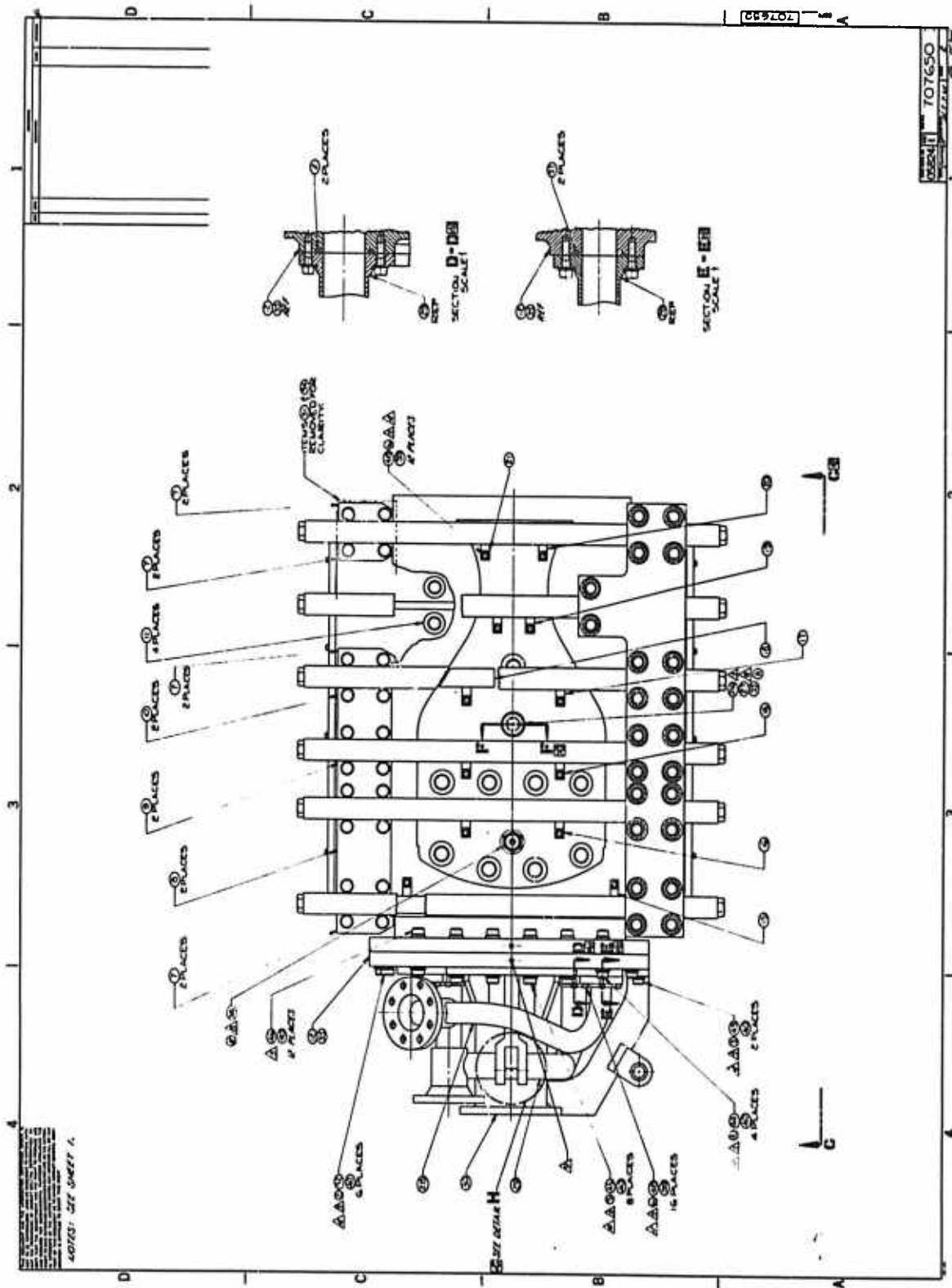


Figure 78b -- Simulator, Injector Chamber









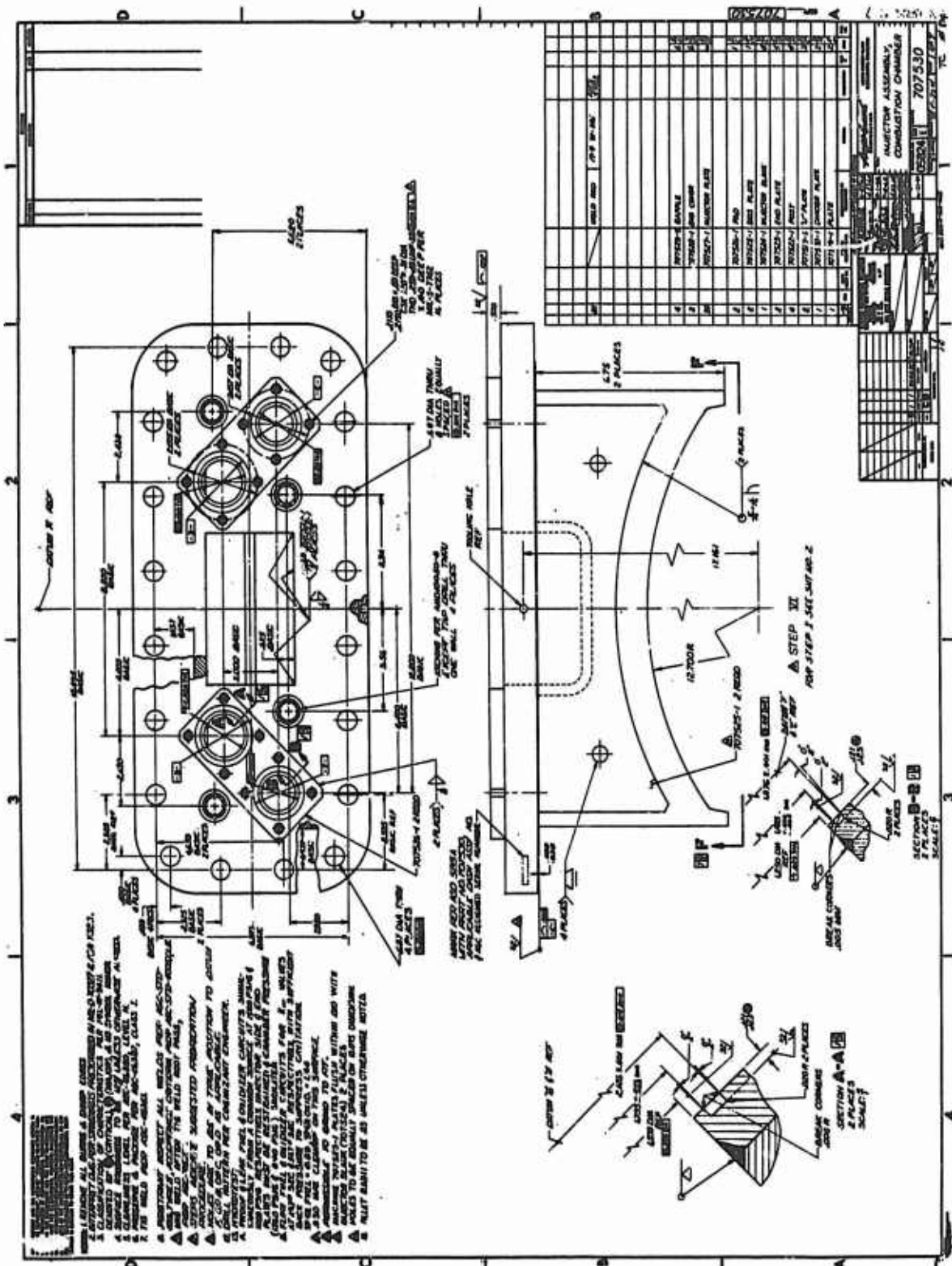


Figure 81a -- Injector Assembly, Combustion Chamber

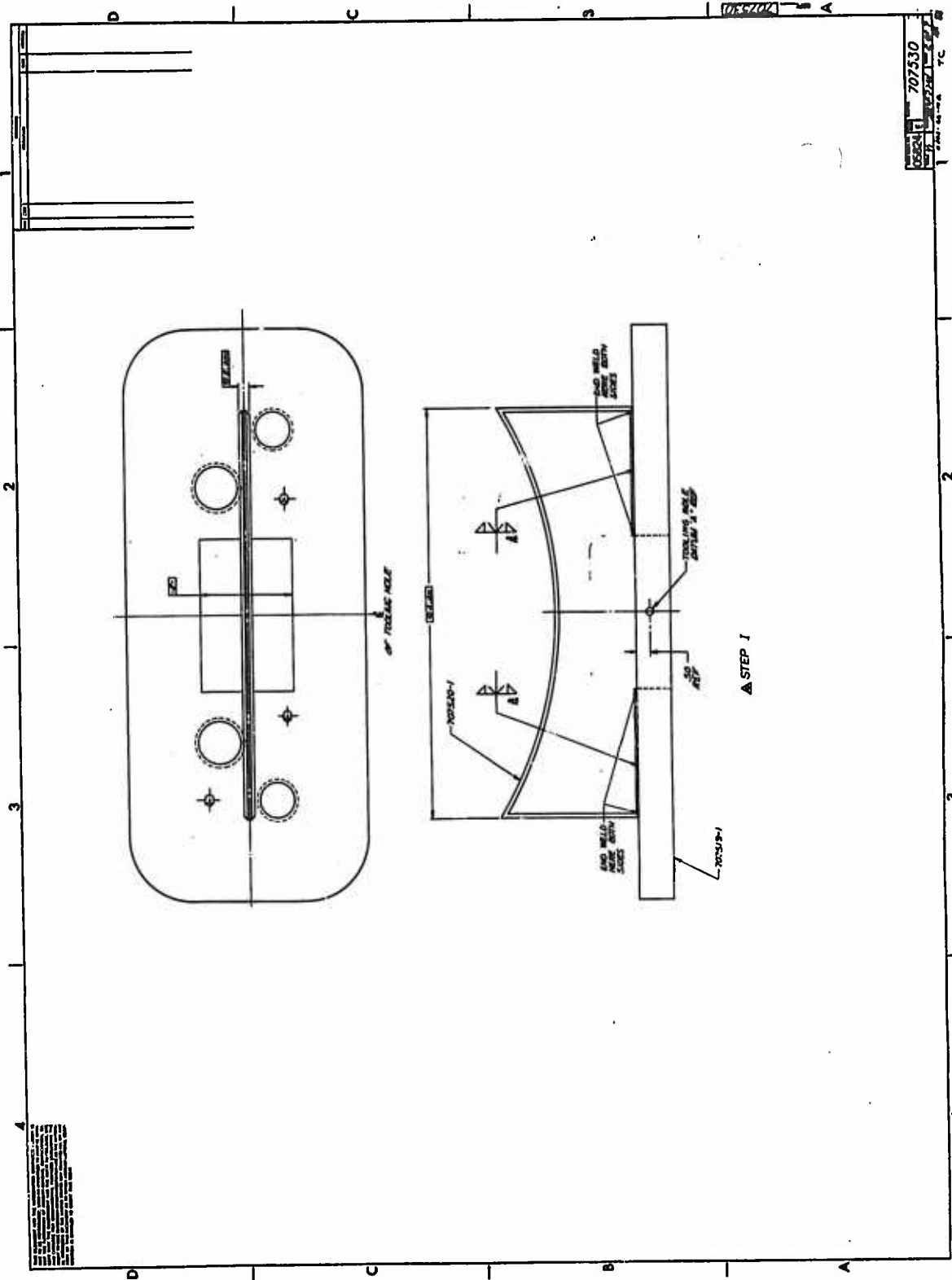


Figure 81b -- Injector Assembly, Combustion Chamber

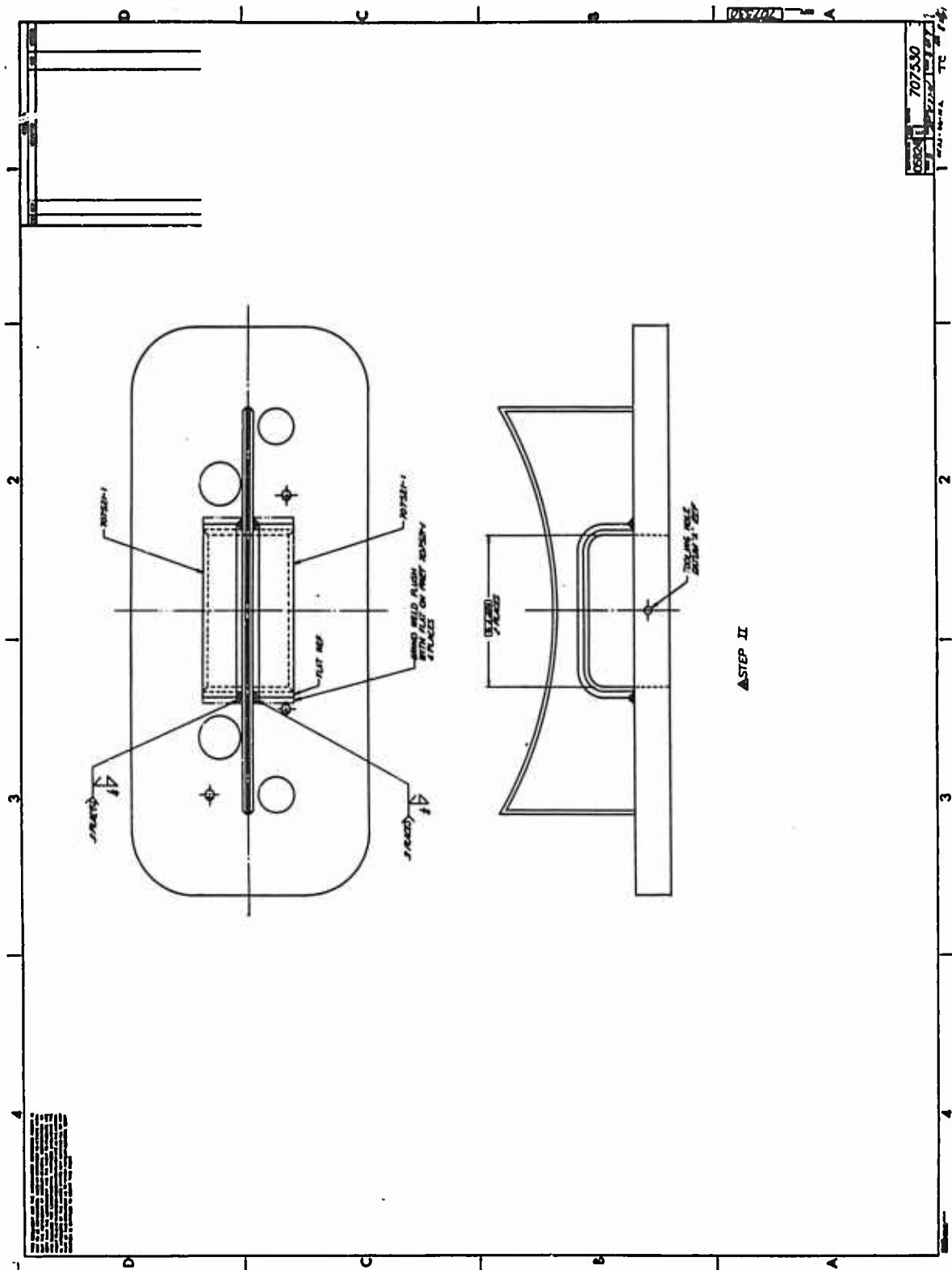


Figure 81c -- Injector Assembly, Combustion Chamber

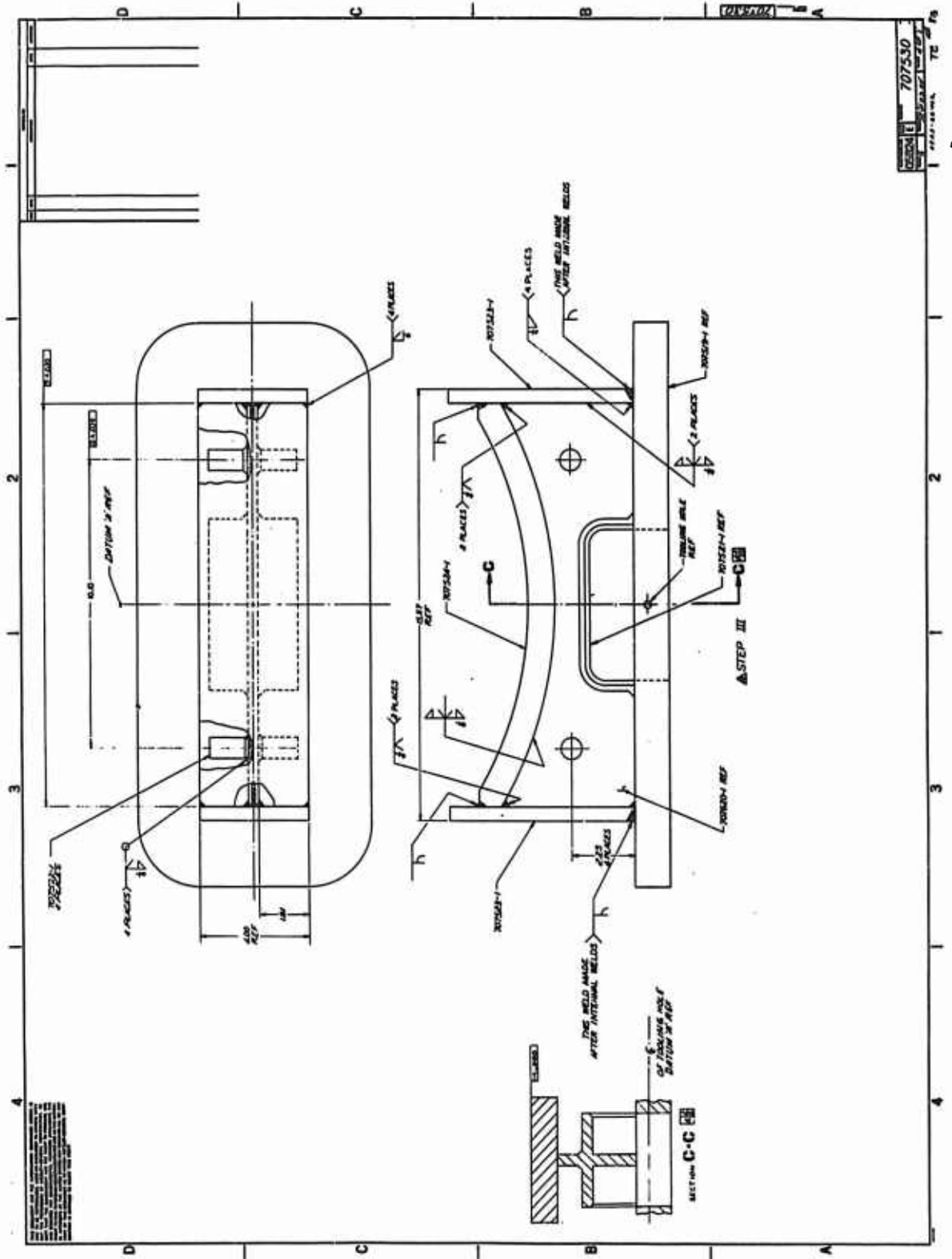


Figure 8ld -- Injector Assembly, Combustion Chamber





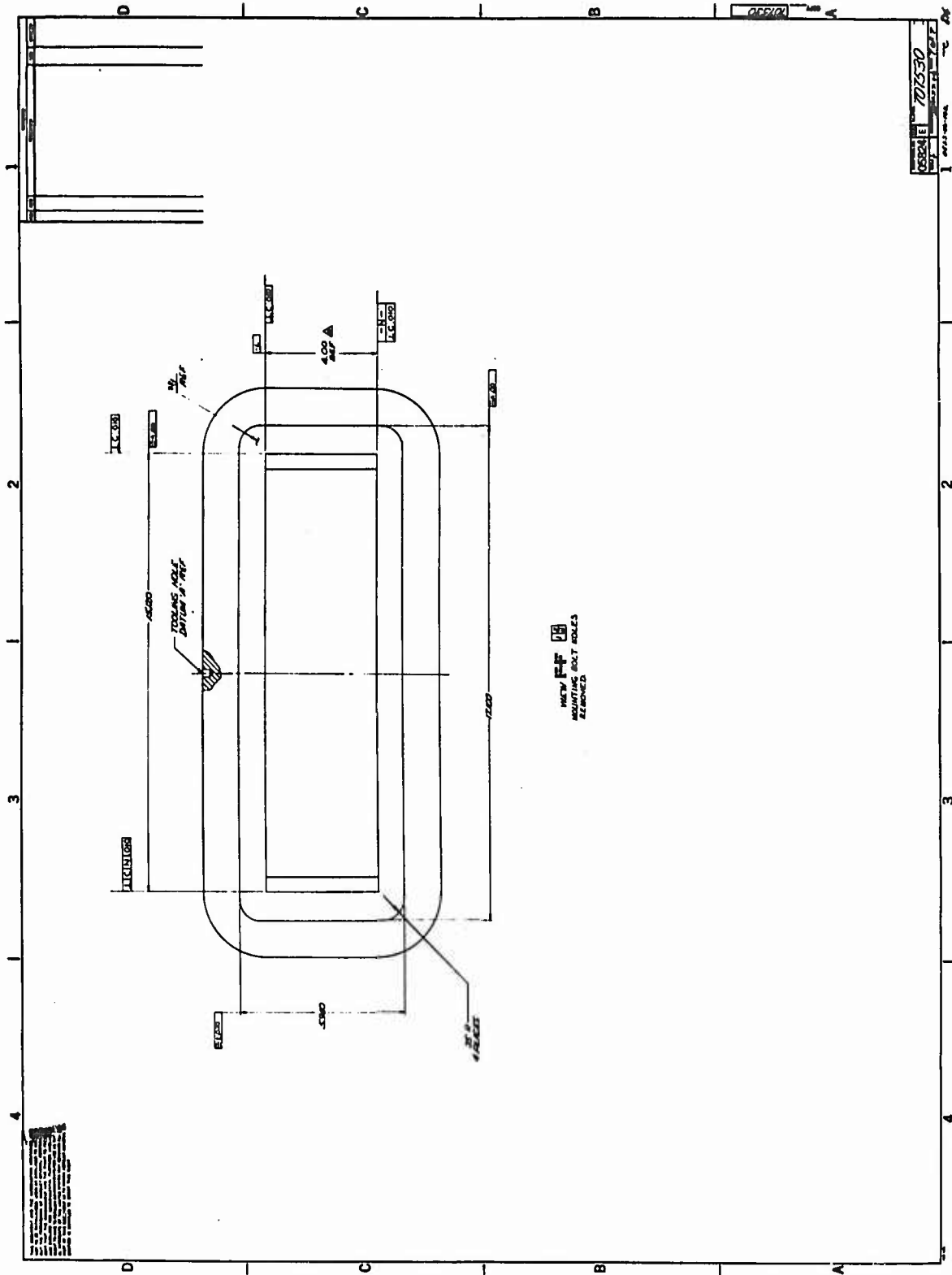


Figure 81g -- Injector Assembly, Combustion Chamber

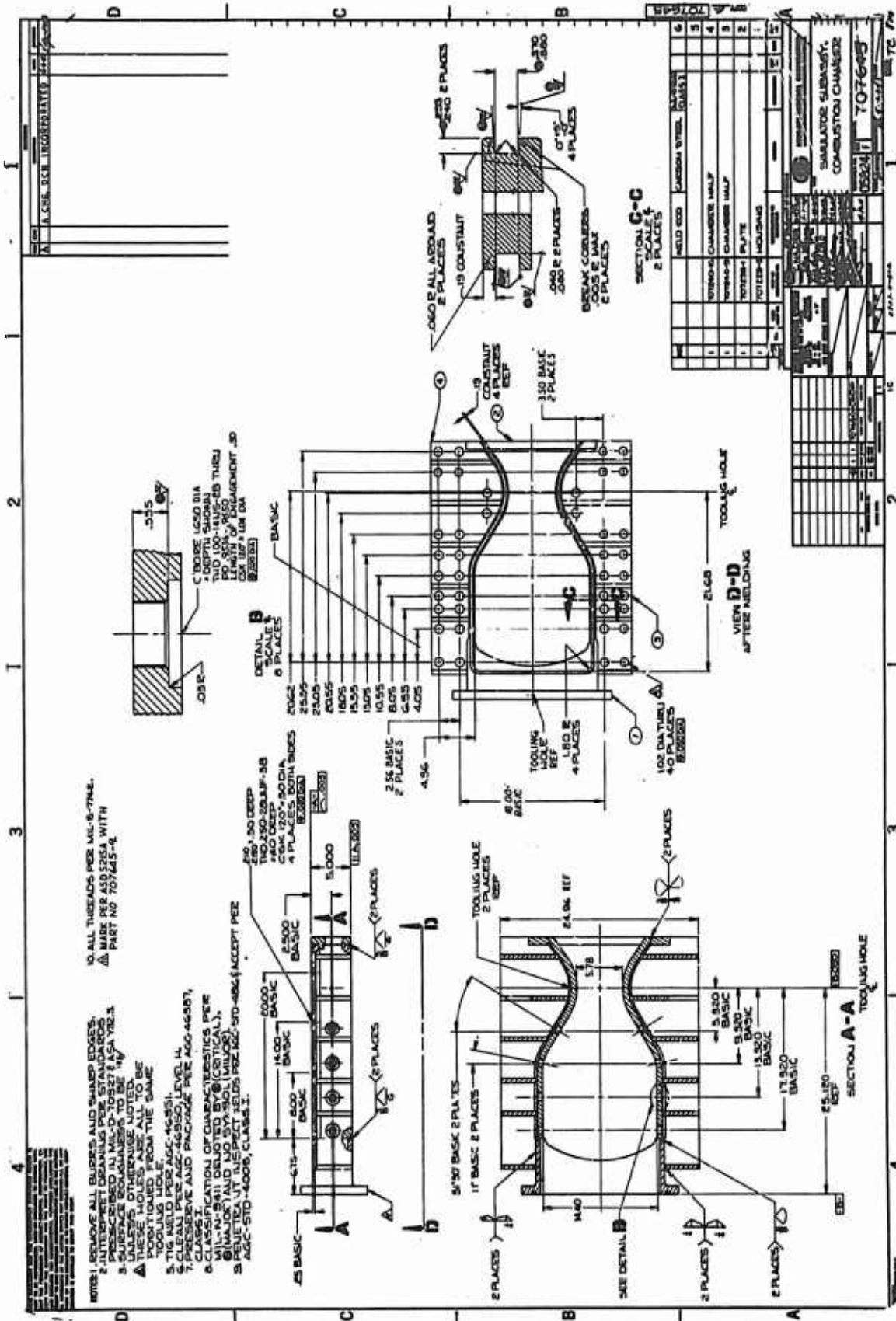


Figure 82 -- Simulator Subassembly, Combustion Chamber





















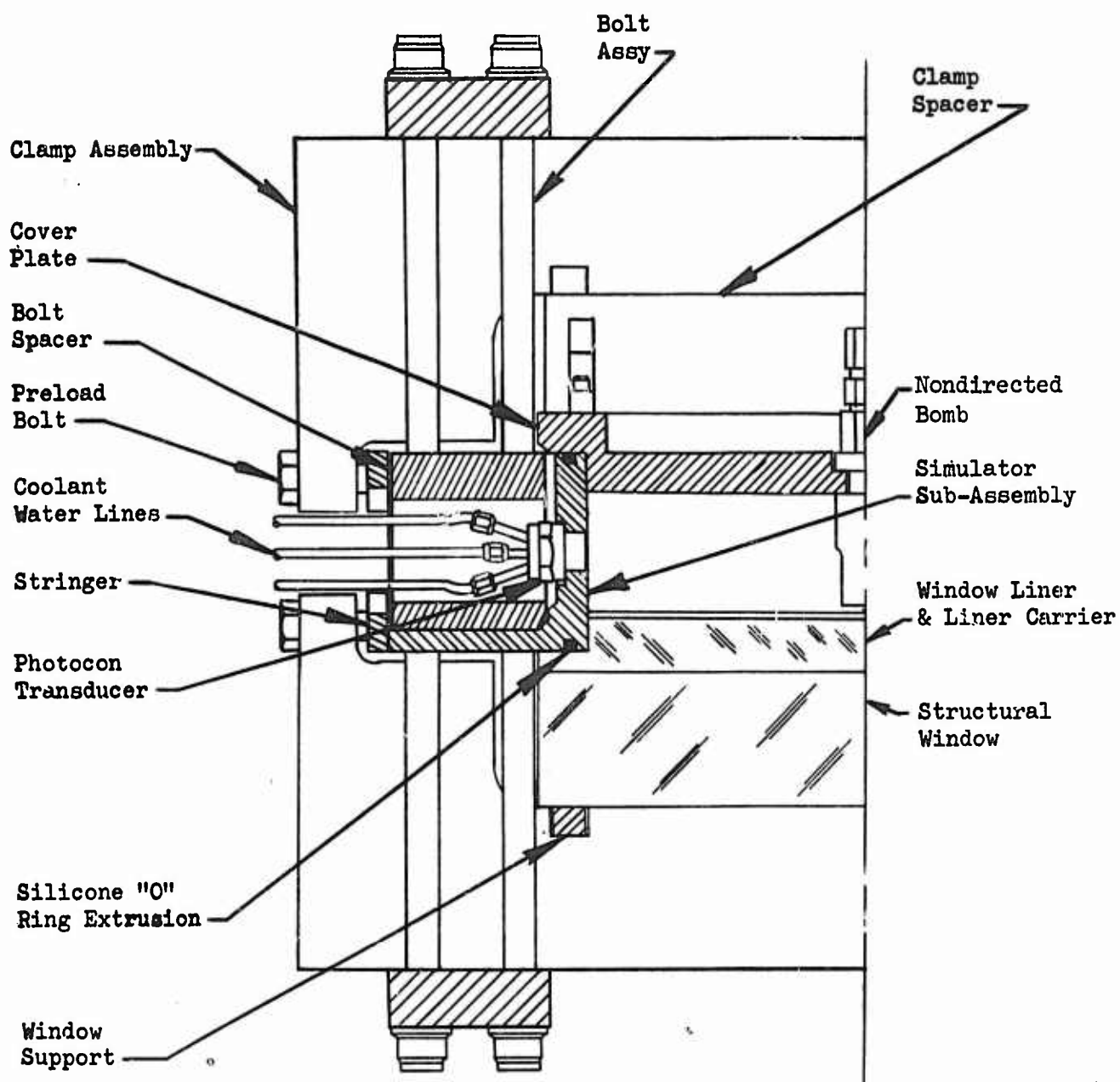


Figure 92 -- Cross-Section of Assembled Motor

## IV, B, Component Description (cont.)

TABLE 8

## OPERATING PARAMETERS, TWO-DIMENSIONAL THRUST CHAMBER ASSEMBLY

<u>Parameters</u>	<u>Units</u>	<u>Symbol</u>	<u>Value</u>
Chamber Pressure (steady state)	Psia	$P_c$	826
Thrust	lb	F	15-20K
Oxidizer weight flow	lb/sec	$\dot{W}_o$	54.7
Fuel weight flow rate	lb/sec	$\dot{W}_f$	29.2
Total weight flow rate	lb/sec	$\dot{W}_t$	83.9
Mixture ratio	--	MR	1.87
Contraction ratio	--	$\epsilon_c$	2.49:1
Expansion ratio	--	$\epsilon$	2:1
Throat Area	in <sup>2</sup>	$A_t$	17.34
Characteristic Exhaust velocity	ft/sec	$C^*$	5500

1. Observation Windows

During the conceptual phase of the motor design it was found that acrylic plastic had been used as the transparent hot-gas-side material for most of the previous work that had been conducted with motors having large viewing areas. It was felt that the acrylic plastics burned during the combustion process, and the flame obscured the combustion of the propellants. A material survey was conducted to evaluate alternative materials for the viewing window. The materials that were evaluated and their properties are listed in Table 9.

The evaluation was conducted by lining hollow acrylic cylinders with the various materials, testing them by hot firing using the same propellant combination used by GEMSIP, photographing the combustion with high speed cameras, and evaluating the photographic data. The primary candidates for selection as the inner liner, based on the results of the evaluation program, were:

GEMSIP FR-1, Volume 5

TABLE 9

ALTERNATIVE MATERIALS FOR VIEWING WINDOW

<u>Material</u>	<u>Cost for 1/2" Window**</u>	<u>Melting or Soft Point</u>	<u>Other Test Experience</u>	<u>Advantages</u>	<u>Disadvantages</u>
Optical Quartz	\$3000	2800- 3300°F	None	Good opt. 's, high melting temp.	Cost 6-8 weeks lead
Industrial Quartz	\$1200	2800- 3300°F	Quartz etched during firing	High melting temp. lower cost	Poor optics 6-8 weeks lead
Vycor	\$3000+	2500°F	None	Best optics High temp.	Cost 8-10 weeks lead
Acrylic (Lucite)*	\$ 4	150-200°F	Most experience High erosion rate grows when hot	Most test experience cheap	High erosion rate flows when hot
Pyrex*	\$ 5	1500°F	Cracks 1/2 sec into firing	Cheap Fair temp.	Susceptible to thermal shock
Kel-F*	\$ 80	390°F	None	High temp plastic Price	--
Teflon, FEP*	\$ 50	550°F	None	High temp plastic	Only fair transparency
Polycarbonate*	\$ 12	300°F	None	High temp. than lucite	Low temp.
Mica	\$ 80	1100°F	None	High temp. Cheap	No information available
Epoxy*	\$ 12	>500°F <sup>▲</sup>	None	Cheap Good ablative	Poor transparency
Silicone Rubber*	\$ 50	600°F <sup>▲</sup>	None	Cheap Easy fabrication	Poor transparency

\* Tested during micromotor test program.

\*\* Material only.

▲ Material does not melt but ablates at this temp.

IV, B, Component Description (cont.)

- 1) Teflon
- 2) Pyrex
- 3) Vycor, in areas of particular interest where the high cost would be justified for experimental reasons.

The observation window was conceived as a two-part design consisting of a massive re-usable acrylic plate for structural support, and an expendable assembly composed of a special purpose liner, and a machined acrylic liner carrier. The liner carrier contained the sealing surfaces for the window-to-simulator sub-assembly interface, and the main portion of the combustion zone cavity. The special purpose liner was attached to the carrier with a transparent adhesive.

The assembly was designed so that different combinations of liners could be utilized on the same or separate tests. Provisions were made for using silica-reinforced phenolic ablative panels in areas of high heat flux or little interest (e.g. throat and divergent segment of the nozzle). The sizes of the components of each liner part were mainly determined by the sheet sizes that were commercially available. Test results with the two-dimensional motor indicated that smaller sheets of the more brittle liners should be used to stop crack propagation through the liner.

2. Injector

The injector was designed to be recessed into the simulator sub-assembly with the face in line with the forward edge of the observation window. The assembly was a weldment of Series 300 stainless steel plate and sheet stock. CRES type 349 weld rod was used throughout. The injector face was designed to have the same contour as the full-scale injector except that the curvature was a segment of a cylinder instead of a sphere.

IV, B, Component Description (cont.)

The fuel and oxidizer manifolds on the back side of the injector simulated the oxidizer dome and fuel pies of the full-scale injector. Sheet metal baffles were installed directly under the propellant inlets to reduce the velocity effects on the injector plate feed slots under the inlets. The injector face propellant channels were milled across the injector and the feed slots were milled through the plate into the propellant manifolds in a manner similar to that used for the Gemini injectors. The channels were milled into the injector face with the center line of the milling head, and therefore the channel walls, perpendicular to the face. On the full scale injector the walls are parallel to the axial centerline of the TCA. This change was made to simplify fabrication of the injector.

The channel cover plates were designed as U-shaped segments of AISI 347 stainless steel plate. The ends of the U closed the open ends of the channels, while the base formed the injector face. This technique was utilized to avoid the close-tolerance weld preparation associated with a conventional cover plate design.

The outer fuel face plates were milled from bar stock and maintained the same shape as the full-scale Channel 17 ring in order to introduce film coolant and wall impingement coolant. Two additional channels were added to the center of the injector to maintain the propellant mass density in that area. On the full scale injector, the circular area enclosed by the first channel is 0.897% of the total projected face area. However on the two-dimensional injector, because the channels are not arc segments but straight, the area between the first channel is 3.19% of the total projected face area. It was felt that serious recirculation and face erosion problems would be encountered if some propellant were not injected in this area. Two fuel channels were added to supply a mass flux at the center and to simulate the absence of oxidizer in this zone on the full scale injector.

The fuel and oxidizer inlets on the injector were set above the injector mounting flange to allow reworking if the sealing surfaces were damaged during the test program and to eliminate the need for finish-machining the entire top surface of the injector to obtain a sealing surface.

IV, B, Component Description (cont.)

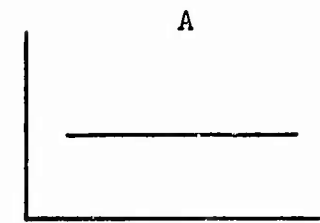
The manifold volume on the backside of the injector was reduced, to simulate full scale conditions, by welding channels to the splitter, side plates, and flange plates of the injector.

Six patterns were designed for the injector. All used the quadlet injection element, and a flat mixture ratio distribution. They were:

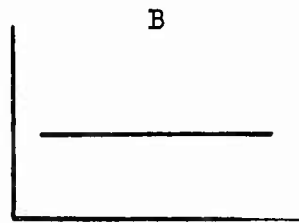
- 1) 100 lb/element, flat mass distribution, Figure 93,
- 2) 300 lb/element, flat mass distribution, Figure 93,
- 3) 100 lb/element, flat mass distribution, long impingement distance, Figure 93,
- 4) 100 lb/element, hump mass distribution, Figure 93,
- 5) 100 lb/element, ramp mass distribution, Figure 93, and
- 6) 100 lb/element, flat mass distribution, with provision for a simulated baffle hub, Figure 93.

A design pressure drop of 120 psig was used for both circuits, and the amount of film coolant per linear inch was kept identical to the full-scale patterns. Since the total face area of a 3-in.-thick segment of the 2D injector is approximately twice as large as two pie-shaped segments of the full-scale injector having the same arc length, and the total mass flow rate per unit area was held the same, the percent of total fuel flow rate used as a film coolant decreased from 13.76% in full-scale operation to 8.22% in the 2D motor.

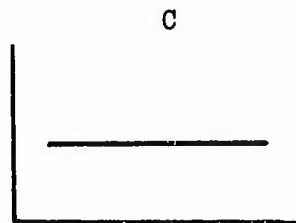
The point-by-point magnitude of mass distribution of the two-dimensional injector also deviated from the full-scale injector when the distribution was not flat, because of the face area differences. The slopes of the hump and the ramp mass distribution curves were the same as the corresponding full-scale patterns.



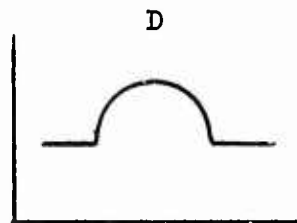
Thrust/Element 100-lb  
Flat Distribution  
No Baffles  
Std. Impingement



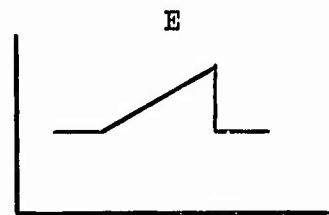
Thrust/Element 300-lb  
Flat Distribution  
No Baffles  
Std. Impingement



Thrust/Element 100-lb  
Flat Distribution  
No Baffles  
Long Impingement



Thrust/Element 100-lb  
Steep Ramp Distribution  
No Baffles  
Std. Impingement



Thrust/Element 100-lb  
Steep Ramp Distribution  
No Baffles  
St. Impingement



Thrust/Element 100-lb  
Flat Distribution  
1 Injecting Baffle and  
1 Noninjecting Baffle  
Std. Impingement

Figure 93 -- Injector Configurations--Two-Dimensional Chamber

IV, E, Component Description (cont.)

Fuel and oxidizer manifolds were designed to channel the propellants from the LR91-AJ-5 valve interface to the injector inlets. The material selected was AISI 347 stainless steel for corrosion resistance. The tubing was sized to provide fluid velocities on the order of 30 fps or lower to reduce the dynamic pressure losses in the system. The upstream flanges were designed to mate with the downstream face of the LR91-AJ-5 propellant lines and the seal glands were sized for "RACO" seals or butyl O-rings as an acceptable alternate.

3. Simulator Subassembly (Chamber)

The simulator subassembly was designed as a weldment of chamber halves, end plate, and injector housing. All components were fabricated from mild steel plate. After welding, the bosses for Photocon water-cooled high-frequency-response pressure transducers were machined in the contour walls of the subassembly. The window mating surfaces were machined flat, and the contour seal grooves were cut. Clearance holes for the clamp bolts were drilled through the L-supports of the chamber halves.

The chamber halves were designed as L-segments with supporting ribs spaced to support the pressure load on the contour plates and to carry the load from the contour plates to the clamp assemblies. Other concepts considered were box beam, weld assembly and bolted assembly, and I-beam support. The I-beam concept was discarded since Photocon bosses were required down the center of the contour plates. The box beam concept was discarded because the physical limitations of placing the Photocon transducers into the box structure with enough space for wrench access required a bolted box beam assembly.

The bolted assembly was not attractive from the viewpoint of fabrication, because, compared to the L-structure, additional machining would be required to insure mating of the components, and on-stand assembly would be complicated by requirements for bolting the assembly together.

IV, B, Component Description (cont.)

The spacing of the supporting ribs was dictated by space requirements for the Photocon transducers and the allowable free span of the observation windows.

4. Cover Plate and Spacers

The cover plate was designed for use in place of a window on either side of the simulator sub-assembly to provide the capability for locating pressure transducers or nondirected bombs. The material selected was mild steel. The plate was a weldment assembly of two machined plates which was recessed into the simulator sub-assembly to produce, with the opposite side of the chamber, the desired 3-in.-thick combustion zone depth. Ten bosses, all of which were capable of accepting transducers or nondirected bombs, were machined into the plate.

In order to provide access to the bosses, the spacers were bolted to the cover plate after the transducers, bombs, or plugs were installed in the bosses. An all-welded concept was discarded when it was shown that the number of bosses would have to be reduced to allow wrench access to the bosses.

5. Bridge Clamp Assembly and Window Support

The bridge clamp assembly secured the windows and/or cover plates in place and transmitted the pressure load to the bolt assemblies. A high strength weldable steel with good impact resistance was required to keep the size of the clamps to a minimum so that the largest window area would be available for viewing.

The original concept utilized separate clamps with welded on bolting plates. The material selected was U.S. Steel "T-1" regular quality quenched and tempered alloy steel. "T-1" plate, up to  $2\frac{1}{2}$  in. thick, has a yield strength of 100 ksi and a weld joint efficiency of 100% in the as-welded condition. The high weld efficiency in the as-welded condition was desirable for the original concept.

IV, B, Component Description (cont.)

It became apparent that a welded assembly of all the clamps and two common retaining plates was much easier to handle and assemble into the motor, so the design was changed as shown.

The distance between the clamps in the assembly was determined by the allowable span of the window assembly. The maximum height of the clamps was set at 4 in. because, if the clamps were higher, parallax would cause restricted views of the window area between the clamps. To reduce the bending moment on the clamps, the clamp bolts were placed as close to the contour walls as possible, and the clamps were pre-loaded by 0.750-in.-dia machine screws through the ends of the clamps bearing on the stringers and the simulator sub-assembly. Notches were machined in the window side of the clamps to accept the window support bar, which was designed for positive clearance above the clamp, and insured even loading of the contour seal between clamps.

6. Bolt Assemblies and Bolt Spacers

The bolt assemblies and bolt spacers were designed as a unit since a through bolt could not be used between the clamp assemblies because of interference with the Photocon transducers in the contour walls of the simulator sub-assembly.

The bolt assemblies were buildups of commercially available 0.875-in.-dia threaded rod, and lock nuts. The locking action of the nut against the stud threads was sufficient to hold the nut on the stud during assembly and disassembly of the motor.

The bolt spacers were designed to carry the bolting load around the Photocon transducer in the contour walls of the simulator sub-assembly. The material selected was mild steel. Clearance holes for the Photocon water cooling lines and electrical connections were provided in the bolt spacer blocks. The bolt spacers were inserted after installation of the Photocon transducers, and the bolt assemblies threaded into the spacers through the clamp assemblies.

IV, B, Component Description (cont.)

7. Thrust Mount Assembly (P/N 708149)

The thrust mount was designed to carry the thrust load from the motor to the test stand and to partially support the weight of the motor while mounted on the test stand. The material selected was Series 300 stainless steel plate and tubing. Stainless steel was selected to minimize corrosion problems which could result from potential propellant leakage from the manifolds and propellant transfer lines.

The assembly was designed as a machined weldment of tubing and plate which was bolted, through the main injector flange, to the main flange of the simulator sub-assembly. Clevises were provided for the attachment of LR91-AJ-5 dummy gimbal actuation rods for additional support.

8. Auxiliary Components

In addition to the main components of the motor, several auxiliary components were designed. These include plugs for the instrumentation bosses, an adapter for the tangential pulse gun, and stringers to distribute the clamp preload along the side of the simulator subassembly.

The instrumentation boss plugs were designed to plug the bosses that were not in use during hot firings, and provided the capability of using low frequency response Tabor transducers if desired. The material selected was Series 300 stainless steel for corrosion resistance and to eliminate thread galling.

The pulse gun adapter utilized Inconel 718 high strength nickel alloy. This material was selected for the high strength required in the comparatively thin adapter walls needed for clearance in the 2D motor.

IV, B, Component Description (cont.)

The material selected for the stringer was AISI 4130 steel. This material was selected so that it could be heat-treated to a high surface hardness to take the concentrated load applied by the clamp preload bolts.

C. PHOTOGRAPHIC INSTALLATION

An isometric drawing of the photographic installation is presented in Figure 94. Nine cameras are employed. Five are used to obtain streak films, both in the visual and in the infrared regions, through long narrow slits mounted on the cameras. These are focused on the sides of the chamber from a distance of 3 ft, instead of mounting the slit directly on the chamber walls. This permits greater flexibility in selecting the field for observation and likewise eliminates many of the technical difficulties arising from the heat rejected by the chamber. Three slits are parallel to the chamber axis--one down the middle and the other two near the wall. Two slits normal to the axis are employed--one near the injector face, the other 2 in. downstream. One general observation camera is used.

The remaining cameras are used to obtain special effects, such as: (1) examination of the operation of a single injector element, (2) determination of the size and rate of vaporization of an individual droplet, and (3) the study of recirculation regions.

In the hope of obtaining a better idea of the actual droplet formation and combustion mechanism involved in the rocket engine it was decided to investigate the possibility of providing a backlight source better to illustrate the combustion process immediately forward of the injector face. The source envisioned would have to meet the following requirements:

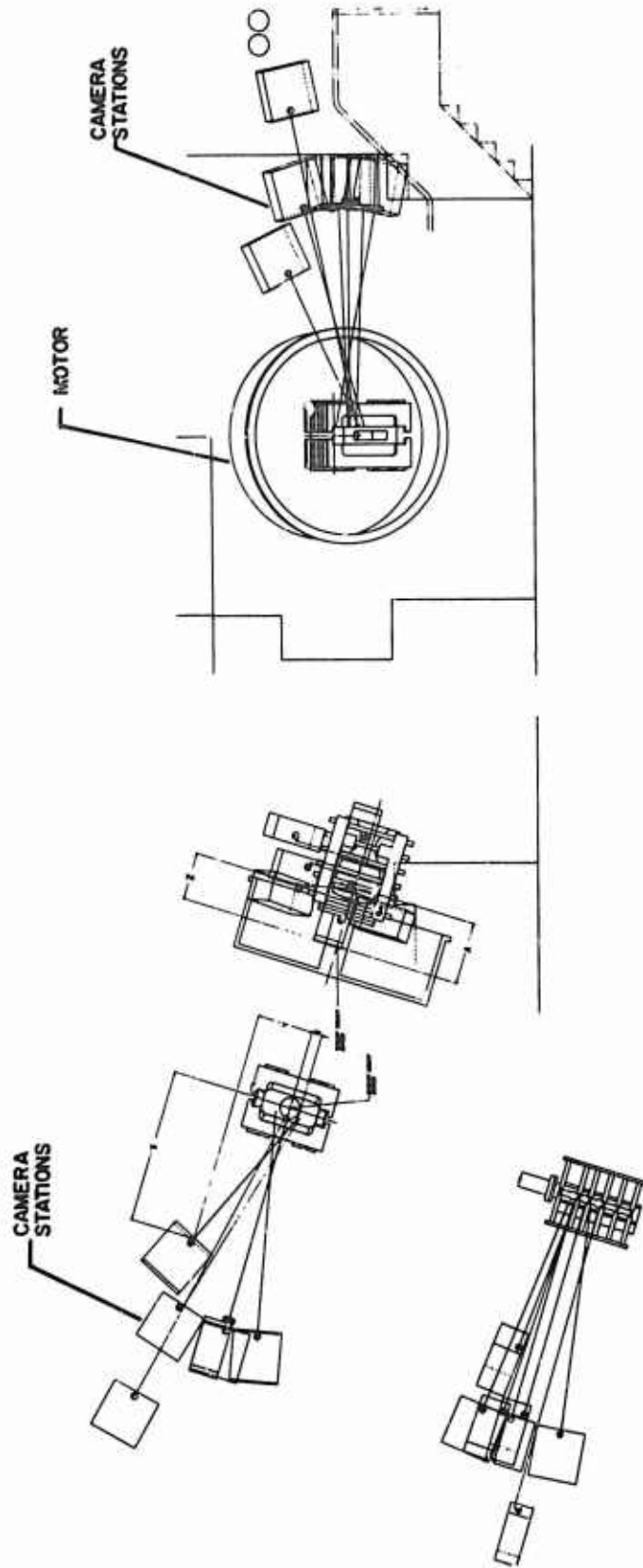


Figure 94 -- Photographic Installation--2-D Chamber

IV, C, Photographic Installation (cont.)

- 1) Extremely high intensity.
- 2) Collimated beam approximately 6 in. in diameter.
- 3) High degree of portability, light weight, compact.
- 4) Spectral emission primarily in the visible portion to prevent excessive heating of the subject.

Since budgetary limitation precluded the purchase of backlighting equipment an effort was made to find existing sources. To this end, a high-intensity light source was borrowed. The source, the Mole-Richardson 356 line flash is a compact mercury-vapor lamp. This lamp operates on direct current and is overloaded to give an extremely bright flash of light over a period of several seconds. Under rated conditions, the light source has a brightness of 35,000 candles/cm<sup>2</sup> and a luminous efficiency of about 47 lumens/watt.

Cadmium vapor is added to the lamp to improve the spectral distribution, which otherwise would be weak in the red end of the spectrum. The spectrum of the source is discontinuous and consists mainly of yellow, green, and blue lines superimposed on a relatively weak continuous spectrum. With the addition of the cadmium vapor, a powerful red line in the spectrum is produced and gaps in the blue-green region are filled by additional lines which give the spectrum a better balance. A fixed, rather than variable, focus ensures that the light output from the unit is constant so that the photographic exposure can be repeated accurately by setting the lamp at predetermined distances from the subject.

A reciprocal relationship exists between the power that can be supplied to the lamp and the duration of the flash. For use with the two-dimensional motor, the flash was set for 1-sec duration at 10 kw. At that power consumption the lamp provides 150,000 ft-candles at a distance of 4 ft from the light.

IV, Two-Dimensional Motor (cont.)

D. TESTING

1. Test Objectives

Only one test was performed before the program redirection caused stoppage of the two-dimensional motor effort. The basic objectives of this test were:

a. Window Material Evaluation

It was hoped that high speed motion pictures taken during this test would show a clear reason for selecting between the two candidate materials, FEP Teflon and a form of Pyrex. Each material had shown promise as a window through which to view combustion. A decision was made to try both materials in hopes of making a selection from the results of the balance run.

b. Camera System Evaluation

The mechanical complexity of the camera system has meant in the past that many runs were necessary in order to set up the system so that good data were obtained. An effort was initiated to design the camera system in advance of the test data so that the necessary material could be procured without delay to the test and so that the first setup could be as highly optimized as possible.

A system of seven basic high-speed cameras was selected. Five of these cameras were to record the images of a particularly located slit; two were to record framed images of the whole thrust chamber and the injector. To compare the Teflon window and the Pyrex window, it was decided that the basic system of seven cameras would be used on the Teflon side of the thrust chamber (the south side) and that additional cameras would be placed on the north side with the purpose of evaluating the Pyrex.

IV, D, Testing (cont.)

Camera position, image size, image clarity, image readability, exposure, choice of film, the efficacy of the timing lights and the means of photographing through the Teflon and Pyrex, were all to be evaluated. The basis of evaluation was to be "how well the camera system accomplished the objectives stated on Sketch 9756-64-1526." This sketch was not fully employed, and so the means of evaluation must be altered and the cameras evaluated on an individual basis.

c.  $P_c$  Rise and Mixture Ratio Selection

Determination of an acceptable pressure rise rate for the thrust chamber assembly and verification of the chosen pressure values for staging of propellant tanks were desired.

d. Development of the Seal Design

Two methods of potting gaps which are inherent to the design were employed. It was hoped that the first hot firing would show one of these methods to be superior.

Several techniques incidental to the previous objectives were employed for the purpose of proving the techniques themselves. These were the use of an 8000-frame/sec Fastex camera for obtaining images of the propellant droplets, the use of slits behind the lens in the streak cameras to serve the same purpose as those formerly placed at the thrust chamber assembly, and the use of slits in the framing cameras in order to obtain sharper images.

2. Data Obtained

An evaluation of the success achieved on each of the objectives follows.

IV, D, Testing (cont.)

a. Window Material Evaluation

The condition of the Pyrex window after the test reveals that the bonds employed are satisfactory. Most of the Pyrex remained attached after shutdown, but it was crazed and cracked extensively. No movies were obtained of the Pyrex window because of camera malfunction. The Teflon window shows a great deal of erosion; the bottom part is missing altogether.

Framed pictures of the Teflon are not of sufficient image size or clarity of focus to determine whether the Teflon is an acceptable material. The results are not conclusive and do not point to a definite course of action. Certain modifications in the Pyrex design will be used to reduce the cracking. New camera techniques will be required to photograph the Teflon window so that an acceptable image is obtained.

The condition of the FEP Teflon after shutdown varied along the axis of the thrust chamber assembly. Grooving occurred at the injector area. These grooves follow the propellant path downstream. Rippling occurred from a distance five inches below the injector to the convergent section of the thrust chamber assembly. The throat piece of the Teflon was completely gone at the end of the run.

b. Camera System Evaluation

The basic coverage (seven cameras) of the Teflon window may be evaluated as follows:

(1) Longitudinal Slit (Upper) - Film No. L66047. In this streak film there was not a clear indication of the position of the injector, and so no distances along the axis of the chamber could be determined. The film was taken through a 0.125-in. slit at  $f/11$  at a voltage which would expose 4000-frames/sec on

IV, D, Testing (cont.)

a framing camera (110 volts ac). The film image was severely overexposed. The images of the bars are disproportionately sharp compared to Film No. L66049, indicating that the camera was not sharply focused when loaded. The slit size should not be used again because it is too large and causes too much rewrite of information. Timing lights were recorded on this film. The whole run was not recorded.

(2) Longitudinal Slit (Central) - Film No. L66045. In this streak film timing lights were recorded, but they were of an erratic nature, the light failing to de-ionize several times and firing erratically. The slit size was 0.010 in. and the image was sharp, but the image was overexposed. No accurate position for the injector face can be established so that some artificial fiducial marks will have to be employed. The flashbulb which indicated FS-1 received a disproportionately small exposure compared with other films of this test. The whole test was not recorded. This film achieved a velocity of 107 ft/sec.

(3) Longitudinal Streak (Lower) - Film No. L66044. No timing lights were recorded on this film. The film was overexposed, out of focus and did not record the whole run. The slit size was 0.125 in.

(4) Transverse Streak (At injector) - Film No. L66043. This film did not get timing lights, and is over exposed. The edges of the thrust chamber are not discernible from the background fog. The whole run was not recorded.

(5) Transverse Streak (At P<sub>c</sub>A1) - Film No. L66046. No timing lights were obtained on this film. The slit size was stated to be 0.030 in., but the exposure was so vastly different from the others that it is probable that the actual size was 0.003 in. Exposure on this film was very close to the ideal value, but slightly over. This film did not record the whole run and the end of the run (the end of the film) was ruined by exposure to sunlight.

IV, D, Testing (cont.)

(6) Framing Picture of Injector - Film No. L66048. This film is overexposed, but is satisfactory in most other ways. Timing lights are recorded as red blips. A distinct image was not achieved.

(7) Framing Picture of TCA - Film No. L66051. This film was recorded at 1000 frames/sec. This film is only useful for possible failure analysis at that rate. It is recommended that this requirement be deleted (as originally requested at 4000-frames/sec) to be replaced by a 1000-frame/sec film of the whole thrust chamber for purposes of analyzing failures. This would relieve a scarcity of Fastex cameras which would occur should Fastex be required for this job.

The timing system initiated in this test does not appear to be any more reliable than that formerly used. Exposure appears to be determinable from the films obtained, and it is anticipated that a correct exposure can be used on future thrust chamber assembly tests. Black and white film will be advantageous for all photographic records. Exposure latitude is larger and this also allows a process of selective filtration to be used. In many cases the image was out of focus, indicating too little attention paid to this detail. The 8000-frame/sec camera failed to function properly.

In no case was the full firing recorded, and the timing sequence must be checked to be sure that a correct one is being used.

Fiducial markings will have to be employed to make the images recorded on the streak films meaningful. It is not yet clear what distances are recorded.

The longitudinal streak film (Film No. L66049) taken of the Pyrex window showed no timing lights and was overexposed. Image sharpness appears to be good. As before the images show dimensions rather poorly and readings can be made only with poor accuracy. The slit size was 0.125 in.

IV, Testing (cont.)

Slits were not available to use in the framing cameras. Behind-the-lens slits appear to be most feasible for obtaining streak data in this program.

c. Mixture Ratio and Pressure Rise Rate

The mixture ratio was nearly achieved. Measured MR was 2.071 and the shutdown pressure was 802.83 psia. A spike of 1500 psia occurred on startup. The pressure rise rate will be revised to accommodate less time at full  $P_c$  and a more gradual rise rate.

d. Development of Seal Design

A method of potting has been selected and will be employed in test two. Potting will fill all possible gaps in the thrust chamber assembly.

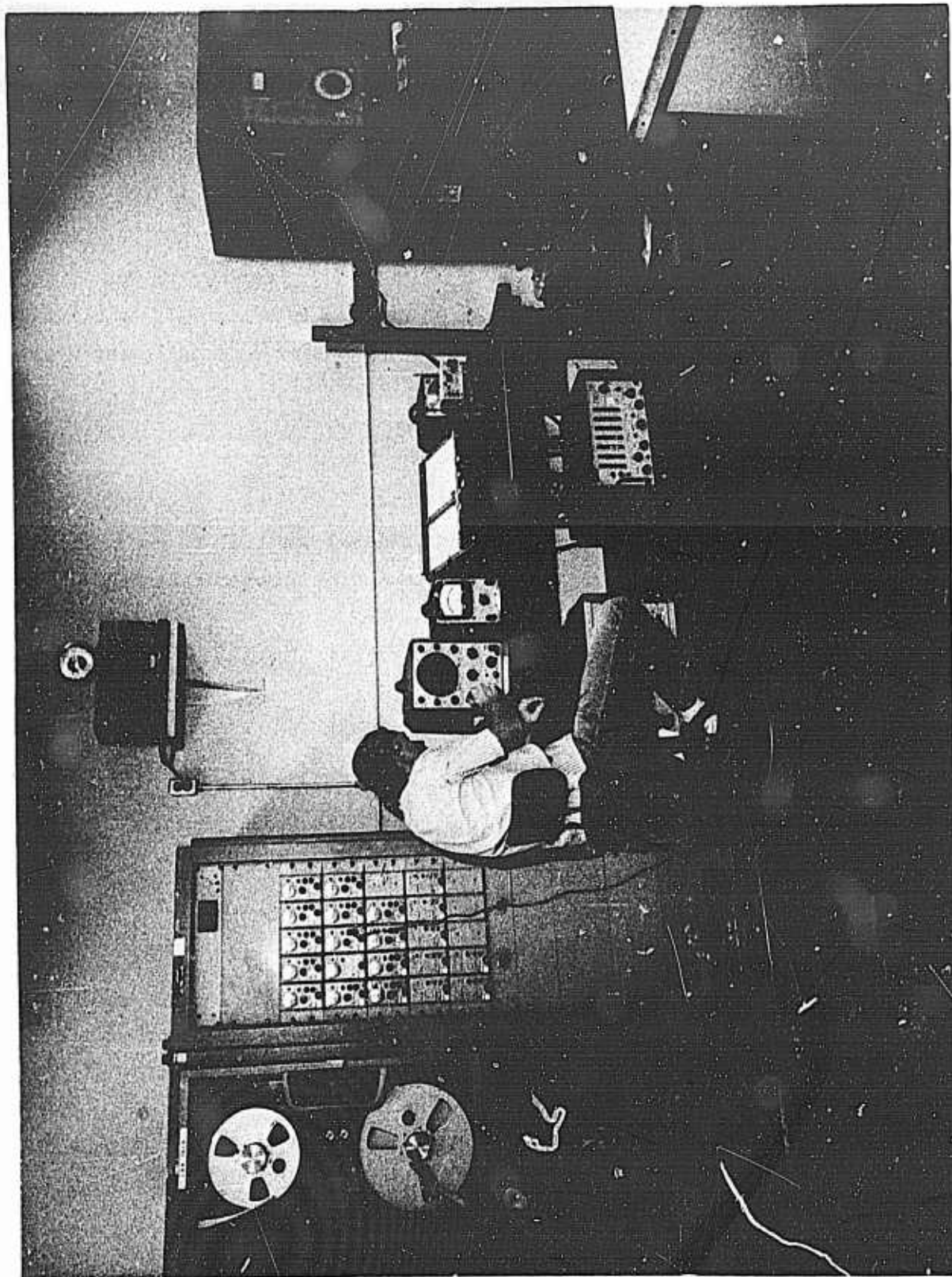


Figure 95 -- Acoustic Test Setup

V. ACOUSTIC TESTING

The following section summarizes the experimental work to evaluate various baffle configurations. This work was conducted during the interval from June to November 1964. The acoustical technique described originated because of a need for an experimental procedure to replace the cold pulse tests originally proposed for the injector candidate screening. It was found that the cold pulse tests were inadequate for defining the damping characteristic of a baffle configuration because of the difficulty in analyzing the data. The cold pulse tests were also damaging to the hardware and required that the injector be reworked prior to subjecting the baffle configuration to firing.

The principal objectives were:

- 1) To develop an experimental procedure for evaluating candidate baffle configurations for the purpose of selecting the "best" configuration based on acoustic test results.
- 2) To determine the validity of the technique as a means for comparing the stability characteristics of various baffle configurations.

A. DISCUSSION OF APPARATUS

The acoustic test setup is shown in Figure 95. Testing was conducted at ambient conditions using both the full and half-scale models of the Gemini combustion chamber. Figure 96 is a schematic of the system used in the various procedures. The initial requirement was to determine the resonant frequencies of the chamber. This was accomplished with a variable frequency oscillator feeding through an amplifier and driving a speaker mounted through a hole in the chamber. The frequency of the oscillator was increased at a logarithmic rate throughout the frequency range to be investigated, while the response of the chamber cavity to this signal was picked up by a microphone mounted in the chamber and observed on an oscilloscope.

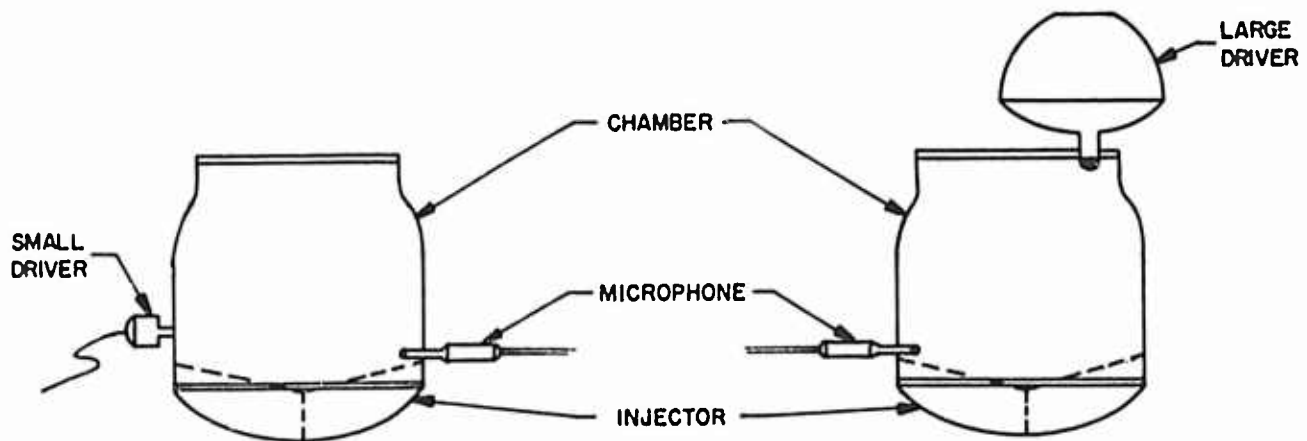
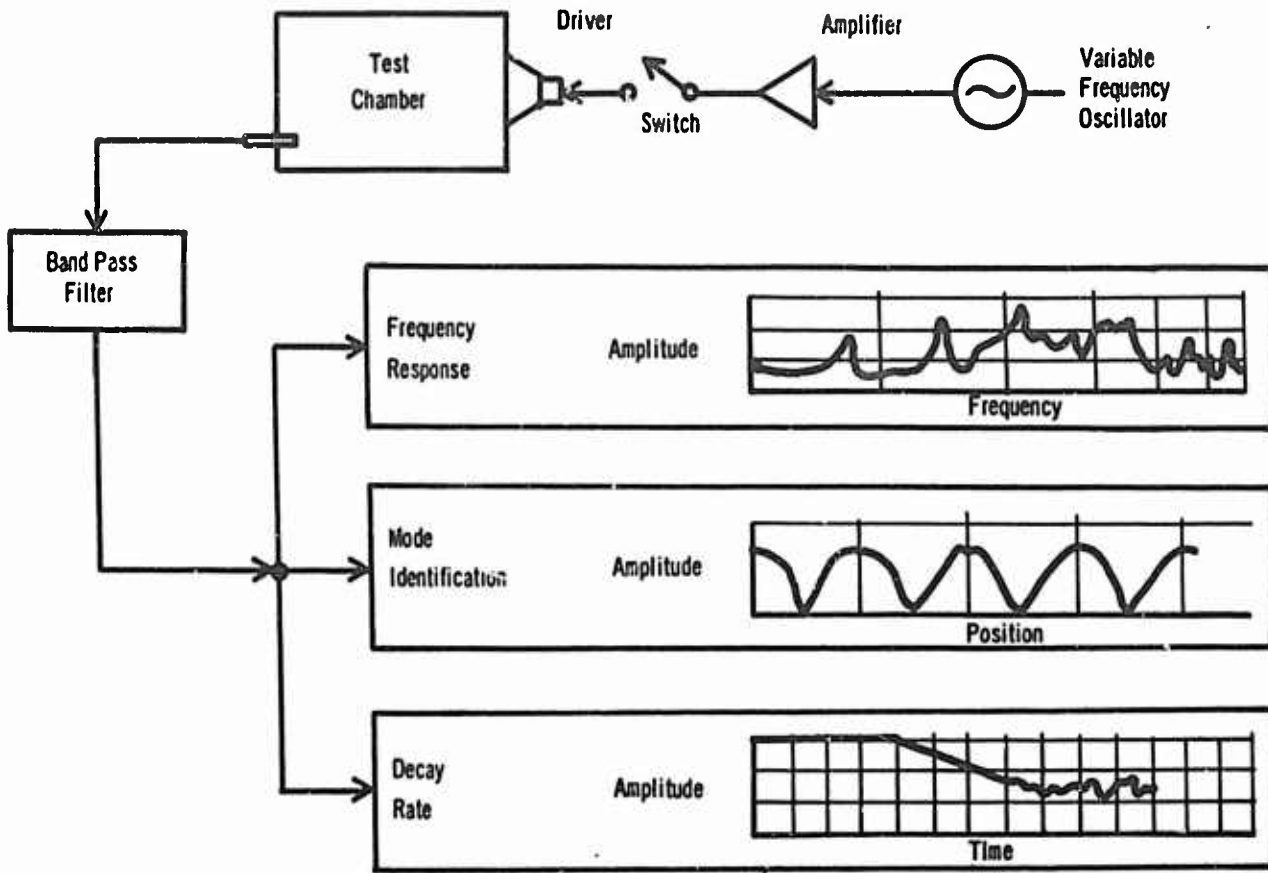


Figure 96 -- Schematic of Acoustic Test Setup

V, A, Discussion of Apparatus (cont.)

After all the resonant frequencies were recorded, the mode at each resonance point was identified. This was done by setting the oscillator signal at a resonant frequency of the cavity with the speaker positioned at an appropriate point in the chamber. The nodal and antinodal points were then located by traversing the chamber in three directions; radially, axially and circumferentially (see Figure 97). The type of mode was determined by the direction of microphone traverse and its order identified by counting the nodes.

The decay rate of each mode was measured by driving the mode at its resonant frequency, stopping the oscillator signal by shunting the driver circuit, and then measuring the decay of the oscillations. These data were used to compare the relative damping rates of the various baffle configurations for the acoustic modes of the chamber cavity.

B. FREQUENCY

The identification of the resonant frequencies for the various acoustic modes was not considered to be of major significance because past experience had indicated that these could be calculated with a fair degree of accuracy. However, measurements made during the acoustic tests showed a shift in the resonant frequencies for nearly all modes as a function of baffle length, the most noticeable changes being associated with the transverse modes. Experimental results for the transverse modes showed that for the tangential modes the variation in frequency was a function of the height of the radial baffle legs,  $h_T$ , and to some extent the hub height,  $h_R$ , while for the radial modes it was a function of  $h_R$  (see Figure 98). For the longitudinal modes the change in the resonant frequency was a function of both the baffle height,  $h_T$ , and the baffle area normal to the chamber axis.

In the case of the transverse modes the frequency is depressed below that of the transverse resonant frequencies for an unbaffled injector-chamber assembly.

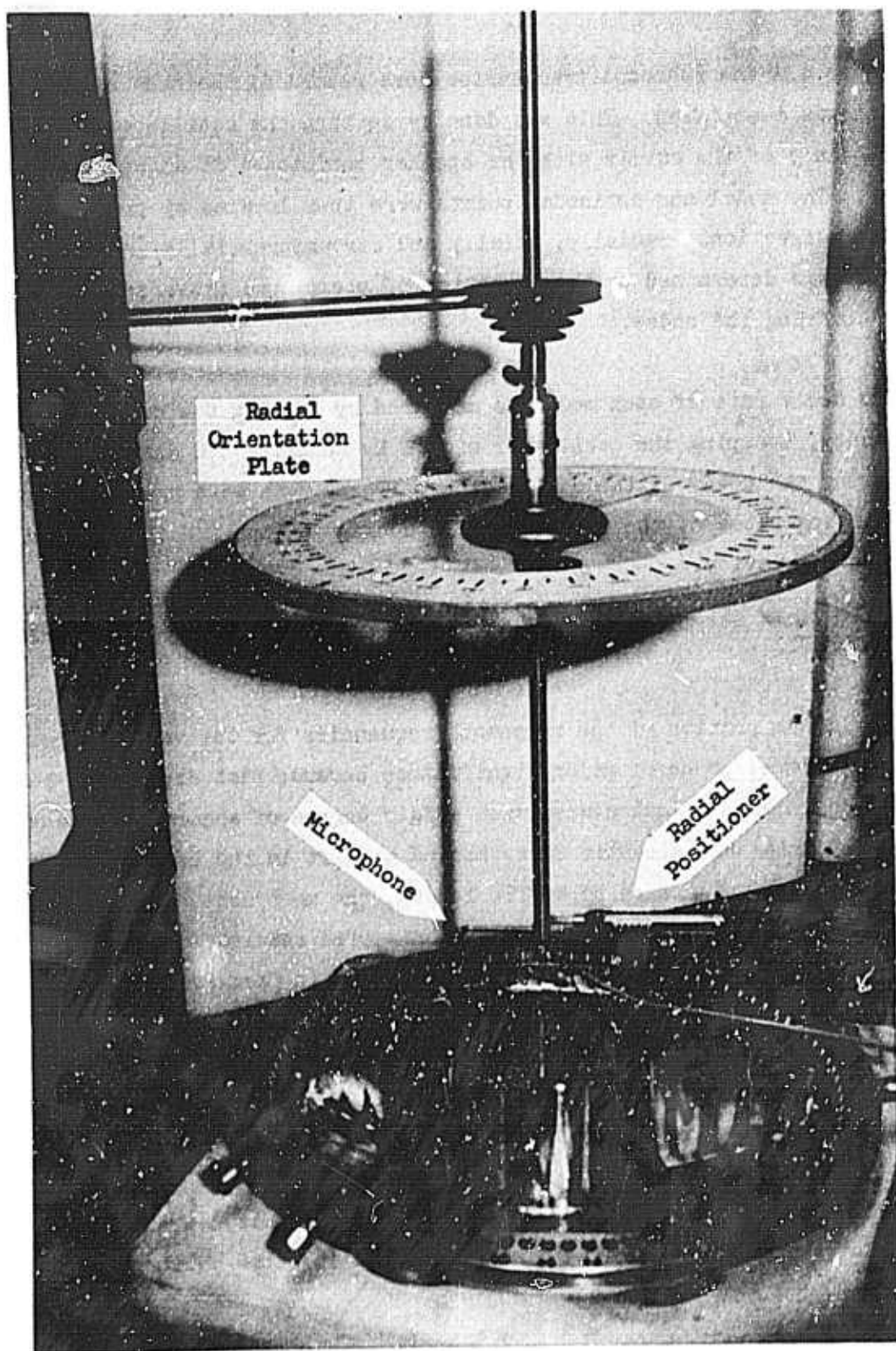
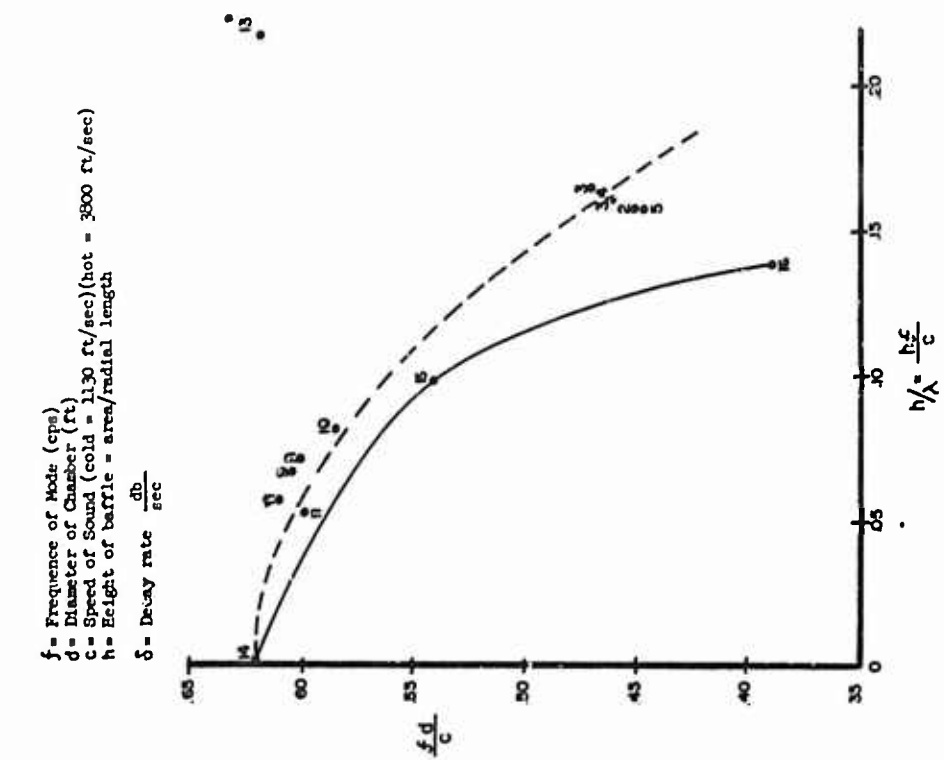
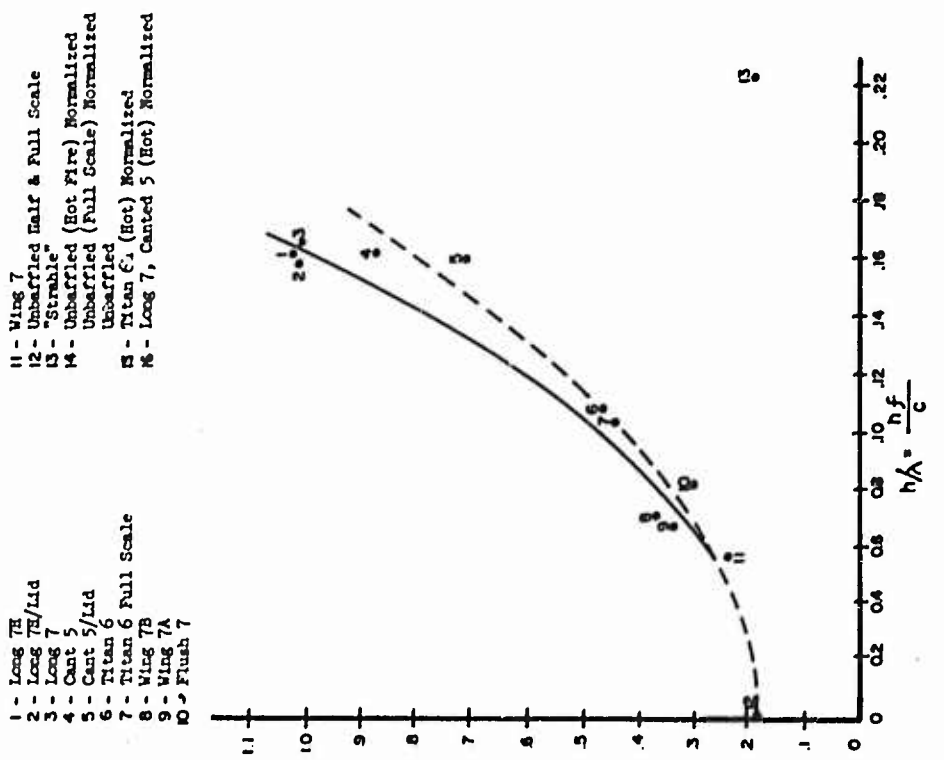


Figure 97 -- Traversing Fixture



a. Decay Rate Correlations Half-Scale Model -- Full-Scale Chamber



b. Effect of Baffle Height on Frequency Depression

Figure 98 -- Experimental Results for First Tangential Mode

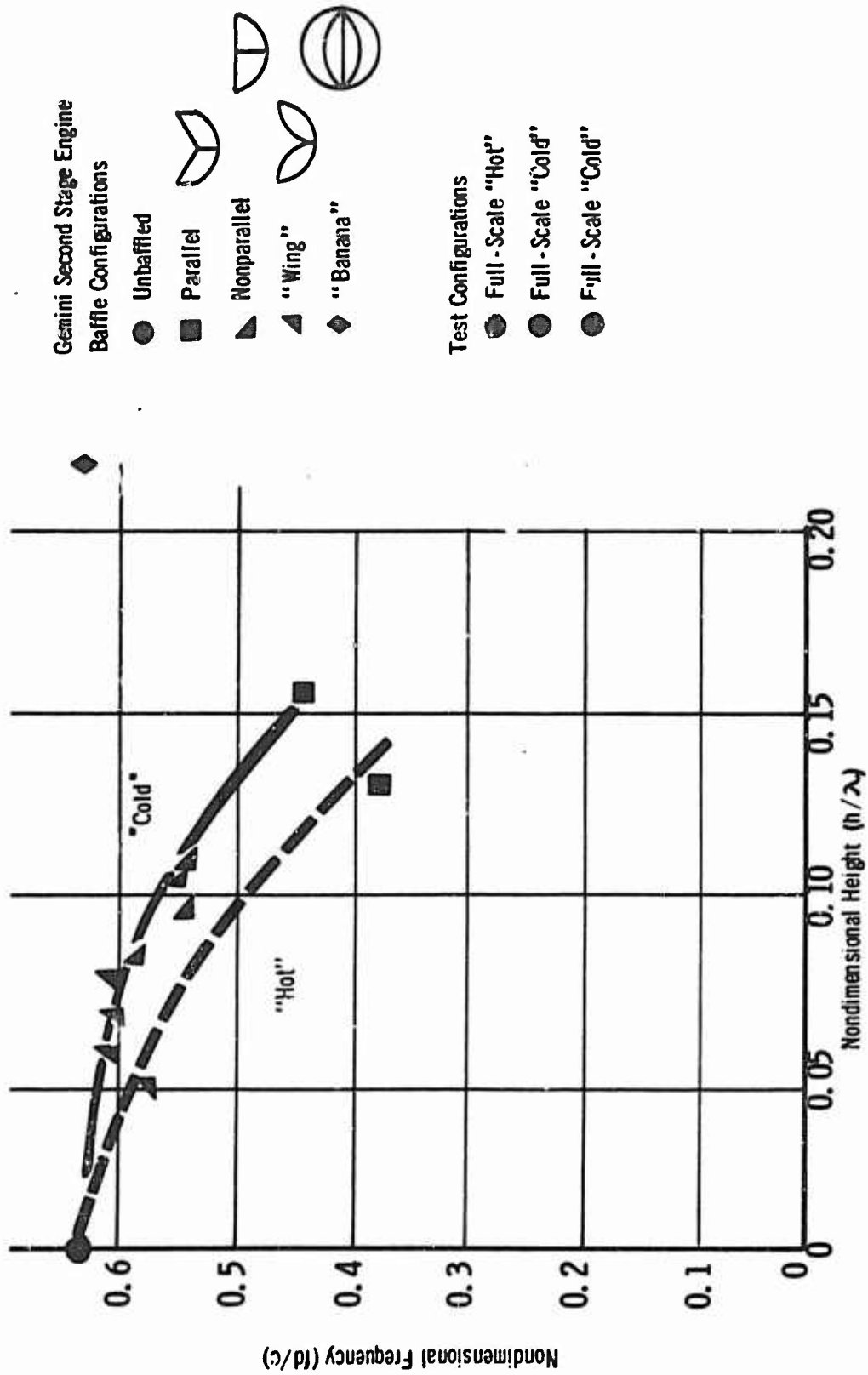


Figure 100 -- Effect of Baffles on First Tangential Frequency

## V, B, Frequency (cont.)

There are exceptions to this rule. If the wavelength for the resonant frequency is such that the half wavelength ( $\frac{\lambda}{2}$ ) is of the same order as the mean distance between baffle legs, in the case of the tangential modes, the frequency is not significantly altered from that of the un baffled configuration. For the radial modes the distance between baffle hubs and between the baffle hub and the chamber are significant. As a special case, if the baffle configuration is compatible with the transverse mode, such as the one shown in Figure 99 was with the first tangential mode, no significant frequency depression is obtained.

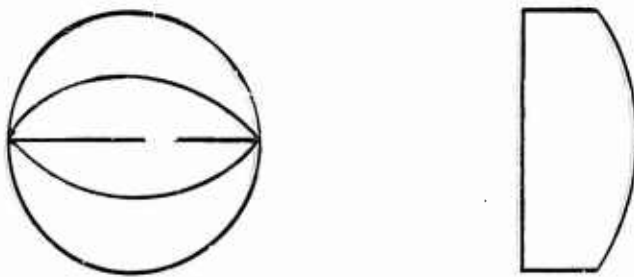


Figure 99 - "Banana" Baffle

Figure 100 shows the correlation between resonant frequency for the first tangential mode as a function of baffle length for the baffle configurations shown. For baffles which have a trailing edge which is not parallel to the injector face, an effective height was determined by the following relationship:

$$h_T = \frac{1}{A} \int_0^{r_b} h(r) dr$$

$A$  = Surface area of baffle leg  
 $r_b$  = Radial length of baffle

GEMSIP FR-1, Volume 5

V, B, Frequency (cont.)

The coordinates for Figure 100 have been made nondimensional in order that both full and half scale ambient tests as well as hot test data could be presented on the same graph. In terms of actual frequency depression experienced during hot testing, the un baffled frequency would be  $\approx 1900$  cps, while with a 5-inch baffle ( $h_T = 0.15$ ) the first tangential frequency would be  $\approx 1200$  cps.

Based on the observed effect of baffles on the transverse modes, an analytical model (see Appendix, this section) of the injector chamber assembly was developed. The basic assumptions made in developing the model were:

- 1) The baffle cavities can be replaced by a highly compartmented structure which allows only axial or longitudinal oscillations in the baffle pocket.
- 2) The admittance is zero at the injector face and the chamber throat.
- 3) No mean flow.

The chamber cavity between the baffle tip and the chamber throat was analyzed using the three-dimensional wave equation. The boundary condition at the baffle tip was defined by a one-dimensional analysis of the baffle cavity to determine the admittance at the baffle tip. This admittance was matched to the axial (Z-direction) admittance of the chamber cavity by varying the frequency in both relationships until a match of the admittance at the baffle tip was obtained. This then defined the resonant frequency. In general, the calculated frequency agreed within 5% of that actually measured.

The analytical model is limited in that it makes no distinction between baffle configurations having different numbers of blades. The degree of agreement between the calculated and measured values is improved ( $\pm 2\%$ ) if the calculated values are normalized by the ratio of the measured to the calculated values to the calculated values for the un baffled case.

V, B, Frequency (cont.)

Indications are that the accuracy of the calculated values could be further improved by consideration of the area changes in the chamber normal to the chamber axis at the baffle tip as well as consideration of the concave injector face in the calculation of the baffle admittance. However, it is felt that the degree of complexity introduced by the latter consideration is not warranted. The former consideration would be easily introduced and will be applied in future applications of the analysis.

In the case of the longitudinal mode, it was noted that the introduction of the baffle resulted in the harmonics of the longitudinal mode no longer being approximately interger multiples\* of the fundamental frequency. Analysis showed that such a variation in the resonant frequencies for the longitudinal modes is mainly due to the area change normal to the chamber axis introduced by the baffles and the location of the area change along the chamber axis. Shown in Figure 101 is the measured variation in frequency from that of the unbaffles case as a function of the baffle length, in terms of wave lengths, for the area change indicated.

These data were obtained from a half-scale model of the Gemini chamber using the baffle configurations indicated. A simple one-dimensional analysis of a closed tube with an area change as shown in Figure 102 can be used to show the variation in the longitudinal frequencies as a function of locations of the area change for a tube of constant overall length. The results give good qualitative agreement with the measured data. Refinement of the analysis to include the nozzle admittance should greatly improve the quantitative agreement.

Included in Table 10 are the measurements of resonant frequency and decay rate for a number of baffle configuration. These data are questionable from the

---

\* The harmonics of the longitudinal mode are not exact intergers of the fundamental because of nozzle effects.

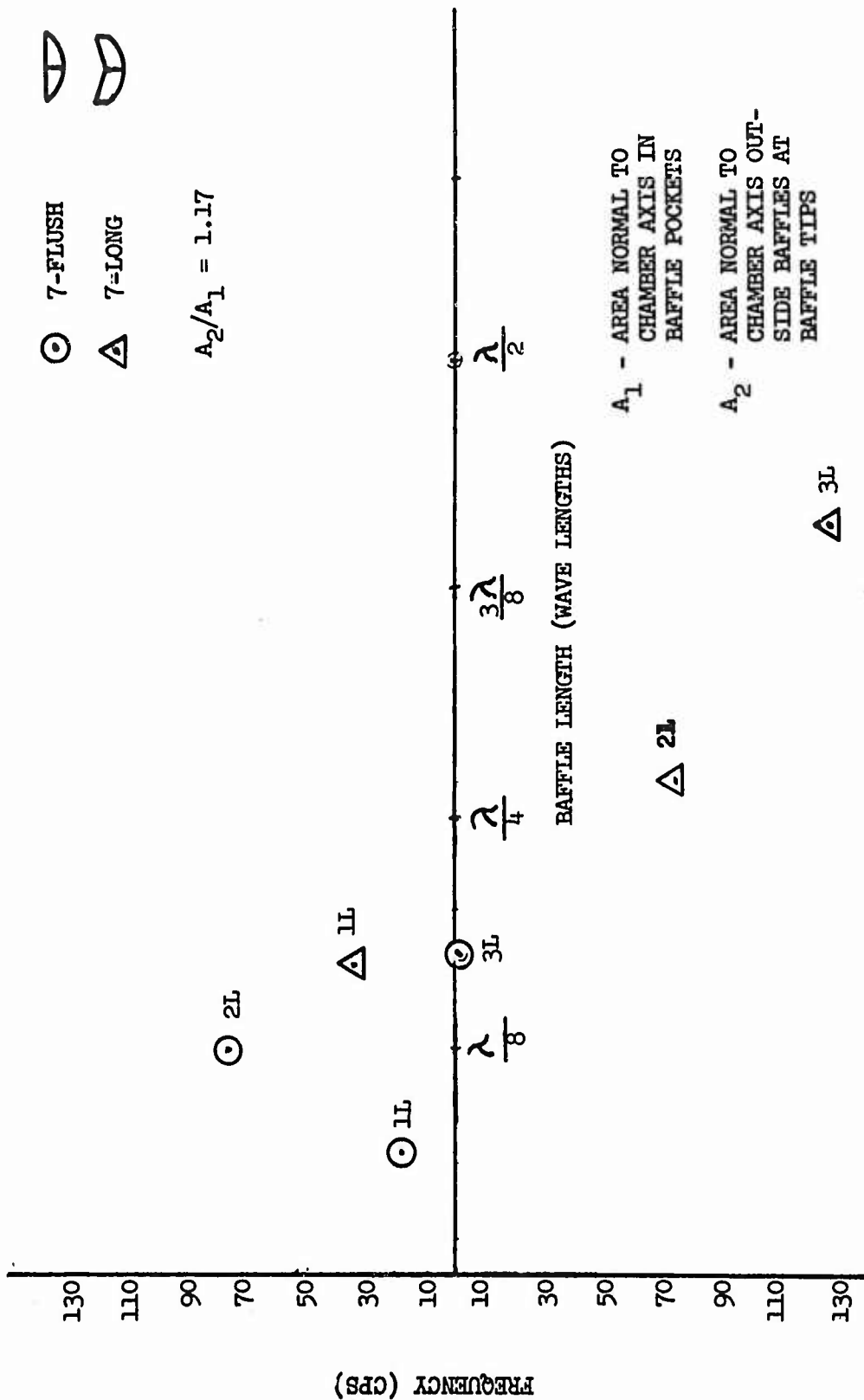


Figure 101 -- Effects of Baffle Length on L-Modes--Acoustic Tests

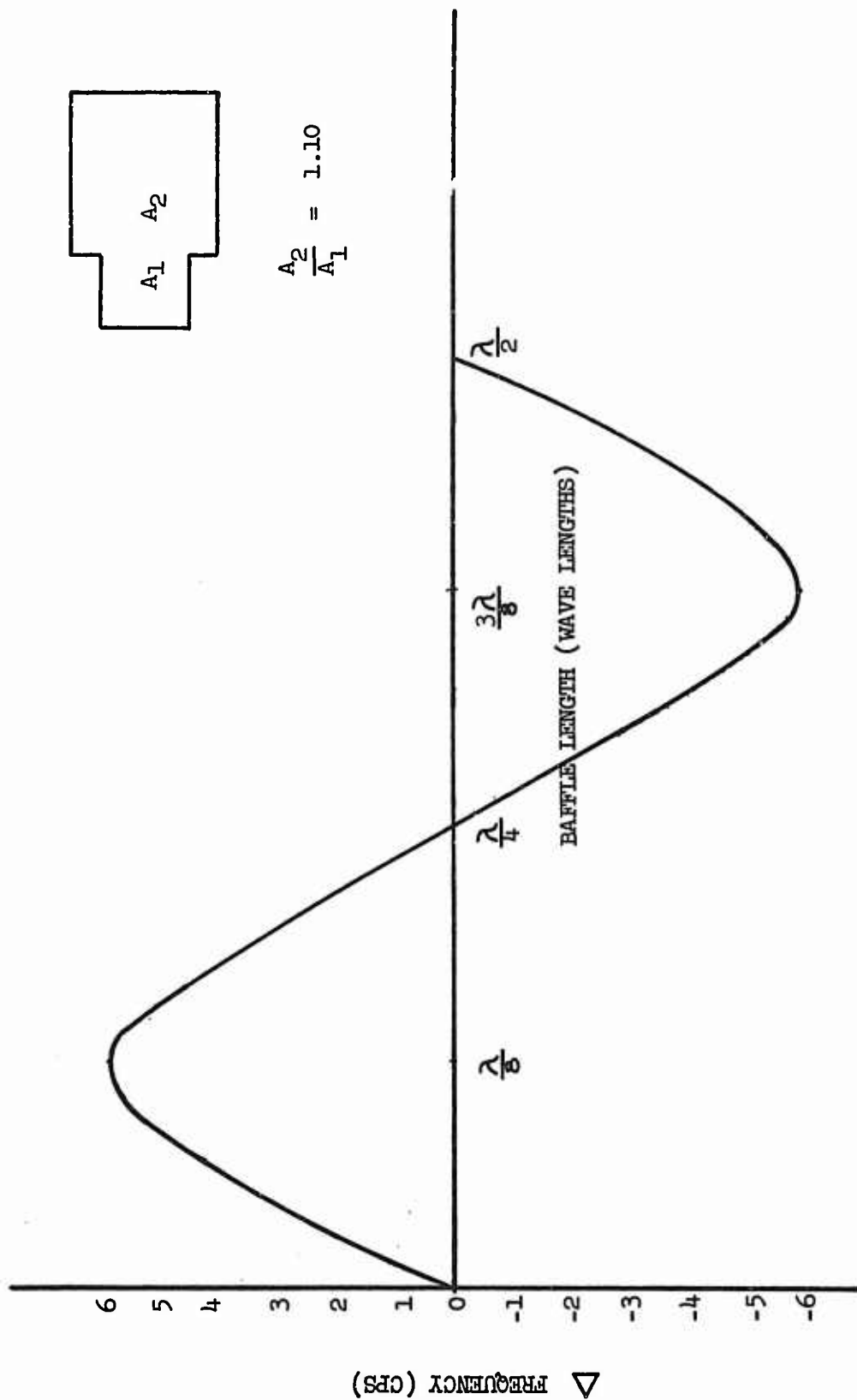


Figure 102 -- Effects of Baffle Length on I-Modes--Calculated

Table 10 -- Resonant Frequency and Decay Rate Comparison for Half-Scale Chamber

Gemsip Chamber Acoustic Frequencies

TABLE 10- RESONANT FREQUENCY AND DECAY RATE COMPARISON FOR HALF-SCALE CHAMBER

MODE	BAFFLE CONFIGURATION		UNBAFFLED		7-WING		7-FLUSH		7-LONG		6H-TITAN		5-CANTED		"STRAHLE"	
	CALC* FREQ cps	OBSERV. FREQ cps	DECAY RATE db/sec	OBSERV. FREQ cps												
1L	890	885	890	893	680	904	1050	918	800	901	800	895	680	893	600	
1T	1112	1178	380	1158	420	1115	480	NONE	NONE	1024	700	1030	260	1177	380	
1L-1T	1424	1523	1050	1533	1200	NOT RECORDED	1300	1485	590	1365	240	1475	580	1503	580	
2L	1626	1600	990	1590	900	1535	1300	1526	900	1510	500	1650	980	1545	710	
2T	1844	1910	210	1858	320	1802	350	NONE	NONE	NONE	700	1998	400	1907	800	
2L-1T	1970	2157	660	2146	830	2110	1000	2090	900	2101	700	2010	520	2080	520	
2T-1L	2042	2216	315	2236	330	2280	420	2288	360	2285	360	2260	380	2285	480	
3L	2366	2395	750	2392	550	2365	560	2350	650	2387	500	2393	450	2312	780	
1R	2316	2468	710	2454	550	2436	450	2416	700	2486	150	2464	600	NOT RECORDED	NOT RECORDED	
2L-2T+	2460+	2665	290	2664	900	2554	700	2507	540	2554	700	2648	400	2529	310	
1L-1R+	2480+	2870	520	2802	480	2702	380	2603	590	2652	450	2648	1400	2595	610	
3T+	2538+	3078	500	3116	580	2968	750	2705	320	2958	270	2958	270	2685	710	
3L-1T+	2620+	3315	220	3230	630			2892	450	2892	450	2791	560	2791	560	
1L-3T+	2690+							3037	200	3037	200					

UNIDENTIFIED RESONANT FREQUENCIES

\*LONGITUDINAL FREQUENCIES CALCULATED WITH FREELINE RESONANCE PROGRAM.  
 +POSSIBLE MODES AND ASSOCIATED FREQUENCY (CALCULATED).

V, B, Frequency (cont.)

standpoint that the identification of modes other than the first tangential was not completed because of discontinuation of the program.

Work on other development programs (M-1 and Apollo) has shown that extreme care must be used in identifying the resonant modes because of the complications introduced by the baffles. Results of these programs has confirmed the observations mentioned previously and has shown that the frequency depression of the first tangential mode experienced during the GEMSIP program will also occur with the higher order transverse modes.

#### C. EFFECT OF BAFFLE ON DECAY RATE

One of the major parameters which is a measure of the effectiveness of a baffle is decay rate. No analytical treatment has yet been devised which will predict the effect of baffles on decay rate; for this reason, the experimental procedure presented here represents a valuable tool in the development of baffles. During the GEMSIP program no attempt was made to explain why one baffle configuration exhibited better decay characteristic than another. The tests were not intended or designed to give basic information as to how baffles work and by what mechanism they suppress instability.

The major emphasis was placed on obtaining the decay rates for the various modes and using these data as a yardstick for measuring the effectiveness of the baffles. Particular emphasis was placed on the effect of the baffle configuration on the first tangential mode since this was the major problem area for the injectors undergoing test. Decay rate measurements made for the higher order transverse modes are in question because of the insufficient identification of the modes for reasons previously mentioned.

The data in Table 10 are presented only as a matter of record in hope that future investigations and analytical treatment of baffles will prove these

V, C, Effect of Baffle on Decay Rate (cont.)

data useful. All reference to particular modes of resonance has been labeled as questionable with the exception of those cases where such identification is warranted. The discussion to follow will be limited to the effects of the baffle configurations evaluated for the first tangential mode of instability.

Extension of the correlations to higher order modes would be without basis. Even in the case of the first tangential mode, extension of the trends indicated would be questionable for baffle configurations which deviate significantly from those tested as can be seen from the results with the "banana" baffle.

The decay rate as a function of baffle length is shown in Figure 98b for the configurations indicated. It is interesting to note that for a baffle configuration which is compatible with the first tangential mode, ("banana" baffle) there is no measurable change in the decay rate, which would indicate that the additional surface area introduced by a baffle does not contribute significantly to the damping of the system.

This information, coupled with the observation that baffles which are not compatible with the transverse modes tend to force longitudinal oscillations into the baffle pocket would indicate that the major contribution of baffles to the damping of a system is the scattering of energy to the longitudinal modes. Some theoreticians consider this simply coupling between a transverse mode and a longitudinal mode occurring in the baffle pocket. However, the baffle does not alter the characteristics of the transverse mode in that it has still the characteristic modes and antimodes; it is only its frequency which is changed. No mechanism for transfer of energy from the transverse to the longitudinal modes is proposed. However, the longitudinal oscillations in the baffle cavity were observed directly and the possibility of such a transfer was indicated, not demonstrated. This mode of oscillation apparently has a greater ability to dissipate the energy. The source of this dissipation is not known and will require further investigation.

V, Acoustic Testing (cont.)

D. CORRELATION OF HOT TESTS WITH ACOUSTIC TESTS

1. Frequency

The correlation between the hot and cold test frequency depression as a function of baffle length is shown in Figure 100. The degree of correlation leaves no doubt as to the ability of the acoustic tests to predict and explain some of the observations made during the hot testing of the various baffle configurations. In this respect the acoustic tests were of significant value in explaining the instabilities which were identified by the phase relationships of the various transducers as a first tangential but had a significantly lower frequency. The positive identification of this mode of instability gave additional confidence in the corrective action taken. The discovery of the phenomena also brought to light a possible effect of baffles not previously considered, that being that they can provide phase stabilization or destabilization by altering the resonant frequency of the chamber cavity away from or toward the peak response frequency of the combustion process. This suggests a fruitful line of approach for further investigation.

2. Decay Rate

The results of hot tests concerning the various baffle configurations tested confirmed the observations made as to the effect of increasing the baffle length on the decay rate of the system. The data presented in Figure 103 shows that the measured increase in decay rate as a function of baffle length had the expected effect, in that a stable configuration was obtained at a certain minimum length and configurations above this length were all stable for the 200-lb-thrust-per-element injector. In the final phases of the development program, data obtained on baffles of various profile (modified "wing" baffles) was extremely useful in optimizing the baffle from the standpoint of hydraulic considerations without compromising stability characteristics.

Additional evidence of the validity of the acoustic tests in defining the relative damping characteristics of various baffle configurations can be found in measurements of the decay rate of stable baffle configurations during hot test. The hot test data reflect the same trend in the decay rate of the system as the acoustic tests.

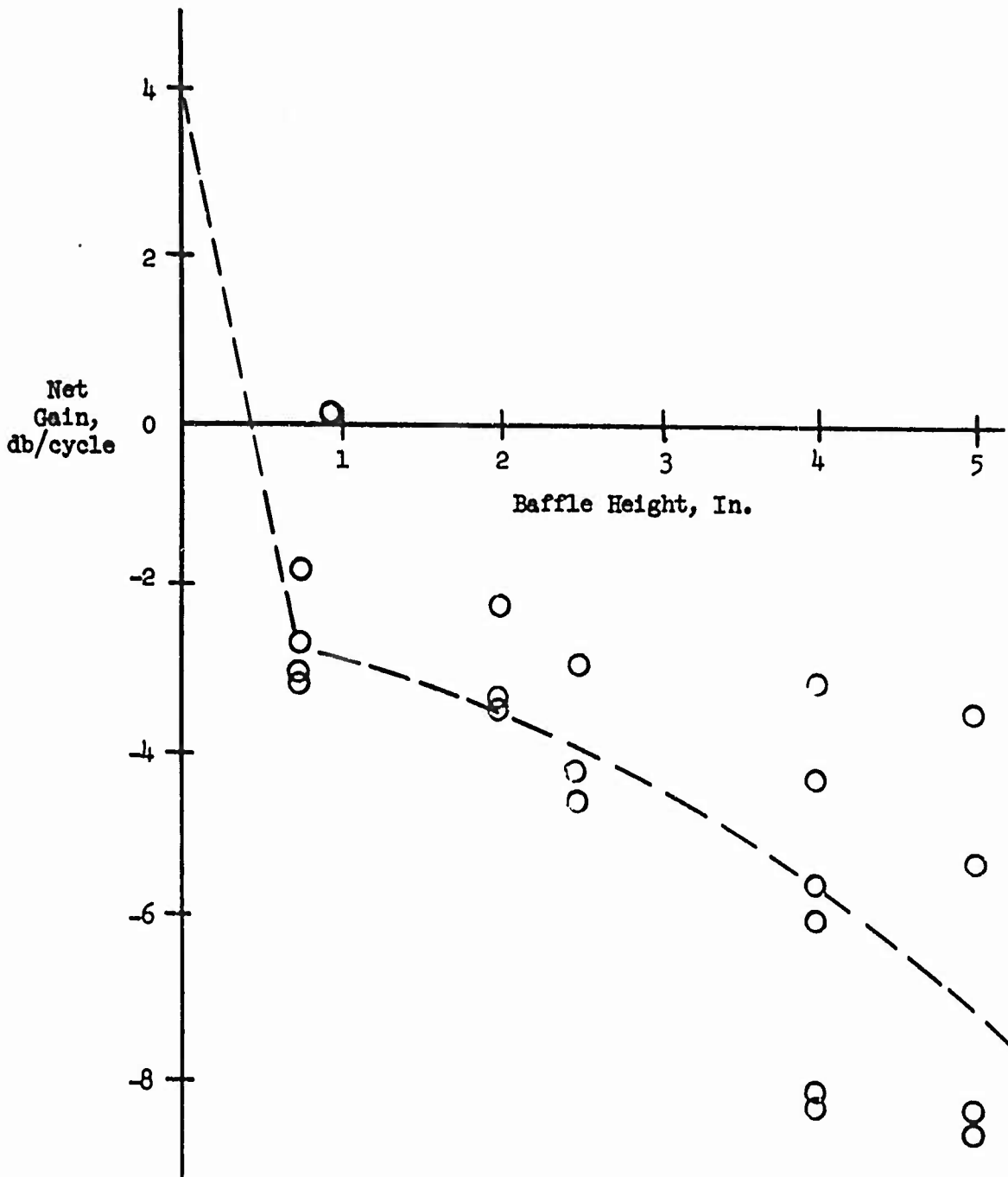


Figure 103 -- Effect of Baffles on First Tangential Mode

GEMSIP FR-1, Volume 5

APPENDIX, SECTION V

ANALYTICAL MODEL OF INJECTOR CHAMBER ASSEMBLY

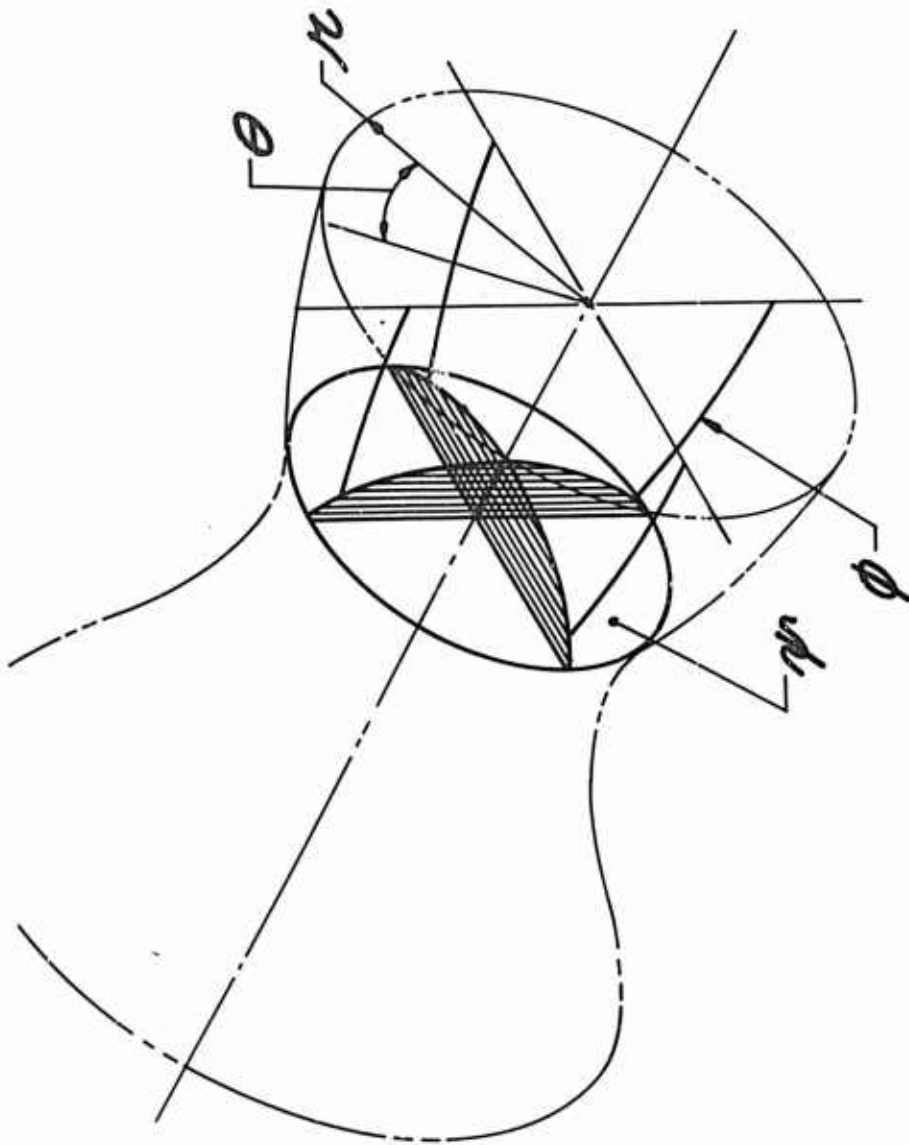


Figure 104 -- Curvilinear Coordinate System

GEMSIP FR-1, Volume 5, Appendix, Section V

The following is a discussion of the analytical model developed to investigate the effect of baffles on the frequency response of a combustion chamber cavity.

The analysis makes the following assumptions;

- 1) The baffle cavity is equivalent to a highly compartmented structure which allows only axial or longitudinal oscillations in the baffle pocket.
- 2) The admittance at the injector face and the nozzle throat is zero.
- 3) The effect of mean flow is negligible.
- 4) In the chamber cavity between the baffle tip and the chamber throat the three dimensional wave equation applies.

Based on assumptions 1, 2 and 3, the acoustic admittance at the baffle tip can be calculated from the relationship for a closed - open tube

$$G_B = \frac{-iAg}{c} \tan \frac{h_T}{c} \omega \quad \text{Eq.(1)}$$

Where  $G_B$  = admittance at baffle tip  
 $A$  = Area of baffle normal to chamber axis (thickness of baffles negligible)  
 $c$  = speed of sound in medium  
 $h_T$  = height of baffle  
 $\omega$  = frequency in radians/sec

For a three-dimensional analysis of the chamber cavity it is necessary to define a curvilinear coordinate system  $\psi$ ,  $\phi$ , and  $\theta$  as defined in Figure 104 where  $\psi$  is the local radius ( $r$ ) divided by the radius to the wall ( $r_w$ ) at that axial location.

At the chamber wall  $\psi = 1$ .  $\varphi$  is the same coordinate as in the cylindrical coordinate system, the angle between  $r$  and the  $x - z$  plane in cartesian coordinates.  $\theta$  is orthogonal to the other two coordinates.

Any differential element  $dL$  can be expressed as:

$$(dL)^2 = (ds)^2 + (dn)^2 + (dm)^2 \quad \text{Eq.(2)}$$

where

$ds$  is the differential element  $\perp$  to the  $\varphi$  constant surface

$dn$  is the differential element  $\perp$  to the  $\psi$  constant surface

$dm$  is the differential element  $\perp$  to the  $\theta$  constant surface

for the coordinate system shown in Figure 104

$$dm = r d\theta = \psi r_w(x) d\theta ; \quad \text{Eq.(2a)}$$

$$dn = dr = r_w(x) d\psi . \quad \text{Eq.(2b)}$$

In order to simplify the analysis it is assumed that the  $\phi$  constant planes represent planes of constant pressure potential.

$$\text{Then } \frac{dP}{dx} = \frac{dP}{d\varphi} \text{ giving } dx = d\varphi \quad \text{Eq.(2c)}$$

For an arbitrary orthogonal coordinate system

$$(dL)^2 = (h\varphi)^2(d\varphi)^2 + (h\psi)^2(d\psi)^2 + (h\theta)^2(d\theta)^2$$

Substituting Equations (2a), (2b), and (2c) into Equation (2) and solving for  $h\varphi$ ,  $h\psi$  and  $h\theta$  gives

$$h\psi = r(x), \quad h\varphi = 1, \quad \text{and } h\theta = \psi r_w(x)$$

The Laplacian  $\nabla^2 P$  can be written in terms of an arbitrary orthogonal coordinate system  $h\varphi$ ,  $h\psi$ , and  $h\theta$  as

$$\nabla^2 P = \frac{1}{h\varphi h\psi h\theta} \left[ \frac{\partial}{\partial \varphi} \left( \frac{h\psi h\theta}{h\varphi} \frac{\partial P}{\partial \varphi} \right) + \frac{\partial}{\partial \psi} \left( \frac{h\theta h\varphi}{h\psi} \frac{\partial P}{\partial \psi} \right) + \frac{\partial}{\partial \theta} \left( \frac{h\varphi h\psi}{h\theta} \frac{\partial P}{\partial \theta} \right) \right]$$

giving

$$\nabla^2 P = \frac{\partial^2 P}{\partial \varphi^2} + \frac{1}{r_w^2 \psi} \frac{\partial P}{\partial \psi} + \frac{1}{r_w^2} \frac{\partial^2 P}{\partial \psi^2} + \frac{1}{r_w^2 \psi^2} \frac{\partial^2 P}{\partial \theta^2}.$$

The acoustic wave equation for a sinusoidal oscillation is

$$\nabla^2 P + \frac{\omega^2}{c^2} P = 0.$$

The acoustic wave equation in our new coordinate system becomes

$$\frac{\partial^2 P}{\partial \varphi^2} + \frac{1}{r_w^2 \psi} \frac{\partial P}{\partial \psi} + \frac{1}{r_w^2} \frac{\partial^2 P}{\partial \psi^2} + \frac{1}{r_w^2 \psi^2} \frac{\partial^2 P}{\partial \theta^2} + \frac{\omega^2}{c^2} P = 0. \quad \text{Eq.(3)}$$

Using the separation of variable technique to solve the equation we assume a solution of the form

$$P = R(\varphi) \bar{\Psi}(\psi) \Theta(\theta).$$

Substituting the assumed solution into Equation (3) and separating variables, three ordinary differential equations are obtained:

$$\Theta'' + A_1 \Theta = 0, \quad \text{Eq.(4)}$$

$$R'' + \left( \frac{\omega^2}{c^2} - \frac{A_2}{r_w^2} \right) R = 0, \quad \text{Eq. (5)}$$

and 
$$\psi^2 \Psi'' + \psi \Psi' + (\psi^2 A_2 - A_1) \Psi = 0. \quad \text{Eq. (6)}$$

Equation (4) has a solution of the form

$$\theta = C_1 e^{\sqrt{A_1} \theta} + C_2 e^{-\sqrt{A_1} \theta}, \quad \text{Eq. (7)}$$

for  $A_1 > 0$

$$\theta = C_1 \sinh \sqrt{A_1} \theta + C_2 \cosh \sqrt{A_1} \theta, \quad \text{Eq. (7a)}$$

for  $A_1 < 0$

$$\theta = C_1 \sin \sqrt{A_1} \theta + C_2 \cos \sqrt{A_1} \theta, \quad \text{Eq. (7b)}$$

For a tangential mode at  $\theta = 0$ ,  $\frac{\partial \theta}{\partial \theta} = 0$ .

Differentiating Equation (7a) gives

$$\frac{\partial \theta}{\partial \theta} = C_1 \sqrt{A_1} \cosh \sqrt{A_1} \theta + C_2 \sqrt{A_1} \sinh \sqrt{A_1} \theta.$$

Evaluating this derivative at  $\theta = 0$  yields

$$0 = C_1 \sqrt{A_1} + 0$$

giving  $\Rightarrow C_1 = 0$ ,

$$\theta = C_2 \cosh \sqrt{A_1} \theta.$$

Since  $\theta$  is everywhere finite and as  $\theta \rightarrow \infty$   $\cosh \sqrt{A_1} \theta \rightarrow \infty \Rightarrow C_2 = 0$  making Equation (7a) a trivial solution.

Differentiating Equation (7b) gives

$$\frac{\partial \theta}{\partial \theta} = -C_1 \sqrt{A_1} \cos \sqrt{A_1} \theta + C_2 \sqrt{A_1} \sin \sqrt{A_1} \theta .$$

Evaluating

$$\frac{\partial \theta}{\partial \theta} \text{ at } \theta = 0 \Rightarrow C_1 = 0 .$$

Therefore

$$\theta = C_2 \cos \sqrt{A_1} \theta .$$

$A_1 = (n)^2$  where  $n$  equals the order of the tangential mode, i.e.,

$n = 1$  for 1st tangential,  $n = 2$  for 2nd tangential, etc.

The solution to Equation (6) is

$$\bar{\Psi} = C_3 J_n (\sqrt{A_2} \Psi) + C_4 Y_n (\sqrt{A_2} \Psi) .$$

Since  $\bar{\Psi}$  is everywhere finite and  $Y (\sqrt{A_2} \Psi) \rightarrow \infty$  as  $\Psi \rightarrow 0$  implies  $C_4 = 0$ .

giving  $\bar{\Psi} = C_3 J_n (\sqrt{A_2} \Psi)$ .

From the boundary condition

$$\Psi = 1, \quad \frac{\partial \bar{\Psi}}{\partial \Psi} = 0 = J'_n (\sqrt{A_2}),$$

$$J'_n (\sqrt{A_2}) = \frac{+n}{\sqrt{A_2}} J_n (\sqrt{A_2}) - J_{n+1} (\sqrt{A_2}),$$

$$\text{or } n J_n (\sqrt{A_2}) = \sqrt{A_2} J_{n+1} (\sqrt{A_2}) .$$

Equation (5) is of the same form as the one dimensional wave equation with the exception that it contains  $r_w$  which is a function of  $x$ , the axial location. In order to solve this equation it must be integrated numerically treating  $r_w$  as a constant for small increments of  $x$ .

$$\text{Assuming } r_w^2 = \text{constant and letting } \frac{\omega^2}{c^2} - \frac{A_c}{r_w^2} = K$$

the solution of Equation (5) is

$$R = C_1 \cosh i \sqrt{K} \Psi + C_2 i \sinh i \sqrt{K} \Psi ;$$

$$R' = i C_1 \sqrt{K} \sinh i \sqrt{K} \Psi - C_2 \sqrt{K} \cosh i \sqrt{K} \Psi .$$

From the momentum equation the flow in the axial direction is given by

$$\dot{W}'_{\Psi} = \frac{-A_c g}{i \omega} R' \Theta \Psi .$$

where  $A_c$  = area of chamber

$$\text{Define the admittance } G_{\Psi} = - \frac{\dot{W}'_{\Psi}}{P'}$$

$$G_{\Psi} = - \frac{i A_c g}{\omega} \frac{R'}{R}$$

$$G_{\Psi} = - \frac{i A_c g}{\omega} \left[ \frac{C_1 i \sqrt{K} \sinh i \sqrt{K} \Psi - C_2 \sqrt{K} \cosh i \sqrt{K} \Psi}{C_1 \cosh i \sqrt{K} \Psi + C_2 i \sinh i \sqrt{K} \Psi} \right]$$

The constants  $C_1$  and  $C_2$  can be determined by considering the value of admittance at  $\Psi = 0$ :

$$G_{\Psi=0} = \frac{i A_c g}{\omega} \frac{C_2 \sqrt{K}}{C_1} ,$$

$$\text{or } \frac{C_2}{C_1} = \frac{G_{\Psi=0} \omega}{\sqrt{K} A_c g}$$

If  $\sqrt{K} \varphi = 0$  (0.1)  $\cosh i \sqrt{K} \varphi \approx 1$  and  
 $\sinh i \sqrt{K} \varphi \approx i \sqrt{K} \varphi$  the equation then becomes:

$$G_{\varphi} = -\frac{iA_c g}{\omega} \left[ \frac{-K \varphi - \frac{G_{\varphi=0} \omega i \sqrt{K}}{\sqrt{K} A_c g}}{1 + \frac{G_{\varphi=0} \omega i \sqrt{K} \varphi}{\sqrt{K} A_c g}} \right]$$

$$G_{\varphi} = G_{\varphi=0} \left[ \frac{1 + \frac{iA_c g K \varphi}{\omega G_{\varphi=0}}}{1 + \frac{G_{\varphi=0} \omega i \varphi}{A_c g}} \right]$$

The method of solution is then to assume a particular mode in the chamber, thus defining  $n$ . Once  $n$  is defined  $A_2$  is solved for.  $A_2$  is multivalued parameter, the value of  $A_2$  being dependent on the presence or absence of a radial mode component and the order of the radial mode. Once  $A_2$  is determined it is possible to integrate  $G_{\varphi}$  numerically -- the resonant frequency for that mode being the frequency for which  $G_{\varphi} = G_B$ .

TABLE 11

List of Symbols

$G_B$	= Admittance at baffle tip
$A_c$	= Area of chamber normal to chamber axis
$\rho$	= Density
$c$	= Speed of sound
$h_T$	= Height of baffle leg
$\omega$	= Frequency (rad/sec)
$r_w(x)$	= Radius of chamber as a function of $x$
$\psi, \varphi, \theta$	= Axes of orthogonal coordinate system
$h_\psi, h_\varphi, h_\theta$	= Sequence roots of metric coefficients for an arbitrary orthogonal coordinate system
$A_1$ and $A_2$	= Eigenvalues
$C_1$	= Integration constants
$n$	= Integer defined by acoustic modes of chamber
$K$	= $\frac{\omega^2}{c^2} - \frac{A_2}{r_w^2}$
$G_\varphi$	= Admittance of nozzle chamber cavity in $\varphi$ direction
$i$	= $\sqrt{-1}$
$\dot{W}$	= Oscillating weight flow
$P$	= Oscillating pressure

VI. FLOW CONTROL SERVO SYSTEM

In order to develop a dynamically stable injector for the Gemini second stage propulsion system, Aerojet-General undertook an extensive program consisting of a series of thrust chamber assembly static test firings. This program required a TCA test stand capable of providing repeatable start transient characteristics identical to those generated by the complete propulsion system. To accomplish this, a method for controlling propellant flow rate was mandatory; further, both transient and steady state flow control was required. To this purpose, it was desirable that both engine start transient simulation and steady state chamber pressure and mixture ratio control be realized with the same control hardware. Two concepts were investigated for the control of propellant flow rates: namely, propellant tank pressurization control and propellant flow rate control by servo valves.

The propellant tank pressurization control technique was analyzed both in terms of control response specifications and system modifications required. It was concluded that extensive modifications would be needed to provide sufficient gas flow rates, particularly during the TCA start transient. Further, gas pressurization control being inherently slow, this system would not be capable of producing a simulated engine start transient at normal rise rates and, moreover, pressure and mixture ratio control would be difficult to achieve.

The direct propellant flow rate control technique also involved modifications to the existing system. In particular, modifications to the existing propellant feed systems were required, together with the installation of fuel and oxidizer flow control valves, close-coupled to the thrust chamber. The direct flow rate control system, however, would be capable of producing rapid and well controlled variations in pressures and flow rates.

Based upon the control criteria and an analysis of modification costs, the direct propellant flow control concept was mechanized on Test Stand C-1.

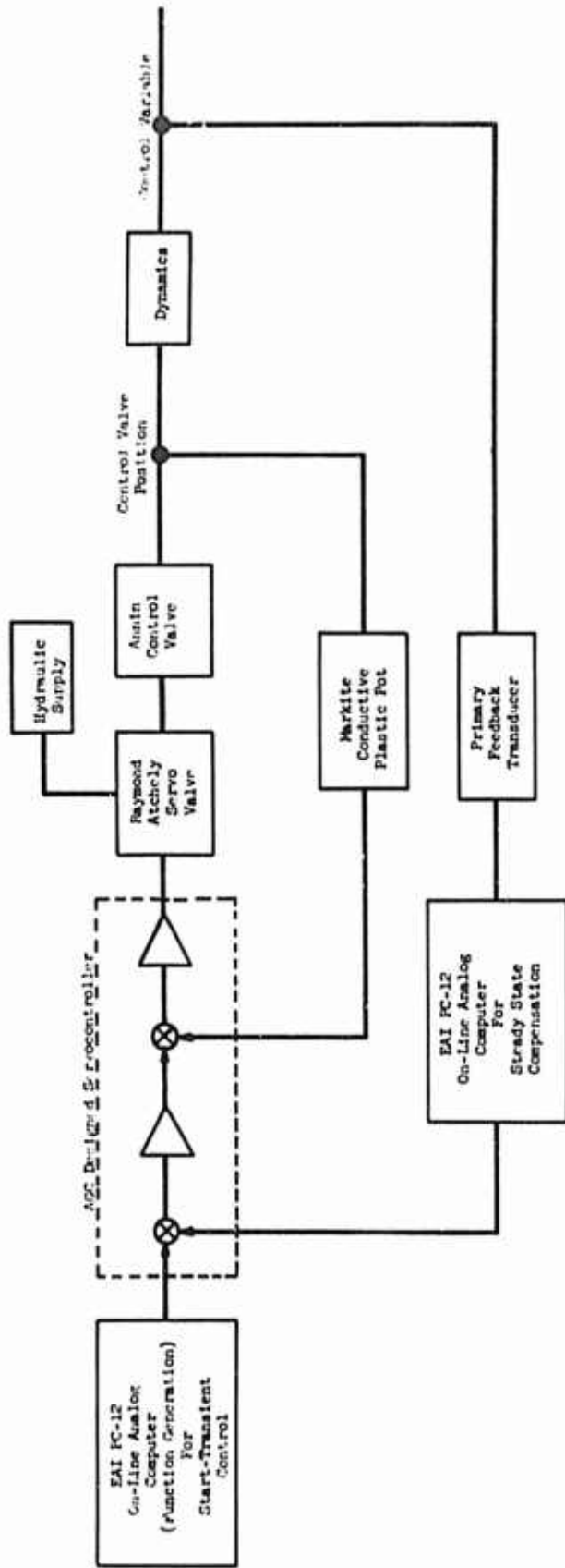


Figure 105 -- Generalized C-1 Control Philosophy

Figure 105 -- Generalized C-1 Configuration Philosophy

VI, Flow Control Servo System (cont.)

The generalized philosophy employed in the C-1 control system is illustrated in Figure 105. An electrical signal is applied across the input terminals of an Aerojet-designed servo controller. The servo controller output drives a Raymond-Atchely servo valve that is hydraulically coupled to an Annin flow control valve actuator. Flow control valve position feedback is used to stabilize the inner loop against gain or dynamic variations in the open-loop components. In general, control valve modulation produces dynamic effects in the downstream line.

The appropriate downstream parameter (flow rates or pressure) is sensed with an applicable transducer; the transducer output signal is then conditioned in the servo controller, and forms the source of primary feedback. Note that an on-line analog computer is included in the loop mechanization. The use of this device (Electronic Associates, Inc., PC-12) was employed to generate the control valve excitation command for transient TCA testing, and also was programmed to mechanize the required feedback signal compensation for closed-loop testing.

During start-transient control, the outer feedback paths were electrically eliminated from the loops so that the systems functioned to position the control valves in accordance with preprogrammed command voltages. In the closed-loop or steady state control mode, however, the outer feedback paths functioned to maintain both mixture ratio and chamber pressure parameters. In this context, the PC-12 analog computer was used to generate the required system compensation.

Based upon the control system of Figure 105, a detailed analysis of the test stand and thrust chamber assembly was performed to define the overall system mathematical model. The model was then simulated on an IBM 7094 digital computer; in particular, the computer was employed to allow the investigation of a wide variety of start transient control modes. The automatic machine approach to analysis was necessary, in the present application, because of the large number of nonlinear differential equations that were required to construct the system model.

## VI, Flow Control Servo System (cont.)

The computer effectively solved the differential equations, while simultaneously closing the control loops into the model. Based upon the computer simulation, an open-loop mode of start transient control was selected. The closed-loop mode was rejected because of the uncertainties associated with dynamic and control hardware mathematical formulations. The final computer design simulated a Gemini engine start transient as illustrated in Figure 106. Sequencing of the control valves, thrust chamber valves, and dump valves were defined by the computer study.

Following the installation of the control system, a series of flow tests were conducted to determine the Annin valve flow resistances as a function of lift. During this preliminary period, a number of problem areas were discovered. Because of difficulties associated with the hydraulic pressurization system, control valve fluctuations were reflected into the actuator supply system, markedly degrading the control valve dynamic response. In addition, it was experimentally verified that the control valves tended to cavitate for small values of lift. This cavitation problem had been anticipated.

Transient valve characteristics were experimentally deduced by subjecting the valves to a series of dynamic response tests. The resulting data were then matched with those of an analytical third-order system on the analog computer; i.e., a general transfer function of the form

$$G(s) = \frac{K (W_u)^2}{s (s^2 + 2 \xi Ws + Wn^2)}$$

was mechanized for computer simulation, and the valve gain ( K ), undamped natural frequency ( wn ) and damping ratio (  $\xi$  ) selected so as to match the experimentally derived valve data. Results of the tests were as follows:

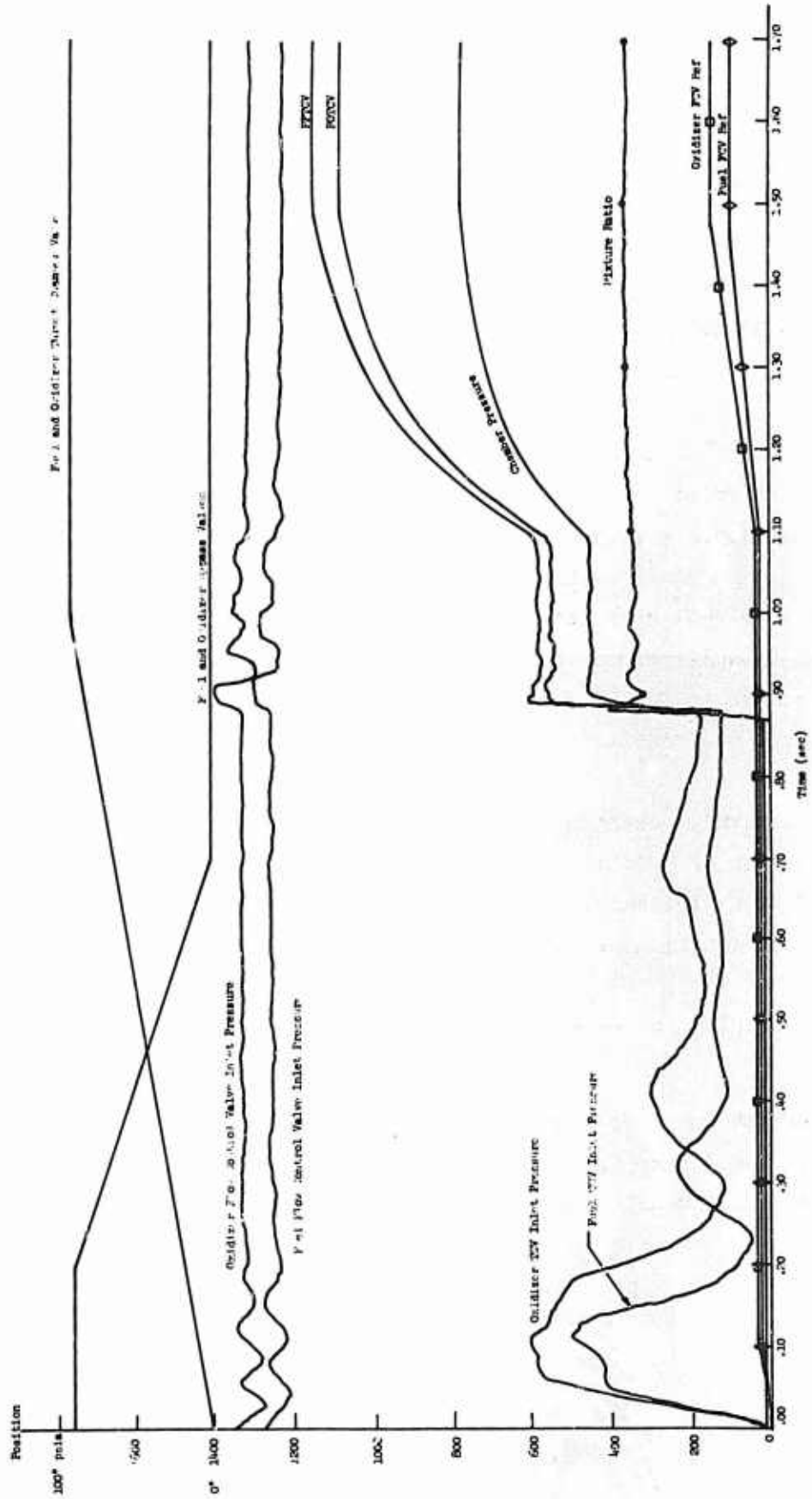


Figure 106a -- TCA transient with Position Feedback Control

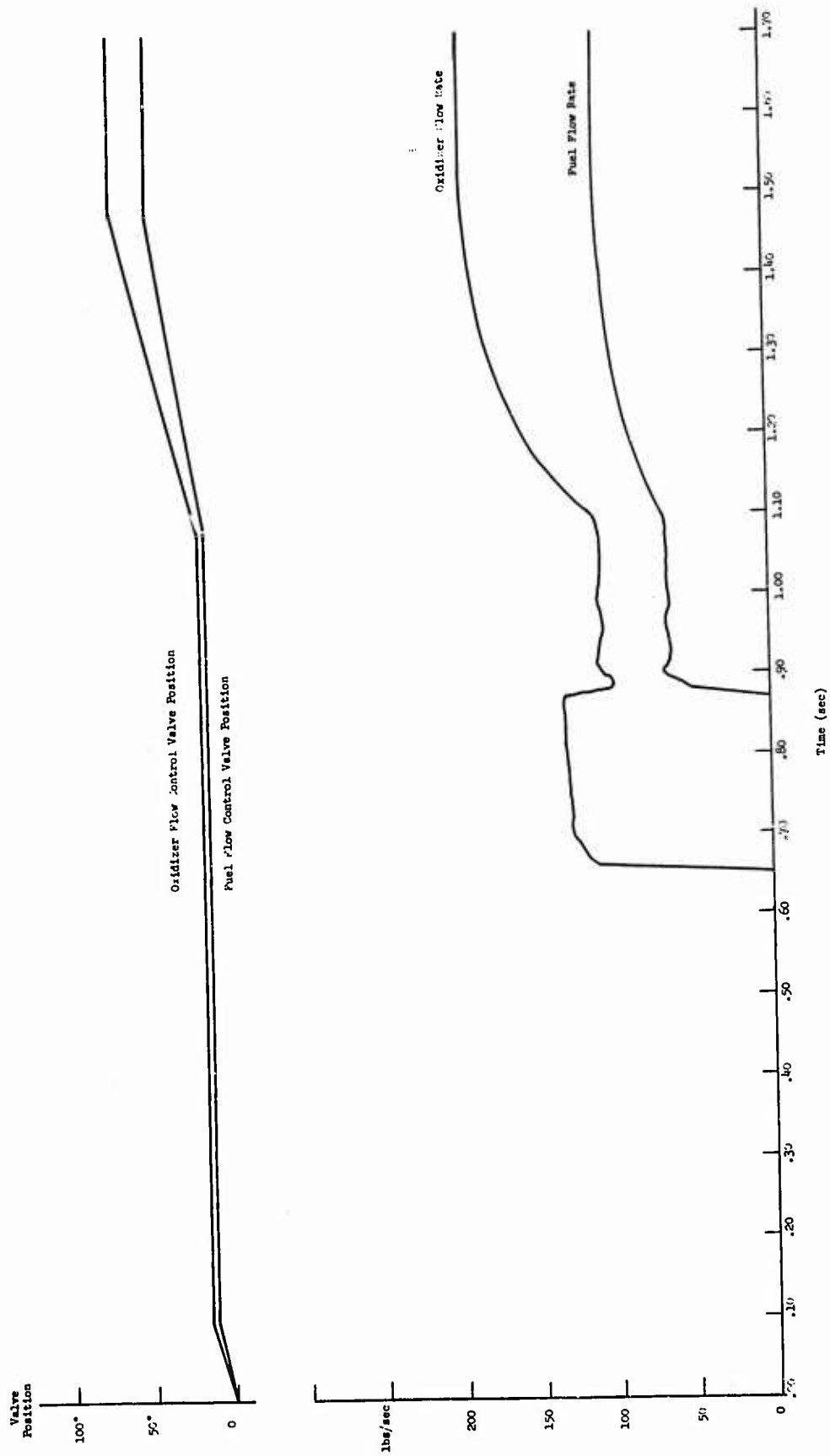


Figure 106b -- TCA Transient with Position Feedback Control

## VI, Flow Control Servo System (cont.)

	<u>Oxidizer Valve</u>	<u>Fuel Valve</u>
K	11.5	12.0
Wn	97.	117.
$\xi$	0.635	0.545

These data were required in the design of both the open-loop start transient control system and the closed-loop mixture ratio and chamber pressure controller.

Based upon the preliminary system design, three transient test firings were conducted. Three distinct problem areas were discovered during initial testing: (1) an extremely high hydraulic gain existing across the Annin valve because of the  $C_v$  vs lift characteristics of the valve; e.g., a 0.5% change in valve position resulted in a 5% variation in flow rate; (2) a valve position "zero-shift" problem due to the use of soft valve seats; and (3) failure to simulate the initial rise rate characteristics of the Gemini second stage engine in the thrust chamber assembly tests.

A typical thrust chamber assembly start transient is illustrated in Figure 107. Note the close agreement between the predicted data of Figure 106 and the achieved data of Figure 107.

The high Annin valve hydraulic gain was reduced by re-contouring the valve plugs to produce exponential rather than linear  $C_v$  vs lift characteristics, and the zero-shift difficulty was obviated by providing a metal-to-metal valve seat. It was thought that the initial rise rate engine ignition condition could be achieved by simulating the pump flow transients that exist prior to engine ignition. The TCA sequencing was thus varied to simulate more accurately the second stage turbopump assembly flow environment in the transient mode. Following additional calibrations of the flow control valves, a test firing with the new method of sequencing produced an acceptable simulated engine start.

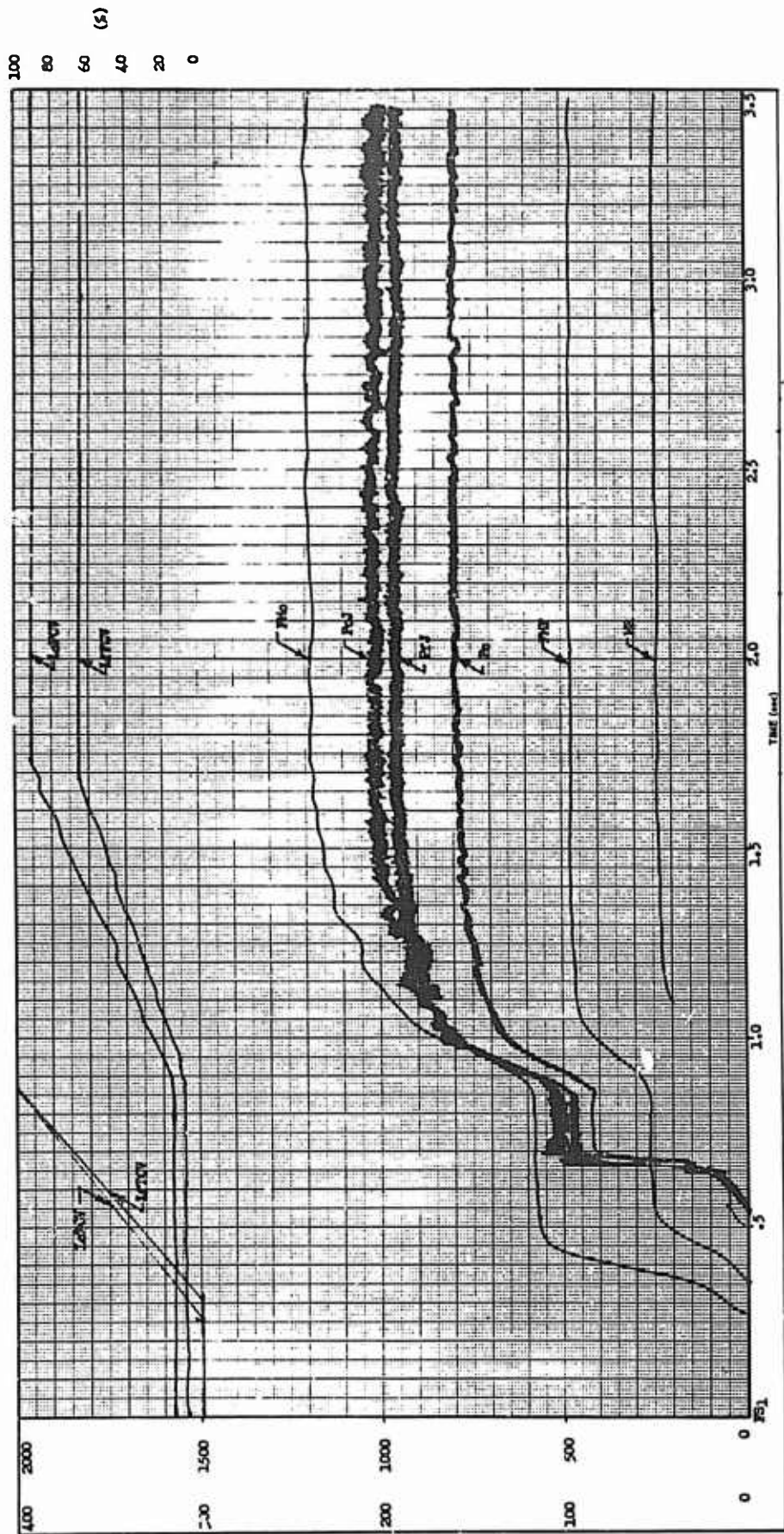


Figure 107 -- C-1 Transient Test Data--Pressure and Flows vs Time

VI, Flow Control Servo System (cont.)

Because of the difficulties encountered with valve sequencing in the open-loop start transient mode, a closed-loop pressure mode was considered. A series of flow tests to determine the effects of modulating valve position based upon thrust chamber valve inlet pressures led to the conclusions that this method of control was indeed feasible. However, problems associated with hardware and test scheduling precluded the application of this technique; the open-loop mode was maintained for start sequence testing with excellent results.

After acceptable transient conditions were achieved, a closed-loop steady state control mode analysis was initiated. Analog computer simulation was employed to design a system capable of simultaneously controlling both chamber pressure and mixture ratio in the steady-state operational mode. As illustrated in Figure 108, an electrical signal proportional to the desired value of steady state chamber pressure is impressed across the command terminals of the fuel valve servo controller. The achieved chamber pressure value is sensed by a pressure transducer. An error between the desired chamber pressure and the achieved chamber pressure then drives the fuel flow control valve in the direction to reduce the error. Integral compensation is employed such that, in the steady state, the error signal degenerates to zero and the correct value of chamber pressure is established and maintained automatically.

Simultaneous control of mixture ratio is realized by the oxidizer flow control valve servo system. Both fuel and oxidizer flow rates are sensed with Potter turbine system. Both fuel and oxidizer flow rates are sensed with Potter turbine meters. The turbine meter produces an electrical signal with a frequency proportional to volumetric flow rate. Because the loop operates in a dc mode, the ac flowmeter output is transformed into a dc electrical signal through the use of an ac-dc converter. Electrical signals, proportional to fuel and oxidizer flow rates, are balanced in the mixture ratio servo controller. The servo controller input gains are established in accordance with the desired predetermined mixture ratio value. Integral compensation is again employed in the mixture ratio control

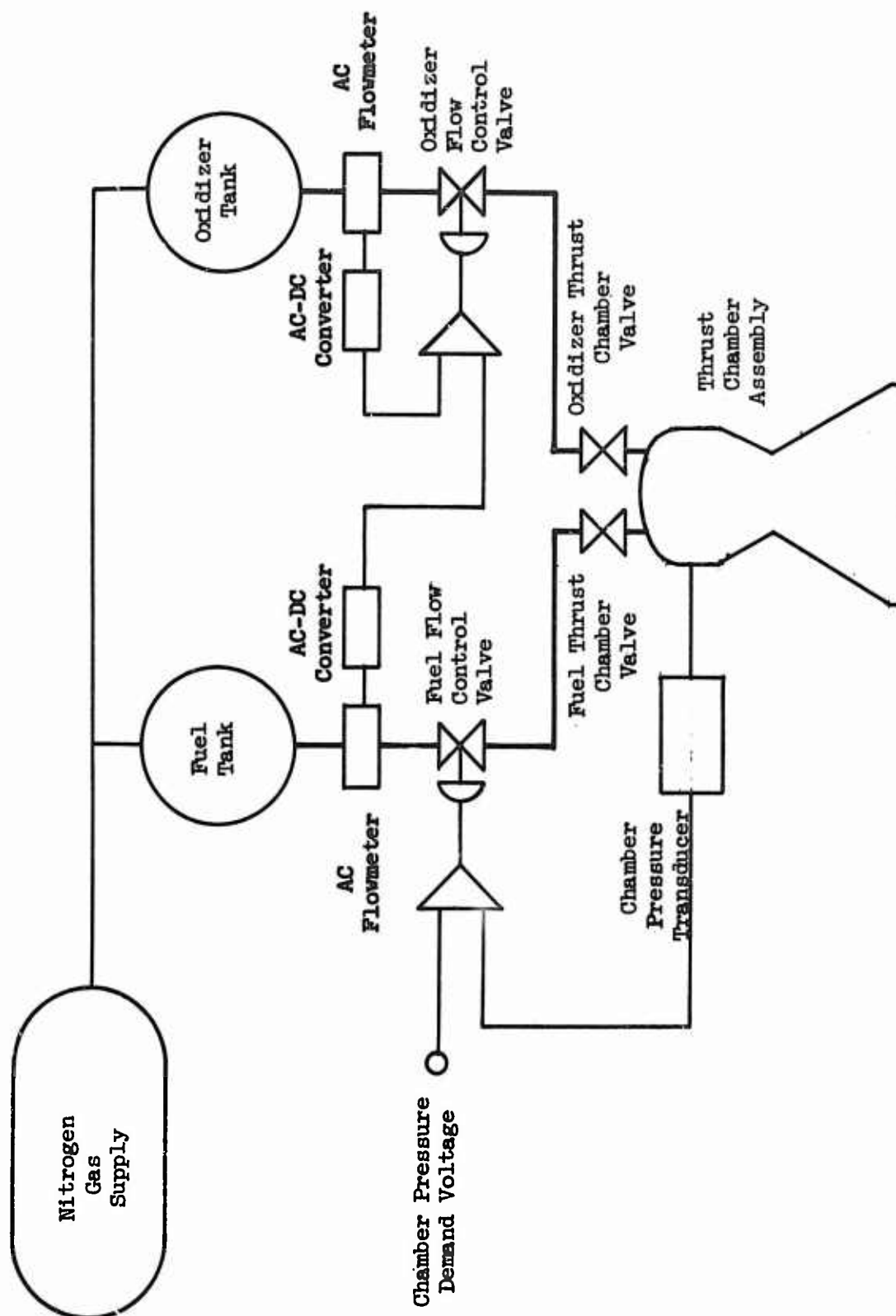


Figure 108 -- System for Simultaneous Control of TCA Parameters

## VI, Flow Control Servo System (cont.)

loop. In the steady state, after all transients have died out, the two loops will control both mixture ratio and chamber pressure to predetermined values. These values can now be varied with time, during the firing, to evaluate TCA performance over a selected range of mixture ratio and chamber pressure.

Representative start transient and steady state test data are illustrated in Figures 109, 110, and 111. Start transient data with a typical open-loop indicate that an excellent simulation of the engine start-transient characteristics can be obtained. The initial high chamber pressure rise rate phenomenon is clearly illustrated in the typical Test Stand C-1 start transient data.

Figure 109 illustrates the benefits derived from the closed-loop  $P_c/$ MR control mode. Note that a large error exists in mixture ratio at the point in time at which automatic closed-loop system control is initiated. The control system senses this error, however, and immediately adjusts the system to the correct mixture ratio. Three distinct values of mixture ratio were evaluated at a constant chamber pressure during this run. Excellent control was established, while the steady state mixture ratio errors were negligible.

The effects of varying mixture ratio at a constant value of chamber pressure is again illustrated in Figure 110. A total of five distinct mixture ratio steps were attained during this typical firing with excellent steady-state accuracy. The small variations noted in chamber pressure correspond to the transient modes occurring at each step-level change in mixture ratio. However, the steady-state chamber pressure remains at the constant preselected value.

Figure 111 illustrates the effects of varying chamber pressure at a constant value of mixture ratio. A total of six useful and accurate data points were obtained during this static test firing. Note that the errors in mixture ratio occurring during the chamber pressure step-level transients are not severe; further, the system automatically adjusts to the correct steady-state value of mixture ratio.

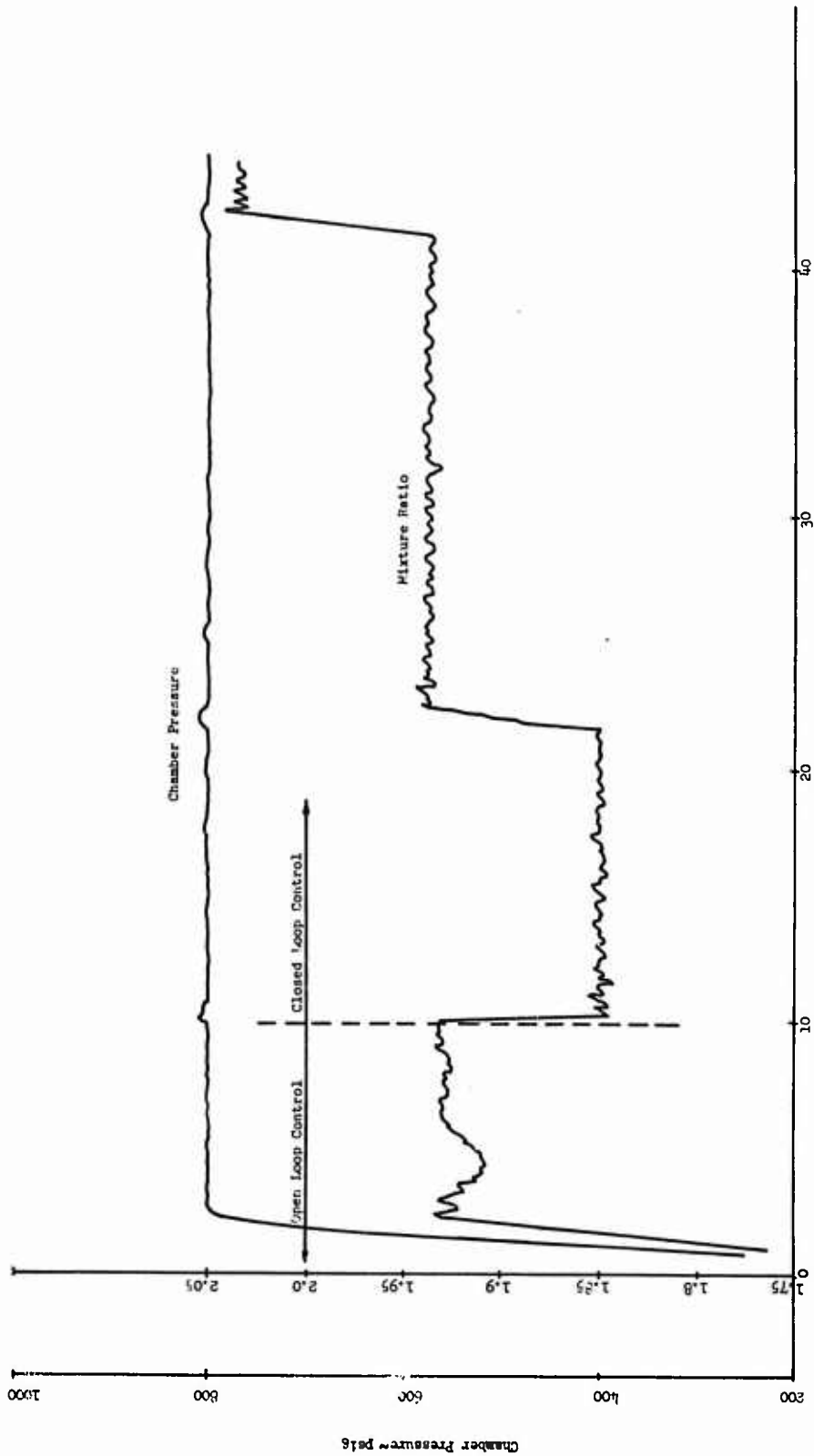


Figure 109 -- C-1 Closed-Loop Control System Response Data--Open-Loop to Closed-Loop Control

Figure 109 -- C-1 Closed-Loop Control System Response Data -  
Open-Loop to Closed-Loop Control

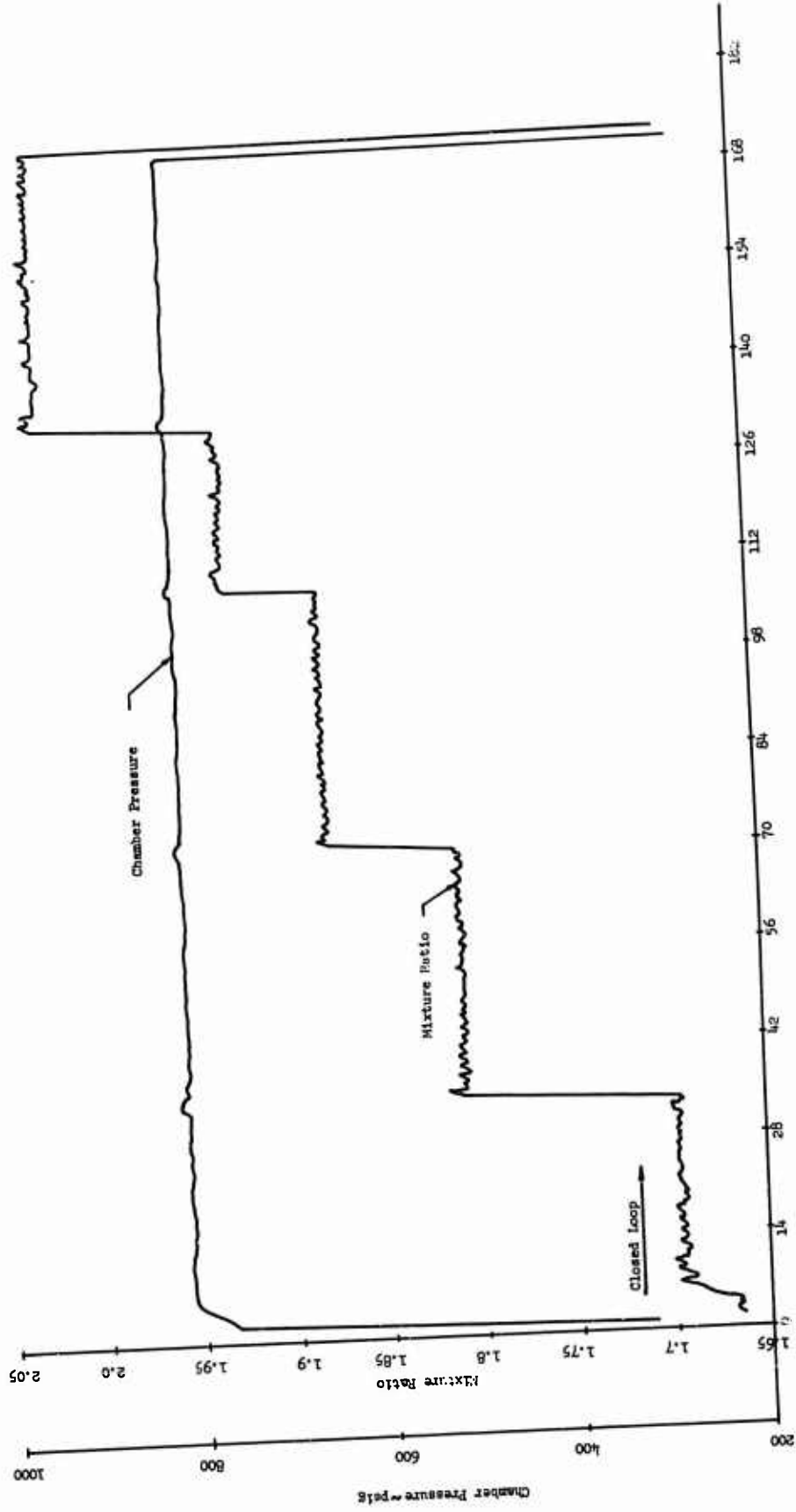


Figure 110 -- C-1 Closed-Loop Control System Response Data

Figure 110 -- C-1 Closed-Loop Control System Response Data

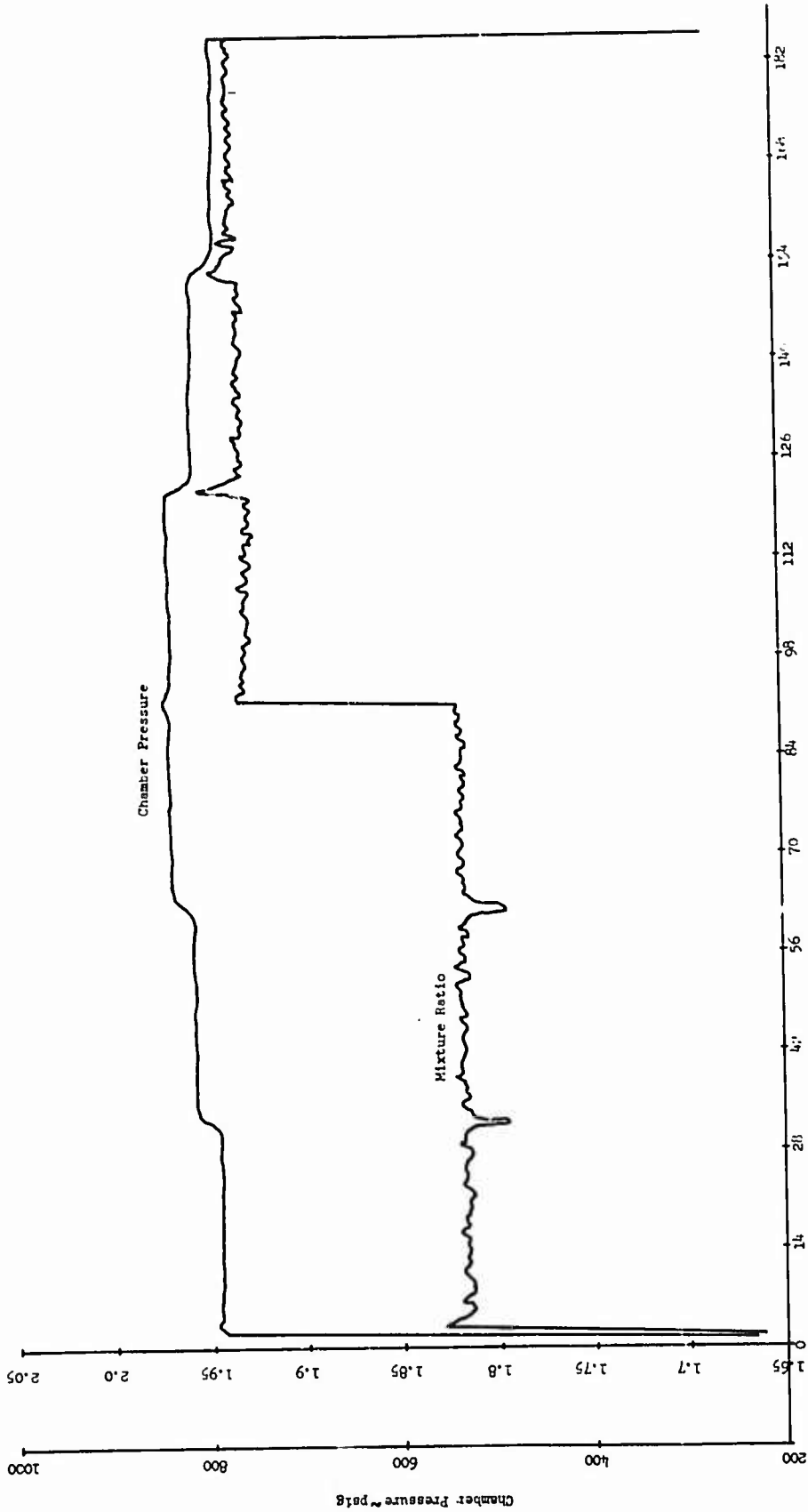


Figure 111 -- C-1 Closed-Loop Control System Response Data

Figure 111 -- C-1 Closed-Loop Control System Response Data

VI, Flow Control Servo System (cont.)

These tests were part of the Cooled Baffle Development discussed in Volume 2, Section II.

From the previous discussion, the following conclusions can be drawn:

- 1) The use of open-loop control during start transient engine simulation testing on test stand C-1 produces a TCA ignition transient very similar to that of the second stage engine.
- 2) Closed-loop pressure-feedback control during the simulated engine start transient is feasible.
- 3) Closed-loop steady state control of mixture ratio and chamber pressure has been demonstrated. In all cases, accurate and repeatable TCA performance data were acquired.
- 4) A considerable cost saving can be realized through the use of the closed-loop  $P_c$ /MR control system; through appropriate programming, a large number of data points were obtained in a small number of static tests.